MODIFICATION

OF THE

SURFACE MECHANICAL PROPERTIES

OF CERAMIC MATERIALS

BY ION IMPLANTATION

by

Steven George Roberts M.A.

of

Queens' College Cambridge

A dissertation submitted for the degree of

Doctor of Philosophy

in the University of Cambridge

S G ROBERTS

Summary: Modification of the Surface Mechanical Properties of Ceramic Materials by Ion Implantation

Implantation to doses greater than ∿4 x $10^{17} N_2^+ cm^{-2}$ at ∿100 kv was known to substantially change the friction and wear behaviour of cemented carbide materials; this study aimed to investigate the mechanism behind such changes. The approach adopted was to study the variation, with dose, of simple surface mechanical properties of a variety of materials (silicon carbide, silicon, cemented carbide, lithium fluoride and metallic and inorganic glasses), covering a wide range of bond types, brittle/plastic behaviour, etc. Tests included microhardness testing and single point diamond scratch testing (observing both plastic and fracture response), and diamond paste and pin-on-disc wear tests. Transmission electron microscopy was used to characterise changes induced in near-surface microstructure by implantation and/or deformation. All implantations were of ∿80 kv nitrogen, in the dose range ∿10^{17}-10^{18} ions cm^{-2}, apart from some boron implantations into silicon carbide.

Significant results included:

a) Surface softening of silicon carbide, silicon and cobalt. This change occurred in the first two ~~metals~~ materials abruptly at dose ∿4 x $10^{17} N_2^+ cm^{-2}$.

b) Suppression of lateral fracture around indentations and scratch tracks in brittle materials, the effect increasing with dose.

c) A hexagonal to cubic phase change was induced in silicon carbide by implantation (of boron or nitrogen) and subsequent deformation.

d) Minor changes were observed in the microhardness, etc, behaviour of cemented carbide, glasses & lithium fluoride.

The suppression of certain types of fracture by implantation is thought to be due to the surface stress state associated with high-dose implantation. Effects on plastic behaviour are more substrate/ion specific, but, in silicon and silicon carbide, are possibly via alterations to the electronic properties of the materials.

PREFACE

This dissertation is submitted for the degree of Doctor of Philosophy in the University of Cambridge. The research described herein is the result of work carried out in the Department of Metallurgy and Materials Science, University of Cambridge, between October 1978 and November 1981 under the supervision of Dr. T.F. Page.

The research was supported by the Science Research Council as a CASE award in collaboration with the UKAEA (AERE Harwell). Laboratory facilities were provided by Professor R.W.K. Honeycombe.

The contents of this dissertation are, to the best of my knowledge, original, except where reference has been made to the work of others. The research was carried out without collaboration, except for parts of sections 5.1.3 and 5.3.6, where S.K. Fromson and T.C. Jones assisted as their Pt. II projects. No part of this dissertation has been, or is currently being, submitted for any other degree, diploma or qualification at any other university. The dissertation is less than 60 000 words in length.

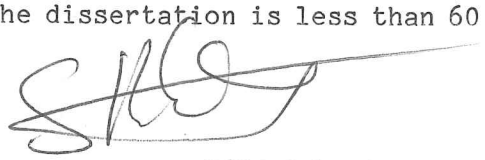

S.G. Roberts

Oxford/Cambridge, November 1982

The work described in this thesis would not have been started or finished without the enthusiasm, advice and practical help generously and patiently given by Dr. T.F. Page, who subverted me from physics at an early age, enticed me into ceramics a little later, and finally coerced me into writing up. Besides, any supervisor who turns not a hair at dismantled motorcycles or ion-beam thinners completely full of water deserves fulsome praise!

Thanks also to the many members of the Metallurgy Department who gave help and advice, including: the ceramics group- Nigel Jepps, Nigel Gibbs, Malcolm Naylor, Philip Sargent and Jocelyn Knight; Brian Derby and Steve 'special K' Kukureka; Dave Ackland and Mike Stocker, who kept 'em running; Derek Starnell, Pat O'Neal and the rest of the workshop staff, who kept 785 FKH and EOY 724J on the road; Steven Lee and Andrew McKnight (Oxford) and Brian Barber (Cambridge) for photographic work; Brian Seymour for X-ray work; Joe 'I tell you one thing' Reich for keeping the ion-beam thinners running; Ian Hutchings and Rob Wallach for letting me play with their PETs; plus others, as they say, too numerous to mention.

At Harwell, I was ably assisted in things I knew little about by Geoff Dearnaley, to whom many thanks. The implantation work could not have been performed without the assistance of Gordon Proctor, 'Spike', Dave Chivers, Phil Goode and Nick Hartley. Thanks to John Turner for the nuclear reaction analyses. Thanks also to Tony Cullis and Nigel Chew of the RSRE for showing me how to make 'edge-on' specimens.

Too many people provided me with beer, food, sympathy and abuse to thank them individually- you know who you are!- however, particular mentions, in no particular order, go to: all the people who've shared houses with me; Ann Ellis, who put up with me on visits to Harwell; Sue; the members of the caving club; Pat; that bunch of eccentrics the BUMPAL (+Gail); Fran; all those who read, corrected and ferried about this thesis; 20GES and its resident troglodytes, who sheltered me in the terminal stages. I notice that Phil and Ukey are in all the group categories above- well done and a Gold Star each.

Finally, I should like to express my gratitude to those people who, knowingly or otherwise, 'got me where I am today': E.A. Scothern, I.L Parker, T.F.Page (again!), and lastly and above all:

my parents,

to whom this thesis is dedicated.

I met a traveller from an antique land
Who said: Two vast and trunkless legs of stone
Stand in the desart. Near them, on the sand,
Half sunk, a shattered visage lies, whose frown,
And wrinkled lip, and sneer of cold command,
Tell that its sculptor well these passions read
Which yet survive, stamped on these lifeless things,
The hand that mocked them, and the heart that fed:
And on the pedestal these words appear:
'My name is Ozymandias, king of kings:
Look on my works, ye Mighty, and despair!'
Nothing beside remains. Round the decay
Of that colossal wreck, boundless and bare
The lone and level sands stretch far away.

P.B. Shelley

CONTENTS

CHAPTER 1

INTRODUCTION

1.1 Project Background

This project arose from the application of a new technology, ion implantation, to the problems of friction and wear, which have a history as old as the science of mechanics. The field of friction, lubrication and wear is now called tribology. It is interesting to note that the effects of ion implantation, and radiation in general, on the structure of materials are quite well understood (see chapter 2), whereas despite the engineering importance and long history of tribology, only a few general principles have emerged and many fundamental problems are still unresolved (see chapter 3).

The first particle accelerators were constructed in the 1930's, but it was not until after the second world war, with the huge civilian and military interest in the possibilities of nuclear fission, that large scale studies of radiation damage in materials were undertaken. Machines to accelerate charged particles to high energies became available; initially these were used to simulate the effects of neutron and alpha-particle impact on possible reactor materials (this line of research still continues, with the growth of fission power and the prospect of controlled nuclear fusion). Interest in the possibility of doping semiconductor materials by accelerated particle beams (of energies typically 30-200kV) grew as the limitations of diffusion doping methods

for these applications became apparent. By the early 1970's a large number of researchers were working in this area, and a series of conferences, on the subject of 'Ion Implantation into Semiconductors' (see conferences in reference list) reflect this interest. Currently, the majority of papers published in the field of radiation damage, and almost the entire literature on ion implantation, are concerned with semiconductor doping and especially the problems of device activation by the annealing of structural and electronic radiation damage while retaining the implanted dopant (see 2.2.1).

It is only very recently that the possibilities of altering the surface chemical and mechanical properties of materials have been realised and systematically investigated. A brief summary of anticipated applications in these areas was published by Brown (in Proc. 2nd Int. Conf, 1971, p430); Subsequent progress in these fields is reviewed in sections 2.3 and 2.4. In a variety of materials, effects of implantation, often significant property improvements, have been reported for corrosion, dry oxidation, hardness, wear, friction and fatigue. The doses required to bring about these changes are much higher than those required for semiconductor doping; typical doses are of the order of 10^{16} to 10^{18} ions cm^{-2}. At these doses, the implanted ions can be present in the surface layer in concentrations of up to 10-50%, and the effects of sputtering often become significant (see 5.1.2).

The work in which this project has its basis is that of Dearnaley and colleagues in the ion implantation group at AERE Harwell, on the friction and wear properties of implanted steels and cemented carbides [eg. Dearnaley (1978b)]. It was found that in these materials, implantation, particularly of nitrogen, to doses greater than $10^{17} cm^{-2}$ could significantly reduce friction and wear rates in both simple geometry laboratory test specimens (eg. pin-on-disc tests) and industrial components such as wire-drawing dies, punches and drills. Wear lifetimes were often extended by factors of 4 or 5. The general aim of the project was to investigate the effects of implantation, especially of nitrogen, on various materials, with the aim of elucidating the mechanisms by which surface mechanical properties could be altered, with particular reference

to cemented carbide materials and wear-related properties. This approach to the project is detailed in the next section.

1.2 Project Overview

The general approach of this project was to examine unimplanted and implanted samples of as wide a range of materials as possible, to see if implantation could produce measurably different responses to macroscopic mechanical tests (eg. microhardness, scratch tests), and to attempt to correlate any such changes with the structural, etc. damage produced by ion implantation and with experimental observations of microstructures of implanted materials. The materials examined were: silicon, silicon carbide, lithium fluoride, silica glass, a metallic glass, WC-Co cemented carbide and cobalt. These materials cover almost the full range of structural and bonding types and plastic/brittle behaviour, although the project is biased towards the study of non-metallic materials for reasons given in section 1.1. The tests performed were those most likely to detect changes in the near-surface behaviour of solids, ie. microhardness and wear tests.

Initially, work was performed on the microhardness behaviour of WC-Co (see 5.3.3), since it was thought that results from such tests might have a bearing on the wear test results reported by Dearnaley (see 5.3.2). However, no changes in such behaviour were found to be produced by nitrogen implantation even to very high doses; moreoever, the microstructure of the material is very complex and its likely response to mechanical tests difficult to predict or model. A broader approach to the investigation, as detailed above, was therefore adopted, concentrating on materials of relatively simple microstructure and well-defined mechanical properties, in the hope of gaining a general understanding of the effects of implantation on a wide range of materials.

The materials used and their properties are listed in table 1.2a; more details are given in the appropriate sections of chapter 5. The growth in the range of materials types studied occurred as the project

progressed and the complexity of the possible effects of implantation, and their interactions and interdependencies, became appreciated (see 2.2). These effects are listed in table 1.2b. For most of the materials studied, almost all of these effects could be active in altering the surface plasticity and/or fracture behaviour, thus changing the wear, friction, hardness and fatigue reponse. Table 1.2c lists, for each material, the 'a priori' most likely active effects of implantation. In chapter 6, these are re-examined in the light of the experimental results presented in chapter 5, especially from the comparison of results for different materials types and (for SiC) different ion species.

The experimental techniques used are described in detail in chapter 4. Choice of techniques was limited by the equipment available and by the difficulties of studying the behaviour of a thin, non-homogeneous, near-surface layer. Detailed studies of the microhardness response, particularly the indentation size effect (ISE - see 4.4.1), were used to gain semi-quantitative results for the plastic behaviour of the implantation-affected layer. Transmission electron microscope (TEM) studies, of both plan-view and cross-sectioned specimens (see 4.6), were undertaken for SiC, Si and WC-Co, so as to examine the deformation mechanisms in or near the implanted layer. The fracture response of the surfaces was studied by examination, by light microscopy and scanning electron microscopy (SEM), of crack patterns around and beneath indentations (4.4.2) and around single-point diamond scratch tracks (4.5.1). Other techniques used were electron channelling (5.2.6), examination of pin-on-disc wear specimens of WC-Co (4.5.3, 5.3.4, 5.3.5), laser beam annealing of silicon specimens (5.2.5) and nuclear reaction analysis of implanted specimens (4.2, 5.1.2, 5.3.6).

Results included:

i) Changes in the microhardness behaviour of silicon (5.2.2), silicon carbide (5.1.3) and cobalt (5.3.6), in all cases showing a surface softening after implantation.

ii) Changes in the fracture behaviour of all the brittle materials studied, lateral fracture around indentations, in particular, being suppressed (5.1.4, 5.2.3, 5.4.4).

iii) Phase changes induced by implantation and deformation in silicon carbide (5.1.7).

Not surprisingly, for an investigation into 'virgin territory', many of the results found were serendipitous rather than anticipated. In several cases, results opposite to those expected were found, for example, the effect of boron implantation on the phase change in silicon carbide, or the reduction in the surface microhardness of cobalt by nitrogen implantation. Perhaps the only general conclusion one could draw about the effects of implantation on the hardness, friction and wear of materials is that each ion/substrate/property combination merits individual investigation. The results to date, however, indicate that such investigations may yield scientifically and commercially useful results.

TABLE 1.2a

Experimental Materials and their Properties

Material	Bond Type	Brittle/ Plastic (room temp)	Hardness ($kgmm^{-2}$)	Notes
		Single Crystal Materials		
Si	covalent	brittle	~2000	Semiconductor. Effects of low-dose implantation extensively studied.
SiC	covalent	brittle	~3000	Polytypic Semiconductor.
LiF	ionic	semi-plastic	~200	
		Amorphous Materials		
SiO_2	covalent	brittle	~1300	
Metglass	metallic	plastic	~850	Deforms by 'shear bands'.
		Composite and Polycrystalline Materials		
REFEL	covalent	brittle	~3000	Composite of SiC & ~5% Si.
WC-Co	mixed	'plastic'	~2000	Wimet 'N' grade - 6% Co.
Co	metallic	plastic	~200	

TABLE 1.2b

'Simple' Effects of High-Dose Ion Implantation

1) Displacement damage to the Crystal Structure:
   In the implanted layer, each parent atom is displaced many times, leading to an amorphous or highly recrystallised structure.
2) Production of a Surface Stress Field:
   Predominantly in-plane compressive in most cases, due to the expansion of the damaged parent structure and the high concentration of foreign atoms.
3) Electronic Effects of the Implanted Atoms:
   In covalent materials, the band structure may be altered by the structural damage and by the doping by the implanted atoms.
4) Physical Effects of the Implanted Atoms:
   These include solid solution dislocation pinning, 'Cottrell atmosphere' effects of implanted interstitial atoms, etc.
5) Chemical Effects of the Implanted Atoms:
   Chemomechanical effects are known to exist in a wide variety of materials, and altering the surface chemistry by implantation may produce such effects.
6) Phase Stabilisation Effects:
   In polymorphic materials, the presence of implanted atoms may affect the relative stabilites of the possible phases.

TABLE 1.2c

'A priori' Most Probable Effects in Experimental Materials

Material / Effect	Si	SiC	LiF	SiO_2	Metglass	WC-Co	Co
Amorphisation	*	*	*			*	*
Surface Stress	*	*	*	*	*	*	*
Electronic Effects	*	*	(*)			*	
Physical Effects	*	*	*		(*)	*	*
Chemical Effects	*	*	*	*	*	*	*
Phase Stabilisation		*				(*)	*

CHAPTER 2

LITERATURE SURVEY: ION IMPLANTATION

2.1 Basic Radiation Damage Processes

The ways in which energetic particles or photons interact with single stationary atoms and non-crystalline or crystalline agglomerations of atoms are reasonably well understood. Several elementary and advanced textbooks exist on the subject eg. those of Chadderton (1965), Thompson (1969), Carter and Grant (1976), and most of the material in this section is drawn from these sources. References will therefore only be given where specific items of information, eg. regarding the characteristics of materials used in the work, are used. The line diagrams in this chapter are taken from the book by Carter and Grant (1976).

2.1.1 Collisions With Single Atoms

Even the simplest radiation damage event is in reality rather complex; an atom or ion, consisting of a small nucleus surrounded by a cloud of electrons approaches and interacts with another similar entity, with resultant changes in their energies and momenta. Essentially two different types of interaction can occur, though these are extreme cases of the real 'mixed' situation. Momentum can be transferred to the target atom as a whole ('elastic' collision), or to its electron cloud alone, leaving the nucleus unaffected ('inelastic' collision). It is found (see

later) that the electronic processes predominate at high energies and the elastic collisions at low energies. The transition between the two regions is gradual; however it is a useful approximation to define an energy at which the transition in behaviour is taken to occur sharply. The two types of interaction and the value of the 'cut-off' energy are discussed below.

i) Elastic Collisions

Except for the case of neutron irradiations, the forces between approaching particles are electromagnetic. Even for this special case, much of the damage resulting from neutron irradiation is due to 'knocked-on' parent atoms, and so electromagnetic interactions are the most important ones. Electromagnetic forces are, in principle, effective at any distance, and various models of the interactions of atoms have been proposed, based on the orbital dynamics of particles under the influence of some variant (with corrections for 'screening' by orbital electrons, etc.) of the Coulomb potential, V(r):

$$V_{(r)} = \frac{Z_1 Z_2 e^2}{4\pi\varepsilon_0 r} \quad f(r, Z_1, Z_2, \text{etc.}) \qquad 2.1.1a$$

[e=electronic charge, Z=atomic no., subscripts
1 & 2 refer to incident & target atoms respectively]

These approximations to the true interactive potential lead to roughly similar results. A very drastic, but still reasonably experimentally accurate approximation is simply to assume the 'hard-sphere' model-

$$V_{(r)} = \begin{cases} \infty & \text{for } r<r_c \\ 0 & \text{for } r>r_c \end{cases} \qquad 2.1.1b$$

The value of r_c can be derived by experiment, or from calculations from the models of the type expressed by equation 2.1.1a; it is found to vary with the energy of the incident ion (see later). From these models, the various scattering parameters of ion-atom interactions can be calculated (eg. distribution of scattering angles and energy transfer).

However, the fundamental questions from the point of view of ion-implantation studies are:

a) How likely is a collision? (ie. what is the mean free path of a moving atom?)

b) How much energy is transferred in a collision?

c) How do these energies compare with those needed to remove an atom from its position in the solid?

The first question is the most difficult to answer, even at a high level of approximation, and is discussed more fully in section 2.1.4. The general approach adopted is to consider the mean free path of the incident ion in an amorphous substrate, and to regard any modifications due to crystallinity as 'exceptions' (see 2.1.2). The interaction cross-section (related to the probability of collision) must then be evaluated as a function of particle energy, etc.

The question of transferred energies is relatively simple to solve if the hard-sphere approximation is used; the maximum energy that can be transferred to a stationary atom (ΔE_{max}) is given by:

$$\Delta E_{max} = \frac{4M_1M_2}{(M_1+M_2)^2} E_1 \qquad 2.1.1c$$

[M = mass, E = energy, of particle; subscripts 1 and 2 refer respectively to the incident and target particles]
The mean energy transferred ($\overline{\Delta E}$) is exactly half this value, assuming a random distribution of collision geometries.

The energy $\overline{\Delta E}$ should now be compared with that required to displace a target atom from its site in the solid (E_d). This obviously varies with the direction in which the target atom is displaced with respect to the crystal structure; it is therefore convenient to define an energy $\overline{E}_d$ which when imparted to a target atom has a 50% chance of displacing it. $\overline{E}_d$ has been evaluated by both theoretical and experimental studies, as detailed below.

A simple approach to a value for $\overline{E}_d$, based on a knowledge of the sublimation energies for solids (E_s), is originally due to Sietz [Carter and Grant (1976) p123]. An atom displaced from its site inside the crystal breaks twice as many bonds as one leaving the surface by sublimation, and one would therefore expect $\overline{E}_d \simeq 2E_s$. This estimate must be increased since sublimation is an equilibrium process and a displacement collision is a highly non-equilibrium one. If it is estimated that the non-equilibrium nature of the process doubles the energy required (or alternatively, if the energy of the interstitial atom formed is included in the total), then $\overline{E}_d \simeq 4E_s$. E_s for most solids is 5-6eV, and so $\overline{E}_d$ is deduced to be 20-25eV. Approaches based on discrete bond breaking have also been applied to covalent solids, and lead to roughly the same values.

$\overline{E}_d$ has been measured experimentally for many solids; methods used have included:

a) Luminescence studies [eg. Loubser et al. (1969)];

b) Electron spin resonance [eg. Gieczy et al. (1967)];

c) Direct observation in the HVEM, using the electron beam both as the source of displacing particles and as a means of observation.

The last method has been used by Hudson and Sheldon (1973) and Hønstvet et al. (1980) for SiC; E_d is found to be 50-100eV, depending on orientation. This high value reflects the strength of the covalent bonds in this material. $\overline{E}_d$ for Si is given by Carter and Grant (1976) (p128) as ~15eV, but no source is cited.

The displaced atom may have a much higher energy than E_d, and thus cause further displacements. The incident particle may also retain enough energy to displace other parent atoms. Thus a single energetic incident particle can create, directly and indirectly, many defects. The geometry of such damage tracks is discussed in section 2.1.3.

ii) Inelastic Processes

These are interactions between the charge (or charge dipole, etc.) of the incident particle and the electron cloud of the target atom. Proper treatment of such interactions would require quantum mechanical calculations; however, estimates of the energies at which such interactions occur can be obtained by use of equation 2.1.1c:

$$\Delta E = \frac{4M_1M_2}{(M_1+M_2)^2} E_1 \qquad 2.1.1c$$

Taking M_2 as M_e, the mass of an electron, so $M_1 >> M_2$:

$$\Delta E = \frac{4\ M_e}{M_1} E_1 \qquad 2.1.1d$$

For energy transfer to occur, ΔE must exceed a critical value for electronic transitions, which will typically be of the order of a few eV (Rydberg energy = 13.6eV), so that:

$$E_1 > \frac{M_1}{4M_e} \Delta E_{crit} \qquad 2.1.1e$$

Since $M_e \simeq 1/2000$ Daltons, and if $\Delta E_{crit} \simeq 1\text{-}4$eV:

$$E_1 > cM_1 \text{ keV} = E_c \qquad 2.1.1f$$

with M_1 in Daltons and c a constant near unity.

If E_1 falls below the critical value (E_c), only elastic processes can occur; above this value, inelastic processes assume increasing importance. Although the transition between predominantly elastic and predominantly inelastic processes are not sharp in reality, it is convenient to define an energy E_c at which a sudden transition between the two modes is assumed to occur. At energies $>E_c$, it is important for the determination of ion ranges (see 2.1.4) to know the rate of energy loss of the incident particle. Different approaches by Firsov (electron interaction model) and Lindhard (multi-process model), give similar expressions [Carter and Grant (1976) p38]:

$$\frac{dE}{dx} = -C\ f(Z_1, Z_2, M_1, M_2, a_0)\ E_1^{1/2} \qquad 2.1.1g$$

where a_0 is the Bohr radius.
In fact, both these approaches are only fair approximations to experimental results, which yield non-monotonic variations of dE/dx with E.

Thus the interaction of a high energy particle with a solid can be seen to consist of:

a) a high energy regime, where processes of electronic interaction predominate ('inelastic regime');

b) a low energy regime where whole-atom collision processes are dominant ('elastic regime'). The dividing energy, E_c, between these two regimes is of the order of M_1keV, though the transition is not sharp.

2.1.2 Effects of Substrate Crystallinity

The existence of long range order in the material through which an ion or knocked-on atom travels can act so as to extend the range of such particles beyond that for travel through an amorphous material. The operative processes can be divided into two classes: channelling effects and collision ordering effects; both are strongly direction dependent.

i) Channelling Effects

In crystalline materials, particularly those with open structures (such as silicon and silicon carbide), there are certain directions in which continous spaces, either pipelike or planar, exist. The directions in which these channels are oriented tend to be certain low index lattice vectors or planes. In silicon (diamond cubic stucture), <110> directions and {110} and {111} planes can act as channels (see fig. 2.1.2.1).

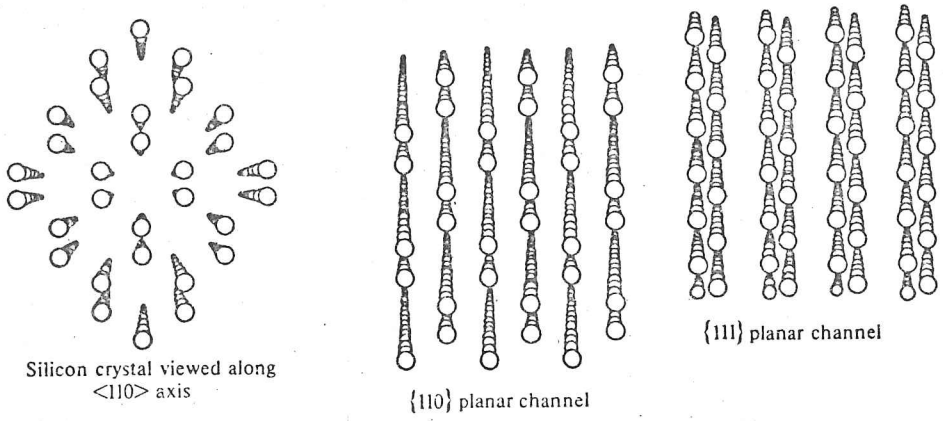

FIG. 2.1.2.1 Channels in silicon.

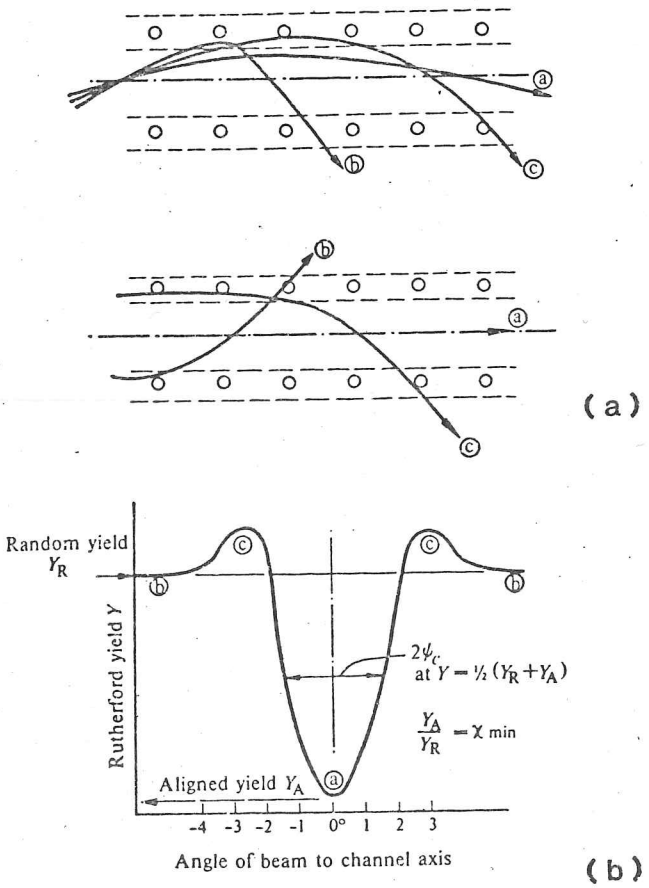

FIG. 2.1.2.2 (a) Paths of ions close to a channelling direction; (b) The expected variation of Rutherford backscattering yield with angle close to a channelling direction.

If a particle is projected along such a direction, and happens initially to be correctly positioned with respect to the substrate atom positions, it can travel a long way down the channel before interacting with a substrate atom. These effects have been the subject of computer modelling [eg. Carter and Grant (1976) p71] from which the general conclusions are:

a) The majority of ions projected down a channelling direction are channelled to some extent. A small fraction (~5%) collide with the end members of atom rows, and have their directions randomised.

b) Ions with a small angular misorientation with the true channelling direction (either from the orientation of the whole beam, or from a grazing collision with a 'row end' atom), move down the channel in an oscillatory manner. Such motion may be stable or may rapidly decay, with the ion being dechannelled.

c) Ions within a certain angular range of the true channelling direction can have a greater interaction probability than ions travelling in a random direction.

It follows that, if the back reflection from an ion beam entering a crystal near the channelling direction is monitored, the variation with angle is of the form shown in fig. 2.1.2.2. This angular variation will change if interstitial atoms are present in the channels; this forms the basis of a powerful technique for studying the site distribution of displaced atoms [eg. Carter and Grant (1976) p87].

A well-channelled ion loses energy only by inelastic electron exitation processes. These processes are inefficient at energies less than E_c, and once a channelled ion has lost energy to this extent, it will travel a long way in the crystal before halting. The range theories discussed in the next section will therefore be modified if large crystals are implanted in these channelling directions. In this study, evidence for channelling was found in lithium fluoride (see 5.5.3).

ii) Ordered or Focussed Collisions

This type of event is analogous to the 'Newton's Cradle' toy; an impulse is given to an atom in a long closely packed row, and momentum is transferred from one to the next along the row [eg. Thompson (1969) p196]. It is not necessary that the original impulse be along the line of atoms, as, under certain circumstances, a part of the obliquely applied momentum can be 'focussed' along a line of atoms. If the hard sphere approximation is applied, it can easily be shown that such an ordered series of collisions can only occur if the spacing between atoms is less than their diameter, with the incident angle range within which focussing can occur increasing with decreasing atomic spacing. At each collision stage in a focussed sequence, some energy will be lost, and eventually the sequence will finish, having transferred energy away from the initial collision site.

iii) Replacement collisions

These are similar to the focussed collision sequences, but involve transfer of matter as well as of energy. If an atom strikes another with an energy of between E_d and $2E_d$, it can displace the target atom, but becomes itself trapped within the vacant site. Along closely packed rows, this process can continue in a focussed manner, finally producing an interstitial in the row (a 'crowdion'). More complex versions of this type of effect exist, where the collisions occur between widely spaced atoms, but with short channels between them, giving an additional focussing effect [eg. Thompson (1969) p216]

2.1.3 Damage Tracks from a Single Incident Particle

The interactions of particles with non-structured solids (see 2.1.1) and the extra effects that can occur if the substrate is crystalline (see 2.1.2) have been described. Generally, the track of a high energy incident particle consists of an initial section of inelastic interaction, followed by a length of track around which atoms are displaced.

The description of this latter part of the track was first attempted by Brinkman (1954), who considered the damage produced by a primary knock-on in a neutron-irradiated solid. Brinkman distinguished between two sections in this final displacement-rich section of the track:

i) that where the distances between diplacement collisions are large, ie. the higher-energy part (the 'thermal spike');

ii) that where the collision interval is of the same order as the interatomic spacing (the 'displacement spike').

The transition between the two regimes is determined by the variation in the effective hard-sphere radius with energy. In the thermal spike, energy is lost between the spread-out displacement events by non-displacive 'glancing' collisions, giving rise to high local temperatures. In the displacement spike, Brinkman assumes that all atoms within a certain region are displaced, temporarily forming a vacancy-rich core region with an interstitial-rich outer layer; this is followed by a collapse and recrystallisation with many defects in the forms of dislocation loops, microtwins, etc.

The model of the sequence described above now needs to be quantified, in two ways:

i) How many atoms are displaced ?

ii) How long are the various sections of the track ?

The second of these questions requires elaborate calculations to gain a quantitative answer; models are reviewed in section 2.1.4. The first question can be relatively easily modelled in a way first suggested by Kinchin and Pease [eg. Chadderton (1965) p35].

It is assumed that all the available energy is dissipated in displacive events, this energy being E_c for incident atoms of energy $>E_c$, and the incident energy itself if it is between E_c and $2E_d$. It is also assumed that an atom is displaced if it receives energy $>E_d$, but not if the received energy is $<E_d$. With these assumptions, at the n^{th} stage of the collision process, $N = 2^n$ atoms will have been displaced. The initial energy available will then have been distributed so that each of the N atoms has, on average, energy = $E/N = E/2^n$. No further displacements will occur when this value falls below $2\overline{E}_d$ (for energy $>E_d$ but $<2E_d$, the displacing atom will replace the displaced atom). Collisions stop when:

$$E_c/N < 2\overline{E}_d \qquad 2.1.3a$$

so that

$$N = E_c/2\overline{E}_d \qquad 2.1.3b$$

Using equation 2.1.3b for the cases under consideration in this study (Si, SiC, Co), the following results are obtained:

Material	$\overline{E}_d$ (eV)	N for >14kV nitrogen
Si	~15	~450
SiC	~70	~100
Co	~25	~300

A value of $\overline{E}_d$ for WC is not available, but in view of the strength of the bonding, it is probably close to that for SiC.

It can therefore be seen that ions of even moderate energies displace very large numbers of atoms. Also, for 40kV nitrogen atoms, nearly 2/3 of the incident ion energy is lost as heat by electronic transfer above E_c. For this reason, ion flux rates were kept low enough to ensure that temperature rises sufficient to allow damage self-annealing did not occur (see 4.1).

2.1.4 Ion and Damage Ranges in Solids

While the processes described in the preceding sections are of interest in considering the origins of the characteristics of implanted surfaces (see 2.2), the most important parameter of an implanted layer for many purposes is the depth distribution of the implanted ions. There are several methods of determining the mean ion range and the magnitude and form of the scatter of the distribution, which range from the purely theoretical approach of Lindhard, Scharff and Schiøtt (LSS) (1963), to purely experimental methods, eg. secondary ion mass spectroscopy (SIMS). Intermediate, computer modelling, approaches have also been used. All these approaches are reviewed briefly below.

i) L.S.S. Theory

Results from the LSS analysis are widely used to estimate ion concentration profiles. The theory derives functions for the inelastic and the elastic scattering energy loss rates by using a Thomas-Fermi interaction potential (a non-analytic function with a good fit to real potentials), and then uses numerical integration to obtain the ion ranges. The results are given in terms of dimensionless parameters for energy (ε) and distance (ρ)* which have been interpreted by various authors into more usable graphs and tables of ion range for various ion/substrate/energy combinations [eg. Channing and Turnbull (1968), (1969)]. The LSS method gives directly only the total ion range (R). However, the parameter most often required is the projected ion range (R_p) and the scatter in this (see fig. 2.1.4.1). Consideration of the basic mechanisms of the stopping processes shows that all the scatter in R_p occurs in the elastic scattering regime. Thus light ions would be expected to show relatively little scatter compared to heavier ions, as E_c is proportional to the ion's mass. Because of the randomness of the elastic collisions, the

---

* $\varepsilon = E_1 a_0 M_2 / Z_1 Z_2 e^2 (M_1+M_2)$

$\rho = RN4\pi a^2 M_1 M_2 / (M_1+M_2)^2$ where N=the atomic density of the solid, a_0=the Bohr radius and R=the Rydberg constant.

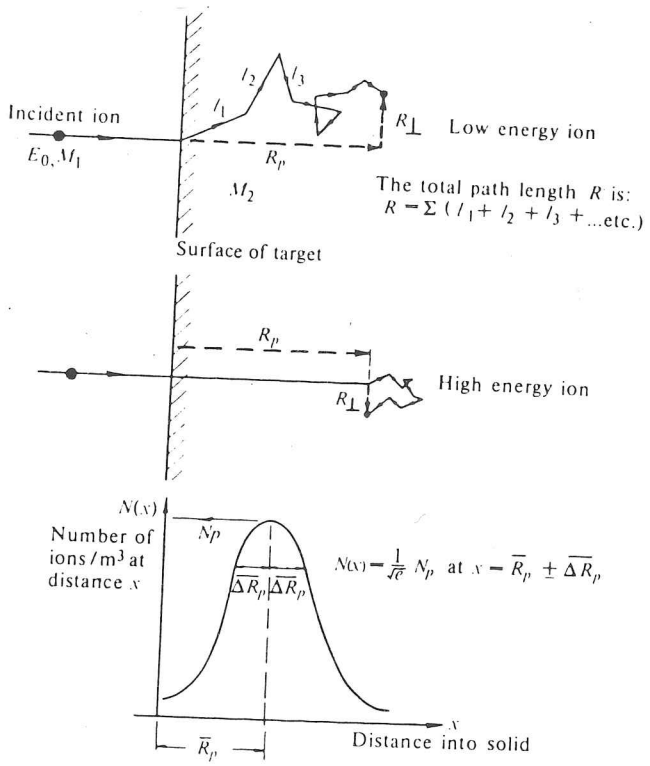

FIG. 2.1.4.1 Range parameters: total path length, R; projected range, R_p; mean projected range, $\bar{R}_p$; standard deviation of $\bar{R}_p$, $\Delta\bar{R}_p$. For high energy or light ions, R_p approaches R.

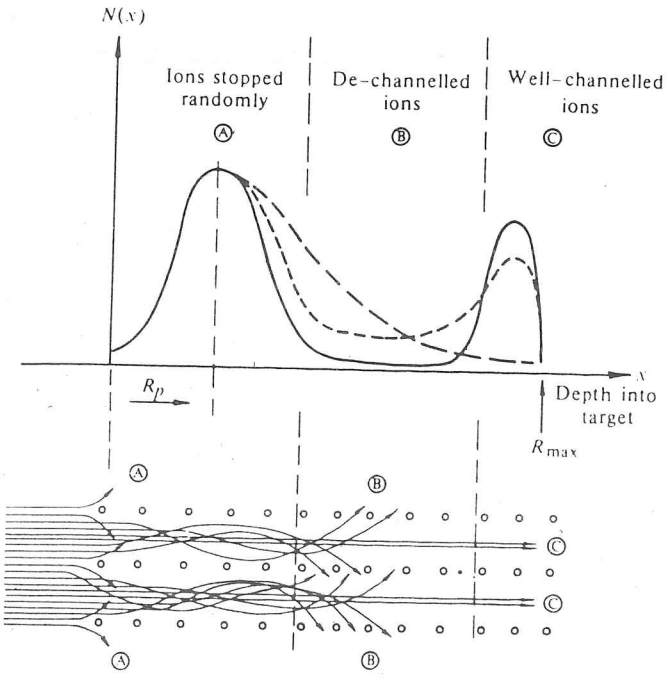

FIG. 2.1.4.2 Effect of channelling on ion profiles. Well-channelled ions can form a concentration peak at a considerable depth within the crystal.

distribution of ions around the mean range is usually assumed to be Gaussian, and experimental results (see below) show a good fit to this. The parameter of interest is therefore ΔR_p, the standard deviation of the distribution. The LSS theory is able to predict values of ΔR_p. Also the ratio R_p:R can be calculated; it is found to vary from ~1 for very light ions (mostly inelastic stopping) to $\sim 1+M_2/M_1$ for very heavy ions (mostly elastic stopping).

The LSS approach takes no account of channelling, etc. If a single-crystal substrate is at or near the right orientation, this can substantially affect the range characteristics (see 2.1.2). Fig. 2.1.4.2 shows the effect of channelling on an ion profile; a long tail of poorly channelled ions lies beneath the Gaussian profile, with a final peak where the well channelled ions come to rest.

ii) Computing Methods

Computer modelling techniques of various types have been employed. That of (eg.) Johnson and Gibbins [Carter and Grant (1976) p58] is to use the basic LSS equations to evaluate numerically the projected ion range and scatter for various ion/target/energy combinations. Fig. 2.1.4.3 shows an example of such results for boron-implanted silicon; similar results would be expected for nitrogen implantation.

Another approach is that of the 'Monte Carlo' type of method, in which the 'flights' of a large number of individual ions are followed through a computer model of the substrate structure. The method involves a great deal of computer time, but has revealed much about the effects of varying the modelling parameters implicit in the analytical methods. This type of method was also the first to 'discover' channelling (see 2.1.2) [Robinson and Oen (1963)], and has been used to study the shapes of individual collision cascades [eg. Beeler (1964)]

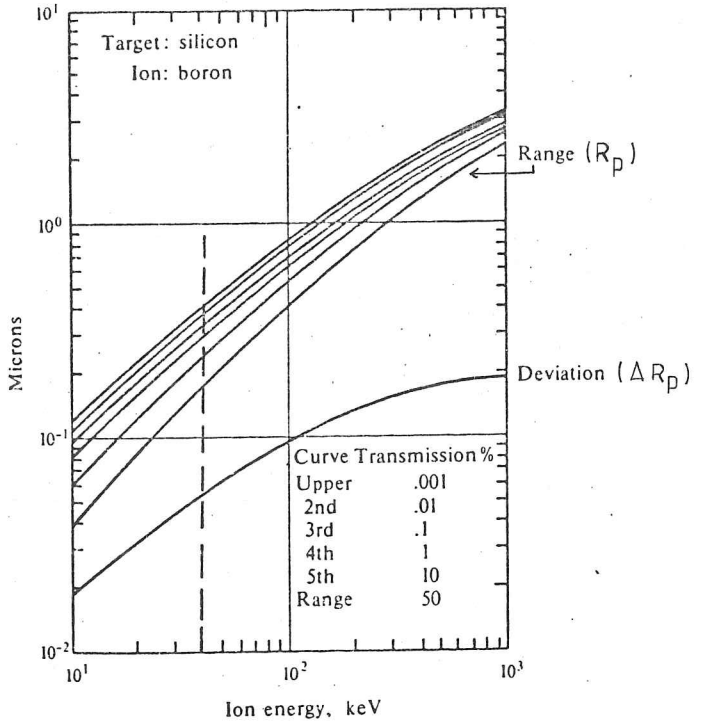

FIG. 2.1.4.3 Depth profile for boron ions in silicon, as a function of ion energy. 'Transmission' lines indicate the thickness of silicon that would transmit only the noted fraction of ions, ie. R_p corresponds to transmission = 50%. The dotted line indicates ions of 40kV energy, as used in this study.

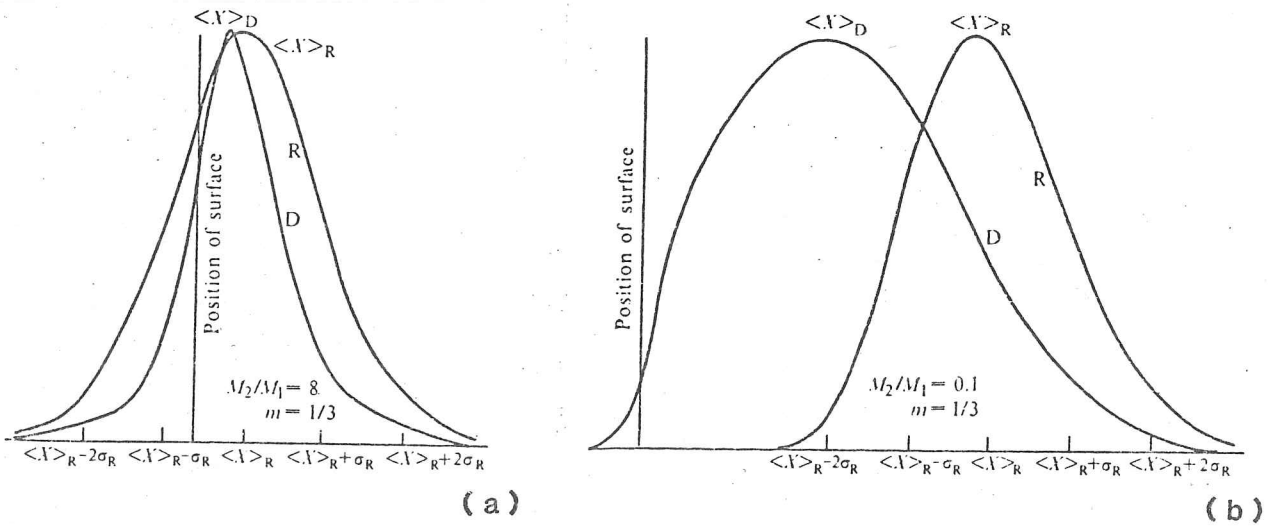

FIG. 2.1.4.4 Ion (R) and defect (D) ranges for: (a) light ions; (b) heavy ions. The defect profile lies closer to the surface than the damage profile, particularly for heavy ions.

The distribution of displacement, etc. damage with depth can be predicted from a knowledge of the characteristics of the collision cascade (see 2.1.3). Such damage will be generated from when an ion's energy falls below E_c, until the ion comes to rest. Generally, the heavier the implanted ion, the closer to the surface the damage profile will lie compared to the ion profile, as:

a) E_c is higher, and so displacement events will occur over a larger part of the track;

b) A heavy ion will suffer less deflection in its elastic collisions.

These effects are shown in fig. 2.1.4.4. For the cases of nitrogen and boron implanted into the materials used in this study, the displacement damage profile would be expected to follow closely the depth profile of the implanted ions.

ii) Experimental Techniques

Measurement techniques for determining ion profiles fall into three broad categories:

a) Surface analysis/stripping;

b) Depth analysis by backscattering/nuclear reactions;

c) Cross-section TEM.

a) Stripping Techniques

These are reviewed by Carter and Grant (1976) (p61). The method is basically to remove a known amount of surface material and then to measure the amount of implanted material either remaining in the substrate or in the material removed. Common techniques of surface stripping include vibratory polishing and controlled oxidation followed by dissolution of the oxide. Detection of the implanted material is often performed by implanting a radio-isotope, or an isotope that is easily detected by eg. neutron activation. A variant of this technique is that employed by Masters et al. (1970), in which the ion-damaged regions were decorated with copper, followed by a series of stripping/neutron activation analyses to

determine the damage profile. Another variant of the stripping technique is secondary ion mass spectrometry (SIMS) (for a general review see eg. Zinner (1980)). This technique is quite difficult to calibrate for depth; in fact ion-implanted samples have been used as calibration samples for SIMS apparatus [Wilson (1980)]. Profiles have also been produced by an SEM/sectioning technique [Bach and Muhle (1976)].

b) Depth Analysis Techniques

These techniques, unlike those above, give direct depth information, generally by examination of the energy losses of the returning radiation/particles. Common techniques are Rutherford backscattering spectroscopy (RBS) and nuclear reaction analysis (see 4.2).

RBS has been developed as a sensitive technique in various ways; a review is given by Carter and Grant (1976) (p82). The technique involves the evaluation of the spectrum of ions elastically backscattered from the substrate/implanted ion combination; typically, MeV He^+ions are used. Depth information is dependent on a knowledge of the rate of energy loss of the analysing ions by inelastic processes. Different implanted species can be detected in the same sample, as the energy lost in the elastic collision depends on the mass of the target atom (see 2.1.1). Also, by making use of the channelling effect (see 2.1.2), ions directed down channels can be used to detect the position of atoms in interstitial sites. In this way, much information can be obtained about the early (pre-amorphisation) stages of implantation [eg. Eskildsen (1982) and other papers from this conference].

The nuclear reaction technique is similar in principle to RBS, except that the detected particle is one emmitted by the implanted atom itself, from a nuclear reaction induced by irradiation by eg. deuterons. Details of the technique as used for analysis of specimens produced in this study are given in section 4.2.

c) TEM Techniques

Both plan-view and cross-sectioned specimens of implanted surfaces have been examined in this study; the specimen preparation techniques are described in section 4.6. These techniques have also been extensively used by workers in the field of annealing of implantation damage (see 2.2.1), especially using electron and laser beams; a large body of literature exists [eg. Cullis et al. (1978), (1980)].

All the above techniques confirm the damage and defect profiles computed by various methods to a good degree of accuracy.

2.2 Characteristics of the Implanted Layer

The composition and microstructure of the implanted surface vary throughout its depth. However, for the purposes of interpreting the results presented in chapter 5, it is convenient to treat the layer as a simple entity having properties different from those of the bulk material. In any case, the methods used (see chapter 4), apart from the TEM techniques, are insufficiently sensitive to detect any variation in properties with depth in the implanted layer. The main ways in which the layer differs from the bulk are:

i) The accumulation of displacement damage often causes the implanted layer to be non-crystalline at high doses.

ii) The high concentration of implanted 'foreign' atoms often causes the layer to be in a chemically metastable state.

iii) The volume changes associated with (i) and the extra material introduced by implantation produce a stressed surface layer.

iv) At high doses, the effects of sputtering (material ejection from the surface) may be significant.

These characteristics are discussed in sections 2.2.1 to 2.2.4.

2.2.1 Amorphisation of Surfaces by Ion Implantation

Ion implantation, particularly into non-metals at low homologous temperatures, is well known to produce amorphous near-surface layers. The materials most investigated from this point of view have been silicon, germanium and other semiconductor device substrates, since it is of great importance for sucessful device fabrication that the doped surface be damage-free. Most papers in this field are concerned with the removal of the amorphous and damaged layers by various annealing treatments, rather than with the mechanisms by which the layers arise (see below).

The most obvious effect of amorphisation on the surface layers of eg. silicon is the colouration of the surface. This has been reported by Beanland and Chivers (1978) and Seidel et al. (1976). These colours have been attributed to optical interference effects between the amorphous layer, the crystalline substrate and (at low doses) a thin surface crystalline layer. Beanland and Chivers describe how the colour produced depends not only on the ion species, energy and dose, but also on the thermal history of the specimen during implantation. Sadana et al. (1980) investigated the structure of variously coloured regions using cross-sectional TEM, and confirmed the differently layered structures in the differently coloured regions, though the layering they observed differed from that predicted by Beanland and Chivers. Colours were normally observed on the silicon and silicon carbide specimens implanted in this study. However, no consistent colour/dose correlation was found from batch to batch of implanted specimens. This is probably due to the variation of process variables in the 'Pimento' implanter (see 4.1.1).

The transition between the crystalline and the amorphous states in silicon has been studied as a function of dose, energy and implanted species by a number of authors [eg. Dennis and Hale (1976)]. The study by Nelson and Mazey (1967), on the influence of channelling on dose for amorphisation, showed that it is energy loss by displacement, rather than through inelastic processes, which is responsible for the crystalline-to-amorphous transition. Suggested mechanisms for the

transition fall into two main groups:

a) Small amorphous regions associated with individual displacement cascades accumulate until they finally overlap. This model was used in the theoretical study of Moorehead and Crowder (1970) in which amorphisation doses at room temperature were successfully predicted. A modification of this approach, taking account of the depth variation of damage, was used by Christel et al. (1981), who estimated that for silicon, low temperature light ion implantation would produce an amorphous layer after displacement of ~10% of the parent atoms.

b) Point defects gradually accumulate throughout the implanted region until their density is so great that the structure collapses into an amorphous state.

Webb and Carter (1979) concluded that results from the study of variations in disorder, as detected by RBS, with dose, energy, etc. are unable to distinguish between the models and their various refinements. Microscopical studies of the accumulation of damage have been performed by Mazey et al. (1968), who found discrete zones of amorphous material in neon-implanted silicon. Studies based on RBS, electron spin resonance (ESR), etc. by Muller and Kalbitzer (1980) conclude that such amorphous regions are only formed by the interaction of light ions with regions with a high density of point defects, while for heavy ions (>100 Daltons) no such 'pre-damage' is required. In the review by Carter and Grant (1976) (chap. 6), this transition between two types of mechanism, accumulation of fine scale damage for light ions, and production of discrete amorphous regions for heavy ions, is also suggested. Direct microscopical evidence for these different mechanisms is sparse.

The structure of the self-implantation-induced amorphous layer (at doses of 10^{14}-10^{15} ions cm^{-2}) has been compared with that of evaporated amorphous material for germanium by Zellama et al. (1978). Their annealing studies indicated that the two structures were identical. The introduction of 'foreign' atoms at high doses, as in this study, may modify this situation, however.

The study by Dennis and Hale (1976) finds amorphisation doses for silicon of the order of 10^{14}-10^{15}ions cm^{-2}, depending on ion mass and energy. For 40kV nitrogen (N^+), the dose for amorphisation was found to be $3x10^{14}$ions cm^{-2}. The general magnitude of this dose is confirmed by the channelling results in section 5.2.6. Studies of implantation amorphisation dose for SiC are rather limited, but that of Makarov et al. (1979) showed that implantation of SiC with 45kV N^+ to a dose of $8x10^{15}$ions cm^{-2} produces an amorphous layer, and the study of Marsh (1974) showed an amorphous layer after $9x10^{14}N^+cm^{-2}$ at 35kV. TEM results in section 5.1.7 and 5.2.7 show that all the Si samples prepared for this study had amorphous surface layers, though implantation produced fine microcrystalline surfaces in SiC and WC (see 5.1.7 and 5.3.5). However, the study by McHargue and Williams (1982) showed that an amorphous surface layer was produced by the implantation of SiC with chromium to a dose of $2.6x10^{17}$ions cm^{-2} at 200kV.

i) Annealing of Damage in Semiconductors

The history of ion implantation as a device-producing route is reviewed by Dearnaley et al. (1973); they note that the first mention of this possible application was made by Shockley in 1954, and that interest grew throughout the 1960's. All early workers appreciated the adverse effects that the radiation damage had on the electrical properties of the implantation-doped layer. These deleterious electrical effects are due to:

a) The reduction of the number of dopant atoms on electrically active substitutional sites;

b) The introduction of 'deep levels' into the band gap, which trap current carriers;

c) The scattering of current carriers by defects.

The annealing treatment required depends on whether or not the surface has been made amorphous. An amorphous layer is best recrystallised by epitaxial regrowth on the bulk material, and this requires rather higher temperatures than those for the annealing of damaged but crystalline surfaces [Dearnaley et al. (1973) p490].

It is, however, difficult to remove all the damage by thermal annealing, even if fairly high temperatures are used ($\gtrsim 800^{o}C$, in silicon); the channelling/TEM studies of Davidson and Booker (1970) revealed large numbers of dislocation loops and other defects even after such high temperature annealing. At higher temperatures, significant loss of the dopant by diffusion can occur, both into the bulk and from the surface. Thermal treatments have been used, in combination with eg. RBS or electrical techniques for the measurement of disorder, to study the annealing characteristics of the implanted layer, and so to estimate the types, quantities and mobilities of the defects present [Carter and Grant (1976) p173], [Tokuyama et al. (1978)]. Some investigations of the thermal annealing of damage in SiC have been carried out [Marsh and Dunlap (1970)], [Marsh (1974)], [Campbell et al. (1974)]. It was found that temperatures in the range 1100-1500^{o}C were required to produce working devices from implanted SiC, as opposed to temperatures of $\gtrsim 1800^{o}C$, and very long times, to produce similar devices by diffusion techniques.

More recently, because of the various problems associated with thermal annealing, rapid annealing techniques have been investigated. These include electron beam and laser light annealing; a very large number of papers have been produced on these subjects. Unlike the thermal techniques, which use (radiation-enhanced) diffusion to anneal out the implantation disorder, the new techniques actually melt the surface [Cullis, Webber and Chew (1980)]. The melting occurs for so short a time that little dopant escapes during the (epitaxial) regrowth of the surface. Laser energies used for silicon are typically in the range 0.5-1 Jcm^{-2}, using nanosecond pulse lengths. Such annealing treatments were tried on the silicon implanted for this study (see 5.2.5), but for these heavily implanted samples, it was found that the annealing treatment stripped off the surface. The laser beam technique has been used with SiC [Makarov et al. (1979)] with pulse energies of the order of 2-10 Jcm^{-2}; high defect densities remained at all but the highest energies.

It is, however, difficult to remove all the damage by thermal annealing, even if fairly high temperatures are used ($\gtrsim 800^{o}C$, in silicon); the channelling/TEM studies of Davidson and Booker (1970) revealed large numbers of dislocation loops and other defects even after such high temperature annealing. At higher temperatures, significant loss of the dopant by diffusion can occur, both into the bulk and from the surface. Thermal treatments have been used, in combination with eg. RBS or electrical techniques for the measurement of disorder, to study the annealing characteristics of the implanted layer, and so to estimate the types, quantities and mobilities of the defects present [Carter and Grant (1976) p173], [Tokuyama et al. (1978)]. Some investigations of the thermal annealing of damage in SiC have been carried out [Marsh and Dunlap (1970)], [Marsh (1974)], [Campbell et al. (1974)]. It was found that temperatures in the range 1100-1500^{o}C were required to produce working devices from implanted SiC, as opposed to temperatures of $\gtrsim 1800^{o}C$, and very long times, to produce similar devices by diffusion techniques.

More recently, because of the various problems associated with thermal annealing, rapid annealing techniques have been investigated. These include electron beam and laser light annealing; a very large number of papers have been produced on these subjects. Unlike the thermal techniques, which use (radiation-enhanced) diffusion to anneal out the implantation disorder, the new techniques actually melt the surface [Cullis, Webber and Chew (1980)]. The melting occurs for so short a time that little dopant escapes during the (epitaxial) regrowth of the surface. Laser energies used for silicon are typically in the range 0.5-1 Jcm^{-2}, using nanosecond pulse lengths. Such annealing treatments were tried on the silicon implanted for this study (see 5.2.5), but for these heavily implanted samples, it was found that the annealing treatment stripped off the surface. The laser beam technique has been used with SiC [Makarov et al. (1979)] with pulse energies of the order of 2-10 Jcm^{-2}; high defect densities remained at all but the highest energies.

ii) Amorphisation in Metals, etc.

Very little has been published concerning implantation damage in non-semiconductor materials. Some work has been performed involving comparisons between quench-produced amorphous alloys and their implantation-produced equivalents, eg. Brimhall et al. (1979) and Rechtin et al. (1978). These studies found the the amorphous materials were very resistant to further damage by ion implantation.

More general studies of implantation into metals have been performed by Ali et al. (1978) and Johnson et al. (1979); earlier work has been reviewed by Grant (1978). It was found that only certain metal/ion combinations give rise to an amorphous layer, typically those combinations that produce a final surface composition similar to that of the normal metal/metalloid type of quench-produced amorphous metal (eg. B^+ into iron). High ion fluences, typically $\sim 10^{17}$ ions cm^{-2}, are required to bring about the transitions, compared with the $\sim 10^{15}$ ions cm^{-2} required to amorphise eg. silicon. Ali et al. suggest that amorphisation is likely to occur if the implanted species has directional bonding and if the target material has a number of polymorphic forms. An interesting case is that reported by Follstaedt et al. (1980), where, in a study of Ti^+ implanted iron, it was found that accidentally introduced carbon (from vacuum contamination) was responsible for stabilising an amorphous phase. Bykov et al. (1975) found that implantation of nitrogen, helium or neon could induce phase changes in iron, molybdenum, nickel or titanium. They speculated that the ion-produced phases (ie. fcc,hcp in Fe and Mo, hcp in Ni, fcc in Ti) were stabilised by a high interstitial density.

These results are not unexpected, considering the difficulty of making metal-based amorphous materials, and reflect the differences in bond type between the covalent semiconductors and the less directionally bonded metals. One would expect that during implantation a process of continuing recrystallisation would occur in metals, and this has been observed by Johnson et al. (1979).

2.2.2 Chemical State of the Implanted Surface

The chemical state of the implanted surface has two interesting aspects:

i) The (meta)stability of the implantation-produced surface compounds;

ii) Possible alterations in the chemical interaction of the implanted surface with the environment (eg. production of corrosion-resistant surfaces).

The former aspect is of interest for the insights it gives into the thermodynamics of non-equilibrium mixtures, and the latter from a more empirical, commercially-oriented viewpoint. The effects of implantation on corrosion resistance are detailed in section 2.3.

Most of the research in the field of implantation-produced metastable surface alloys has concentrated on metal substrates. However, some interest has been shown in synthesising insulating subsurface layers of SiC and Si_3N_4 in silicon by implantation and annealing treatments. Papers on this subject [Tsujide et al. (1980)], [Edelman et al. (1976)], [Pavlov et al. (1976)], [Akimchenko et al. (1977)], indicate that very high doses (10^{17}-10^{18}ions cm^{-2}) and high annealing temperatures (850-1200°C) are required to produce these compounds. Under these conditions, polycrystalline cubic SiC is formed, though Edelman et al. report that single crystal cubic SiC can be formed by implantation of carbon into hot (850°C) SiC. Nitrogen implantation tends to produce α Si_3N_4 at low doses, and a mixture of α and β forms at higher doses. Again, polycrystalline material is usually produced, though large crystals can be produced by suitable heat treatment [Pavlov et al. (1976)].

The formation of metastable alloys in metals has been reviewed by Poate and Cullis (1980), Poate (1978) and (1979), Myers (1978) and Wolf (1980). Poate and Cullis describe ion implantation as the terminal member of a series of increasingly violent mixing techniques, beginning with solidification from the melt and progressing via rapid quenching to ion implantation. Much of the work they describe involves analyses of RBS

spectra from several crystallographic directions in the same sample, so as to determine the lattice sites of implanted and other atoms. They give examples of dilute solid solutions (eg. 0.02% Gd in Be) which cannot be produced by any technique other than ion implantation. The use of Ag/Cu alloys is also mentioned; here concentrated substitutional solid solutions can be obtained by implantation, which are stable up to ~300°C (the Ag/Cu system normally exhibits very limited solid solubility). Non-crystalline mixtures of normally incompatible elements (eg. W/Cu, Ta/Cu) can also be produced, and can be stable up to moderately high temperatures (eg. 400°C for Ta/Cu).

The limits of solubility of implanted alloys have been investigated by Sood (1978), Sood and Dearnaley (1978) and Liau and Mayer (1978). Sood and Dearnaley consider the limits on solubility set by the 'Hume-Rothery' rules, and find that a modification of these fits the data for implantation-produced alloys quite well. The modified rule is that a metastable solid solution will be formed if the implanted species has both:

i) Atomic radius within -15% to +40% of the host atom radius;

ii) An electronegativity within ± 0.7 of that of the host atoms.

These empirical rules are intended to apply only to metals, and so no conclusions can be drawn about the chemical state of the surfaces implanted in this study.

Liau and Mayer (1978) consider the limits set on compositions by the effects of sputtering (see 2.2.4). They estimate that at a dose of 10^{17} ions cm^{-2}, 50-500nm of parent material will be removed (the effect of sputtering on the composition of implanted REFEL surfaces is discussed in section 5.1.2.). They conclude that, for the limitation of sputtering, it is desirable to:

i) Implant with light ions where possible;

ii) Implant to low doses, by implanting ready-doped surfaces;

iii) Recoil-implant where possible (ie. bombard a surface coating of the desired dopant with inert ions).

This last technique is also useful where an expensive dopant is required, since material loss in coating is normally much less than that in

producing an ion beam. However, very careful process control is required [eg. Padmanabhan and Sørensen (1982)].

Poate and Cullis (1980) point out the possiblities of using ion-implanted mixtures in the determination of phase diagrams, as the high defect density present speeds both nucleation and growth of any phases formed during post-implantation annealing. This aspect is reviewed by Myers (1978), who gives as an example the technologically important Cu/Be system; the use of ion implantation allows solid solubility data to be gathered at lower temperatures than would otherwise be possible. Myers also reviews the use of ion implantation in solute trapping studies (eg. Sb in Fe-Ti-C alloys), where use of RBS and TEM during annealing can show the progress of the trapping (in this case of Sb by a Ti-rich alloy).

The review by Wolf (1980) gives examples of the use of Mössbauer spectroscopy in the study of compound formation in implanted materials, particularly complex organo-metallic compounds. This technique has also been used by Longworth and Hartley (1978) in the investigation of nitrogen-implanted iron. It was found that various iron nitrides were formed. This conclusion is reinforced by the X-ray photoelectron studies of Singer and Murday (1980). The state of the nitrogen in iron and steels is important because of such materials' increased resistance to wear after nitrogen implantation (see 2.4.4).

2.2.3 Stresses in the Implanted Layer

Ion implantation to high doses has marked effects on the stress state of the surface. Both displacement damage (see 2.1.1) and the large number of foreign atoms implanted tend to increase the volume of the material, producing a state of compressive plane stress. Several workers have measured the stresses in the implanted layer; two types of method have been used:

i) those based on the bending of the specimen by the stresses;

ii) those using X-ray techniques such as Lang topography, Pendellosung topography, examination of rocking curves etc.

producing an ion beam. However, very careful process control is required [eg. Padmanabhan and Sørensen (1982)].

Poate and Cullis (1980) point out the possiblities of using ion-implanted mixtures in the determination of phase diagrams, as the high defect density present speeds both nucleation and growth of any phases formed during post-implantation annealing. This aspect is reviewed by Myers (1978), who gives as an example the technologically important Cu/Be system; the use of ion implantation allows solid solubility data to be gathered at lower temperatures than would otherwise be possible. Myers also reviews the use of ion implantation in solute trapping studies (eg. Sb in Fe-Ti-C alloys), where use of RBS and TEM during annealing can show the progress of the trapping (in this case of Sb by a Ti-rich alloy).

The review by Wolf (1980) gives examples of the use of Mössbauer spectroscopy in the study of compound formation in implanted materials, particularly complex organo-metallic compounds. This technique has also been used by Longworth and Hartley (1978) in the investigation of nitrogen-implanted iron. It was found that various iron nitrides were formed. This conclusion is reinforced by the X-ray photoelectron studies of Singer and Murday (1980). The state of the nitrogen in iron and steels is important because of such materials' increased resistance to wear after nitrogen implantation (see 2.4.4).

2.2.3 Stresses in the Implanted Layer

Ion implantation to high doses has marked effects on the stress state of the surface. Both displacement damage (see 2.1.1) and the large number of foreign atoms implanted tend to increase the volume of the material, producing a state of compressive plane stress. Several workers have measured the stresses in the implanted layer; two types of method have been used:

i) those based on the bending of the specimen by the stresses;

ii) those using X-ray techniques such as Lang topography, Pendellosung topography, examination of rocking curves etc.

i) Cantilever beam methods

This type of technique was first used by EerNisse (1971a,b). A cantilever beam of silicon was implanted on one face, and the deflection at the free end as the implantation progressed was measured in situ by a capacitance method. This method measures an 'integrated stress'; ie. all the implantation-induced stresses are measured together as a single surface force. At low doses (10^{11}-10^{13} He^+cm^{-2}), a linear dependence of the compressive integrated stress on dose was found. At higher doses the stresses peaked and then levelled off. The dose at which the peak stress occurred varied with ion mass, being ~10^{13} Xe^+cm^{-2}, ~10^{15} Ne^+cm^{-2} and ~10^{16} He^+cm^{-2}. EerNisse considered the peaking of the stress to be due to yielding in the implanted layer. He estimated the peak stresses present to be of the order of 400-500MPa, less than the yield stress of normal silicon, but considered that the yield stress in implanted silicon might be less than the normal value (see 5.2.2). EerNisse also measured the stresses in implanted Si_3N_4, Mo, Al_2O_3, and silica glass (1974) and (1977a), CVD Si_3N_4 (1977b), and various other glasses and metals (1973). For most materials , increasing and peaking compressive stresses in the surface plane were found. In a study on CVD Si_3N_4 (1977b), a variety of ions were used ranging in mass from H^+ to Ar^+; the dose at which the peak stress occurred was found to be that at which a certain amount of energy had been lost by displacment processes (~10^{22}keV cm^{-2}). This indicates that is the accumulation of displacement events, rather than the presence of the implanted ions, which is responsible for the observed stresses. This conclusion is reinforced by the results for copper and gold [EerNisse (1973)], materials in which displacement damage anneals out at low temperatures; here the stresses produced were zero, for gold, and small, for copper.

However, the results for fused silica [EerNisse (1974), (1977a)], showed a tensile stress, ie. compaction in the implanted layer. The ion doses extend only up to 10^{15}ions cm^{-2}, however, and the stresses produced by the implantation of the heavier ions (Ar^+, Ne^+) peaked at lower doses than this and then decreased rapidly. Results presented in section 5.4.4 suggest that at higher doses, compressive stresses are produced. These

results are compatible with initial compaction by break-up and partial collapse of the open silica glass structure, followed by expansion as large numbers of foreign atoms accumulate. It is interesting that such compactions are not found to occur during the implantation of other open-structured solids such as silicon, diamond [Maby et al. (1981)] or the CVD Si_3N_4.

A cantilever beam technique was also used by Hartley (1975a) to measure the stress build up in EN40B steel implanted with nitrogen and argon. Here compressive stresses were observed, peaking at $\sim 5 \times 10^{17} N_2^+ \text{ cm}^{-2}$ (stress $\simeq$ 10GPa) and $\sim 10^{17} Ar^+ \text{ cm}^{-2}$ (stress $\simeq$ 40GPa). These stresses are well above the normal yield stress of the steel (600MPa), perhaps indicating that some hardening has occurred in the implanted layer (see 2.4.3). The technique was used in a modified form by Hoffman and Gaerttner (1980) for the implantation of chromium films with Ar^+ and Xe^+, during the evaporation of the films onto glass. The beam bending was measured by an interferometric method, and compressive stresses were observed.

ii) X-ray methods

These techniques have been applied to silicon and to magnetic bubble materials (garnets) by a variety of workers; in many cases the annealing of the stresses was also studied. X-ray methods (other than Pendellösung topography) measure the surface strain in crystalline material, rather than the integrated stress measured by the cantilever beam techniques. Methods used include:

a) Lattice parameter measurement by 'rocking curves', eg. Lecrosnier et al. (1977), Kyutt et al. (1980);

b) Pendellösung topography, eg. Alstrup (1979);

c) Lang topography, eg. Gerward (1978), Itoh et al. (1978), Zielinska-Rohozinska and Gerward (1980);

d) Interferometry, eg. Gerward (1978).

Results varied greatly depending on the ion species used (especially with the ion's atomic volume with respect to the substrate), the implantation dose and the annealing temperature. Generally, however, compressive

stresses were found after implantation, with annealing tending to reduce the stresses. If an amorphous surface layer is produced, annealing can produce tensile stresses in the surface if the ion implanted is smaller than the host atoms (eg. B^+ in silicon [Larson and Barhost (1980)]), or compressive stresses if the implanted ion is larger than the host atoms (eg. Sb^+ in silicon [Itoh et al. (1978)]). Gerward (1978) found that increasing the dose of Ar^+ in silicon above that required for a saturation of stress brings about a rapid fall-off in the surface stress measured, with almost no stress at a dose of 10^{17}ions cm^{-2}. This result should be compared with those of EerNisse (1971a,b), who found a stress plateau above a certain dose. The differences between these two results are probably because EerNisse's method measures the stress in the as-implanted material, whereas Gerward's method can only measure stress in crystalline material produced by post-implantation annealing. Models for the stress behaviour in annealed material such as that proposed by Alstrup (1979) involve slip at the boundary between amorphous and crystalline layers at high doses. Alstrup's method, Pendellösung topography, is an X-ray method of measuring the curvature of specimen surfaces, and so can evaluate stresses in amorphised material.

Ion implantation into magnetic bubble device materials is used to introduce stress states which improve device performance [North et al. (1978)]. Accordingly, workers have measured the stresses produced by implantation, generally at low, non-amorphising doses up to $\sim 10^{15}$ions cm^{-2}. At higher doses, the amorphous or microcrystalline surface layer produced is magnetically inactive [Komenou et al. (1978)]. In the low dose range, strain is found to be proportional to dose [MacNeal and Speriosu (1981)], [Strocka et al. (1980)], [deRoode and Smits (1981)]. In all cases, X-ray techniques were used; the strains measured were up to 1%.

iii) Other Methods of Detecting Surface Stresses

The expansion of diamond with B^+ implantation has been investigated by Maby et al. (1981), who measured the step height between implanted and unimplanted regions using a Talysurf machine. Linear expansion with dose was found over the dose range 10^{15}-10^{16}ions cm^{-2}. The authors attributed the expansion to a partial conversion to graphite, though no microstructural evidence was produced. Gerward (1978) reported similar step height measurements for implanted silicon. McHargue and Williams (1982) have reported volume increases in silicon carbide implanted with chromium ions, also using the method of measuring surface step heights. The volume increase was estimated to be ~30% at a dose of ~10^{16}ions cm^{-2}.

Jensen et al. (1976) showed the existence of tensile surface stresses in proton-implanted silica glass, by a difference in the median/radial crack lengths as measured at the surface. An extension in crack length of 25% was observed at a dose of $10^{15}H^+cm^{-2}$, the effect decreasing at higher doses. This result should be compared with those for the brittle solids investigated here, (see chapter 5), where no such changes in crack length were observed.

2.2.4 Surface Sputtering

Sputtering is the ejection of atoms from a solid by an ion beam. Use can be made of such processes, eg. in the production of thin foils for TEM from otherwise difficult materials, such as those which are chemically inert, are inhomogeneous in structure, etc. (see 4.6). In the processes considered here, sputtering limits the extent to which a solid can be implanted as an equilibrium is reached between gain of dopant by implantation and its loss by doping (see 5.1.2) [Carter et al. (1978)], [Liau and Mayer (1978)].

The sputtered atoms are those which gain enough of an incident ion's energy, either directly or indirectly, to reach the target's surface and escape from it. Energy can be tranferred by either thermal or elastic

mechanisms (see 2.1.1). The sputtering yield, ie. the number of ejected atoms per incident ion, is a complicated function of ion energy, ion incident angle, and target crystallography and composition [Smith et al. (1981)], [Kang et al. (1979)]. The theory of sputtering is not very well advanced.

For most materials, the sputtering yield is relatively insensitive to process variables, and generally lies between 1 and 10 [Liau and Mayer (1978)], being normally less than 5 for ions of keV energy [Carter and Grant (1976) p4]. Sputtered surfaces tend to be roughened, because of the variation in yield with angle and crystallography; in extreme cases, cones can develop on an originally flat surface [eg. Smith et al. (1981)].

2.3 Ion Implantation for Corrosion Protection, etc.

This section and section 2.4 briefly review the recent 'unconventional' applications found for ion-implanted materials, ie. applications outside the fields of semiconductor doping and radiation damage studies.

During the last decade, interest has grown in studying the surface metallurgy of implanted materials. In particular, an increasing number of papers have been concerned with the corrosion and oxidation properties of implanted solids. Large and commercially advantageous changes in behaviour have been produced by applications of high ion doses ($\gtrsim 10^{16}$ ions cm^{-2}). Several reviews, often covering a wide range of engineering applications of implanted materials, have appeared, eg. Ashworth et al. (1976), Dearnaley and Hartley (1977), Hartley (1978), Dearnaley (1978a), Dearnaley (1978b), Hirvonen (1978), Dearnaley (1981a), Dearnaley (1981b), Dearnaley (1982).

2.3.1 Dry Oxidation

This aspect of the effects of ion implantation on the surface chemical behaviour of solids has been recently reviewed by Dearnaley (1981b). The development of studies in this area is viewed as starting by trial-and-error methods, where ion/substrate combinations were chosen almost randomly, and progressing to an approach based on a better, but still partial, understanding of the mechanisms involved. Such mechanisms include:

i) Implanted elements helping to form a cohesive oxide film;

ii) Blocking of easy diffusion paths (eg. grain boundaries, dislocations);

iii) Catalytic effects;

iv) Alteration of oxide plasticity, so changing the likelihood of flaking;

v) Modification of oxide conductivity.

A large number of papers in this area have been given at the International Conferences on Ion Implantation (1970), (1971), 1972), (1974), (1976), and the conferences 'Applications of Ion Beams to Materials 1975' (1976) and 'Ion Implantation into Metals' (1982). At the 3rd (1972) conference, Dearnaley et al. (p405) reported changes in the oxidation rates of stainless steel and chromium induced by implantation. Results were found to depend on the electronegativity of the ion species, the effects being in opposite directions in the two substrates (low electronegativity ions were found to inhibit the oxidation of Ti, and high electronegativity ions to increase it). In contrast, the results of Bentini et al. (1980) on the oxidation of implanted zinc indicated that the size of the implanted ion is the important factor (possibly by altering oxide plasticity). Anttila et al. (3rd conf. (1972) p415) investigated the corrosion-rate improvement of stainless steel by yttrium implantation. The effects of implantation on the oxidation of copper have been investigated by Naquib et al. (1976) and Morris et al. (1978); improvements were noted for implantations of B^+ and Ti^+. At the 1975 conference, Muhle et al. (p147) and Goode (p154) reported changes in the oxidation rates of nickel and chromium, respectively, finding that ionic size and electronegativity were the factors

controlling the direction and size of the changes. At the 1981 conference (published 1982), one session of ten papers was devoted to the effects of implantation on the high temperature oxidation of iron, stainless steels and nickel and its alloys; significant improvements were claimed in all cases.

All the above papers deal with the oxidation of metal substrates; however, the work of Ramin et al. (1980) indicates that Si_3N_4 formed in Si by implantation (see 2.2.2) has better oxidation resistance than CVD Si_3N_4. This is possibly because of the different stress states in these two different forms; CVD Si_3N_4 is normally in a state of tension, whereas the implantation-produced material is compressed (see 2.2.3).

2.3.2 Wet Corrosion

The first significant study in this area was that of Ashworth et al. (3rd conf. (1972) p443). The effects of neutral (Ar^+) and active (B^+, Fe^+, Mo^+) ions on the wet corrosion of copper, aluminium and iron were investigated; significant changes in passivation behaviour were found for all ion/substrate combinations. It was suggested that these changes were due to displacement damage in the surface layer, rather than to any chemical effect of the implanted ions. This conclusion was reinforced by the work of Pankove et al. (1981), who investigated, by Auger analysis, the oxide layers produced on implanted aluminium. They found no differences between the oxide layers on implanted and unimplanted substrates; in particular, the possiblity of the changes being due to recoil-implanted carbon contaminants was eliminated. The polarisation characteristics of various implanted materials have been investigated by Wolf (1980). For a given substrate, he found that the identity of the ion chosen made no difference to the polarisation curve, though implanted materials behaved differently to unimplanted materials.

More recent work has concentrated on implanting with ion species known to improve the corrosion properties of metals when incorporated into bulk alloys, in particular Cr^+ and Ni^+ into iron and steels. Such

implantation treatments, not suprisingly, produce surfaces resistant to corrosion. Ashworth et al. (4th conf. (1974) p367) found that the corrosion performances of Cr^+ implanted iron alloys were similar to those of such alloys conventionally produced. Improvements were also found to be produced by implantation of Ta^+, where conventional methods cannot produce an equivalent alloy [Ashworth et al. (1977)]. Similar studies in the implantation of iron and steels for corrosion resistance include the use of: phosphorus [Clayton et al. (1980)], which can be deleterious to mechanical properties if used in bulk; lead [Ashworth et al. (1978)], impossible to alloy conventionally with iron; chromium and nickel [Sartwell (1978)], [Wang et al. (1979)]. The 1981 conference (published 1982) included twelve papers on the influence of ion implantation on wet corrosion, varying from the surface production of conventional alloys (eg. Cr^+ into iron) to alloys otherwise impossible to produce (eg. Cl^+ into aluminium and stainless steel).

2.3.3 Other Non-mechanical Applications of Ion-implanted Alloys

Some of these applications have been mentioned briefly in the appropriate part of section 2.2. In many cases, only a little preliminary research has been published:

i) Phase diagram determination (see 2.2.2); annealing from the metastable implanted state can give otherwise unobtainable information about phase field boundaries [Myers (1978)], [Smugeresky and Myers (1978)].

ii) Diffusion kinetics studies; the radiation damage introduced by ion implantation can enhance diffusion, and the diffusional kinetics of the substrate and impurity atoms can be studied under these conditions [Poate and Siedel, 3rd conf. (1973) p317], [Myers et al. 3rd conf. (1973) p455]. Most of such studies have been carried out on semiconductor materials.

iii) Improvement of magnetic bubble device performance; the strain induced by implantation (see 2.2.3) can favourably affect the directionality of the magnetic field at the surface [Komenou et al. (1978)], [MacNeal and Speriosu (1981)]

iv) Integrated optics; changes in atomic volume (see 2.2.3) can alter

the refractive index of the substrate or produce optically absorbing layers. These effects could have applications in the development of integrated optical devices [Townsend (1977)], [Bagley and Townsend, 2nd conf. (1971) p575].

v) Superconductivity research; raising of the critical temperature for superconductivity by implantation has been found for aluminium [Meyer, 4th conf. (1974) p309]. Large ions with a high electronegativity were found to be the most effective. Linker and Meyer (4th conf. (1974) p301) found that for vanadium, niobium and tantalum, the critical temperature was only decreased by implantation.

vi) Crystallisation of glasses; glass ceramics can be produced on the surface of silica glass by implantation with Li^+ions, and on lithia-silica glasses by neutral ion implantation [Arnold (1975)], [Arnold and Peercy (1980)], [Arnold (1980)]. This could have beneficial effects on their surface mechanical properties.

2.4 Mechanical Properties of Implanted Surfaces

Work in this area began to be published in the early 1970's [eg. Hartley et al. (1973)], slightly after interest in the chemical properties of implanted surfaces developed (see 2.3). Effects of implantation on most of the near-surface mechanical properties of materials have been examined to some extent, eg.

i) Friction [Hartley et al. (1973)];
ii) Wear rates [Hartley (1975b)];
iii) Adhesion [Roy Chowdhury et al. (1980)];
iv) Low-cycle fatigue (LCF) [Sleeswyk et al. (1980)];
v) High-cycle fatigue (HCF) [Hu, Clayton et al. (1980)];
vi) Microhardness [Kant et al. (1979)].

However, the literature is sparse and consists, to a large extent, of preliminary results. Such results have been almost exclusively concerned with property changes in metals, especially steels, and so complement, rather than supplement, the results presented in chapter 5. Generally, authors have simply presented experimental results, and have not proposed other than tentative mechanisms for the implantation-induced property

changes they observe.

Several general reviews of the use of implantation for the modification of surface mechanical properties have been published, notably by Dearnaley (1978a), (1978b), (1980b), Hartley (1979a) and Hirvonen (1978). These reviews stressed the importance of industrial applications of implanted surfaces; some case studies have been presented by Dearnaley and Delves (1980), Delves (1982) and Hartley (1979b). The review here concentrates on specific quantitative results drawn from the above and similar reviews and from more specialised papers.

2.4.1 Adhesion between Implanted Surfaces

Roy Chowdhury et al. (1980) investigated the effects of nitrogen implantation on the adhesion energies of titanium surfaces. The apparatus used measured the force between a fine titanium probe (unimplanted) and a flat surface (implanted or unimplanted). For unimplanted surfaces, adhesion energies of ~0.45 Jm^{-2} were found; after implantation of the flat surface to $2x10^{17} N_2^+ cm^{-2}$ at 200kV, the adhesion energy decreased to ~0.15 Jm^{-2}. It was speculated that such adhesion energy reductions, if applicable to steels, etc., might help to account for the lower wear rates of such metals after implantation.

2.4.2 Ultra-microhardness Tests

This type of test uses apparatus similar to that for the adhesion experiments described above, but uses loads high enough to cause plastic deformation of the surface. In the experiments performed by Pethica (1982) and Newey et al. (1982), specially-profiled diamond indenters were used, loaded by a capacitative method. The penetration depth and the force applied were continously measured. Depth resolution of ~2.5nm and load sensitivity of ~10μN were claimed. At such low loads, microhardness varies strongly with depth (see 3.1.2), and so care must be taken that tests on different surfaces are comparable. In particular, the surface preparation

state is important.

Newey et al. (1982) studied the effects of 300kV N_2^+ implantation on electropolished iron, and found significant hardness increases. However, a dose of 10^{17} ions cm^{-2} was found to have a large effect, and higher doses up to $6x10^{17} N_2^+$ cm^{-2} had progressively smaller effect on the hardness. Pin-on-disc wear tests were also performed, and a positive correlation was found between hardness and wear resistance. The implantation of titanium into steel was also found to produce a hardness increase at dose levels of $\sim 4x10^{17} N_2^+$ cm^{-2}.

Pethica (1982) tested a wide variety of materials (Cr, Au, W, WC-Co, steels), using nitrogen implantation. The results on some materials (Au, Cr, steels) were variable and depended strongly on the surface preparation. Pethica did, however, find that WC-Co was softened by N_2^+ implantation to doses greater than $\sim 10^{17} cm^{-2}$ (see 5.3). He was unable to distinguish between results from the two phases present, but as the composite was only 6% Co, it is clear that the carbide phase at least is softened by such implantation.

2.4.3 Microhardness Tests

Relatively few workers have reported results from microhardness tests on implanted surfaces. Early results have been summarised by Hirvonen (1978); the review also includes some 'scratch hardness' results. Hardening was found in iron, steel and beryllium substrates implanted with nitrogen or carbon, and attributed to carbide or nitride formation at high beam fluxes (and therefore temperatures) or to point-defect dislocation pinning at low temperatures. One often-quoted result is that of Kanaya et al. (1972), where an increase in hardness from 300 to 400 $kgmm^{-2}$ was found at a dose of $\sim 10^{17}$ nitrogen ions cm^{-2}. No experimental details are given of the testing procedure, in particular the loads used in the microhardness tests; however the hardening effect appears to be strong and consistent with results reviewed by Hirvonen (1978).

More recent implantation/microhardness tests on metals include those of Evdokimov and Fischer (1980), who used a recoil technique, with argon ions mixing a nickel coating into the surface of mild steel. They found a large increase in the microhardness (at 5 and 10g) in the nickel-implanted region, where the nickel concentration was ~1-10%, and only a small change in the microhardness in the region implanted with argon alone. It was estimated that the nickel was concentrated within 2nm of the surface, though any diffusion would increase the layer thickness; the indentations were several microns deep, so the hardness changes in the implanted layer must be very large to be detectable by this technique. Suri et al. (1979) have also studied microhardness changes in steels after implantation, in this case of nitrogen and boron at doses up to $10^{17}cm^{-2}$, using low loads (15g). The unimplanted steel had a (Knoop) hardness of ~300 $kgmm^{-2}$; implantation with boron and nitrogen increased the hardness to 410 and 630 $kgmm^{-2}$, respectively.

Suri et al. (1979) also reported implantation-induced changes in the microhardness of aluminium and titanium. The hardness of both metals was slightly increased by implantation with nitrogen or boron. The effect of boron implantation on the microhardness of beryllium (for gas bearing applications) has been investigated by Kant et al. (1979). At doses of $1-2x10^{17}cm^{-2}$, large increases in low-load (5 and 10g) hardness were found, particularly after annealing. Backscattering analysis showed that beryllium boride particles were present. Copper was also reported to be hardened by boron implantation.

In addition to these 'direct' microhardness tests, the surface hardness of metals has been quantitatively inferred from wear rate data by Singer and Bolster (1980), Singer et al. (1980) and Dubovitskaya et al. (1979). Implantation of steel with nitrogen or titanium to doses greater than $\sim10^{17}cm^{-2}$ was found to increase the hardness [Singer and Bolster (1980)], as did implantation of chromium and iron with nitrogen.

It can be seen from the above that the data on implantation-induced hardness changes in metals are sparse and have concentrated on a few ion/substrate combinations of immediate technological interest. The

reported hardness increases, after implantation with both light and heavy ions, appear to result from the formation of dislocation-pinning precipitates.

Very little data exist on the microhardness of implanted non-metallic materials. Hu and Schwenker (1978) found that implantation of silicon with boron, oxgen, arsenic or nitrogen up to doses of 10^{16} cm^{-2} reduced dislocation motion, as revealed by an indentation etch-pitting technique. The authors considered this to be due to an increase in Peierls stress from implantation displacement damage and/or to the pinning of dislocations by clusters of implanted atoms. These results should be compared with those in section 5.2.2, where silicon was found to be softened by nitrogen implantation. However, Hu and Schwenker performed their indentations at 600°C (indentations in ~~this~~ the current study were all made at room temp.), and the softening effect found in section 5.2.2 occurred at doses greater than ~$4 \times 10^{17} N_2^+$ cm^{-2}. McHargue and Williams (1982) found that the Knoop microhardness of SiC was reduced by 20-40% after implantation with chromium in the dose range 10^{14}-10^{16} ions cm^{-2}. They also measured the values of K_{Ic} by an indentation technique (not specified) and found slight increases (~10%) after implantation.

Hauser et al. (1977) found that self-ion implantation in diamond produced a softer, electrically conducting, surface layer, probably due to surface graphitisation.

2.4.4 Friction and Wear Tests on Implanted Materials

Most mechanical property tests on implanted materials have been of this type, because of the technological importance of wear-resistant surfaces. Most studies have been fairly empirical, reporting behaviour changes only, though sometimes qualitative mechanisms are tentatively suggested; this is not surprising in view of the complexity of friction and wear phenomena (see 3.4).

Almost all results reported have been for implanted steels and cemented carbides. The results for the cemented carbides are reviewed in section 5.3.2. It is found that implantation to doses greater than $\sim 10^{17} cm^{-2}$ produces greatly extended wear lifetimes (up to ~5x normal) in both controlled laboratory tests and industrial components subjected to wear. The results for steels, where reductions in both the wear rates and friction coefficients have been achieved by various implantation techniques, are reviewed here. Many results are based on in-service testing of components. For both types of material, it was found that implantation produced significant wear rate improvements only at low wear rates, and that implanted and unimplanted materials behaved identically in 'accelerated wear' tests. This is not surprising, as mechanisms of rapid wear (see 3.4) would tend to act on thicknesses of material much greater than the implanted depth (eg. 'ploughing' type abrasive wear), whereas mild wear mechanisms involve very near surface processes.

The earliest report of the application of implantation in this field was by Hartley et al. (1973). Various ions were implanted into EN352 steel, and the friction coefficient measured by sliding a loaded WC-Co ball across the surface. Doses of 10^{16}-10^{17} ions cm^{-2} were used, and friction measured under both lubricated and unlubricated conditions. For all the ion species used (Kr,Sn,In,Ag,Pb,Mo,S,Mo+2S), changes in the unlubricated coefficient of friction were found, with the greatest increase in friction (45%) for lead implantation, and the greatest decrease (350%) for tin. Results under lubricated conditions were more variable, and smaller changes in friction coefficient were found. (These results are in contrast to those of Suri et al. (1979) who found greater changes in friction coefficient under lubricated conditions.)

Later studies by the same group [Hartley (1975b)] extended the range of ions used in the low-speed friction tests and concluded, from the lack of effects from the implantation of inert gas ions, that displacement damage alone had negligible effect on friction. The tests performed also included pin-on-disc tests and the implantation of light ions (eg. nitrogen and boron). The light ions were found to be very effective in reducing both friction and wear in a variety of steels. Following these

results, and possibly also because of the comparative ease of implanting nitrogen, a good deal of later work has concentrated on the effects of nitrogen implantation into steel (eg. Varjoranta et al. (1981), LoRusso et al. (1979), Singer et al. (1980), Hirvonen et al. (1979), Hirvonen et al. (1980), Hale et al. (1982), Herman (1982), Singer and Bolster (1980)). It was also found that titanium implantation was effective in reducing wear in steels [Singer et al. (1980)]. This was attributed to the presence of a fine TiC precipitate distribution, the carbon being either that already present in the steel, or recoil-implanted carbon contaminant. Similar effects were achieved by simultaneous implantation of Ti and C [Carossella et al. (1980)]. Wear rate reductions due to carbide formation were also found in cobalt-implanted steels, but not in chromium- or nickel-implanted steels [Hirvonen et al. (1979)].

The mechanisms by which implantation of the light ions boron, carbon and nitrogen might alter the wear rates of steels were less clear. It was found [Dearnaley and Hartley (1978)] that this type of treatment was effective in many types of steel, reducing wear rates by factors of up to 200x, and that such treatments were effective even when depths much greater than the implanted layer thickness were worn away. It was proposed that this was due to the implanted 'interstitial' ions forming Cottrell atmospheres around dislocations, and thus both pinning the dislocations and following them into the substrate during the wearing process. Mössbauer studies [Longworth and Hartley (1978)] showed that the implanted nitrogen was only weakly bound to iron atoms, and mostly not in the form of precipitates, thus reinforcing this conclusion. These mechanisms have been reviewed by Hartley (1979a) and Dearnaley (1980b).

Often reference is made to the operative wear mechanism being 'adhesive' or 'abrasive' (see 3.4.2) (eg. Hartley (1978), (1979b), Singer et al. (1980), Singer and Bolster (1980)), but as all the proposed mechanisms for wear rate reduction depend on an implantation-induced surface hardening it is clear that truly abrasive ('brittle') wear is not being considered and that in steels it is surface plastic flow that is the dominant deformation process during wear [eg. Suri et al. (1979)]. Dearnaley (1982) suggests that in some cases a correlation exists between

wear resistance and oxidation resistance, based on work involving the implantation of rare earth ions into iron alloys. This is possibly connected with the observation that 'mild wear' is controlled by oxide formation and removal (see 3.4.2). The effects of nitrogen implantation into steel on its wear properties have made the process industrially attractive and preliminary in-service tests are being performed (eg. Dearnaley (1978b), Hartley (1978), Dearnaley and Delves (1980), and the reviews noted in the introduction to section 2.4).

Investigations of the wear properties of implanted non-ferrous metals are scarce. However, results for the implantation of copper, aluminium and gold are reported by Hartley (1979a). Here, under abrasive conditions (pin-on-disc with grit in the lubricant) a wear rate improvement was reported for boron implantation into copper, correlating with a hardness increase. Dearnaley (1981d) has reported large reductions of the wear rate of chromium plating on steel by implantation with nitrogen to a dose of $4 \times 10^{17} N_2^+ \text{ cm}^{-2}$, using pin-on-disc testing with silica suspended in the lubricant. Suri et al. (1979) have investigated the wear behaviour of boron and nitrogen implanted titanium and aluminium, under both adhesive and abrasive wear conditions. Under adhesive wear conditions, only nitrogen-implanted aluminium showed any improvement over the unimplanted material, while under abrasive conditions, boron-implanted aluminium showed a slight reduction in wear rate, and boron-implanted titanium a 400% wear rate reduction.

In summary, several workers have found changes in the friction and wear behaviour of steels and other metals after implantation. Whatever the wear conditions, it seems that any wear rate reduction (and perhaps friction reduction) is related to a surface hardening. This may be via either production of fine precipitates [eg. Singer et al. (1980)] or by solute pinning of dislocations [eg. Dearnaley and Hartley (1978)]. The latter mechanism, especially with light implanted ions (eg. nitrogen, boron or carbon), could account for the observations of long term improvement of wear life [eg. Dearnaley (1978b)]. Surface adhesion changes, as reported in section 2.4.1, might also be significant in determining the friction and wear properties of implanted surfaces, but no correlatory experiments in

this area have yet been performed.

Experiments on the friction and wear properties of implanted non-metals have mostly been confined to tests of the technologically important WC-Co cemented carbides, where nitrogen implantation has been found to produce significant improvements in wear lifetimes. These experiments are detailed in section 5.3.2. Hirvonen (1981) has reported results from diamond stylus wear tests on titanium-implanted silicon nitride very similar to those reported for nitrogen-implanted REFEL in section 5.1.5. McHargue and Williams (1982) have reported similar results for silicon carbide implanted with chromium to a dose of $\sim 6 \times 10^{15}$ ions cm^{-2}. These changes, involving reduction in near-track chipping fracture, are possibly due to the surface stresses introduced by implantation, as discussed in section 5.1.8. Hartley (1982) has found that implantation of diamond styli with boron or nitrogen, though not with carbon, to doses of 10^{15}-10^{16} cm^{-2}, can improve wear life by up to 500%. Hartley speculated that these improvements, at least for the nitrogen implanted diamond, might be due to the simulation of nitrogen-containing type 1A natural diamond, which is known to have superior mechanical properties.

2.4.5 Fatigue Behaviour of Implanted Surfaces

As ion implantation had been shown to alter dislocation mobility near the surface (surface hardness; see 2.4.2, 2.4.3) and to produce compressive stresses into the surface (see 2.2.3), the possible applicability of implantation treatments to the fatigue properties of metals (see 3.3) became apparent. The fatigue lifetime for high-cycle fatigue (HCF: stresses lower than the bulk yield stress) is dependent largely on the initiation of surface cracks by plastic processes.

Preliminary results were reported in several review papers in 1975-79 (eg. Hirvonen (1978), Dearnaley and Hartley (1978), Dearnaley (1978b) (steels) and Hirvonen et al. (1979) (titanium)). The materials were in all cases implanted with light interstitial ions, to doses greater than $\sim 10^{17}$ ions cm^{-2}. In all cases, large extensions of the HCF lifetime

this area have yet been performed.

Experiments on the friction and wear properties of implanted non-metals have mostly been confined to tests of the technologically important WC-Co cemented carbides, where nitrogen implantation has been found to produce significant improvements in wear lifetimes. These experiments are detailed in section 5.3.2. Hirvonen (1981) has reported results from diamond stylus wear tests on titanium-implanted silicon nitride very similar to those reported for nitrogen-implanted REFEL in section 5.1.5. McHargue and Williams (1982) have reported similar results for silicon carbide implanted with chromium to a dose of $\sim 6 \times 10^{15}$ ions cm^{-2}. These changes, involving reduction in near-track chipping fracture, are possibly due to the surface stresses introduced by implantation, as discussed in section 5.1.8. Hartley (1982) has found that implantation of diamond styli with boron or nitrogen, though not with carbon, to doses of 10^{15}-10^{16} cm^{-2}, can improve wear life by up to 500%. Hartley speculated that these improvements, at least for the nitrogen implanted diamond, might be due to the simulation of nitrogen-containing type 1A natural diamond, which is known to have superior mechanical properties.

2.4.5 Fatigue Behaviour of Implanted Surfaces

As ion implantation had been shown to alter dislocation mobility near the surface (surface hardness; see 2.4.2, 2.4.3) and to produce compressive stresses into the surface (see 2.2.3), the possible applicability of implantation treatments to the fatigue properties of metals (see 3.3) became apparent. The fatigue lifetime for high-cycle fatigue (HCF: stresses lower than the bulk yield stress) is dependent largely on the initiation of surface cracks by plastic processes.

Preliminary results were reported in several review papers in 1975-79 (eg. Hirvonen (1978), Dearnaley and Hartley (1978), Dearnaley (1978b) (steels) and Hirvonen et al. (1979) (titanium)). The materials were in all cases implanted with light interstitial ions, to doses greater than $\sim 10^{17}$ ions cm^{-2}. In all cases, large extensions of the HCF lifetime

were found, up to 100x in the case of the steels (after ageing treatments). It was noted for the steel specimens that the implanted specimens became hot during testing [Dearnaley (1978b), Dearnaley and Hartley (1978)], indicative of the large amounts of energy being ~~absorbed~~ dissipated, rather than stored, ~~in non-elastic processes~~ in the crack initiation stage. Microscopical examination of the steels [Hirvonen (1978)] and the Ti alloys [Hirvonen et al. (1979)] showed fine (~10nm) precipitates to be present in the implanted layers, which probably act as dislocation pinning centres.

Further investigations were carried out on steels by Hu, Herman et al. (1980), Hu, Clayton et al. (1980), LoRusso et al. (1980), White and Dearnaley (1980) and Bakru et al. (1981). It was found by Hu, Herman et al, Hu, Clayton et al. and LoRusso et al. that the greatest HCF lifetime extensions for nitrogen-implanted steels were obtained after ageing treatments, and it was suggested by White and Dearnaley that ion beam heating could induce such ageing during the implantation process. Investigation of the dose dependence of the effect [LoRusso et al. (1980)] showed that at high doses (greater than $4 \times 10^{17} N_2^+$ cm^{-2}) the treatment was ineffective, though no explanation was proposed. Microstructural studies and internal friction measurements on fatigue-life-enhanced steels [Hu, Clayton et al. (1980)] showed that although nitrides were formed, nitrogen also formed 'Cottrell atmospheres' around dislocations, and it was proposed that this latter effect controlled the surface plasticity and hence the fatigue crack nucleation. This would also account for the effectiveness of ageing treatments, and correlates well with the proposed mechanisms for the wear resistance of nitrogen-implanted steels (see 2.4.4). Study of implanted and fatigued surfaces [Bakru et al. (1981)] showed that persistant slip band formation was also strongly suppressed, which also fits in with this theory.

White and Dearnaley (1980) extended the laboratory fatigue tests above to the industrially important case of rolling contact fatigue in ball bearings. Using a dose of $3 \times 10^{17} N_2^+$ cm^{-2}, a moderate increase in fatigue life (~3x) was reported, even though the ball bearings were not implanted over the whole surface.

Recent work on the effects of implantation on the fatigue life of non-ferrous metals has concentrated on copper, eg. Kujore et al. (1980), Chakrabortty, Spooner and Starke (1980), Chakrabortty, Kujore and Starke (1980), Burr et al. (1980), Sleeswyk et al. (1980), Bakru et al. (1981) and Heydari et al. (1982). A correlation was found between the the extension or reduction of fatigue life and the assumed compressive or tensile nature of the implantation-induced surface stresses [Chakrabortty, Kujore and Starke (1980)], [Bakru et al. (1981)]. In particular, aluminium implantation was found to be effective in increasing HCF lifetimes; surface slip was observed to be more homogeneous, retarding the formation of persistant slip bands. This was also found to improve the low-cycle fatigue life (where stresses are above the bulk yield stress) in copper; this result contrasts with those of Sleeswyk et al. (1980), who found that carbon implantation shortened the LCF life of copper and stainless steel. These authors proposed that surface stresses (assumed to be compressive) might aid surface rumpling and so reduce fatigue life. The actual effect of the surface stresses is therefore in some doubt, at least for low-cycle fatigue; however, these may not be the only effects of implantation operating. Evidence for any particular mechanism for fatigue life alteration in ion implanted copper is, so far, scarce.

CHAPTER 3

REVIEW: SURFACE MECHANICAL PROPERTIES

3.1 Surface and Indentation Plasticity

3.1.1 Plastic Flow

Permanent deformation of materials can be accomplished by a variety of mechanisms, depending principally on the material, temperature, strain rate and the magnitudes and geometry of the applied stresses. The major mechanisms for crystalline materials have been reviewed by Frost and Ashby (1982) and comprise:

i) Dislocation glide controlled by structure resistance (Peierls-Nabarro force);

ii) Dislocation glide controlled by obstacles;

iii) Power-law creep;

iv) Diffusional flow;

v) Dynamic recrystallisation.

At the low temperatures of the tests used in this study only the first two mechanisms are relevant. Non-crystalline materials can deform by other mechanisms as yet incompletely understood (see 5.4), in which shear deformation is concentrated in highly localised and heavily strained 'shear bands'. In hardness tests (see 3.1.2), hydrostatic and shear stresses are transiently extremely high, and 'exotic' yield mechanisms can operate, particularly in materials of high yield stress. Such mechanisms include:

twinning, phase transitions (see 5.1.7), block shear and crowdionic diffusion [Sargent (1979)], [Sawyer et al. (1980)].

The materials used in this study cover a very wide range of mechanical properties, from covalently bonded hard brittle ceramics (Si, SiC) to a tough, plastic metal (Co). Given the experimental conditions used in this study, the materials can be classified by which of the above-mentioned deformation mechanisms control their plastic behaviour. Such a classification then divides the experimental materials into four groups:

i) Those where the Peierls-Nabarro force controls dislocation movement, eg. silicon and the silicon carbide materials [Davidge (1979) p65]. In such materials, dislocations move by the formation and propagation of kinks, generally requiring relatively high shear stresses at low (ie. room) temperatures [eg. Alexander and Haasen (1968)]. Unless crack nuclei are absent or of subcritical size (see 3.2), such materials tend to fracture before substantial bulk plastic flow occurs, except where large compressive hydrostatic pressures suppress such fracture - as in the quasistatic and moving single point contacts that are the basis of this study. The nucleation and motion of the kinks are controlled by the electronic band structure of the material [Alexander and Haasen (1968)], [Hirsch (1979),(1981)], [Westwood and MacMillan (1973)]. Ion implantation could therefore modify the flow behaviour of this type of material by modification of the band structure, either by doping effects, by structural changes (amorphisation) or by altering the electrochemical potentials near the surface. Such mechanisms may act either to promote or restrict plastic flow. Flow in these materials may also be affected by the presence of phase or grain boundaries, as in REFEL, which can act as barriers to dislocation motion. It is possible that implantation could produce precipitate distributions (in these normally fairly homogeneous materials) that could restrict dislocation motion, but it appears from the results in section 5.1 and 5.2 that this is not the case here, at least for low-temperature implantations. In addition, displacement damage alone could inhibit dislocation motion. At low doses, displaced atoms would produce local strain centres that could pin dislocations. At high doses,

the amorphous or microcrystalline materials produced (see 2.2.1) would be unlikely to have the same flow properties as their crystalline counterparts.

ii) Ionic materials, where flow is by dislocation motion, usually controlled by the density of localised charged defects (eg. 'colour centres'). The Peierls-Nabarro force in these materials tends to be lower than in the covalent solids ((i) above), as the bonding is less directional. However, dislocation cores, particularly kink and jog sites, have associated electrical charges, and these can interact strongly with charged defects (vacancies, dissolved ions, or more complex entities) and become pinned [eg. Davidge (1979) p68]. Lithium fluoride (see 5.5) is typical of this type of material, and implantation might be expected to alter plastic flow behaviour by introduction of charged defects if the implanted species is of a different valency from the substrate atoms. For this to occur, the temperature must be high enough for diffusion (enhanced by displacement damage) to incorporate the implanted ions into the structure of the substrate. At lower temperatures, displacement damage disruption of the structure may interfere with dislocation motion, as above. Also, displacement damage, when combined with radiation damage that produces ionisation (eg. X-irradiation) could produce large numbers of charged colour centres (see 5.5.3).

iii) Metals, which have low Peierls-Nabarro stresses, because of the non-localised nature of their bonding and the lack of charge effects. Dislocation motion is limited by interactions with local stress fields and with phase or grain boundaries (ie. 'obstacle controlled' in Frost and Ashby's classification). The various effects of implantation would be expected to introduce extra obstacles to dislocation motion, in the forms of dislocation loops, solute atoms, microtwins, precipitates, etc. (in addition, as described in section 2.2.1, some implantations into metals may produce an amorphous surface layer). Implantation would therefore be expected to inhibit dislocation motion, especially if the conditions are such as to produce a fine precipitate distribution (see 2.4). However, if the substrate is already in a highly hardened state (eg. iron-carbon martensite), the displacement damage from the implantation would be

expected to reduce the hardening. The metal tested in this study, cobalt, is exceptional in that it has a very low stacking fault energy, so that dislocations are highly dissociated (see 5.3.6). Thus the metal work-hardens rapidly, as dislocations cannot cross-slip easily. Implantation-induced changes in the stacking fault energy may explain the observed post-implantation softening. Also, the metal can exist in two crystal forms (one metastable) at room temperature, and implantation may affect phase stabilities. Phase transformation could be a yield mechanism during hardness indentation.

iv) Amorphous solids; deformation processes in these materials are not well understood (see 5.4). At low temperatures, both metallic and inorganic glasses deform inhomogeneously in narrow, highly strained, shear bands. It is not clear how implantation might affect the flow processes in these shear bands though, as it is thought that local dilation occurs there, the compressive stress state associated with implantation may cause hardening. In these studies, no such effect was found (see 5.4).

It can therefore be seen that, except where the Peierls-Nabarro stress is high and controls dislocation motion (ie. in single- or large-crystal covalent solids), implantation would generally be expected to harden solids by introduction of obstacles to dislocation motion. This is particularly the case if charged defects can be produced in ionic solids, or fine precipitates in metals. In covalent solids, the influence of implantation on the band structure, via damage or doping, may alter the dislocation mobility, and might generally be expected to increase it [Hirsch (1981)].

Quantitative testing of the plastic properties of a thin near-surface layer is difficult. In this study, microhardness testing was used extensively. The following section reviews the technique. Details of the experimental and analytical procedures used in this study are described in section 4.4.1.

3.1.2 Microhardness Testing

This section draws information mainly from 'The Science of Hardness Testing and its Research Applications' [Westbrook and Conrad (Eds.) (1973)] and 'Factors affecting the Microhardness of Solids' [Sargent (1979)].

Hardness testing involves the making of a permanent, measurable indentation in a material's surface; the pressure required to do this is taken as a measure of the material's 'hardness'. The indenting tools commonly used have a wide variety of geometries, but the commonest are spherical (eg. 'Brinell' and 'Rockwell' hardness) or pyramidal (eg. 'Vickers' and 'Knoop' hardness). In some studies, conical indenters have been used [eg. Weiler (1973)], so that the influence of indenter shape on the result is minimised. Vickers profile indenters were used in all the tests in this study. Hardness values produced by differently shaped indenters are generally only roughly comparable; an analysis by Studman et al. (1977) gives a basis for correlation. Generally, use of loads greater than ~1kg is referred to as macrohardness, or simply hardness, testing, and is common in industrial tests on metals. For work on brittle materials, lower loads must be used in order to avoid gross cracking, which would render the indentations unmeasureable. Low-load testing is also useful in a number of research applications (see 'Science of Hardness Testing etc.'), such as tests on individual grains in metals, following hardness profiles induced by heat treatments, and the tests performed in this study. Tests using loads less than ~1g are not possible without very specialised apparatus, eg. as used by Pethica and by Pollock (see 2.4.2). Microhardness testing, using the load range ~1-~1000g, can be routinely carried out using standard equipment.

Models of the indentation process for non-strain-hardening solids fall into two categories [Sargent (1979)]:

i) Surface-directed displacement models;

ii) Radially-directed displacement models.

The former type of model best describes the behaviour of relatively soft

materials, where the material displaced by the indenter forms a 'pile-up' around the indentation. The application of slip-line field analysis to this situation yields the result:

$$H/Y = C \qquad 3.1.2a$$

[H=hardness, Y=yield stress, C=a constant≃3]

For harder materials (eg. the ceramics used in this study), the radially-directed displacement (RDD) model gives a better fit to experimental data. In this model, the material displaced from the indentation is absorbed as elastic strain in the bulk of the specimen, with a plastically deformed region close to and beneath the indentation preventing full strain relaxation. The geometry of such plastic zones has been investigated in SiC by Lankford and Davidson (1979), who found them to be approximately hemispherical, with radius ≃5x that of the indentation. However, the model of Yoffe (1982) for indentation in hard materials suggests that the plastic zone might be no larger than the indenter in width, and fairly shallow in depth. The results from the cross-sectioned indentations in sections 5.1.4 and 5.2.3 conform to this suggestion. The RDD model has been analysed as being similar to that of a spherical cavity expanding into an elastic body (though Yoffe (1982) has pointed out several defects of this type of model). The results of two analyses, due to Studman et al. and Gerk both yield similar expressions [Sargent (1979)]:

$$H/Y = f(E/Y, \tan(\beta), \nu) \qquad 3.1.2b$$

[E=Young's modulus, β=indenter 1/2 angle, ν=Poisson's ratio]

and the functions are shown graphically in fig. 3.1.2.1. It can therefore be seen that the hardness number for a material is some small multiple (~1-3) of the yield stress.

In both these models, the hardness is assumed to be constant for a given material, independent of testing time, load, etc. For all real materials, it is found that hardness varies with indentation size (ie. applied load) [Sargent (1979)], indenter orientation with respect to specimen crystallography [Brookes et al. (1971)], [Sawyer et al. (1980)], and testing time [Brookes et al. (1975)], [Fairbanks et al. (1982)]. The variation of hardness with orientation has been used to indentify the slip systems active during indentation [Sawyer et al. (1980)], and can be

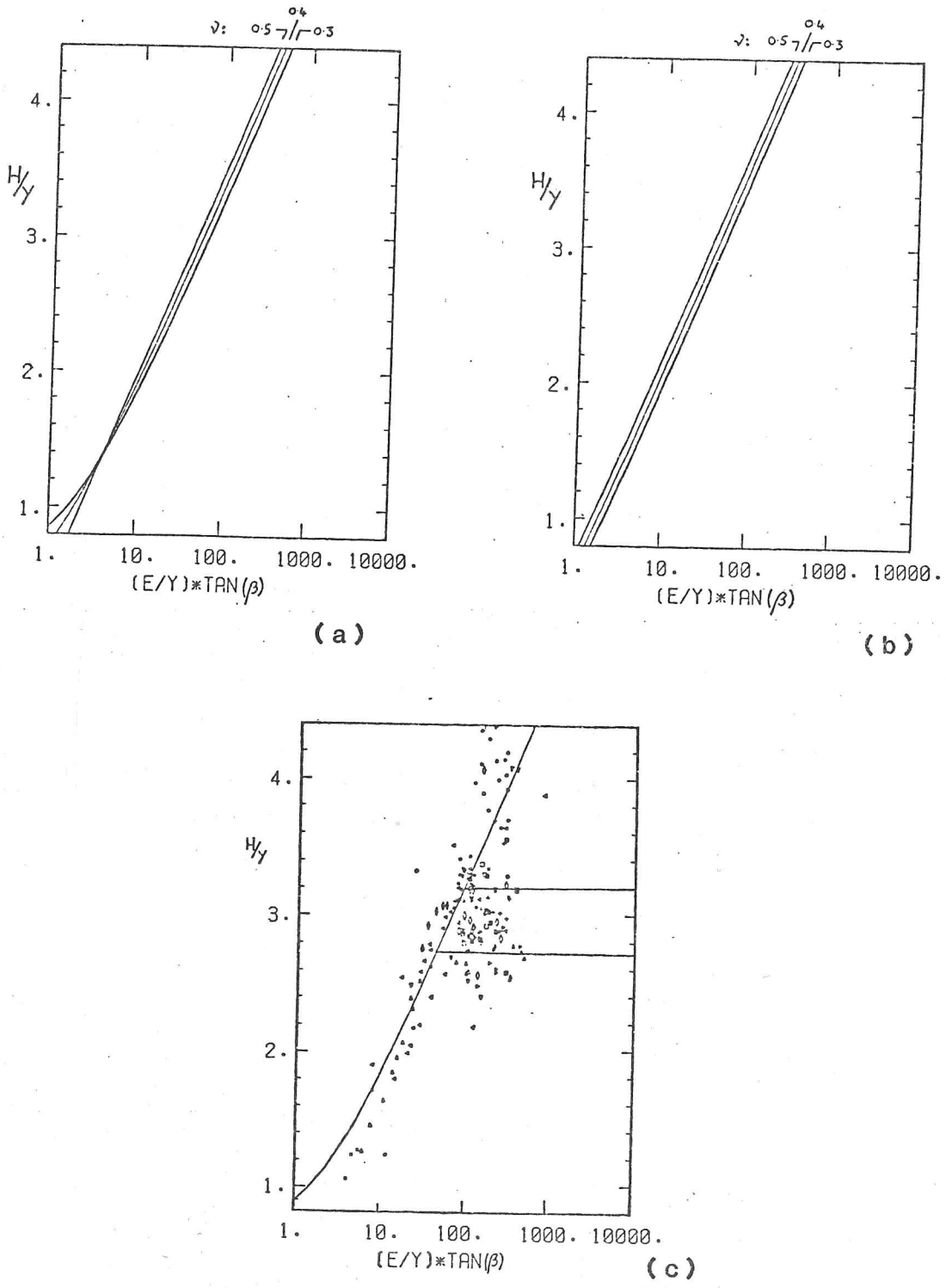

FIG. 3.1.2.1 Computed relationships between hardness, yield strength, Poissons ratio, and elastic modulus, for radially-directed displacement, according to: (a) Studman et al. (b) Gerk. These are compared with some experimental results in (c); the lines are that of the model in (a) with ν=0.3, and those of H/Y=2.75 and 3.2 corresponding to lower and upper bounds for surface-directed displacement models. (From Sargent (1979)).

allowed for in comparative tests on the same material (as here), by keeping to a standard indenter orientation. The effect of loading time variation can also be eliminated by keeping to standard conditions (see 4.4.1). The indentation size effect (ISE), a genuine variation in measured hardness with load, is less accountable and allowable for. There are four basic classes of reasons for this effect, and these have been modelled by Sargent (1979):

i) The existence of surface layers, the mechanical properties of which differ from those of the bulk. Such 'layers' could arise from dislocation image forces at the surface, oxide films, surface charge effects, and, as here, ion implantation.

ii) Microstructure scale effects. Here the grain size, precipitate spacing, etc. give a definite scale to the microstructure, and when the indentation deformation volume becomes smaller than this, the plastic behaviour may alter.

iii) Deformation structure scale effects. As the deformation volume decreases, the average curvature of dislocation loops will tend to increase, and the spacing between slip planes will tend to decrease. Both these scale changes would be expected to result in an increased flow stress.

iv) Work-hardening effects. As indentation size increases, increasing work hardening in the deformation volume would be expected to increase the flow stress. This effect would be strongest in pure annealed metals.

The combination of these effects in a given material in a particular microstructural state give rise to a characteristic and well-defined variation in hardness with indentation size [Sargent (1979)]. The size and direction of such variations can be quantified by an ISE (Meyer) index, as decribed in section 4.4.1. The Meyer index is useful for the comparison of different near-surface microstructural states of the same material, as in this study; if the Meyer index were not used in such comparisons, the normal variation of hardness with indentation size would partially obscure hardness variations due to the presence of an ion-implanted layer.

3.2 Indentation Fracture

At low temperatures, most ceramics fail in service not by plastic flow but by fracture, whether in the bulk or by surface chipping. For such materials, quantification of fracture behaviour is important. The basic methods of so doing are reviewed below.

3.2.1 Fracture Mechanics

The basic approach of fracture mechanics [eg. Lawn and Wilshaw (1975a) chap. 1] is due to Griffith, who in 1920 established the importance of energy balance in crack propagation. A crack would only expand if by so doing it released enough stored elastic energy to compensate for the surface energy increase of the lengthened crack, and any external work done. Depending on the loading geometry, this means that, given a set of stress conditions, there is a critical crack length (c_{crit}), below which a crack will not expand, and above which it will do so. In plane stress:

$$\sigma_f = (2E\gamma/\pi c_{crit})^{1/2} \qquad 3.2.1a$$

[σ=applied tensile stress, E=Young's modulus, γ=surface energy]

This is more usually expressed as:

$$K^2 = GE \qquad 3.2.1b$$

where $G=2\gamma$ + any additional crack extension work) and $K=\sigma(\pi c)^{1/2}$.

The value of K_{Ic}, the critical K (stress intensity) value for crack extension in the 'mode I' geometry (tensile forces normal to the crack plane), is then a measure of the ease of brittle fracture of a material, and is commonly known as the fracture toughness. For brittle materials (eg. SiC, Si, Al_2O_3, etc.), $K_{Ic} \simeq 0.5\text{-}5$ MPam$^{1/2}$; for ductile metals (eg. mild steels), $K_{Ic} \simeq 50\text{-}200$ MPam$^{1/2}$ [Ashby and Jones, (1980) p127].

If it is assumed that for brittle materials, such as Si and SiC, $G=2\gamma$, ie. no plasticity occurs at the crack tip (as Lawn et al. (1980) have shown for silicon), then K_{Ic} can be calculated from estimates of the surface energy, γ. However, surface energies of solids are difficult to calculate or determine directly, and so K_{Ic} is more usually determined

experimentally; for more ductile materials, where $G > 2\gamma$, this is the only possible approach. The surface energy and elastic moduli vary with direction with respect to the structure in crystalline materials, and so K_{Ic} will be to some extent direction dependent. This is apparent in the existence of preferred fracture planes, eg. (0001) in SiC. The fracture properties of each of the materials used in this study are detailed in the appropriate sections of chapter 5.

K_{Ic} is a useful measure of fracture toughness; however, the assumption is made that cracks already exist in the solid or that nucleation of cracks is easy. In practice, for most real brittle solids, cracks or 'psuedo cracks' (eg. grain boundaries, pores, precipitates) are plentiful [eg. Davidge (1979) p75]. Even for homogeneous single crystal material, surfaces normally have a high density of microcracks from handing damage, etc. Griffith performed experiments on flaw-free glass whiskers and showed that such samples only fractured at stresses so high that c_{crit} was of the order of the bond lengths, while introduction of any flaws caused whiskers to fail at much lower stresses [Lawn and Wilshaw (1975a) p12]. Surface flaws can therefore be seen to have great importance in determining the usuable strength of hard brittle materials. The size distribution of surface flaws can be deduced from certain types of indentation experiments, as can values of K_{Ic}; such techniques are described in section 3.2.2.

Even in the absence of pre-existing flaws, microcracks can be nucleated by plasticity mechanisms within a solid (though in hard solids, such mechanisms can only operate at very high shear stresses, notably beneath hardness indentations, and in abrasive wear contacts). Such mechanisms are discussed by, eg. Lawn and Wilshaw (1975a), chap. 2; all basically involve some obstacle to dislocation motion (or shear band propagation), eg. grain boundaries, precipitates or other slip systems. These give rise to dislocation pile-up, where high stresss (and, in some models, the 'wedge' effect of piled-up edge dislocations) initiate fracture. An interesting variant on this is the mechanism observed by Hagan (1980), where cracks formed at the intersection of shear bands in indented silica glass.

Ion implantation could influence such mechanisms either by changing the plastic flow homogeneously (eg. by Cottrell atmospheres around all dislocations) or by providing the barriers to flow which might nucleate cracks (eg. by forming precipitates). At very high doses, the effects of sputtering might be expected to alter the surface flaw distibution. However, in the cases studied here, the main effects of implantation on fracture behaviour appear to be at the propagation, rather than the initiation, stage (see chapter 5).

3.2.2 Indentation Fracture Mechanics

This area of study has recently expanded rapidly, and an extensive body of literature exists. The basic principles have been reviewed by Evans, Lawn, Wilshaw and others, eg. Lawn and Wilshaw (1975b), Lawn and Marshall (1979), Evans (1980). Indentations can be divided into two classes: blunt or 'Hertzian', where deformation is principally elastic, and sharp contacts, where plastic deformation occurs (combined with a surrounding elastic stress field - ie. the radial displacement model in 3.1.2). The stress fields for the two cases are rather different (though they converge at large distances from the indentation), and give rise to different crack geometries, as described below.

i) Blunt Contact

The stress field for this type of contact, as first analysed by Hertz for a spherical indenter, is illustrated in fig. 3.2.2.1. It can be seen that the maximum surface tensile stresses are on the indentation periphery. As the indentation progresses, this maximum stress 'samples' an increasing area, until a flaw of size greater than critical is found; this then grows into a surface 'ring' crack. Further loading propagates the crack down into the solid, along the surface of maximum crack opening stress (σ_{11} in fig. 3.2.2.1), forming a 'cone' crack, as shown in fig. 3.2.2.2 [Lawn and Wilshaw (1975b)]. Thus the Hertzian indentation test can be used to investigate a surface's flaw distribution, given a solution for the

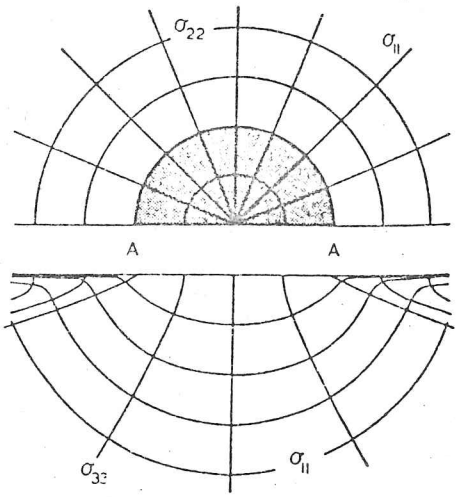

(a)

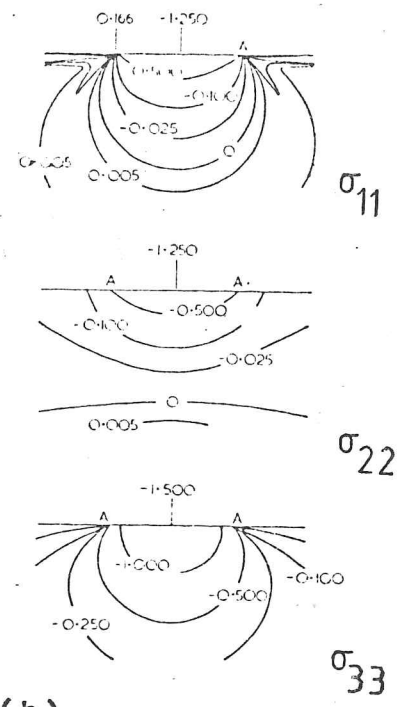

(b)

FIG. 3.2.2.1 Hertzian (blunt contact) stress field: (a) stress trajectories; (b) stress magnitudes, in units of the applied indentation pressure (compressive stresses negative). The contact area is shaded in (a). Note that σ_{11} is a maximum on the surface at the contact area boundary. (From Lawn and Wilshaw (1975b)).

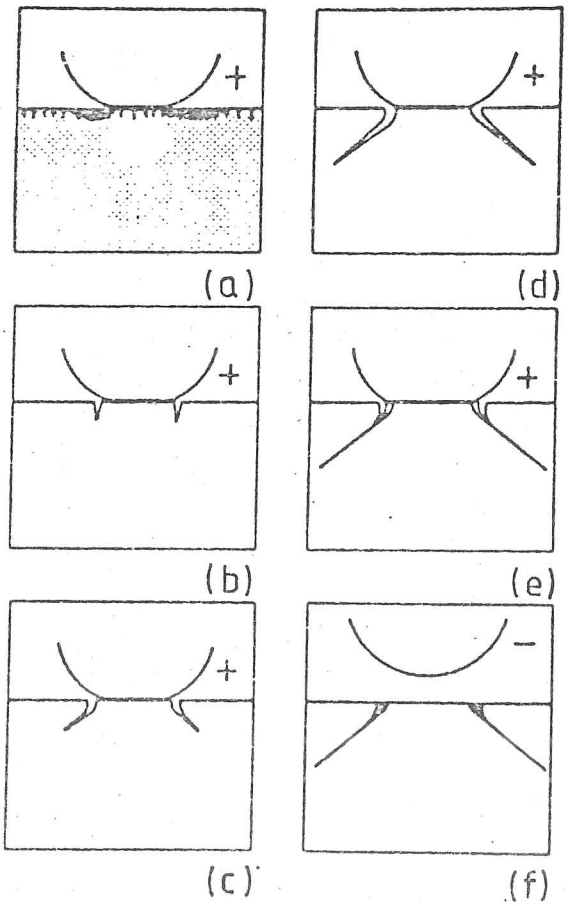

FIG. 3.2.2.2 Growth of 'cone crack' under Hertzian loading conditions, along lines of maximum σ_{11}. (from Lawn and Marshall (1978)).

surface stresses (these can be modified from the ideal elastic values by frictional tractions between the indenter and the test surface). Blunt indentations were not used in this study; however, indentations on silica glass produced cracks closely resembling cone cracks, even though a sharp Vickers profile indenter was used (see 5.4.3).

ii) Sharp Contact

The idealised stress field for this case (first analysed by Boussinesq) is shown in fig. 3.2.2.3. However, the situation for a real sharp indenter is complicated by the plastic flow that occurs in the near-indentation region (see 3.1.2). The modified stress fields have been assessed, by eg. Chiang et al. (1982) and Yoffe (1982), and lead to crack types rather different from those for blunt contacts [Lawn and Swain (1975)], [Lawn and Wilshaw (1975b)]. The cracks can be divided into two classes (see fig. 3.2.2.4):

a) Cracks normal to the surface. These are the 'median' cracks, which form below the surface on loading the indenter, and which may extend on unloading so as to break through to the surface, and the 'radial' cracks, which nucleate at the surface on both loading and unloading the indenter.

b) Cracks approximately parallel to the surface, the 'lateral' cracks. These nucleate on unloading the indenter, at the boundary between the plastic zone and the surrounding material. The lateral cracks may either remain below the surface, or break out to from plate-like chips.

The final extension of all crack types is determined by the residual stress field of the indentation. All types of crack degrade the mechanical properties of the material; median and radial cracks act as surface flaws, thus lowering fracture strength, and lateral cracks (especially when they intersect with median or radial cracks) can lead to material loss from the surface.

The analysis by Lawn and Marshall (1979) indicates that there is a critical indenter load, P^*, below which median cracks will not form; associated with P^* is a minimum viable crack size, c^*. These parameters, together with K_{Ic}, give an indication of a material's resistance to

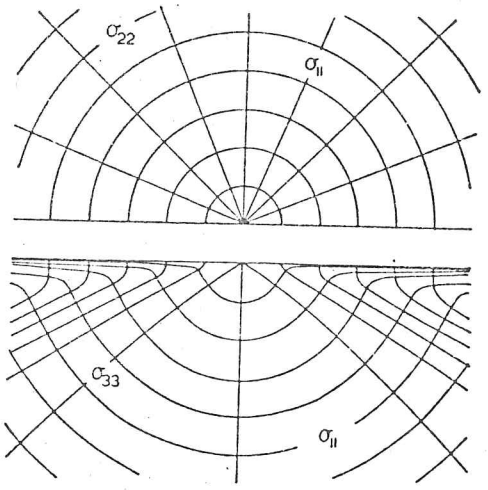

(a)

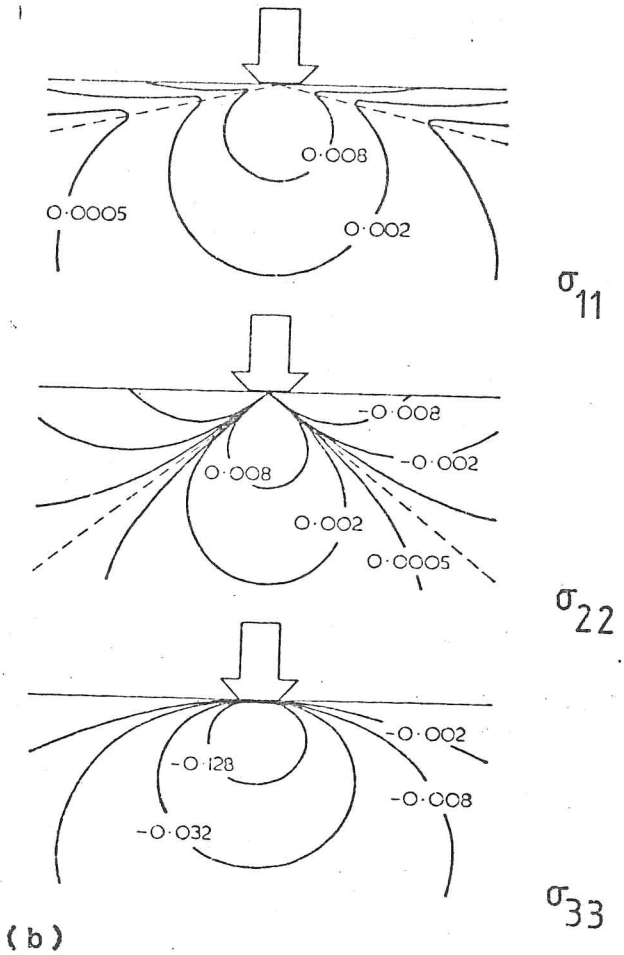

(b)

FIG. 3.2.2.3 Boussinesq (sharp contact) stress field: (a) stress trajectories; (b) stress magnitudes, in units of the applied pressure (compressive stresses negative). Note that σ_{11} is tensile throughout. (From Lawn and Wilshaw (1975b)).

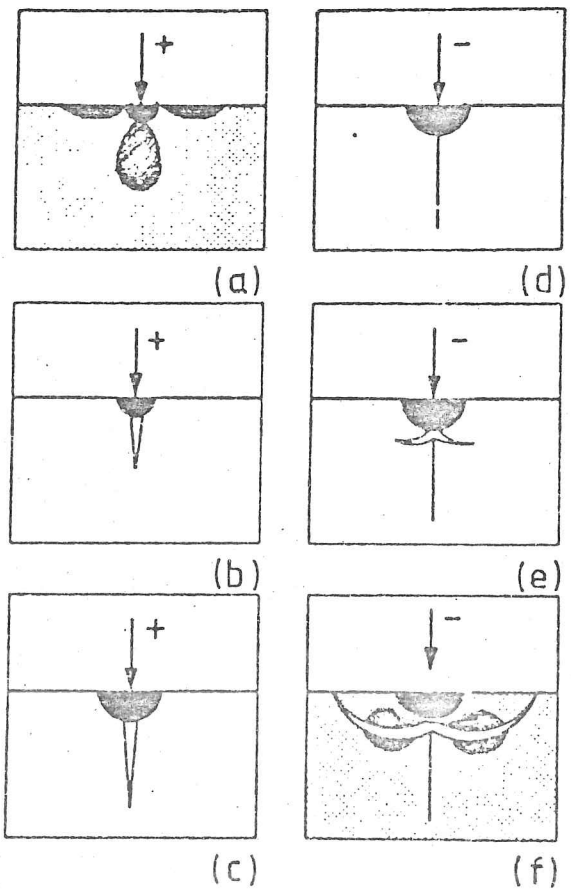

FIG. 3.2.2.4 Cracks from sharp contacts. Median cracks (normal to the surface) form on loading; lateral cracks from unloading and propagate in the residual stress field. Shaded areas in (a) show areas of high tensile stress, and those in (f) the residual stresses around lateral cracks. Radial cracks can also form, at the surface, on loading or unloading. (From Lawn and Marshall (1978)).

fracture. Lawn and Marshall showed how study of the variation of median/radial crack length with indenter load can be used to evaluate P^*, c^*, and K_{Ic}:

$$K_{Ic} = B_0(E/H)^m Pc^{-3/2} \qquad 3.2.2a$$

$$P^* = \lambda_0 K_{Ic}(K_{Ic}/H)^3 \qquad 3.2.2b$$

$$c^* = \mu_0(K_{Ic}/H)^2 \qquad 3.2.2c$$

[H=hardness,P=indenter load,c=median crack length, m, β_0, λ_0 and μ_0 are constants , whose values were determined by best fit to data from a variety of materials.]

Such methods have been used by Naylor (1982) to study the variation in fracture toughness of ceramics with temperature, etc.

The relationship between applied loads at point contacts (P) and P^* determine the cracking response of the surface. There are three regimes of behaviour:

a) $P < P^*$ - macrocracks do not form and surface deformation is wholly plastic;

b) $P > P^*$ - macrocracks form and surface deforms both plastically and by large-scale fracture;

c) $P \simeq P^*$ -fracture and plastic flow are of roughly equal importance, and on roughly the same scale.

Naylor (1982) calculates values of P^* for SiC to be 1-50g, depending on microstructure, and for Si to be ~1g (for Vickers indenters, at room temperature). In all the indentation tests performed in this study on these materials, fracture would therefore be expected, and was observed (see 5.1, 5.2). Only well-developed fracture was studied, in terms of the effects of implantation on fracture paths. Any possible effects of implantation on P^*, c^* and K_{Ic} were not studied, as the fine-scale layering of the implanted surface invalidates the models used to evaluate these parameters from crack-length data.

The effects of pre-existing surface stresses on fracture paths have been studied by, eg. Marshall and Lawn (1977), Lawn and Marshall (1977) (tempered glasses) and Jensen et al. (1976) (proton-irradiated glass). In the study by Jensen et al., the median/radial crack span was observed to be

greater in the irradiated material, and this was attributed to irradiation-induced surface tensile stresses. No such effects, in either direction, were observed in this study, but marked alterations in lateral crack paths were found to be produced by implantation (see 5.1.4, 5.2.3). The observations made in this study could only identify the surface stress states as in-plane compressive; other techniques (see 2.2.3) would be needed to quantify the stresses.

Such qualitative tests can also provide information on preferred crack paths in materials (especially polycrystalline materials) [Sawyer (1979)], [Naylor (1982)], provided account is taken of the influence of indenter shape on crack directions. Simply observing the number of cracks of various types formed can also yield valuable qualitative information about the brittleness/toughness of a material.

iii) Moving Indenters

The crack patterns formed by single sharp points loaded and moving across the surface of a brittle material are closely related to those formed around a sharp indentation [Broese van Grenou et al. (1975)], [Veldkamp et al. (1978)], [Sawyer (1979)]. Tracks made by moving blunt indenters can show partial cone cracks in the track base [Misra and Finnie (1979)]. Numerous examples of typical crack geometries from the motion of loaded diamond cones across SiC and Si surfaces are shown in sections 5.1.5 and 5.2.4. The generally observed crack types are those shown in fig. 3.2.2.5. The chipping fracture mode, ie. that related to lateral cracking, can be an important wear mechanism in ceramic materials (see 3.4). This type of fracture can be initiated at very low loads in sliding contacts (ie. P^* for sliding fracture is lower than that for quasistatic indentations) [Swain (1978)].

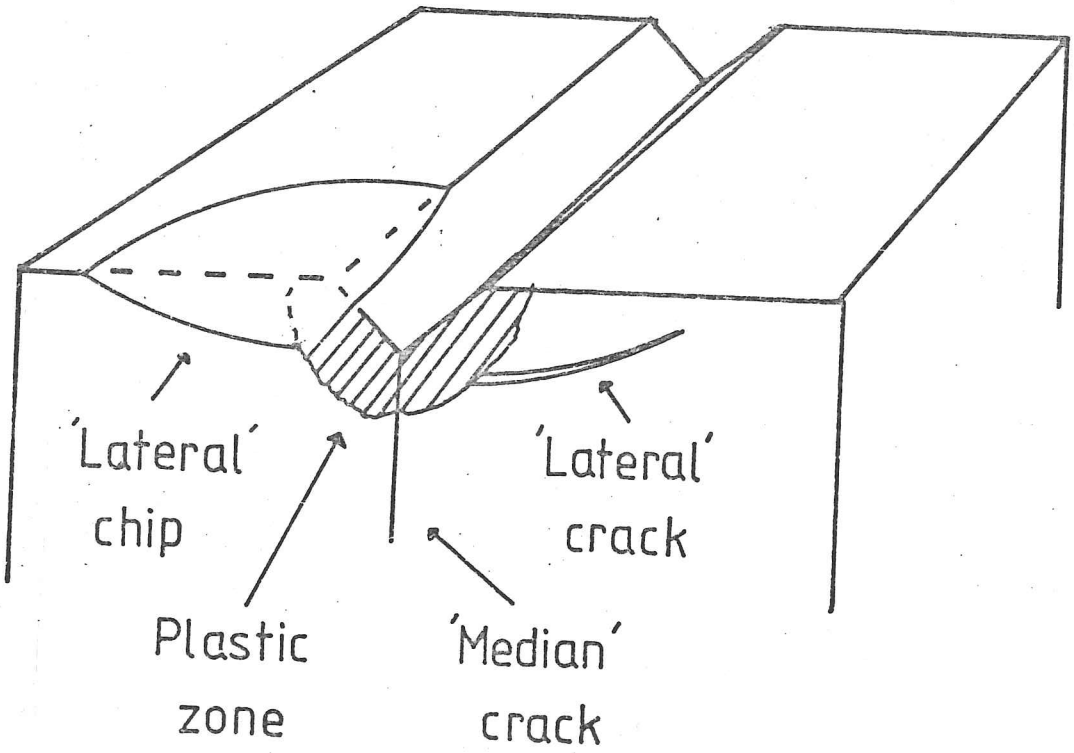

FIG. 3.2.2.5 Fracture types around the path of a moving sharp indenter. Chips may be formed by the breakout of lateral type cracks or by the interaction of cracks from several tracks.

3.3 Fatigue

Fatigue is the slow growth of cracks in a material subjected to cyclic stresses [eg. Frost et al. (1974)]. Fatigue mechanisms may be classified into those of high-cycle fatigue (HCF: stresses lower than the bulk yield stress) and low-cycle fatigue (LCF: stresses higher than the bulk yield stress). In high-cycle fatigue, flow occurs near the surface in a few favourably-oriented grains; within these, the arrangement of dislocations becomes permanently changed in regions where their movement is easiest (persistant slip bands). Eventually such plastic flow in the surface leads to the nucleation of cracks, by the formation of intrusions and extrusions where the persistant slip bands meet the surface. These cracks then grow with continued cyclic stressing, by plastic processes at the crack tip, until the remaining material section is insufficient to support the loads on it. In HCF, the initial crack formation stage occupies the greater part of the fatigue life, and can be lengthened by surface polishing, surface hardening and avoidance of sharp changes in surface contours. In LCF, crack nucleation is easy, and the fatigue lifetime is determined by the crack growth rate.

3.4 Friction and Wear of Materials

The body of literature on friction and wear is large, but for the most part consists of 'engineering' studies of specific wear/friction situations; general surveys are few. The material in this section is drawn mainly from the books of Bowden and Tabor (1974) and Rabinowicz (1965). As in the rest of this chapter, a brief summary only of the state of knowledge in the field is presented, with a few specific references to the materials and processes of specific relevance to this study.

3.4.1 Friction

The historical growth of knowledge in this area has been surveyed by Bowden and Tabor (1974). The basic empirical 'laws' of friction for unlubricated sliding contact were first formulated by Amontons in 1699, these being:

i) Frictional force is proportional to the normal load on the interface (the constant of proportionality being known as the coefficient of friction, μ);

ii) Frictional force is independent of the apparent, macroscopic, area of contact;

iii) Frictional force is independent of the relative velocties of the surfaces (this 'law' is less rigourously obeyed than the others, especially in that static friction is generally slightly greater than moving friction).

The range of μ for most materials in unlubricated contact lies between 0.1 and 1.5. The basis on which these laws are understood, especially the intuitively non-obvious (ii), is that the real areas of contact between the two surfaces are isolated points where asperities meet. The real contact area (A) can be estimated by assuming that the asperities (hardness H) deform until they support the applied load (P):

$$A = P/H \qquad 3.4.1a$$

If it is assumed that the frictional force is proportional to the true

contact area, the laws (i) and (ii) above follow. Further, if it is assumed that the frictional forces arise from the breaking of junctions formed in the above process, the force (F) is then equal to the tensile strength of the (weaker) contacting material (σ_{UT}):

$$F = A\ \sigma_{UT}$$

$$= P\ \frac{\sigma_{UT}}{H}$$

so

$$\mu = \sigma_{UT}/H \qquad 3.4.1b$$

This relation then accounts for the small range of observed values of μ, as the ratio of hardness to tensile strength varies very little from material to material (as hardness is closely related to yield stress (see 3.1.2)); though the relations between hardness, yield stress and tensile strength may be different at asperity contacts from those in the bulk [Gibbs (1982)]. This mechanism for friction is closely related to those proposed for 'plastic' wear (see 3.4.2). In both the above mechanisms the energy lost to friction is absorbed in heating and work-hardening; temperature rises, particularly at asperities, may be quite high, but are very difficult to measure.

In addition, frictional energy can be lost to 'ploughing', where hard asperities on one surface cut through material on the other. This is most likely to happen for mixed frictional couples (eg. steel on copper), and in fact such combinations generally have higher values of μ than those for identical contacting surfaces. Energy can also be lost, and so friction arise, through other mechanisms; energy loss by elastic hysteresis can be important in such situations as rolling contact, and in brittle materials energy can be lost in fracture processes (though normally a relatively small proportion).

3.4.2 Wear of Materials

Wear mechanisms can de grouped into five major types:

i) Adhesive wear;

ii) Abrasive wear by ploughing, in ductile materials;

iii) Abrasive wear by fracture, in brittle materials;

iv) Delamination wear and fatigue wear;

v) Erosion.

Many of the above mechanisms can be influenced, and usually the wear accelerated, by the presence of a corrosive environment. In real wear situations, various combinations of these processes can occur at different stages of the wear life. The above categorisation of mechanisms is only a framework, within which each wear couple must be regarded as unique; extrapolation from one wear situation to another, even if apparently closely related, can lead to confusion.

i) Adhesive wear

This class of wear mechanisms is closely related to the 'normal' friction mechanism outlined in section 3.4.1. It is reviewed by Rabinowicz (1965) and Finkin (1979). The basic mechanism is that of adhesion at the asperity junctions, followed by breaking of the junctions along a plane different from that of the original interface, and subsequent loss of some of the transferred material. On this basis, Archard (1953) modelled the wear process, and arrived at the expression:

$$V = \frac{k\,P\,l}{3H} \qquad 3.4.2a$$

[V=wear volume, P=applied pressure, l=sliding distance, H=hardness of the softer material]

The dimensionless constant k then represents the fraction of junctions that lead to a wear particle; the factor of 1/3 arises from Archard's assumption that the particles would be hemispherical. This expression is usually followed by the wear of unlubricated metals, when values of k are

found to be $\sim 10^{-3} - 10^{-5}$.

The semi-empirical Archard model does not explain how loose wear fragments can arise from the junctions; it might be supposed that the junctions must be as strong as the original material if they are to break on a plane other than that of the original interface. Rabinowicz (1965) proposed that the fragments are formed by the action of residual stresses, as the junction is formed uder a high compressive stress. When the junction is free again, strain incompatiblity at the interface may cause it to break and so form a wear particle.

Adhesive wear of metals can be divided into 'mild' and 'severe' wear. In mild wear, the debris found is principally fine oxide particles. In severe wear, where wear rates are often thousands of times greater than in mild wear, large metallic particles are formed. Transition between the two types of behaviour occurs at a critical load. Bowden and Tabor (1967) consider that this is because at low loads the oxide film supports the load, whereas at higher loads the asperities can penetrate the oxide film. The difference in mild and severe wear rates thus reflects the different wear properties of metals and oxides.

Adhesive wear occurs to some extent in all cases where moving surfaces are in contact, but can be almost eliminated by suitable lubrication. Lubrication is a complicated subject beyond the scope of this review; the books of Bowden and Tabor (1967), (1950) and Rabinowicz (1965) contain much information.

ii) Plastic Abrasive Wear

This type of wear occurs when a hard rough surface rubs against a softer one, for example in the polishing of a metal with SiC paper. It is reviewed by Rabinowicz (1965) and Moore (1978). A model by Moore (1978) gives the expression:

$$V = \frac{k` P l}{H} \qquad 3.4.2b$$

which is identical in form to the Archard equation for adhesive wear, 3.4.2a. The constant k` depends on the abrasive particle shape, size and distribution. Moore also notes that, for a given substrate hardness and abrasive material, metallic substrates wear much more rapidly than non-metallic ones, though no explanation was offered. Moore's model involves the formation of a groove in the soft surface, by plastic flow around the moving hard asperity, with a constant proportion of the groove material being lost from the system, though no mechanism for this was suggested. However, it was suggested that the material, particularly that piled up ahead of the asperity, was lost by fracture when it became strained to a certain critical level.

Even brittle materials, such as silicon, can deform in this way, as observed by Stickler and Booker (1962) and as in section 5.2.7.

iii) Brittle Abrasive Wear

Here the material loss mechanism is by fracture through material deformed elastically rather than plastically. The interaction of lateral and median crack types , analagous to those around hardness indentations (see 3.2.2) causes chips of material to be removed from the surface. This situation has been modelled by Evans (1979), who derived the expression:

$$V = k`` l P^{7/6} K_{Ic}^{-2/3} H^{-1/2} \qquad 3.4.2c$$

This expression is different in form from those for adhesive wear and plastic abrasive wear (3.4.2a and 3.4.2b); in particular, the fracture toughness of the material, K_{Ic}, is now important. The constant k`` is material-independent. Evans (1979) also presented experimental resuts for the wear of various ceramic materials which fitted equation 3.4.2c. A threshold load, P^*, is required for the initiation of fracture.

Very little work has been done on the wear rates of abraded brittle materials, Most workers, eg. Broese van Grenou et al. (1975), Adewoye and Page (1976), Veldkamp et al. (1978) and Page et al. (1978) have studied the types and sizes of cracks generated in a single point, single pass, wear test (as has been done in this study). Stickler and Booker (1962) studied the transition from plastic to brittle abrasive wear with increasing abrading particle size in silicon. Gibbs (1982) investigated the wear rates of several ceramic materials abraded by variously sized diamond grits, and concluded that wear rates are strongly dependent on the number and type of interfaces (eg. between grains and phases) in the surface. Increasing the number of interfaces (eg. by decreasing the grain size) was found to tend to increase wear rates.

iv) Wear by Delamination and by Fatigue

Both these mechanisms involve the generation of subsurface cracks by plastic processes near the surface [Jahanmir (1980)]. The two mechanisms are related to one another in roughly the same way as low- and high-cycle fatigue (see 3.3). In delamination wear (a mechanism first proposed by Suh (1973)) the active surface undergoes repeated plastic deformation, whereas in fatigue wear (such as occurs in repeated rolling contact) the surfaces are deformed for the most part elastically, with plastic flow occuring in 'favoured' regions, eg. at inclusions. In both cases, voids or cracks nucleate when sufficient plastic work has accumulated. These tend to form some distance below the surface, as the tractional stresses from the frictional interactions die away rapidly with increasing depth, but the high hydrostatic stresses associated with the interacting surfaces suppress void or crack nucleation at the surface itself. Inhomogeneities in the microstructure (eg. precipitates) can act as void/crack nucleation centres. The cracks grow with repeated deformation until a large plate is generated, which eventually breaks off from the surface.

v) Erosion

Erosion is caused by the impact of rapidly moving solid or liquid bodies onto a surface. Material loss is by methods similar to those of abrasive wear ((ii) and (iii) above). However, the very high strain rates involved mean that there is very little correlation between material properties (eg. hardness, fracture toughness) measured under normal conditions and the erosion rates [Hutchings (1979)].

vi) Other Wear Mechanisms

These include:

a) Fretting; this type of wear results when two metallic surfaces are in oscillatory contact. Adhesive wear produces oxide debris, which are trapped in the wear couple and cause accelerated wear by abrasion or delamination. Corrosive environments have a strong effect on fretting wear.

b) Effects of corrosive environments; the combination of the various wear mechanisms described above and chemically active environments can lead to greatly accelerated wear, particularly when oxide formation and removal is important in the wear process (ie. in adhesive wear). It is also well known that (slow) crack growth can be accelerated by the presence of corrosive agents, eg. in the case of fatigue.

3.4.3 Wear Mechanisms and Ion Implantation

From the preceding summary of wear mechanisms, it can be seen that ion implantation, which can alter the plastic flow properties of almost all classes of materials (see 3.1, 2.4), is likely to have effects on wear rates. The depth of the implantation treatment (~0.5μm) is comparable with the asperity height that might be expected on industrial surfaces, and rather greater than the probable asperity height on a well polished surface.

For the adhesive wear mechanisms, a hardening of the surface would be expected to reduce the wear rate and experimental results (see 2.4.2, 2.4.3) show that the hardness of certain metals (especially steels) can be increased by implantation. Another route by which implantation might affect adhesive wear is suggested by the results of Roy Chowdhury et al. (1980) (see 2.4.1), which showed that nitrogen implantation reduced the adhesion between titanium surfaces. The probability of forming asperity junctions could thus be reduced; however, this type of mechanism might not apply to all metals, or in non-vacuum environments. In the important mild wear regime, where the mechanical properties of the oxide film control the wear rate, the chemical effects of implantation on oxide film growth might be important (see 2.3). Alternatively, implanted ions incorporated into the oxide film might change its mechanical properties; however, no work has been performed to investigate the deformation behaviour of such oxide films. Hartley (1975b) has suggested that, under lubricated conditions, implantation might lead to the production of a smooth surface either by increased plastic flow (heavy ion implantation) or by asperity fracture (light ions), and thus decrease the wear rate. This possible mechanism cannot apply to unlubricated conditions, where production of smooth surfaces would increase friction and wear.

High surface temperatures can be produced by frictional energy loss, particularly at asperity tips. The mechanical properties of implanted surfaces (or even unimplanted surfaces) under the influence of such transient thermal effects are not well understood. It has been suggested by Dearnaley and Hartley (1978) that the steady state temperature rise, coupled with dislocation motion, might transport light implanted ions into the bulk of the material by 'Cottrell atmosphere drag'. This mechanism was proposed to account for the extended-lifetime wear reductions in WC-Co materials (see 2.4.4, 5.3.2).

Surface hardening could also reduce wear rates where the controlling mechanism is that of plastic abrasive wear. It would be expected that in this case implantation treatment would be most effective when all deformation is near the surface, ie. when fine abrasives are used. If the wear is by very coarse 'ploughing' action, then it is unlikely that

implantation would have much effect. Most results reported for this type of wear have been for cemented carbide materials; wear of this complicated material is discussed below. The results of Singer et al. (1980) for steels worn with very fine abrasives (~5μm diamond) showed wear rate reductions after implantation, which were interpreted by the authors in terms of surface hardening.

Implantation might be expected to affect wear by delamination and fatigue by changing the flow properties of the surface. Any surface hardening would be expected to reduce wear by these mechanisms, and has been found to reduce both high- and low-cycle fatigue in bulk metal specimens, as well as wear rates (see 2.4.5). However, if precipitates or other inhomogeneities were produced by implantation, these might act as nuclei for the formation of subsurface cracks if flow occurred. Conversely, compressive stresses produced by implantation might be expected to inhibit void/crack production.

Much of the work performed so far on the effects of implantation on the wear behaviour of materials has concentrated on metals, where the inhibition of plastic flow by implantation has led to significant improvements in wear (and fatigue) life (see 2.4). These results can be understood in terms of surface hardening, with perhaps some contribution from the implantation-induced stress state.

Clarification of the effects of implantation on the abrasive wear of brittle materials was one of the principal objectives of this study; results are presented in chapter 5 and discussed in chapter 6. Implantation can affect this mode of wear via the nucleation of cracks (particularly lateral cracks) or via their propagation. Changes in crack nucleation can be brought about by the effects of implantation on surface plasticity (see 5.1.3, 5.2.2, where it was found that nitrogen inplantation reduced the surface hardness of SiC and Si). As P^* depends on H^{-3} (3.2.2b), even a small reduction in hardness could achieve a transition from brittle to plastic behaviour. The stress state induced by high dose implantation (see 2.2.3) can influence the paths and extent of cracks formed, if the load exceeds P^* (see 5.1.4), and possibly also influence the nucleation of

cracks (see 5.1.4, 5.1.6, 5.2.3). Alterations in surface plasticity could be effective in long-term wear reduction, but stress-related effects are likely to be effective only initially, as:

i) Friction-induced annealing could eliminate or reduce the stresses;

ii) Intersection of subsurface cracks from many tracks will eventually produce debris (in the cases where crack nucleation is not altered by the stress state).

Tungsten Carbide/Cobalt composite

The response of this material to the pin-on-disc wear test and nitrogen implantation is discussed in sections 5.3.4, 5.3.5 and 5.3.7; the results of industrial and laboratory tests by the Harwell group are summarised in section 5.3.2. Wear rates were found to be markedly reduced after implantation, under both adhesive and abrasive wear conditions. Various mechanisms have been proposed. It appears from the long-term effectiveness of implantation that brittle behaviour alone does not account for wear, so that plastic deformation in the binder and/or the carbide phase is important. However, all results so far indicate that WC and (pure) Co are softened by implantation (see 5.3.3, 5.3.6); possible effects of implantation on the cobalt-rich binder phase in real materials are less clear (though Mazey, quoted, by eg. Hartley (1979b), has observed a martensitic transformation to be induced in this material by nitrogen implantation). It has been suggested that wear occurs by the the loss of whole WC grains [Dearnaley and Hartley (1978)], but little evidence was found for this in this study. Experiments by Dearnaley and Hartley (1978) indicate that the effective nitrogen and carbon implantations do not change the oxidation behaviour of the material. Work by Greggi and Kossowsky (1981) indicates that adhesion at the WC-Co interfaces might be improved by implantation, though this would be expected to affect wear by whole-grain loss only. The route by which implantation alters wear rates in this material is therefore still unclear.

CHAPTER 4

EXPERIMENTAL TECHNIQUES

4.1 Implantation Techniques

Three types of machine were used to implant the specimens used in this study: the 'Pimento' prototype industrial implanter, the Cockcroft-Walton accelerator and the Harwell-Lintott isotope separator. All machines were at AERE Harwell. The majority of nitrogen implantations were performed using the 'Pimento' machine, the Cockcroft-Walton being used for some higher energy implantations and the Harwell-Lintott being used for boron implantation. The characteristics of each machine are described below.

4.1.1 Pimento Implanter

This machine is shown in fig. 4.1.1.1. It consists of a large vacuum chamber, 0.5x0.5x0.7m, with removable side panels for the attachment of special workpiece handling devices [eg. Dearnaley and Goode (1980)]. At the top of the chamber is a beam scource of the twin anode type [Fitch et al. (1970)] which uses electrostatic fields to contain ions in long-lifetime paths prior to extraction [McIlraith (1966)]. The source as fitted to the 'Pimento' can only be used for the production of ions from gaseous elements. The beam area at the specimen is roughly 15x8cm; however the ion flux is highly non-uniform within this area (see fig. 4.1.1.2). For

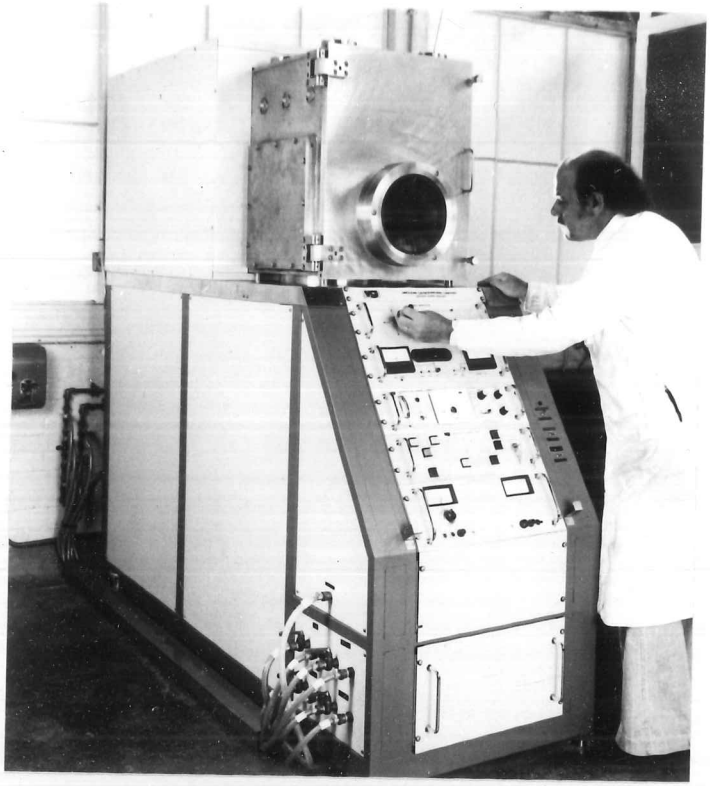

FIG. 4.1.1.1 The 'Pimento' implantation machine.

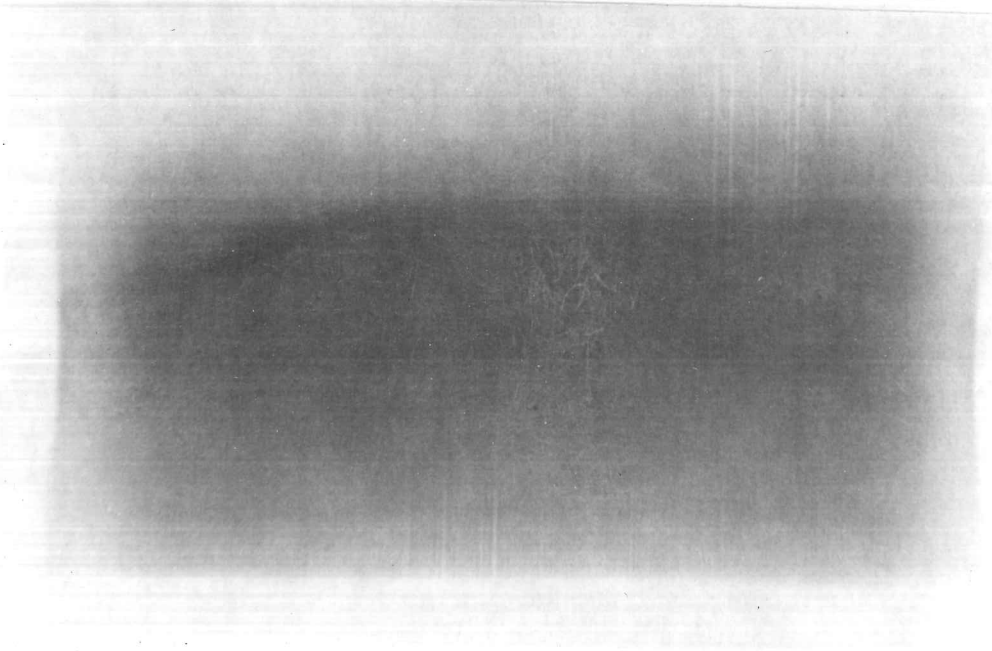

FIG. 4.1.1.2 'Burn' formed by implanting plastic-coated card in the Pimento implanter. Note the non-uniformity of the beam. (~80% full size)

some of the early implantations, the severity of the variation was not appreciated, and the specimens were simply placed in the beam area (see eg. 5.2.2). For later specimens, a rotating table was used so that each specimen passed through both the weak and the strong flux areas. This arrangement also allowed more specimens to be treated during any one run. The first series of implantations established a set of standard conditions, which were kept to, as closely as possible, for the remainder of the project. When the rotating table was used, the dose rate was increased so that each specimen recieved the same average flux rate as the stationary specimens.

Initially, implantation conditions were set so as to limit the specimen temperature to 300°C. As annealing of implantation damage in silicon is not effective below ~600°C, and as higher temperatures are required to anneal SiC (see 2.2.1), it was thought that such a temperature limitation would ensure that minimal annnealing of damage would occur. These conditions are also similar to those used for industrial implantations at Harwell (see eg. 5.3.2).

Implantation Conditions - Pimento

Ion Species	Nitrogen, beam estimated ~80% N_2^+
Energy	90 keV (±~5 keV)
Average Dose Rate	4.7μA cm^{-2}
Implantation Rate	56 mins per 10^{17} ions cm^{-2}
Max Specimen Temp.	~280°C
Base Vacuum	2.5×10^{-6} torr
Running Vacuum	2.5×10^{-5} torr

Dose control was achieved by timing the implantation process and frequently checking that the implantation conditions remained constant. Where necessary, specimens were masked using thick aluminium foil. Total beam current could be measured by inserting a flap into the beam, and this was related to the ion current at the specimen using charts from calibration implantations performed by the Harwell implantation group. Where possible, doses were checked by nuclear-reaction analysis, as described in section 4.2, either of the specimens themselves, or of stainless steel discs included in the specimen batch.

some of the early implantations, the severity of the variation was not appreciated, and the specimens were simply placed in the beam area (see eg. 5.2.2). For later specimens, a rotating table was used so that each specimen passed through both the weak and the strong flux areas. This arrangement also allowed more specimens to be treated during any one run. The first series of implantations established a set of standard conditions, which were kept to, as closely as possible, for the remainder of the project. When the rotating table was used, the dose rate was increased so that each specimen recieved the same average flux rate as the stationary specimens.

Initially, implantation conditions were set so as to limit the specimen temperature to 300°C. As annealing of implantation damage in silicon is not effective below ~600°C, and as higher temperatures are required to anneal SiC (see 2.2.1), it was thought that such a temperature limitation would ensure that minimal annnealing of damage would occur. These conditions are also similar to those used for industrial implantations at Harwell (see eg. 5.3.2).

Implantation Conditions - Pimento

Ion Species	Nitrogen, beam estimated ~80% N_2^+
Energy	90 keV (±~5 keV)
Average Dose Rate	4.7μA cm^{-2}
Implantation Rate	56 mins per 10^{17} ions cm^{-2}
Max Specimen Temp.	~280°C
Base Vacuum	2.5×10^{-6} torr
Running Vacuum	2.5×10^{-5} torr

Dose control was achieved by timing the implantation process and frequently checking that the implantation conditions remained constant. Where necessary, specimens were masked using thick aluminium foil. Total beam current could be measured by inserting a flap into the beam, and this was related to the ion current at the specimen using charts from calibration implantations performed by the Harwell implantation group. Where possible, doses were checked by nuclear-reaction analysis, as described in section 4.2, either of the specimens themselves, or of stainless steel discs included in the specimen batch.

Generally, correspondence between calculated and analysed doses was found to be good except at higher doses where substantial sputtering occurred, as described in section 5.1.2. However, miscalibration of the beam after modification of the pumping system caused gross dose overestimation when the cobalt specimens were implanted (see 5.3.6); the real dose was only 40% of that estimated. Unless each implantation run is checked by post-implantation analysis, this machine is not very suitable for non-industrial research uses. It does, however, have the advantage of a high specimen throughput compared with the other two machines used.

4.1.2 Cockcroft-Walton Accelerator

This machine was originally built in 1950 as a neutron generator, and was adapted for implantation work in 1967. The machine is illustrated in fig. 4.1.2.1. A detailed description of the machine's construction and capabilities has been given by Goode (1971).

The accelerator has a maximum working voltage of 500kV; voltages up to 150kV were used in this study. Ions are produced by a sputtering ion source, capable of generating a wide range of ion species. Production of ions of gaseous elements is relatively simple. Acceleration takes place in the vertical section of the machine. The ions then pass through an analysing magnet and are scanned electromagnetically over the specimen surface. Only small specimens (~30mm diameter) can be implanted in the standard target chamber, though several specimens can be held in a cassette under vacuum, so that pumpdown is not necessary between each implantation. However, the running vacuum (2×10^{-7} torr) is much better than that in the 'Pimento', and implantation conditions are continuously monitored and adjusted, thus ensuring good dose control.

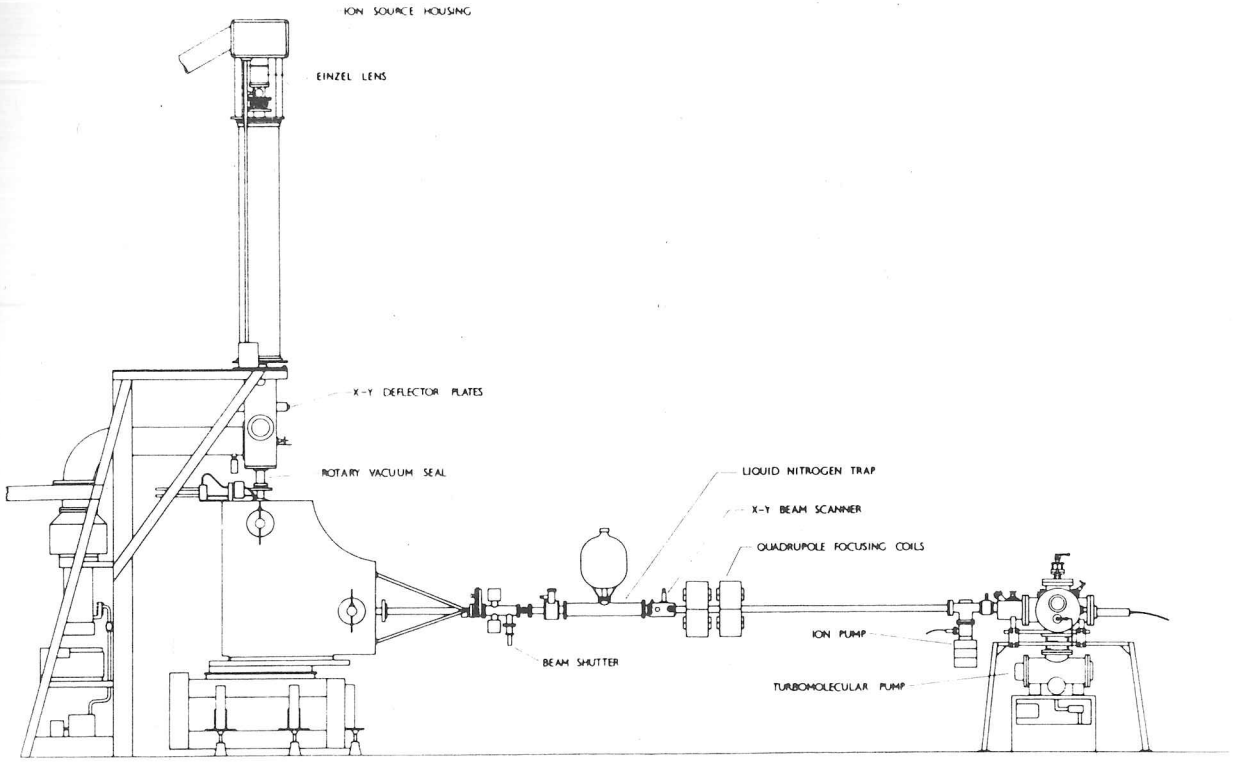

(a)

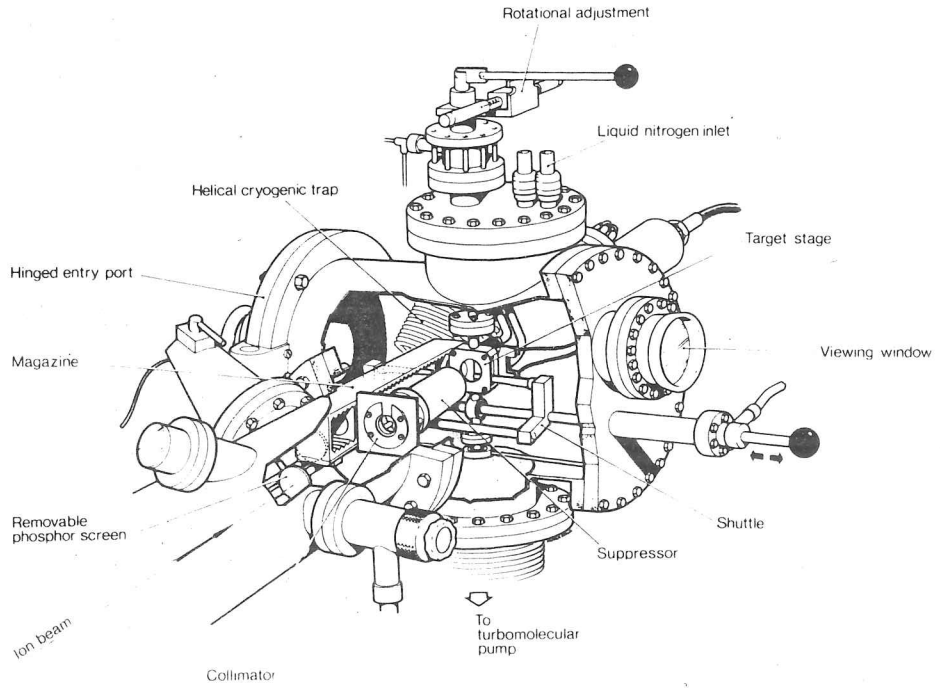

Ion implantation chamber

(b)

FIG. 4.1.2.1 (a) Cockcroft-Walton implantation machine; (b) Implantation chamber.

4.1.3 Harwell-Lintott Isotope Separator

This accelerator, though developed principally for semi-conductor industry implantations, can be used to produce ions of almost any element [Freeman et al. (1977)]. The machine was used in this study to implant silicon carbide with boron (see 5.1.6, 5.1.7). Figure 4.1.3.1 shows the machine and ion source.

The Harwell low-voltage discharge ion source [Freeman (1969)] was used with a BF_3 feed for the implantations performed in this study. A wedge-shaped beam is produced, which can be accelerated up to 80kV before magnetic analysis, and can be further accelerated up to 200kV afterwards. The specimens are mechanically scanned within the stationary beam; a specimen area of approx. 60mmx40mm can be covered. The beam variables are constantly monitored, giving accurate dose control. Background vacuum is $\sim 10^{-6}$torr.

For the boron implantations, conditions were chosen to be equivalent to those for the nitrogen implantations described in section 4.1.1, ie.

$$10^{17} N_2^+ \text{ at } 80\text{kV} \equiv 2\text{x}10^{17} B^+ \text{ at } 40\text{kV}$$

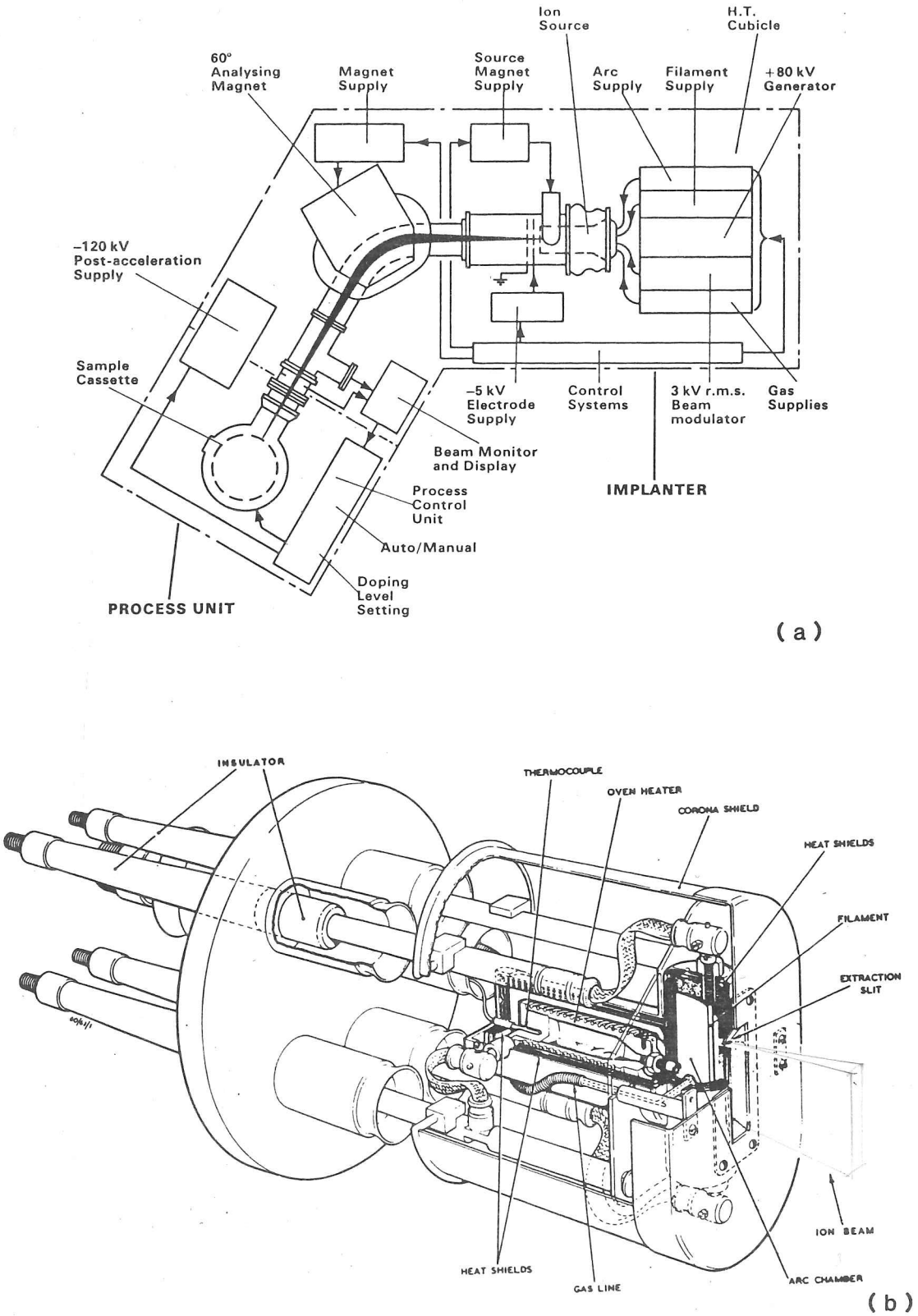

FIG. 4.1.3.1 (a) Harwell-Lintott implantation machine; (b) Ion source (from Freeman (1979)).

4.2 Nuclear Reaction Analysis

This method was used to check the total doses of nitrogen implanted into both actual samples (see 5.1.2) and into stainless steel test discs included in implantation runs (see 5.3.6). The technique in general involves the inducement of a nuclear reaction by injection of an accelerated particle or a high-energy photon, followed by quantitative detection of one of the reaction products. These, and similar, methods have been reviewed by DeConninck (1978).

Nuclear reaction analysis is a particularly useful method for the detection of light elements, such as nitrogen and boron, for which other common techniques (eg. energy dispersive X-ray analysis, neutron activation) are inadequate [DeConninck (1978)]. Individual elements or isotopes can easily be distinguished by selection of reactions yielding products of well-defined energies. In the analyses performed for this study, the reaction used was:

$$^{14}N + d \rightarrow {}^{12}C + \alpha + 13.575 \text{ MeV}$$

[d=deuteron, α=helium nucleus]

This is conventionally written as $^{14}N(d,\alpha)^{12}C$.

The analyses were performed using the 6 MeV Van der Graaf accelerator at AERE Harwell, using 2.4 MeV deuterons. Detection of α particles was by silicon surface barrier devices (Ortec Inc.). An area $\sim 1mm^2$ of the surface was analysed and calibration was by comparison with a standard sample.

If a reaction producing particles of a low, very well-defined energy is used, then the loss of energy of such particles penetrating from the bulk to the surface (see 2.1.4) can be used to evaluate the depth at which the reaction occurred, and so a concentration profile can be produced. The reaction $^{14}N(d,\alpha)^{12}C$ is not of this type, and so only total nitrogen concentrations could be determined. Concentration profiles of nitrogen can be produced if the implantation is of the rare isotope ^{15}N (0.37% of natural nitrogen), and by using the reaction:

4.2 Nuclear Reaction Analysis

This method was used to check the total doses of nitrogen implanted into both actual samples (see 5.1.2) and into stainless steel test discs included in implantation runs (see 5.3.6). The technique in general involves the inducement of a nuclear reaction by injection of an accelerated particle or a high-energy photon, followed by quantitative detection of one of the reaction products. These, and similar, methods have been reviewed by DeConninck (1978).

Nuclear reaction analysis is a particularly useful method for the detection of light elements, such as nitrogen and boron, for which other common techniques (eg. energy dispersive X-ray analysis, neutron activation) are inadequate [DeConninck (1978)]. Individual elements or isotopes can easily be distinguished by selection of reactions yielding products of well-defined energies. In the analyses performed for this study, the reaction used was:

$$^{14}N + d \rightarrow {}^{12}C + \alpha + 13.575 \text{ MeV}$$

[d=deuteron, α=helium nucleus]

This is conventionally written as $^{14}N(d,\alpha)^{12}C$.

The analyses were performed using the 6 MeV Van der Graaf accelerator at AERE Harwell, using 2.4 MeV deuterons. Detection of α particles was by silicon surface barrier devices (Ortec Inc.). An area $\sim 1mm^2$ of the surface was analysed and calibration was by comparison with a standard sample.

If a reaction producing particles of a low, very well-defined energy is used, then the loss of energy of such particles penetrating from the bulk to the surface (see 2.1.4) can be used to evaluate the depth at which the reaction occurred, and so a concentration profile can be produced. The reaction $^{14}N(d,\alpha)^{12}C$ is not of this type, and so only total nitrogen concentrations could be determined. Concentration profiles of nitrogen can be produced if the implantation is of the rare isotope ^{15}N (0.37% of natural nitrogen), and by using the reaction:

$$^{15}N + p \rightarrow {}^{12}C + \alpha + 4.964 \text{ MeV}$$

In this study, the concentration profiles were assumed to be similar to those calculated for various ions in silicon (see 2.1.4). The cross-section TEM results in section 5.2.7 correspond well with such profiles. For 80 keV (di)nitrogen, peak concentration is at a depth of ~0.3μm.

4.3 Specimen Sectioning and Polishing

Smooth, damage-free, polished surfaces were required for all the tests performed in this study. For each material, a different surface preparation technique was required:

i) Silicon - wafers could be used as supplied (one side lapped and chemo-mechanically polished), after cleavage along {110} planes into smaller specimens.

ii) Silica glass - discs (10mm diameter, 3mm thick) were used as supplied in a good state of polish.

iii) Lithium fluoride - crystals required cleavage along {100} to produce a fresh usable surface.

iv) Metglass and cobalt - supplied as ribbon or thin sheet; required polishing.

v) WC-Co - supplied as large discs (25mm diameter, 3mm thick). Required polishing, and for some purposes, sectioning.

vi) Silicon carbide materials - required sectioning from compacts (eg. rod) or single crystal, followed by polishing.

Roughly the same sectioning and/or polishing techniques were used for all materials, making due allowance for their particular ductile/brittle characteristics, and these are detailed below.

4.3.1 Sectioning

All sectioning was performed using a Capco Q35 high speed diamond saw. Bulk material was stuck to friable ceramic blocks using a high melting point wax ('Tanwax', m.p. ~150°C). These blocks were similarly waxed to a brass bar which was clamped to a two-axis goniometer head on the saw. Specimen alignment was performed by eye. Slices as thin as ~150μm could be cut; the blade thickness was ~250μm. Cutting speed was of the order of 1mm per minute.

It was found that any thickness of SiC could be cut, but the cemented carbide tended to clog and jam the blade if blocks wider than ~5mm were cut. However, no other satisfactory method of cutting WC-Co could be found (apart from spark erosion cutting of 3mm discs for TEM), so large blocks of this material were cut on the Capco saw by mounting them in such a way that only a small width of WC-Co was in contact with the blade.

4.3.2 Polishing

It was found useful to mount small sections of WC-Co in bakelite, using a conventional metallurgical hot-mounting press, prior to polishing. Attempts to mount SiC materials in a similar way usually cracked the specimens so badly as to render them useless. Accordingly, these and all other brittle materials were polished after mounting by low melting point wax ('Lakeside 70', m.p. ~70°C) to aluminium blocks. The more delicate slices and foils were wax-mounted onto glass slides, then onto the aluminium blocks.

Polishing was performed using a range of diamond pastes on laps and cloths using an Engis Ltd. 'Kent' Mk2A machine, the sequence being:

i) Cast-iron laps - 14μm and 6μm diamond
ii) Copper lap - 6μm diamond
iii) Hydrocell Pellon Cloth - 6μm diamond
iv) Microcloth - 1μm and 1/4μm diamond

These were followed in sequence, the polish being checked after each stage using an optical microscope. For some delicate specimens, lapping was omitted and initial polishing was on Hydrocell Pellon using 14μm paste. Initial lapping was continued until a flat surface was obtained; each of the subsequent polish stages usually occupied 5-10 minutes, longer if examination showed this to be necessary at any stage. Applied load was 1.75kg for the 14μm and 6μm pastes and 0.5-1kg for the finer pastes. Final polishing was performed by hand on the 1/4μm paste. The metglass specimens were finished by polishing on 0.05μm alumina slurry in a vibropolisher (see 5.4.1).

4.4 Indentation Plasticity and Fracture Techniques

4.4.1 Microhardness Testing

A large proportion of the work in this study involved microhardness testing of the various materials before and after implantation, followed by analysis of diagonal measurements and examination of the fracture patterns and surface topography around the indentations. Indentation plasticity and fracture have already been discussed in sections 3.1.2 and 3.2.2; this section is limited to a discussion of the indentation and analysis techniques used in this study.

All microhardness testing was carried out using a Leitz 'Miniload' microhardness machine. A Vickers profile indenter was chosen as it is widely used and as results are less dependent on indenter orientation with respect to specimen crystallography than is the case for the Knoop profile indenter. Indentations were performed at room temperature in air, using an indenter dwell time of 15 seconds. Indentation diagonals were measured using the micrometer eyepiece of the microhardness tester, except for the indentations made on silica glass, where extensive cracking around the indentation made this impossible (see 5.4.3). In this case, diagonals were measured from scanning electron micrographs; care was taken to ensure that

the level of scanning distortion was low (by checking the squareness of indentations and the indentation arrays), and magnifications were calibrated using the inter-indentation spacings.

The basic problem with using conventional microhardness testing equipment to examine changes in plasticity in implanted layers is that even for the hardest materials (eg. SiC, Si) and using the lowest loads practicable, the indentation depth is at best of the order of, and usually much greater than, the implantation depth. For example, use of loads below 50g on SiC produces small (<3μm diagonal), irregular (the indenter may not be well shaped near the tip) indentations which are impossible to measure accurately in the microhardness tester, and virtually impossible to find in the SEM. Even in the SEM, such small, irregular indentations would be very difficult to measure with any degree of accuracy. However, a 3μm diagonal indentation still has a depth of ~0.5μm, and the plastic zone associated with the indentation will be of considerab ly larger size (see 3.1.2). The ions implanted in this study give a 'layer' depth of ~0.5μm, so even the smallest indentation practicable with conventional microhardness testers samples a thickness of material much greater than that at which the bulk of the implanted ions and the implantation damage lie (see 2.1.4).

An approach taken by Pethica and others is to use specially designed ultra-microhardness testing devices, which monitor the penetration of a specially profiled diamond into the specimen surface, together with the applied load at each stage [Pethica (1982)]. In this way, the variation in hardness at each stage of the indentation process from the time of the first contact can be evaluated. Typical loads are in the μN range, and penetrations down to a few nm can be monitored (see 2.4.2). Roy Chowdhury et al. (1980) used similar equipment, but with such low loads that no plastic deformation occurred; the results obtained were related to the adhesion behaviour of the surfaces (see 2.4.1). These techniques require careful specimen preparation, and require sophisticated equipment not generally available.

An alternative approach has been used in this study, based on the work of Sargent (1979), in which use is made of the concept of the indentation size effect (ISE) (see 3.1.2). The change in measured hardness with indentation size is evaluated in terms of the Meyer index (see below), and comparisons made between the ISE in unimplanted and implanted materials. In this way, the influence of an implantation-affected layer of fixed thickness on indentations (and thus indentation-induced plastic zones) of varying size can be studied. While it is not possible, by this method, to determine directly the mechanical properties of the implanted layer (which is in any case not uniform with depth), a semi-quantitive comparison of the properties of the implanted and bulk materials can be made, and direct comparisons can be made between the microhardness behaviour of variously dosed specimens of the same material.

The raw data (indentation diagonal sizes) were processed using the ISEMH suite of programs written by Sargent, and described in detail by him [Sargent (1979)]. Only a brief descrition of the input, processing methods and output will be given here.

i) Input- This is in the form of a series of indentation diagonal measurements at various loads. To ensure the production of an internally consistent and meaningful set of results, data from a particular series of specimens should be as alike as possible; that is, the same number of measurements should be made at each load used, and the load range should be the same for each specimen in the series.

ii) Processing - the program first calculates a hardness value for each of the diagonal measurements and from these a mean value (with standard deviation) for each load. All data are then fitted to the ISE equation:

$$L = a.d^m \qquad 3.1.3a$$

[L=applied load, d=indentation diagonal, m=derived Meyer index]

The fit is performed by transforming the equation to logarithmic form:

$$\ln(L) = \ln(a) + m.\ln(d) \qquad 3.1.3b$$

followed by data fitting to the best straight line by a 'weighted least squares' method (the weighting is to compensate for the distortion in the Gaussian error function by the tranformation to logarithmic form). The data fitting is performed by minimising the squared errors in ln(d), since L is assumed to be known accurately. This analysis enables the Meyer index

and 'a' to be evaluated, with the errors in each; these errors are not independent of each other. The value of 'a' is that of the extrapolated hardness at an indentation diagonal of 1μm; such a parameter for a material is useful for comparison purposes (see above). However, a diagonal size of 1μm is an extrapolation well beyond the limits of the input data, and so the program interpolates a hardness value for an operator-specified diagonal size. In all the results presented in chapter 5, this fixed reference indentation size is 10μm, being as small a size as could confidently be interpolated from the input data.

iii) Output - this consists of a listing of the diagonal values, derived hardness values, and the mean hardness and error at each load. Best values of the Meyer index and 10μm hardness, with standard deviations, are produced. Graphs are output of the variation of hardness with load, and of the variation of hardness with diagonal size. A graph of the fitting to equation 3.1.3b is also produced, showing the 'best fit' line. A plot in 10μm hardness vs. Meyer index space is drawn, showing the best values and the area surrounding this in which there is a 95% probability that the true values lie. This area is elliptical in shape, as the limits of error of these two are not independent, being derived from the same line fitting. Examples of the graphical output are shown in figs. 4.4.1.1.

In all the results presented in chapter 5, values of the Meyer index and 10μm hardness are given for various materials at each implantation dose used. In all cases, results were derived from 5 indentations (10 diagonal measurements) at each load used, the loads being chosen to cover the diagonal size range from ~30μm to the smallest size measurable, usually ~5μm. When changes were found in the indentation behaviour after implantation, these were usually only apparent at the smaller indentation sizes ($\lesssim$15μm). There were no cases where the larger diagonal sizes varied significantly with implantation. Changes in the Meyer index can therefore be taken as reflecting the characteristics of the near-surface material.

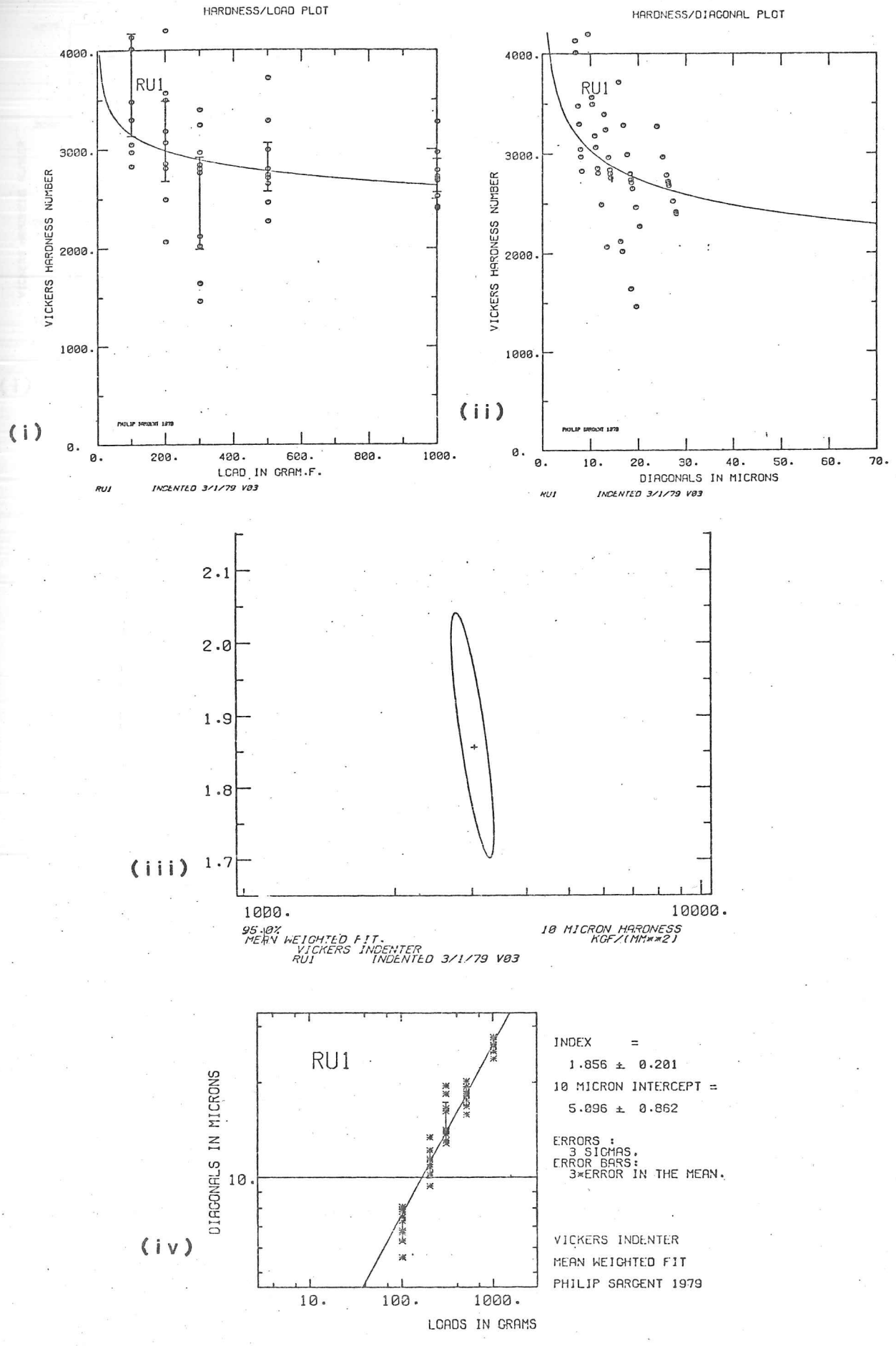

FIG. 4.4.1.1(a) ISEMH output for unimplanted REFEL: (i) Hardness vs. load; (ii) Hardness vs. indentation diagonal; (iii) Meyer index / 10μm hardness 'space', with best fit values and 95% certainty contour; (iv) line fitting for (iii).

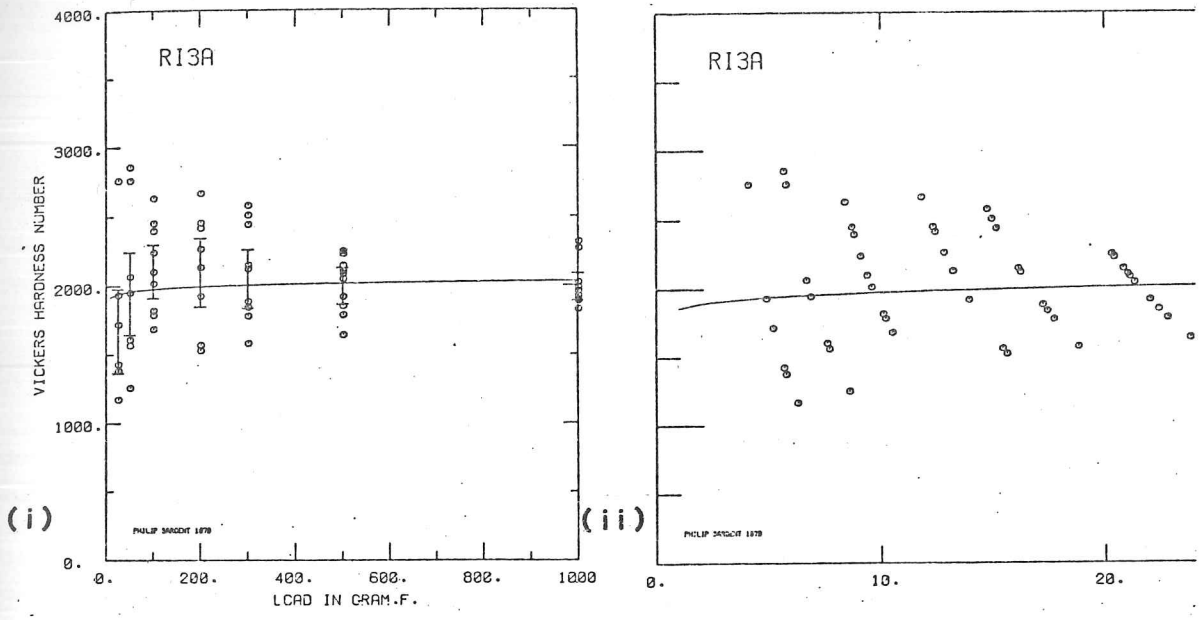

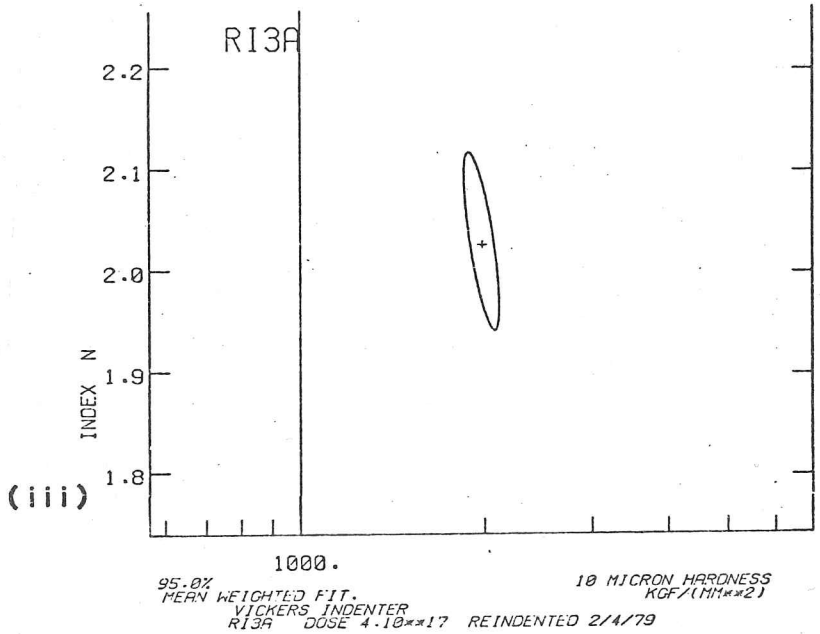

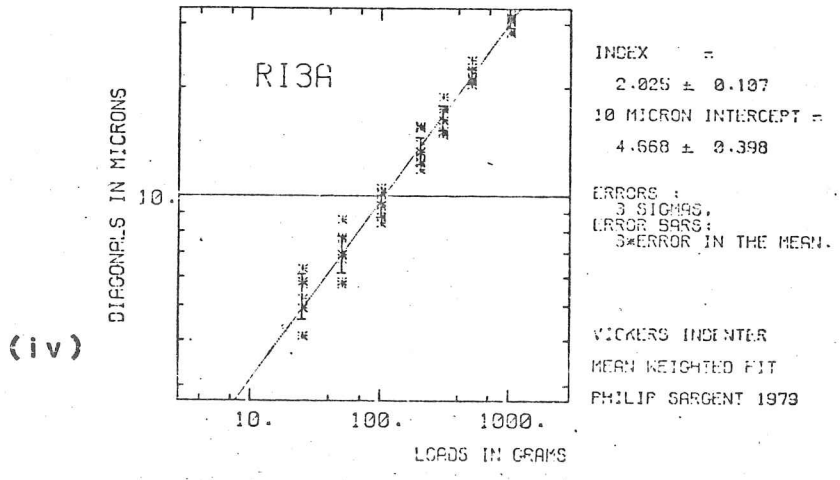

FIG. 4.4.1.1(b) ISEMH output for implanted REFEL, dose $4 \times 10^{17} N_2^+$ cm^{-2}: (i) Hardness vs. load; (ii) Hardness vs. indentation diagonal; (iii) Meyer index / 10μm hardness 'space', with best fit values and 95% certainty contour; (iv) line fitting for (iii).

4.4.2 'Broken-open' Indentations

This technique was developed to study the subsurface lateral fracture paths in SiC and Si, by sectioning the specimen normal to the surface through a line of indentations.

Indentations were made in a closely spaced line across a thin (less than 500μm thick) specimen, so that the median/radial cracks were in line in a cleavage direction and almost joining. The specimen was then placed over the edge of a glass slide, held in place by a second slide; pressure was applied on the projecting half of the specimen with a third slide until it fractured by extension of the line of cracks. For some very small specimens, three slides used in a three-point bend configuration were found to be a more effective method of breaking. The two halves of the specimen were then mounted on an SEM stub for examination. Results from this type of specimen are given in sections 5.1.4, 5.1.7 and 5.2.3.

FIG. 4.5.1.1 Scratch testing machine. The specimen on the stage is driven beneath the loaded scriber by the motor/gearbox.

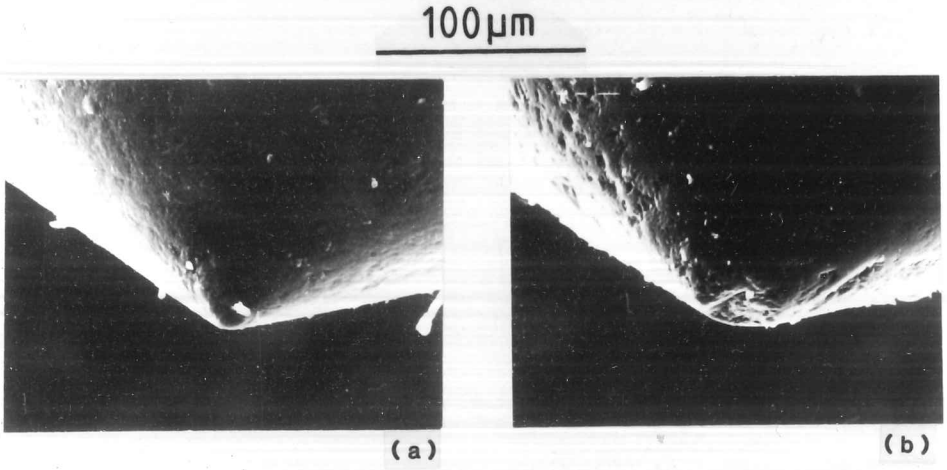

FIG. 4.5.1.2 90° diamond cones, before (a) and after (b) wear tests. The diamond in (b) had made tracks on silicon carbide to a total length of ~25mm at loads 10-50g.

seen under a microscope, it was withdrawn from use. At each stage of blunting when testing implanted materials, reference tracks were made on unimplanted material so that the effects of implantation on chipping could be distinguished from those of the progressive diamond blunting.

4.5.2 Diamond paste Abrasion Tests

These were performed on silicon surfaces for plan and profile TEM examination (see 4.6). Specimens were lightly rubbed by hand on a cloth impregnated with 6μm diamond paste, until microscopical observation revealed that a sufficient density of tracks had accumulated to ensure that some would cross the limited area usable in the TEM after thinning. Tracks on all the specimens treated in this way appeared in the optical microscope as purely plastic grooves.

4.5.3 Pin-on-Disc Wear Tests

Discs of WC-Co (~25mm diameter) were worn on an Avery-Denison pin-on-disc machine at AERE Harwell. In this machine, shown in fig. 4.5.3.1, a 0.5mm diameter cylindrical WC-Co pin bore against the disc, rotating at 2000 rpm, under a load of 100N. Wear rates were measured by monitoring the vertical movement of the pin load arm. The test couple were immersed in a recirculating bath of 'white spirit' as coolant and lubricant. Wear rate results for such tests are detailed in section 5.3.2; specimens of this type were examined by SEM and TEM techniques (see 5.3.4, 5.3.5).

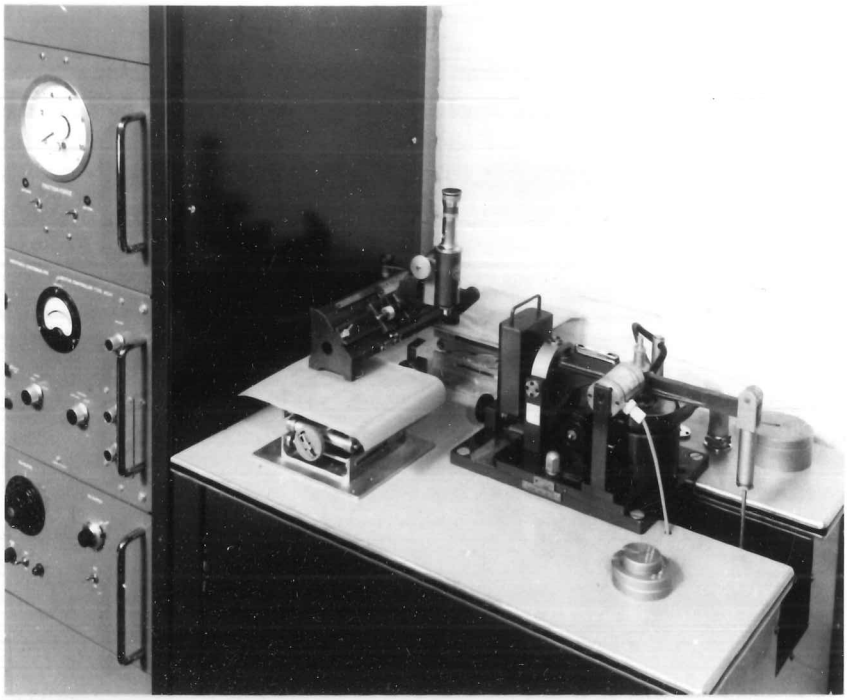

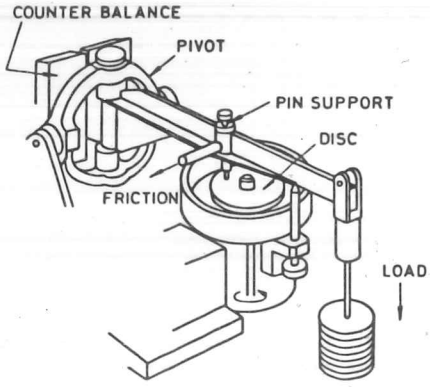

FIG. 4.5.3.1 Avery-Denison pin-on-disc wear testing machine. The lubricant recirculating system has been removed for clarity; the disc/pin couple run immersed in white spirit.

4.6 Electron Microscope Specimen Preparation Techniques

The early stages of this project found several ways in which ion implantation could change the near-surface plasticity and fracture behaviour of materials. In order to investigate the interaction between implantation damage (see 2.2) and near-surface deformation structures, transmission electron microscopy (TEM) was performed on several of the materials investigated, these being SiC, Si and WC-Co. Plan views of the implanted layer and the surface were obtained by back-thinning of specimens. A cross-sectioning technique, allowing the near-surface material to be seen in profile, was employed on some of the silicon specimens.

4.6.1 Plan-view Specimen Preparation Techniques

All such specimens were initially prepared by waxing a specimen to a glass slide, using 'Lakeside 70' low-melting point wax, the implanted/deformed layer facing the glass, then polishing the specimen to ~50μm thickness. Initial specimen size was usually ≤1cm^2 in area and ~250-500μm thick. Silicon wafers were easily cleaved to a useful size, whereas specimens of silicon carbide and WC-Co were cut using the 'Capco' saw (see 4.3.1). Polishing required different techniques for each material. Silicon was polished on 500 grit SiC paper until ~100μm thick, then by hand on the sequence of laps and cloths listed in section 4.3.2. The SiC and WC-Co specimens required machine polishing at all stages, as described in section 4.3.2. It was often found useful, particularly for the thicker WC-Co specimens, to surround the specimen with a box of glass cut from slides so that the specimen lapped down flat.

Cutting of 3mm discs from the thin sections was performed by ultrasonic machining for the Si and SiC specimens, and by spark machining for the WC-Co. Ultrasonic machining was performed using a Kerry Ultrasonics 'Sonorode' model KT 150 drill and a slurry of boron nitride as the cutting fluid. Initial specimen cutting used the drill's own weight

(lessened by internal springs) to drive the bit into the specimen; however, even using the lightest load setting and with sharp tool bits, specimens frequently broke up or were lost from the slide during cutting. Following a suggestion by Cullis (1980), the machine was altered so that the height of the bit remained constant and the specimen was raised up to be cut, using a three way micrometer stage. This arrangement gave consistently good results. After cutting of the discs, they were removed from the slide by soaking in warm methanol.

WC-Co proved to be too plastic to be effectively cut by the abrasive process of ultrasonic machining. Discs were therefore cut by spark machining, using a Metals Research Ltd. 'Servomet' Type SMD machine. The lapped and polished strips of WC-Co were fixed using a mixture of 'Durofix' and graphite powder to a metal plate , which was clamped to the machines work table. It was found important to glue the specimen with the polished face uppermost; if this was not done, sparking at the glue-specimen boundary spoiled the surface finish.

All foils were thinned to perforation by ion beam thinning. Some early specimens were thinned on Edwards IBMA-2 machines, later ones on Ion Tech 4004 'Microlap' machines. Specimens were lapped from the unimplanted side, using argon ion currents of 0.5mA (0.05mA on the Edwards machines) at 4-6kV, at an incidence angle of 10-20^{o}. One of the Ion Tech machines was fitted with a liquid nitrogen cooled stage, but examination of the profile-view specimens (see 5.2.7) showed that negligible annealing had occurred during specimen preparation, and so this facility was not used.

4.6.2 Cross-sectional Specimen Preparation

Although plan view specimens were found to produce usable specimens of the implanted and/or deformed surface (see 5.1.7, 5.2.7), such specimens give little information about the variation with depth of the structures of such surfaces. Cross-sectional specimens were therefore prepared.

The method adopted was essentially that of Fletcher (1973), subsequently used by several workers in semiconductor field [eg. Cullis, Webber and Chew (1980)]. The method allows comparison of two juxtaposed surfaces in the same specimen, so that a 'control' surface can be examined at the same time as the one of interest, and any artefacts of the specimen preparation route can be allowed for. The technique as described here is that for the preparation of cross-sectional specimens from silicon wafers; however, it could be extended to other materials of suitable size and thickness, provided they can be bonded by some form of low-viscosity adhesive. The technique is described below in the form of a detailed set of instructions for specimen preparation.

i) Materials required:

a) backing blocks - ~10x3x2mm, cut from silicon, with faces flat and accurately at right angles;

b) specimen silicon - cut or cleaved to ~3x10mm;

c) adhesive - a low viscosity, rapid-drying epoxy resin ('Devcon' modelling epoxy resin was found to work well);

d) two small engineers' clamps;

e) miscellaneous: glass slides, 500 grit SiC paper, large glass polishing plate, cocktail sticks, filter papers and alcohol.

ii) Pre-preparation notes:

a) Cleanliness is vital. Silicon dust from specimen cleavage is a particular nuisance - any filter paper used for cleaving should be thrown away immediately. All glass slides, silicon, etc, should be washed in alcohol and wiped on a clean filter paper before use.

b) The epoxy resin should be mixed well, and enough should be made at once to ensure a good 50:50 mixture of resin and hardener. If the glue appears cloudy after thorough mixing, it should be thrown away and a new tube used.

c) The clamp faces sould be well-linnished on SiC paper, and covered with sellotape to prevent the epoxy from sticking irretrievably.

iii) Preparation method (see fig. 4.6.2.1):

a) Place on a clean glass slide the two specimen halves, one polished face up, the other polished face down, and two backing blocks, working faces (2x10mm) uppermost.

b) Mix the glue. Pick up one backing block in tweezers, dip the working face in glue and press on to the unpolished specimen half. Dip the pair thus formed into the glue, wetting the polished face, and press this to the polished face of the other specimen half. Similarly attach the other backing block, and put the assembled specimen down on a clean glass slide.

c) Using cocktail sticks, move the components of the specimen against one another so as to clear excess glue from the joints, keeping the assembly flat on the slide.

d) Apply one clamp, keeping the faces parallel. Lift the specimen from the slide and tighten the clamp fully.

e) Leave the assembly to dry under a light bulb for at least an hour, using the other clamp as a stand.

f) Remove the specimen from the clamp, and hand-polish one side flat on the SiC paper on the glass plate. When all the joints are exposed on a flat surface, transfer to hand polishing on a 14μm lap, 6μm laps and 1μm cloth (see 4.3.2).

g) Wax the polished side to a glass slide, using 'Lakeside 70' wax, and hand polish the specimen on 500 grit SiC paper until it is ~200μm thick. Carefully polish on a 14μm lap until ~100μm thick, then on 14μm, 6μm and 1μm cloths, aiming for a final thickness of ≤50μm. If the specimen is found to chip at the joints during lapping, polish on 14μm paste applied directly to the glass plate.

h) Using an ultrasonic drill, as described in section 4.6.1, cut 3mm discs from the specimen, centering the drill carefully.

i) Separate the disc from the slide by soaking in warm methanol or trichloromethane, until the discs float off. The discs can then be scooped up on an EM grid held in tweezers. At this stage it is quite likely that the backing blocks will have detached themselves from the central part of the specimen. Good specimens can still be easily produced if this occurs.

j) Mount the specimen in an ion beam thinner, using 'hole' type EM grids

as support if only the central portion is left, and thin from both sides in the usual way (see 4.6.1). Often perforation leaves a central glue and silicon 'spine'. This should be thinned until it breaks in two, when the needles thus produced are normally good specimens.

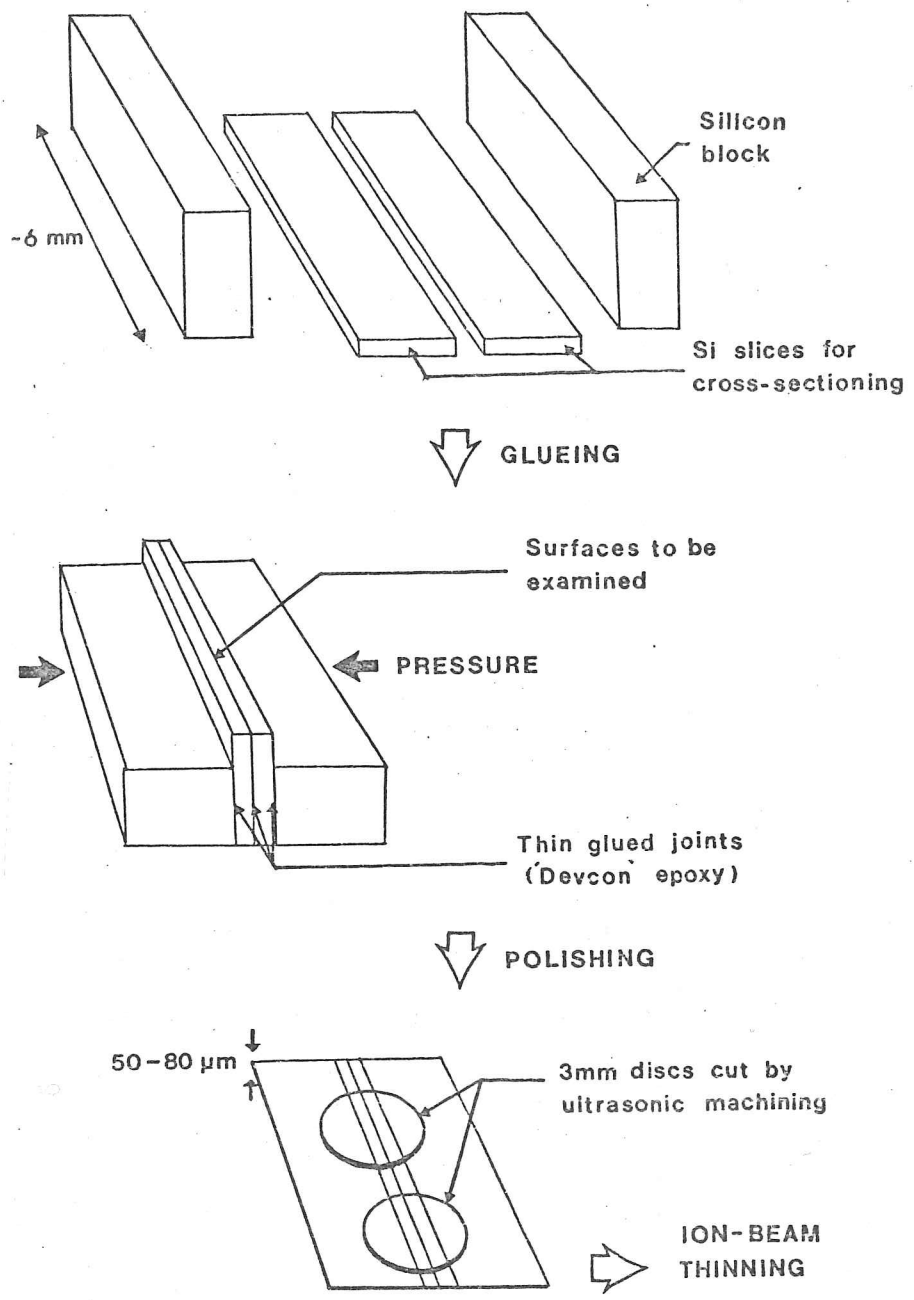

FIG. 4.6.2.1 Construction of cross-sectional TEM specimens. See text for details.

CHAPTER 5

EXPERIMENTAL RESULTS

5.1 Experiments with Implanted Silicon Carbide

5.1.1 Description of Materials

Silicon Carbide (SiC) is a very hard, brittle material. It exhibits polytypism (see below), that is, it has many crystal structures which differ from each other only in the sequences in which identical layers of SiC tetrahedra are stacked. It is a semiconductor with a band gap of ~2-3eV, depending on polytype [Parché (1964)]. Silicon carbide is available as single crystals and in a variety of polycrystalline forms (see below). Experiments were performed on single crystals and on a reaction bonded form, REFEL*. The different forms of silicon carbide are described below; the results of experiments performed on both the single crystals and REFEL followed the same pattern, and are described together in sections 5.1.2 to 5.1.7.

---

* 'REFEL' is a regd. trademark of the UKAEA.

i) Polytypism of SiC

As the archetypal polytypic material, silicon carbide has been extensively investigated by crystallographers [eg. Verma and Krishna (1966)]. Hundreds of regular variants of the stacking sequence are known, some with very large 'c' spacings. There are several commonly found room-temperature (meta)stable forms; these are listed below:

Polytype	Zhdanov Symbol	Remarks
6H	(33)	Commonest Polytype
15R	$(23)_3$	
4H	(22)	
3C	(∞)	The only cubic polytype

Several symbolisms are used to describe the polytypes. The simplest classification is the division into α (non-cubic) and β (cubic) polytypes. The α polytypes can be divided further into hexagonal (H) and rhombohedral (trigonal) (R). The polytype name then consists of the number of layers of C-Si tetrahedra in one c-repeat, and a letter giving the crystal class. The structure of the basic C-Si layer is shown in fig. 5.1.1.1. These layers are parallel to (0001) in the α polytypes and to (111) in the β polytype. Each layer in the three dimensional structures is related to the ones 'above' and 'below' it by a translation of $a/3\langle 1\bar{1}00\rangle$; adjacent layers may also be related by a rotation of 180°. The 'Zhdanov symbol' for a polytype then gives the number of succesive steps in one $\langle 1\bar{1}00\rangle$ direction before such a rotation, followed by the number in the reverse direction, etc. The unit cell of 6H SiC (Zhdanov symbol: (33)) therefore has three successive layers related to each other by steps of $a/3\langle 1\bar{1}00\rangle$, followed by three layers in the 180° rotated orientation related to each other by steps of $a/3\langle \bar{1}100\rangle$. The stacking sequences for the various polytypes can be illustrated on tramline diagrams, ie. schematic cross-sections on a $\{11\bar{2}0\}$ plane [Verma and Krishna (1966)]. Figs. 5.1.1.2 illustrate the stacking sequences of two common polytypes, 6H and 3C; the structures of these two polytypes are particularly relevant to the TEM observations reported in 5.1.7.

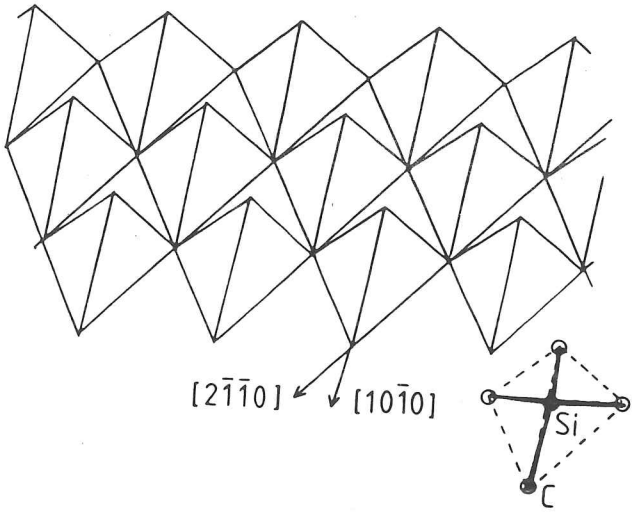

FIG. 5.1.1.1 All SiC polytypes can be considered as consisting of planes of SiC tetrahedra joined at the corners.

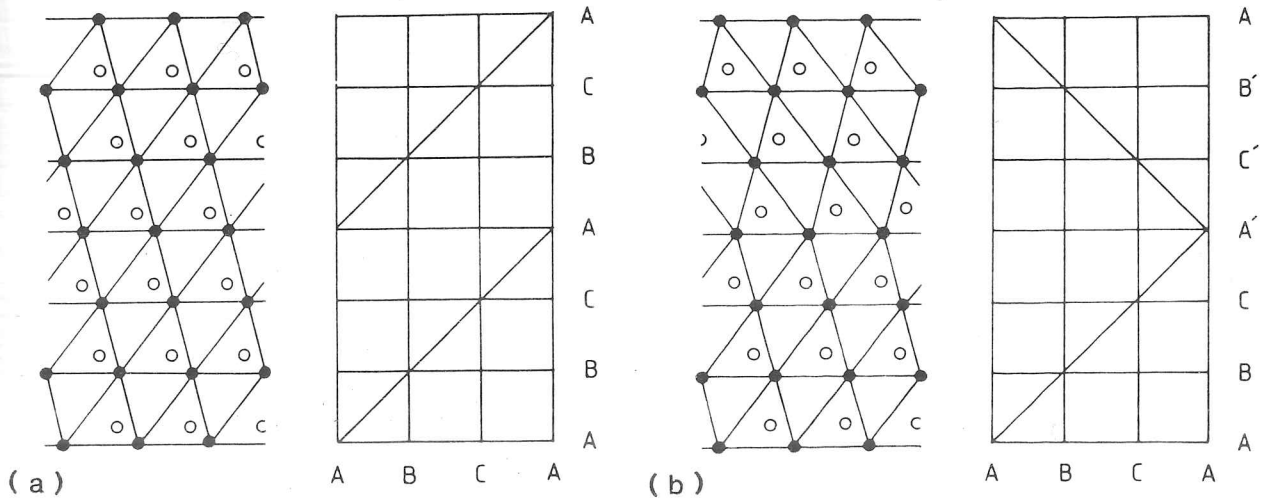

FIGS. 5.1.1.2 The structure of two common polytypes of SiC: (a) 3C; (b) 6H, as viewed down the <10$\bar{1}$0> direction, and as represented in 'tramline diagrams'.

Polytypes differ from each other only in long-distance co-ordination (3rd nearest neighbour and further) and so the energy differences between them might be expected to be small. Furthermore, transformations between one polytype and another involve a good deal of reconstruction (though mechanisms involving partial dislocations may ease transformations in some cases [eg. Jepps and Page (1979)]. It is not, therefore, surprising that a large number of polytypes of SiC are stable at room, and higher, temperatures. Conditions for the formation of, and transformations between, various SiC polytypes have been studied by several workers [eg. Jepps and Page (1979)], but many aspects are still not well understood. It is known that β-SiC is only produced directly by low temperature (<1400°C) syntheses [Popper (1960)], and that the β form transforms irreversibly to the 6H polytype at temperatures greater than 1600°C [Jepps and Page (1979)]. The stabilities of polytypes are also thought to be influenced by their impurity content [Verma and Krishna (1966)]. In particular, nitrogen is thought to stabilise the β polytype [Kieffer et al. (1969)] (see, however, the results in 5.1.7). Most of the very long-period polytypes are thought to arise from the growth of a faulted short-period polytypes around a screw dislocation [Verma and Krishna (1966)].

The analysis of polytypes of SiC has been performed by a variety of techniques, including:

a) X-ray methods [Tung and Faust (1974)], [Verma and Krishna (1966)];

b) Examination of etch pits on the (0001) plane [Faust et al. (1974)];

c) Observation of lattice fringes in the TEM [Jepps and Page (1980)].

The last technique is particularly suited to the study of structures at transformation, etc. interfaces. In this study, simple TEM diffraction techniques were used to distinguish between polytypes (see 5.1.7).

ii) Single Crystal SiC - Mechanical Properties

Silicon carbide is a covalent solid, with the typical properties of such materials; it is hard, brittle and has a high elastic modulus:

VHN	2500-3500 $kgmm^{-2}$	(see 5.1.3)
K_{Ic}	3-5 MPa	[Naylor and Page (1980)]
Young's Modulus	390 GPa	[Parché (1964)]
Poisson's Ratio	0.16-0.18	[Parché (1964)]

Fracture paths in hexagonal SiC are most likely to be along the $\{1\bar{1}00\}$, $\{11\bar{2}0\}$ and (0001) cleavage planes, in increasing order of calculated work of fracture (8.4, 10 and 21 Jm^{-2} [Shaffer (1964)]). Fracture is observed around microhardness indentations and diamond cone scratch tracks [Page et al. (1978)]; the changes in such behaviour with ion implantation are detailed in sections 5.1.4, 5.1.5 and 5.1.6.

Since silicon carbide is so brittle, microhardness testing is the only effective way of studying its plastic flow characteristics at low temperatures. Study of the Knoop hardness anisotropy of α-SiC [Sawyer et al. (1980)] on various crystallographic surfaces has identified the active slip systems as $(0001)\langle 11\bar{2}0\rangle$ and $\{1\bar{1}00\}\langle 11\bar{2}0\rangle$. Similar conclusions have been reached as a result of X-ray topographic studies [Posen and Bruce (1974)], and TEM observation and etching of dislocations [Adewoye and Page (1976)]. The $\{1\bar{1}00\}\langle 11\bar{2}0\rangle$ slip system has the lower critical resolved shear stress (CRSS), by a factor of ~1.5 [Sawyer et al. (1980)]. Slip systems of the type $\{h\bar{h}01\}\langle 11\bar{2}0\rangle$ are also possible. The value of the yield stress was estimated to be 12-52 GPa. Silicon carbide crystals are normally obtained in an impure state (nitrogen and aluminium being common impurities). It is possible that the impurity type and concentration could influence flow behaviour, as is known for silicon (see 5.2.1). Comparison of theoretical stresses for 'exotic' deformation mechanisms such as block shear, densification and crowdionic diffusion with the transient stresses occcuring during indentation indicates that such mechanisms may also operate, though no experimental evidence for this has been produced [Sawyer et al. (1980)] (see 3.1.1).

The mechanical properties of cubic (β) SiC have not been well investigated, due to the difficulties of preparing large crystals. Shaffer (1965) investigated its microhardness behaviour, and found a hardness of 2500-2900 $kgmm^{-2}$ (at a load of 100g), with very little anisotropy. This hardness value is similar to that for α-SiC. The slip system in α-SiC has

been found to be {111}<1$\bar{1}$0> [Stevens (1970)], identical to that in diamond and silicon, which have crystal structures closely related to that of β-SiC. This slip system is equivalent to (0001)<11$\bar{2}$0> in the α materials. Given the similarity of the structures of SiC polytypes at a local level (1st and 2nd nearest neighbour distances and orientations), and the narrowness of dislocation cores in such a strongly covalently bonded material, it is not surprising that the stresses for dislocation movement in the various polytypes are so similar.

No data are available on the fracture properties of β-SiC, but K_{Ic}, etc, would not be expected to vary markedly from those for α-SiC. The easy fracture planes, like those in Si and diamond, would be expected to be {110}, {112} and {111} (see 5.2.1).

The single crystal material used in this study was supplied by Arendal Smeltewerk (Norway) in the form of blue-black crystal agglomerates. These were prepared by the Acheson process (described by Parché (1964)), where coke and silica are heated to temperatures of 2000-2500°C in an electric furnace. Well-formed crystals of hexagonal habit were broken from the agglomerates and cut (parallel to (0001)) and polished as described in section 4.3.

iii) Polycrystalline SiC Materials

The most common industrial use of SiC, in the form of powder or small grains, is as an abrasive, 'carborundum'*. However, interest is growing in the possibilites of using SiC as a high temperature semiconductor, because of its thermal stability and large band gap (see numerous papers in 'Silicon Carbide 1973' [Marshall et al. (Eds.) (1974)]), and as a high temperature structural and bearing material, eg., 'Ceramics for High Performance Applications' [Burke et al. (Eds.) (1974)]. The difficulties associated with the production and machining of large single crystals of SiC have led to the development of several polycrystalline forms for engineering applications. The 'bulk' forms of the material (there are also

---

* 'Carborundum' is a trade mark of the Carborundum Co., USA.

techniques such as chemical vapour deposition (CVD) for applying coatings) can be divided into three broad classes:

a) Those formed from a powder compact by simultaneous heat and pressure ('hot-pressed') [eg. Lange (1975)];

b) Those where the bonding is by thermal effects (diffusion, etc.) at low or zero pressure ('sintering');

c) Those formed by pressureless methods where a chemical reaction binds the powder together ('reaction-bonded').

Of these, only reaction-bonded material, REFEL, was used in this study.

The preparation route of REFEL has been described by Popper (1960) and Forrest et al. (1972). A mixture of α-SiC and graphite, in a polymeric binder, is formed by any standard polymer-forming process (eg. extrusion). The compact is then heated in vacuum to 1600-1700°C in contact with molten silicon. The silicon is drawn by capillary action into the body of the material and reacts with the graphite to form SiC, which deposits epitaxially on the 'old' grains. The final microstructure has been described by Sawyer and Page (1978) and is illustrated in figs. 5.1.1.3. It consists of the original angular SiC grit, epitaxially deposited SiC, 5-10% residual silicon, and <0.1% porosity. Note that the SEM secondary imageing mode (fig. 5.1.1.3b) shows contrast between the original and epitaxial SiC; this has been attributed by Sawyer and Page (1978) to differences in purity between these regions. Jepps (1980) has confirmed, by etching experiments, that the purity variation in REFEL is consistent with this proposal. The SiC, both original and reaction-formed, is predominantly of the 6H polytype, with some 15R and other polytypes; the fine precipitates in the silicon are mostly 3C SiC [Sawyer and Page (1978)].

The mechanical properties of REFEL, hot pressed and sintered silicon carbide materials have been reviewed by Edington et al. (1975a), (1975b) and their hot hardness and fracture behaviour have been investigated by Naylor and Page (1979), (1980). Relevant parameters for REFEL are:

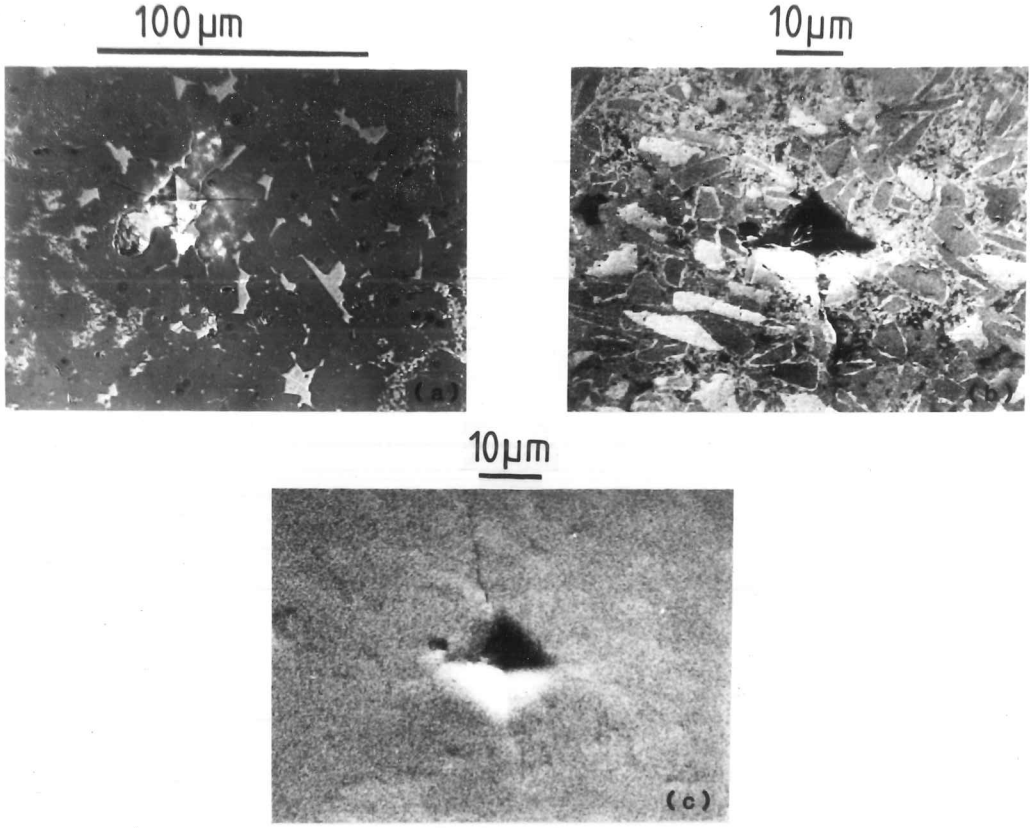

FIGS. 5.1.1.3 Microstructure of REFEL reaction-bonded SiC: (a) optical micrograph; (b) SEM (secondary electron) image; (c) SEM (back-reflected electron) image. Areas of SiC and Si can be distinguished in (a),(b) and (c) (barely). (b) Shows additional contrast, enabling original and new SiC to be distinguished. (b) and (c) show the same area. All indentations are at 500g load.

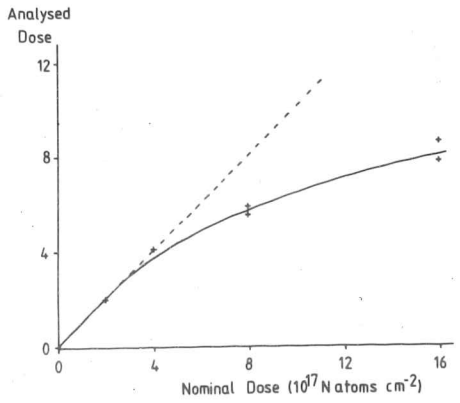

FIG. 5.1.2.1 Comparison of estimated and analysed doses for nitrogen-implanted REFEL. Note divergence from expected values at high doses, due to sputtering.

Young's Modulus	400-430 GPa	[Edington et al. (1975a)]
Poissons ratio	0.24	[Edington et al. (1975a)]
Density	3.12 gcm^{-2}	[Edington et al. (1975a)]
Tensile Strength	203 MPa	[Edington et al. (1975a)]
K_{Ic}	4-5 $MPam^{1/2}$	[Edington et al. (1975b)]
Microhardness (1kg)	2400 $kgmm^{-2}$	[Naylor and Page (1979)]

The REFEL used in this study was cut from a bar supplied by UKAEA (Springfields, UK), and polished to a 1/4μm finish as described in section 4.3. Its indentation plasticity and fracture and single-point-scratch behaviour were studied as a function of dose of N_2^+ ions (see following sections).

5.1.2 Specimen Implantation, Analysis and Sputtering

Specimens of single crystal (0001) SiC (which will be referred to simply as SiC) and REFEL were cut and polished as described in sections 5.1.1 and 4.3. Implantation was performed at AERE Harwell using the 'Pimento' machine for the nitrogen implantation (see 4.1.1) and the Harwell-Lintott machine for boron implantation (see 4.1.3). In addition, some REFEL specimens were implanted using the Cockcroft-Walton machine (see 4.1.2). Doses were from 10^{17} to 1.6×10^{18} ions cm^{-2}. The nitrogen implantations were performed over a period of approximately a year, as gaps in the data were found. During this period, the problems with dose control for the 'Pimento' machine became apparent, and analyses of a representative series of samples were performed (see 4.2). Not all samples could be analysed, because of time restrictions on the use of the Harwell 6MeV Van-der-Graaf facility for (d,α) analysis. Results are shown in fig. 5.1.2.1.

It can be seen that athough the analysed dose corresponds well to the estimated dose at low dose levels, there is a steady divergence between the two as the dose increases. The simplest interpretation of this is that surface sputtering at the higher doses has removed some of the previously implanted nitrogen along with the silicon carbide matrix. Examination of heavily implanted samples (see fig. 5.1.2.2) shows their

FIG. 5.1.2.2 SEM (secondary electron) image of REFEL surface implanted to $8 \times 10^{17} N_2^+ cm^{-2}$. Note surface dimpling due to sputtering. The silicon areas are just distinguishable. Indentation is at 1kg load.

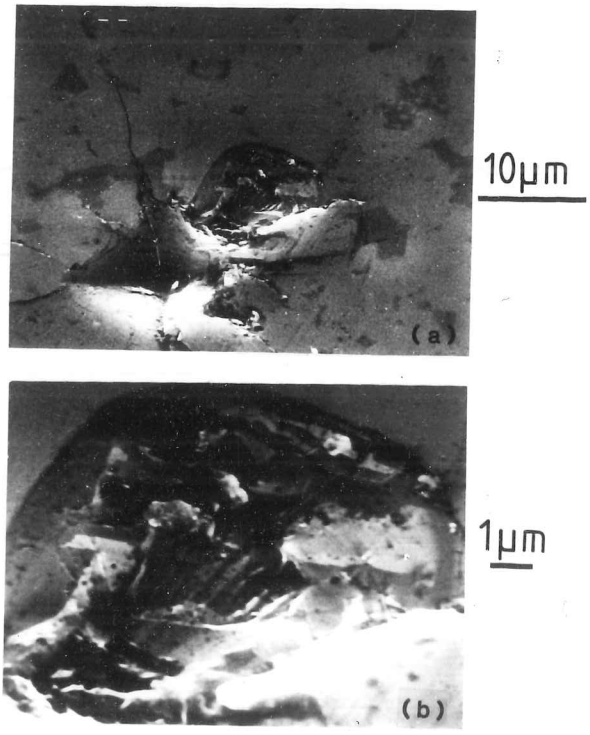

FIGS. 5.1.2.3 Suppression of 'REFEL contrast' by low-dose implantation ($2 \times 10^{17} N_2^+ cm^{-2}$). SEM (secondary electron) images: (b) shows a close-up of the lateral crack in (a). REFEL contrast can be seen right up to the crack edges; the contrast suppression is a very shallow effect.

surfaces to be severely pitted as a result of sputtering.

Given a few simple assumptions about the implantation process, the sputtering rate can be estimated. For the samples of dose $8 \times 10^{17} N_2^+$ cm^{-2}, half of the implanted nitrogen has been sputtered away. If it is assumed that the peak of the nitrogen depth distribution in silicon carbide is at roughly the same depth as it is in silicon (~0.3μm), and that the distribution is roughly symmetrical, then the specimen has had roughly this amount of material removed. In fact, this must be an underestimate of the removal rate, as the implantation penetrates deeper with respect to the original surface as this surface is sputtered away. A more detailed knowledge of the precise shape of the ion distribution curve, and rather more complete analysis data would be required for a better estimate of the sputtering rate. The estimated rate is equivalent to the removal of 3.75 $Å^3$ of SiC, or approximately 2 SiC units, per incident ion. The number of atoms displaced per (di)nitrogen ion is about 200 (see 2.1.3), ie. 100 SiC units. Thus, for the observed sputtering rate, 2% of the displaced atoms escape the surface; this seems quite credible.

Despite the above, all doses quoted later in this report will be those estimated from implantation rates, etc, and not estimated sputtering-corrected doses. This is because it is the implanting dose, rather than the final ion concentration, which is relevant to the actual preparation of the samples. If a knowledge of the actual dose is required, it can be estimated from fig. 5.1.2.1.

The data above shows that within the dose range required for 'mechanical effect' studies, sputtering can have a significant effect on ion concentration and surface finish. Extrapolation of fig. 5.1.2.1 indicates that sputtering will cause saturation of implantation effects at doses $\gtrsim 5 \times 10^{18}$ cm^{-2}.

REFEL Contrast and Implantation

This type of contrast, observable in the secondary electron imageing of uncoated REFEL specimens by SEM, was first described by Sawyer and Page (1978). The original grit particles and the epitaxial SiC are clearly distinguishable (see fig. 5.1.1.3). Sawyer and Page attributed this difference in secondary electron emission coefficients to the different impurity levels in the two materials, the impure original grit material having a large number of available electron-trapping states in the band gap.

At doses lower than any used in this study, the effect of implantation on either the crystal structure or the impurity levels overwhelms the small purity differences that give rise to the 'REFEL contrast'. Fig. 5.1.2.3a shows a secondary electron image of REFEL implanted to $10^{17} N_2^+$ cm^{-2}; no contrast can be observed within the SiC phase. The effect is, however, shallow - the normal contrast can be observed in the bases of lateral fracture around indentations (see fig. 5.1.2.3b).

5.1.3 Microhardness Testing of Nitrogen-implanted SiC Materials

Microhardness tests were performed as described in section 4.4.1. A load range of 50-1000g was used; on the single-crystal specimens the indenter (Vickers profile) was aligned with the growth facets so that one diagonal was parallel to <11$\bar{2}$0>. Five indentations were made at each load, and the resultant diagonal measurements analysed using the computer program described in section 4.4.1. The indentation fracture behaviour was also studied, and is described in section 5.1.4.

The results are shown in figs. 5.1.3.1 (REFEL) and 5.1.3.2 (SiC). These comprise plots of (a) hardness at 1kg load, (b) hardness normalised to a 10μm indentation diagonal and (c) Meyer index, against nominal dose. It can be seen that:

i) The hardness variation with dose follows the same pattern in the single crystal and the reaction-bonded materials.

ii) The 1kg hardness does not change significantly with dose of

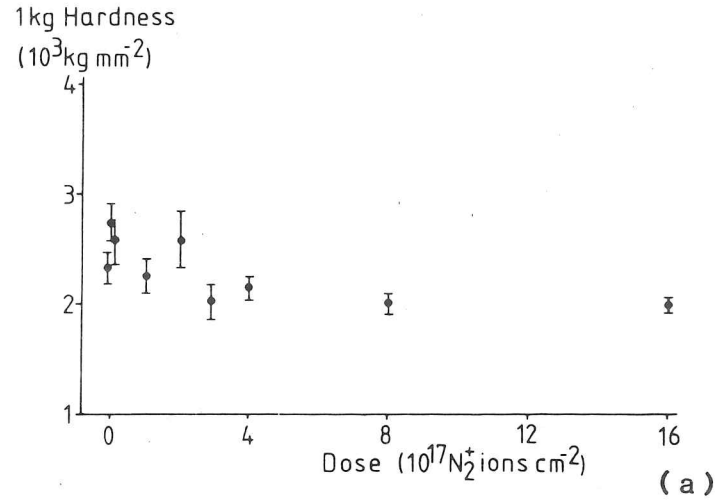

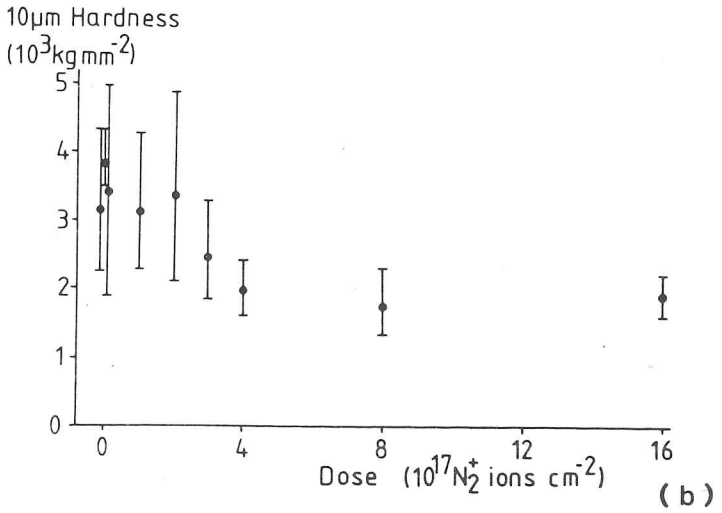

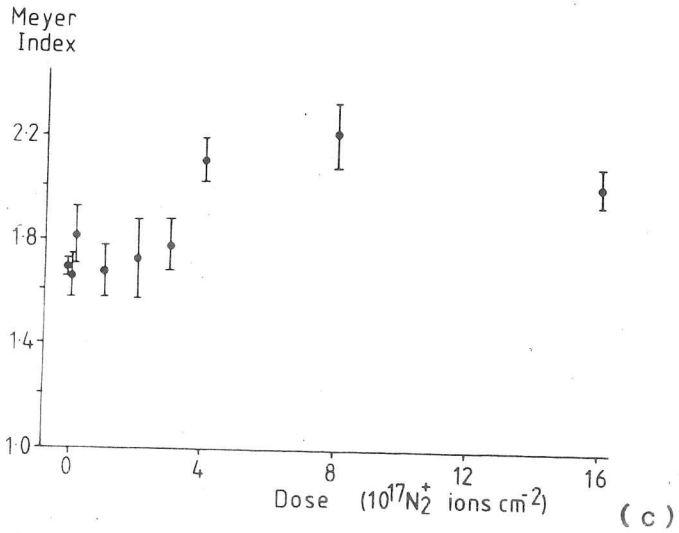

FIGS. 5.1.3.1 Indentation size effect (ISE) behaviour of nitrogen-implanted REFEL: (a) Hardness at 1kg load; (b) Hardness at 10μm diagonal; (c) Meyer (ISE) index. Note the surface softening above a dose of ~$4 \times 10^{17} N_2^+$ cm^{-2}. Error bars: (a),(b), 2σ; (c), 3σ.

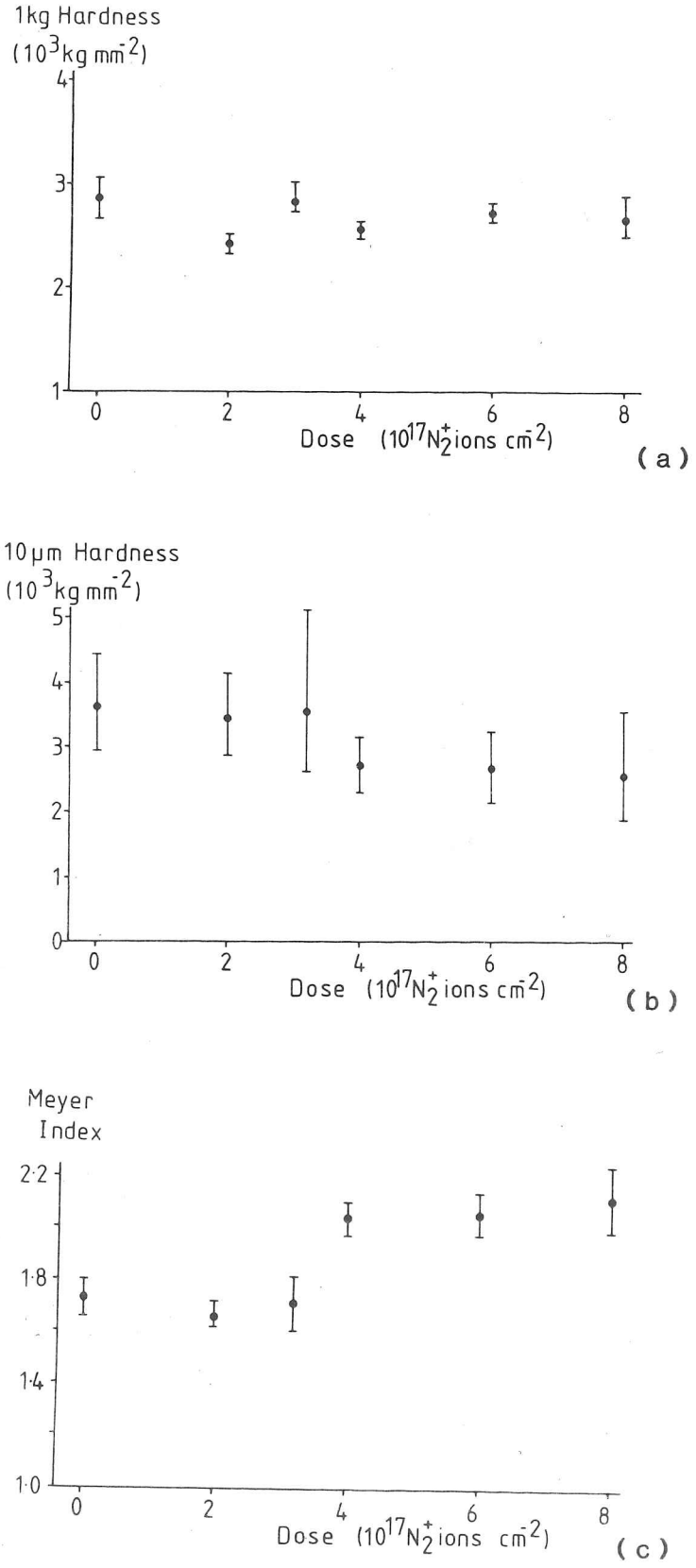

FIGS. 5.1.3.2 ISE behaviour of single crystal (0001) SiC: (a) Hardness at 1kg load; (b) Hardness at 10μm diagonal; (c) Meyer (ISE) index. Note surface softening at doses greater than ~$4\times10^{17}N_2^+$ cm^{-2}. Error bars: (a),(b), 2σ; (c) 3σ.

nitrogen.

iii) The 10μm hardness decreases at doses greater than ~$4 \times 10^{17} N_2^+$ cm^{-2}. This change in behaviour occurs over a narrow dose range.

iv) The plot of Meyer index against dose shows that this parameter (which is derived from all the hardness data for each specimen) is a sensitive indicator of changes in hardness behaviour induced by implantation.

The Meyer index change, from ~1.7 (low dose) to ~2.1 (high dose) implies that the ISE behaviour has changed from the normal case of hardening with decreasing load to a softening with decreasing load (see also figs. 4.4.1.1). The effect occurs at a 'critical dose' of ~$4 \times 10^{17} N_2^+$ cm^{-2}, and low dose specimens behave indistinguishably from zero-dose specimens in microhardness tests. The changes in indentation diagonal at low loads are quite marked, eg:

	Indentation diagonal at 50g load (μm)	
Dose ($10^{17} N_2^+$ cm^{-2})	zero	8
(0001) single crystal	4.4 ±0.4	6.8 ±0.6
REFEL	4.8 ±0.5	7.7 ±0.7

Implantation with nitrogen has dramatically changed the yielding and/or flow characteristics of silicon carbide. The effects observed are large, even though the 'plastic zone' associated with even the smallest indentation used is much deeper than the ion range. The plastic zone depth for a 10μm diagonal indentation in SiC is certainly at least 10μm (see micrographs of broken open indentations in section 5.1.4), and has been estimated by Lankford and Davidson (1979) to be ~25μm. The peak ion range is approximately 0.3μm. These figures imply that either:

i) The implantation-affected depth may be much greater than the projected ion range;

or ii) The softening effect of the nitrogen within the thin implanted layer may be extremely large.

Each of these two possibilities is considered in more detail below, and the microhardness results are also further discussed in 5.1.8 and chapter 6.

i) Enhanced Range Effects

TEM studies of silicon, in which a similar range distribution of 100keV N_2^+ would be expected, show that the thickness of the amorphised layer is ~0.5μm (see 5.2.7). If it is assumed that the large change in hardness values for comparatively large indentations is due to an effective increase in implanted layer depth, several possible mechanisms exist for this:

a) The small amount of nitrogen in the 'tail' of the ion distribution may be effective in altering the flow characteristics, possibly by electronic doping effects [eg. Hirsch (1981)].

b) If the nucleation of yield mechanisms were easier in the implanted layer (ie. during the inital stages of indentation), this might be reflected in subsequent yield and flow behaviour. Since initiation of flow in the initial stages of sharp indentation is not difficult (see 3.2), such a mechanism is not likely to be effective unless the type of deformation behaviour is changed, eg. from (predominantly) dislocation flow to a phase change (see section 5.1.7).

c) A mechanism could exist similar to that suggested by Dearnaley and Hartley (1978) whereby dislocation motion away from the surface carries implanted ions, by 'Cottrell atmosphere' drag, into the bulk. The experimental conditions (pin-on-disc wear tests) for which this mechanism was postulated, with its associated high surface temperatures and slow inward progress from the surface, are rather different from the low-temperature, high strain-rate conditions of the microhardness test, and so such processes would not be expected. Furthermore, the presence of Cottrell atmospheres of implanted nitrogen around dislocations would imply that a hardening effect should occur, whereas in fact the reverse effect is observed.

ii) Large Property Changes

If the softening effect of the implantation is confined to a thin layer, then a simple 'weighted mean hardness' approach (after Sargent (1979)) can yield approximate estimates of the hardness in the layer. The measured hardness is assumed to be the mean of the values for the bulk and

the layer, weighted by the volume of each in the plastic zone associated with the indentation:

$$H = (H_{imp}V_{imp} + H_{bulk}V_{bulk})/(V_{imp} + V_{bulk}) \qquad 5.1.3a$$

ie. $$H_{imp} = [(V_{imp} + V_{bulk})H - H_{bulk}V_{bulk}]/V_{imp} \qquad 5.1.3b$$

For a 10μm diagonal indenter, if the plastic zone volume is taken to be that of a square pyramid of base side 10μm and height 10μm to 30μm, then $V_{imp}=50\mu m^3$ and $V_{bulk}=350-1000\mu m^3$. For SiC at a dose of $8x10^{17}N_2^+$ cm^{-2}, $H_{10\mu m}=2500$, $H_{bulk}=2700$. These give values of H_{imp} between -1500 and 1100 $kgmm^{-2}$. The first of these values is clearly nonsensical; in fact the model is unreliable for a number of reasons:

a) The indentation stress field is not uniform over the plastic zone, and so a simple weighting of yielded volumes is an over-simplification;

b) Effects of work-hardening on flow stress are not taken into account;

c) The implanted volume is not a simple homogenous layer in terms of structure or composition, and therefore probably not in its mechanical behaviour;

d) The model is invalid for cases (such as here) where a very weak layer covers a very strong material. For example, in the limiting case of a material with a zero yield strength covering one of very high yield strength, no indentation would have a diagonal less than 1/7 of the layer thickness. Sargent (1982) has pointed out that this type of analysis, applied to the data for implanted SiC, implies a non-zero hardness for the implanted layer. Extrusion pile-up of the softer material may also complicate measurements.

However, SEM and optical observations of indentations in REFEL and SiC implanted to high doses show that some pile-up has occurred (see figs. 5.1.3.3 and 5.1.4.6). A close examination shows that this pile-up is of a thin surface layer which occasionally breaks away from the substrate, and can be lost altogether. At lower doses, no such pile-up occurs, and the indentation edge is fractured (see 5.1.4(vi)). These observations are consistent with the existence, above the 'critical dose', of a thin, highly plastic surface layer. The incompatibility between the flow properties of this layer and those of the bulk is enough to cause them to separate in

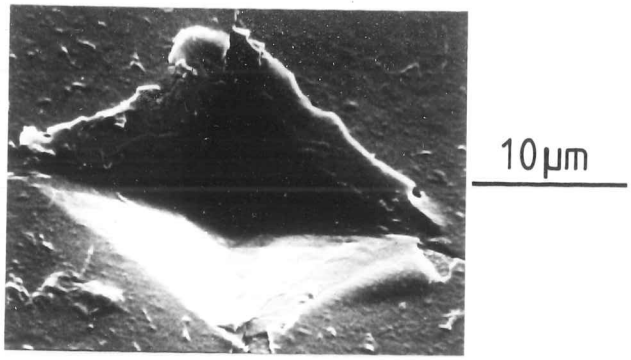

FIG 5.1.3.3 1kg indentation in SiC implanted to $8x10^{17}N_2^+$ cm^{-2}. SEM (secondary electron) image. Note pile-up and partial exfoliation of a thin surface layer.

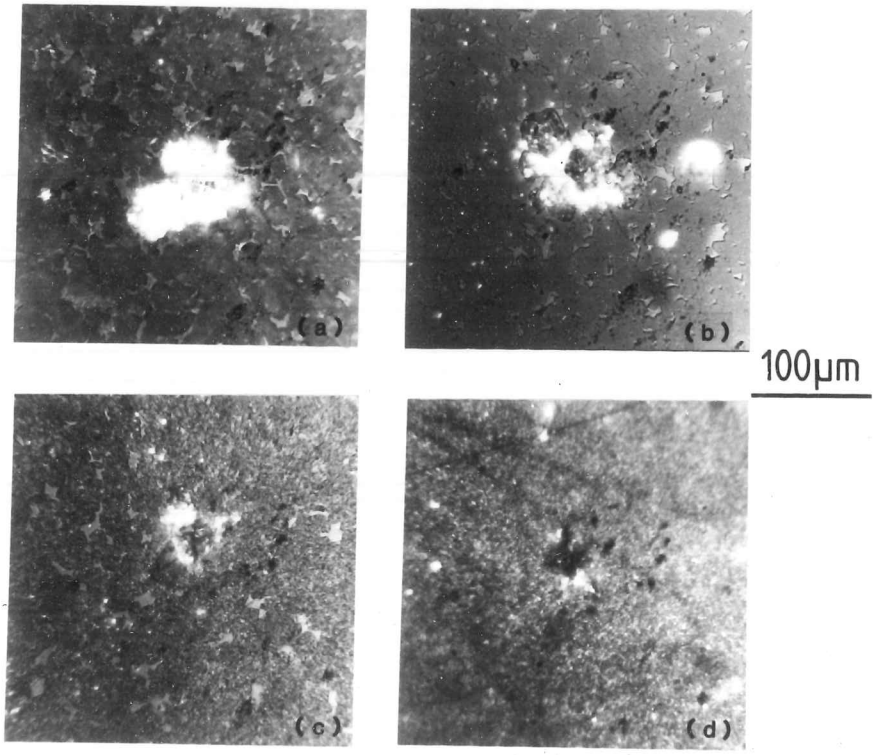

FIGS. 5.1.4.1 1kg indentations on REFEL: (a) Unimplanted; (b) $2x10^{17}N_2^+$ cm^{-2}; (c) $4x10^{17}N_2^+$ cm^{-2}; (d) $8x10^{17}N_2^+$ cm^{-2}. Optical micrographs, polarised light. Note progressive reduction in lateral cracking with increasing dose.

places.

In summary, while the surface softening in these materials is substantial, and phenomenologically quantifiable by, eg., the Meyer index changes, no detailed conclusions can be drawn from the microhardness data alone regarding the yield and flow processes in the implanted layer. So as to examine the possible effects of semiconductor-type doping on plastic flow, experiments were carried out using a different ion species, boron,(see 5.1.6). Also, the structures of implanted and/or deformed SiC were examined in the TEM (see 5.1.7).

5.1.4 Indentation Fracture of Nitrogen-implanted SiC Materials

Nitrogen implantation to high doses was found to have pronounced effects on the fracture behaviour of brittle solids (see also 5.1.5, 5.2.3, 5.2.4, 5.4.4; indentation fracture behaviour is described in section 3.2.2). The effects in the two SiC materials were similar; the incidence of 'broken-out' lateral fracture was suppressed by implantation, while median/radial fracture was not noticeably affected. In the unimplanted state, both materials showed such fracture at loads greater than ~100g. The single crystal material ('SiC') showed less tendency than the REFEL to form lateral cracks around indentations. This is probably due to the alignment of easy (0001) fracture planes parallel to the surface, thus requiring stepping from one such plane to another for breakout to occur (but see results in 5.1.6). In REFEL, the random alignment of fracture planes (both inter- and intra-granular) with the surface increases the likelihood of an easy fracture path being available for breakout.

A variety of techniques were used to observe the fracture behaviour of these materials, and results are listed below:

i) Visible lateral fracture became increasingly suppressed as the dose increased from 10^{17} to ~$10^{18} N_2^+$ cm^{-2}, as can be seen in figs. 5.1.4.1 (REFEL) and 5.1.4.2 (SiC). At the highest doses, no such fracture can be seen. However, observation of the surface alone cannot distinguish easily between the cases of cracks being totally absent and cracks being present but failing to break out.

ii) Observation of unimplanted SiC by light microscopy showed subsurface lateral fracture as a 'halo' surrounding ~200g to 1kg indentations (see fig. 5.1.4.2a). The halo is split into four segments by the median/radial cracks; occasionally one segment of the halo is missing. Observation through crossed polars renders the halos more visible (see figs. 5.1.4.3). These halos are not visible in heavily implanted samples. This may, however, be due to an implantation-induced change in the optical properties of the near-surface layer rather than to a change in the subsurface lateral fracture behaviour, particularly as halos are still not visible in the lower dose specimens where fracture still occasionally breaks out, and as it was observed that all implanted specimens had a higher reflectivity than unimplanted ones.

iii) Observation by the Nomarski differential interference contrast technique can reveal the presence of subsurface fracture by changes in surface tilts. This technique shows the suppression of such fracture in REFEL with increasing dose (see figs. 5.1.4.4)

iv) Subsurface lateral fracture in SiC was also investigated by the technique of breaking open indentations (see 4.4.2). Results from the examination of such specimens in the SEM are shown in figs. 5.1.4.5. Specimens used were of doses of zero, 4 and $6 \times 10^{17} N_2^+$ cm^{-2}. It can be seen that:

a) There is a progressive change in lateral crack type and occurrence as dose increases. In unimplanted specimens, lateral fracture is easily observed on both sides of the indentation, often at several levels, and occasionally breaks out into the surface. In the $4 \times 10^{17} N_2^+$ cm^{-2} specimen, there is usually at least one lateral crack visible; however, these normally propagate well below the surface, some actually being directed away from it. In the $6 \times 10^{17} N_2^+$ cm^{-2} specimen, very little lateral fracture can be seen at all. The observable cracks are all short and closely associated with the highly disturbed zone immediately beneath the indentation, and breakout does not occur.

b) Samples of all doses show the 'classic' median/radial fracture patterns to some extent. However, some indentations show an obvious central penny-shaped crack, while in others there appear to have been separate crack nucleations on either side of the indenter. Both types show distinguishable extensions to the surface, probably occurring both on

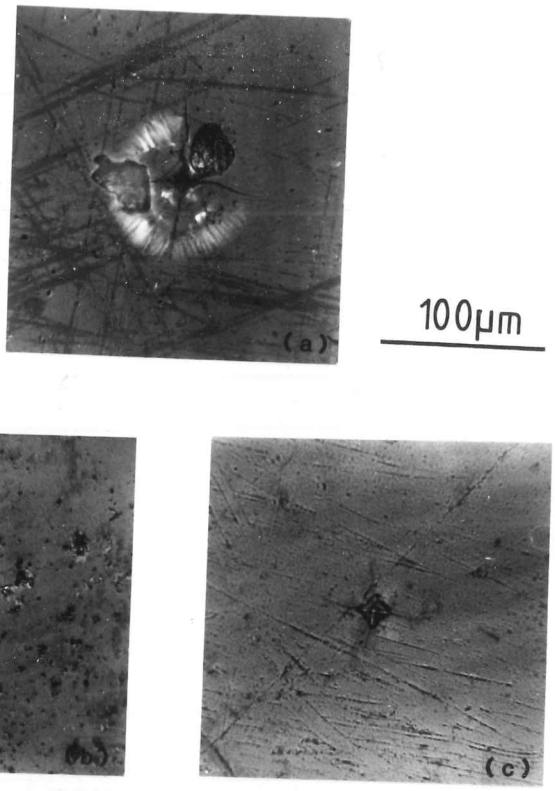

FIGS. 5.1.4.2 1kg indentations on SiC: (a) Unimplanted; (b) $6x10^{17}N_2^+$ cm^{-2}; (c) $8x10^{17}N_2^+$ cm^{-2}. Optical micrographs. Note obvious subsurface and broken-out lateral fracture in the unimplanted specimen, and lack of lateral fracture in the implanted specimens. Pile-up can be seen at the edges of the indentations in the implanted material.

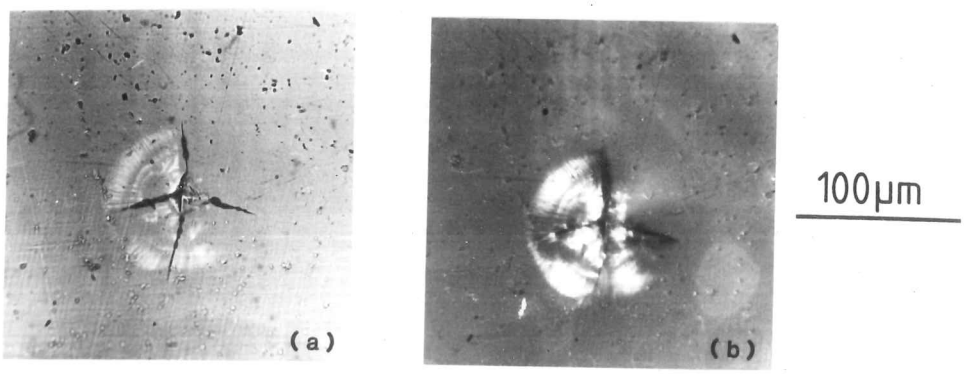

FIGS. 5.1.4.3 1kg indentation on unimplanted SiC. Optical micrographs: (a) Unpolarised light; (b) Polarised light. Note increased visibility of the subsurface lateral cracks when viewed with polarised light.

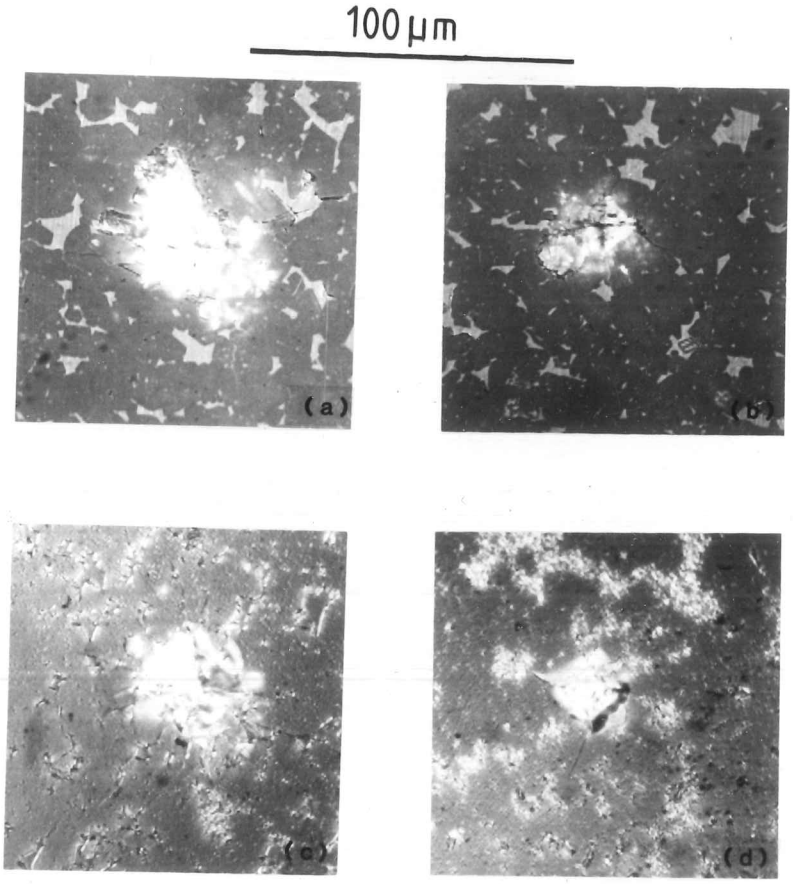

FIGS. 5.1.4.4 Indentations on REFEL. Optical micrographs, Nomarski differential interference contrast: (a),(b) Unimplanted; (c),(d) Dose $4 \times 10^{17} N_2^+$ cm^{-2}; (a),(c) 1kg indentations; (b),(d) 500g indentations. Note suppression of subsurface lateral fracture in the implanted specimen.

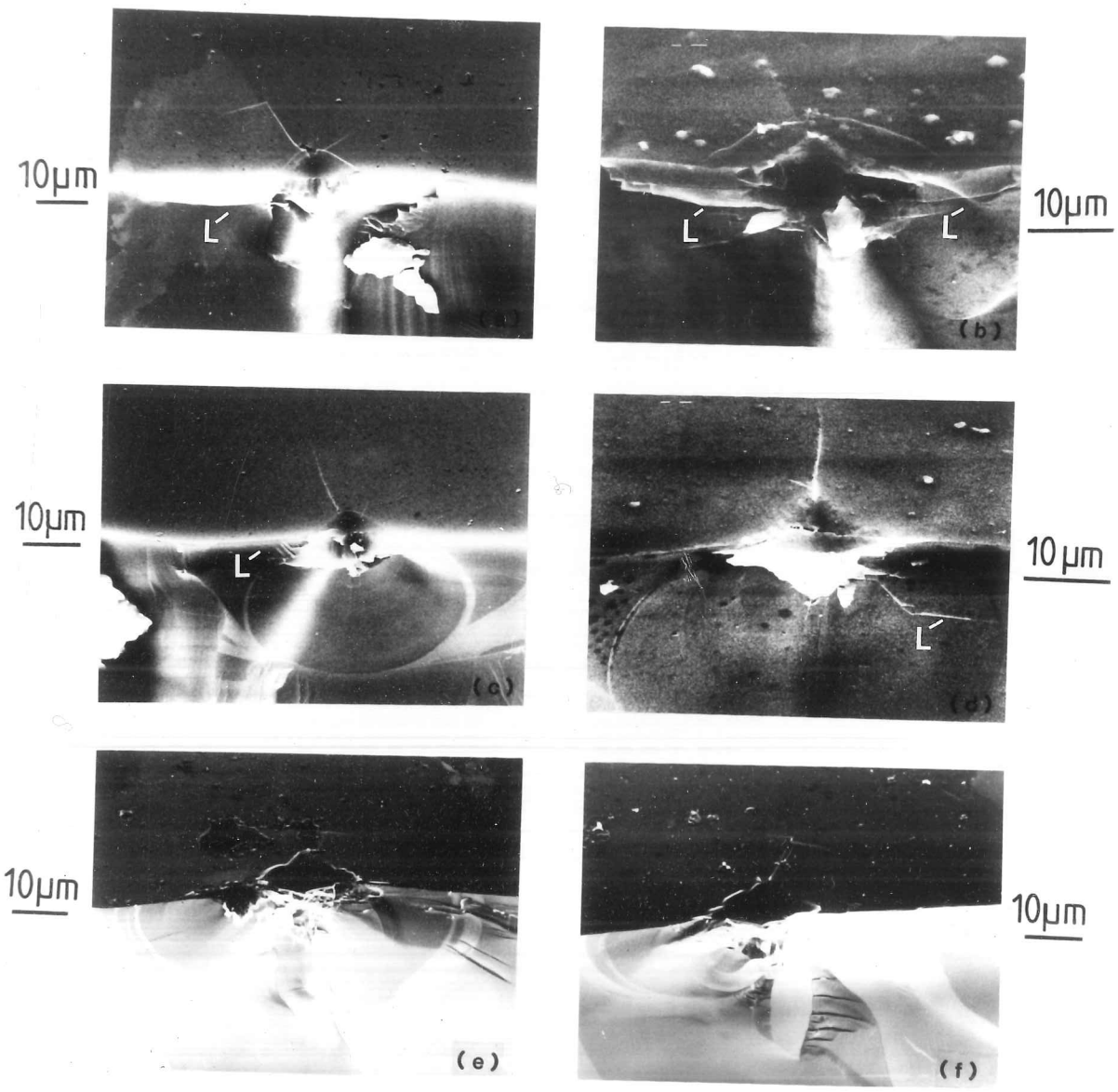

FIGS. 5.1.4.5 Broken-open 500g indentations in SiC. SEM (secondary electron) images: (a),(b),(c) Unimplanted; (d) $4x10^{17}N_2^+$ cm^{-2}; (e),(f) $6x10^{17}N_2^+$ cm^{-2}. Note increasing suppression of subsurface lateral fracture with increasing dose. The shapes of the median/radial cracks can also be seen, as can circum-indentation cracking in (a),(b) and (c), and pile-up in (e) and (f).

unloading the indenter and during the breaking open of the specimen.

c) A highly disturbed region underlies all indentations. No change in character of this region with dose is observable; however, details of the region's characteristics are not easily discernable. The localised linear features might be the remnants of fracture, localised shear or phase transformations, etc. and their appearance is probably altered to some extent by the breaking open of the specimen.

v) Specimens of both materials implanted to doses greater than the critical dose for changes in microhardness behaviour ($\sim 4 \times 10^{17} N_2^+ \text{ cm}^{-2}$) showed evidence of pile-up around indentations. This is illustrated in fig. 5.1.3.3 and figs. 5.1.4.6 and discussed in section 5.1.3.

vi) SEM examination of the surface around high load (500g,1kg) indentations in SiC often showed a type of fracture approximately parallel to the indentation edge and normal to the surface (see figs. 5.1.4.6). The cracks lie along crystallographic directions; the surface intersections are parallel to <11$\bar{2}$0>. The crack planes are therefore of the form {1$\bar{1}$01}, probably {1$\bar{1}$00}. These cracks are only observed around indentations in zero and low dose specimens. At higher doses the pile-up and exfoliation previously described occurs.

Results from fracture in other implanted materials, particularly for boron-implanted silicon carbide (see 5.1.6) imply that indentation and scratch track fracture are chiefly influenced by the stress state introduced by implantation (see 2.2.3). This is discussed in more detail in section 5.1.8 and in chapter 6.

5.1.5 Scratch tracks on Nitrogen-implanted SiC materials

These tracks were made as described in section 4.5.1. 90° diamond cones, and loads of 10, 20 and 50g were used. The tracks were aligned with the <11$\bar{2}$0> directions on the single crystal specimens (ie. parallel to the {1$\bar{1}$00} growth facets); because of bearing looseness, etc. in the scratching equipment, alignment inaccuracies were probably up to ~5°. For most of the scratching experiments (including those in 5.1.6 and 5.2.4), only six fresh, sharp cones were available. Consequently, to ensure consistency of results, the usage of each cone was recorded and the tip sharpness frequently

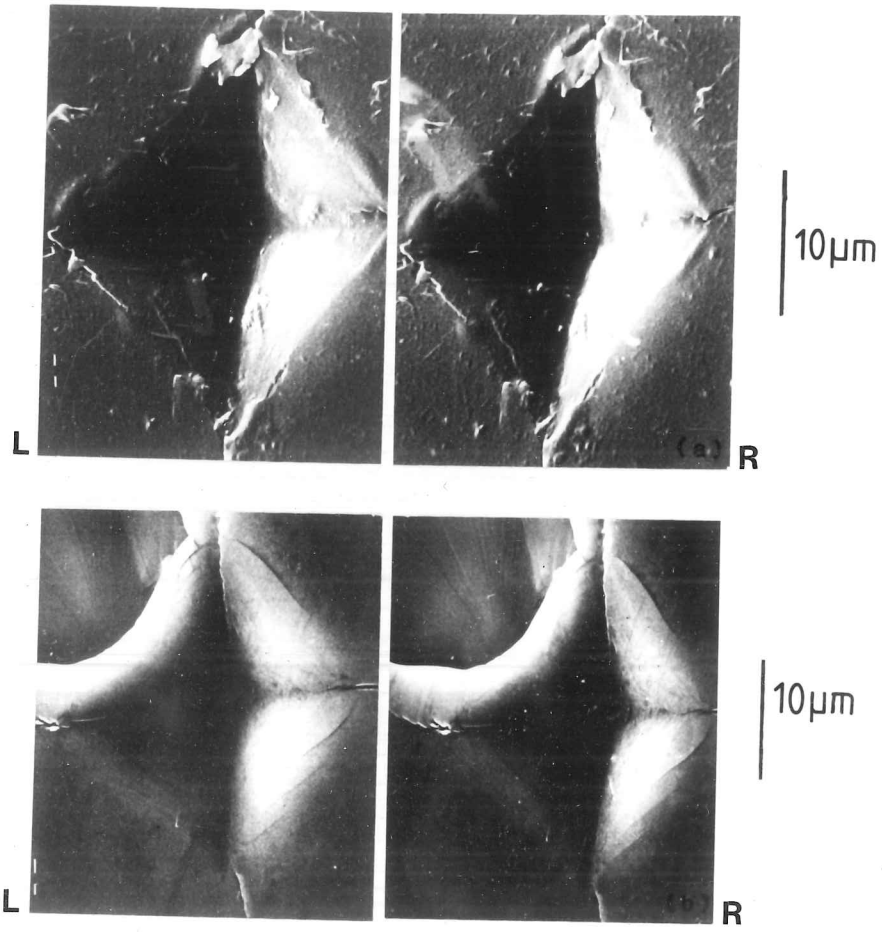

FIGS. 5.1.4.6 SEM stereo pairs (30° & 40° tilts). 1kg indentations on SiC: (a) Dose $6 \times 10^{17} N_2^+ cm^{-2}$; (b) Unimplanted. Note pile-up in (a), and circumferential and lateral cracking in (b).

examined. After each short series of tests on implanted material, a track was made on unimplanted material, so that the effect of cone blunting on track morphology could be distinguished from the effects of implantation. Consistent differences between the behaviour of implanted and unimplanted SiC were seen (see below) once the initial extreme sharpness of the cones had worn off; this occurred after the cones had made about 1/2 mm of track on SiC, during which all samples showed large amounts of chipping fracture.

Tracks were examined by light microscopy and SEM. Debris was removed from the tracks using Bioden RFA replicating plastic. The replicas were examined optically; attempts to examine the debris in the TEM using a two stage carbon replica technique were unsuccessful in the limited time available. Some scratched specimens were back-thinned (see 4.6.1) and examined in the TEM; results from such specimens are reported in section 5.1.7.

Scratch tracks on single crystal SiC were made on specimens covering a dose range of $0\text{-}6\times10^{17} N_2^+$ cm^{-2}. Sideways chipping fracture was found to be suppressed in all the implanted samples (minimum dose $2\times10^{17} N_2^+$ cm^{-2}) at all loads used (10-100g). Even with a very blunt cone, loads as low as 10g produced extensive chipping on unimplanted samples. Typical results are shown in figs. 5.1.5.1. Where chipping is suppressed, the essentially plastic nature of the groove left by the cone can be seen. The track widths appear to be the same (5-7μm for 10g loads) for both implanted and unimplanted samples, but it is difficult to measure the track widths on the highly fractured unimplanted samples accurately.

Because of the limited number of cones available, only a small number of tracks were made on REFEL. Specimens used were of doses of zero, 1 and $8\times10^{17} N_2^+$ cm^{-2}. As with the single crystal material, the unimplanted sample was used as a reference for checking the effects of cone blunting. Tracks on the low dose specimen showed almost no chipping, even at high loads and with relatively sharp diamonds. For the high dose specimen, chipping was similarly absent. Tracks on the unimplanted material showed large amounts of chipping, even at low loads and with blunt diamonds. Typical tracks are shown in figs. 5.1.5.2. Measurement of track widths showed the zero and low dose specimens to have track widths of ~3μm at 10g

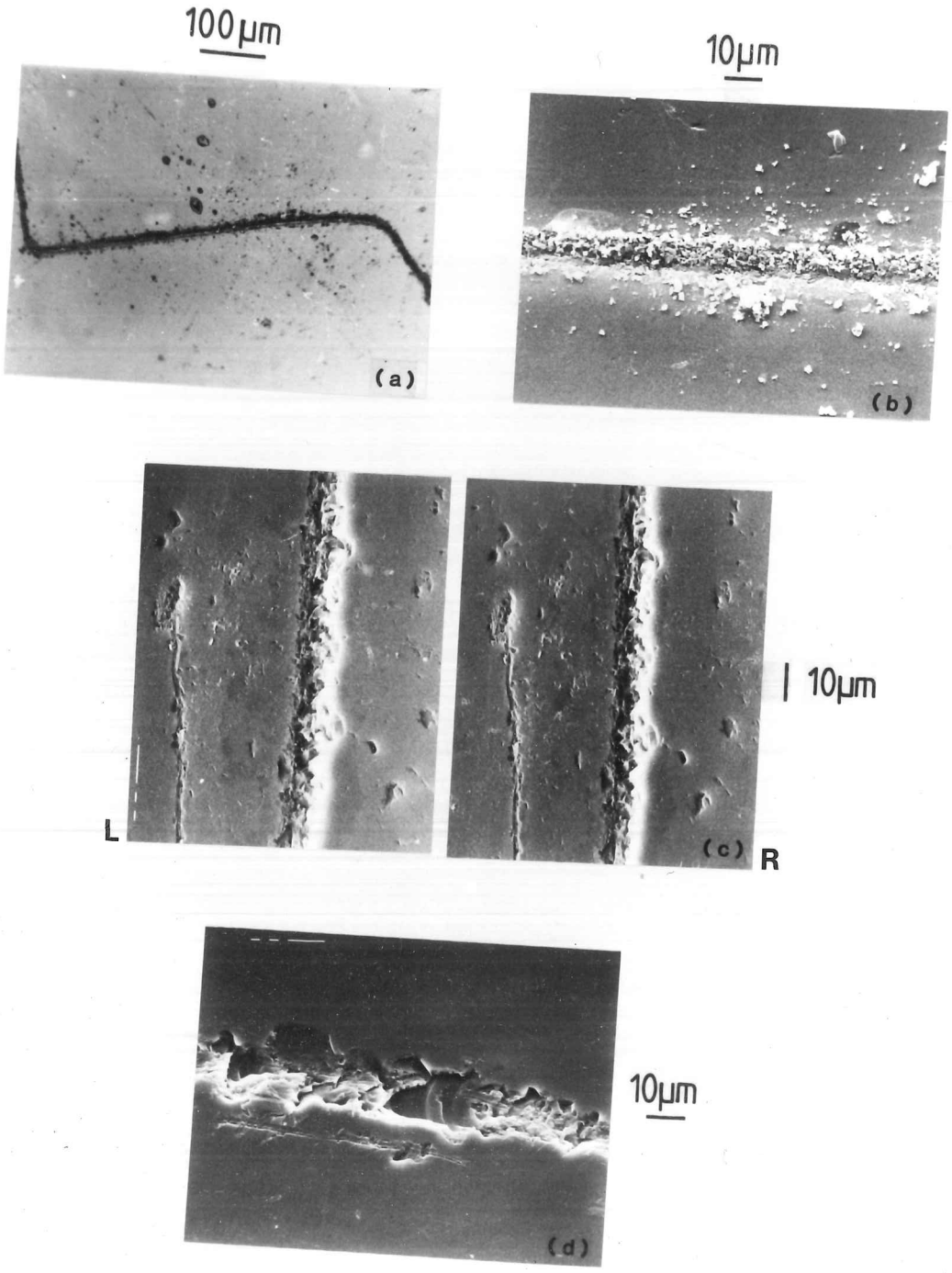

FIGS. 5.1.5.1(a)-(d) Single-point scratch tracks in unimplanted SiC: (a) Optical micrograph, 10g load; (b) SEM (secondary electron) image, 10g load; (c) SEM stereo pair (30^{o}& 40^{o} tilts), 10g load; (d) SEM (secondary electron) image, 100g load. Note substantial chipping at both loads.

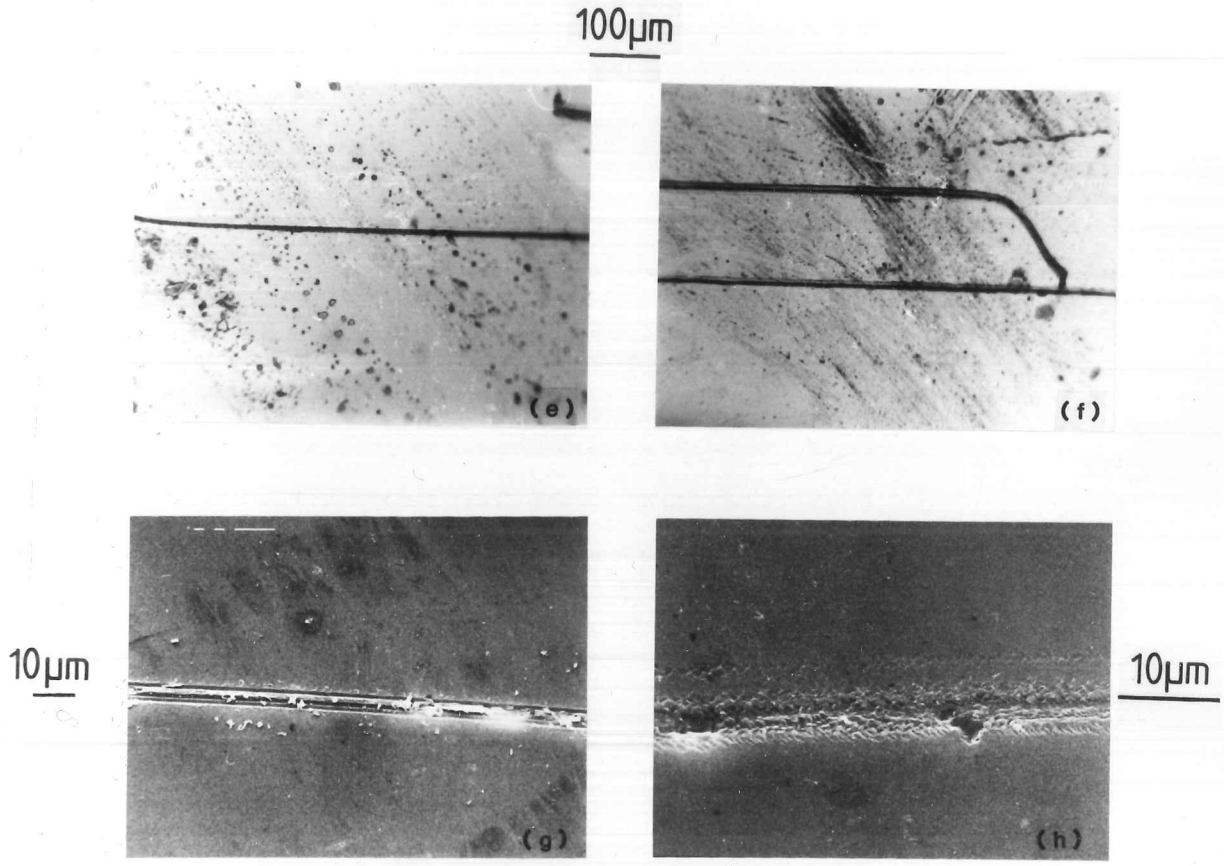

FIGS. 5.1.5.1(e)-(h) Single-point scratch tracks on implanted SiC: (e),(f) Dose $2x10^{17} N_2^+ cm^{-2}$ (optical micrographs); (g),(h) Dose $3x10^{17} N_2^+ cm^{-2}$ (SEM (secondary electron) images). Loads: (e) 10g; (f) 20g and 50g (upper); (g) 10g; (h) 100g. Note lack of lateral chipping at all loads, and the plastic appearance of the wear tracks and debris.

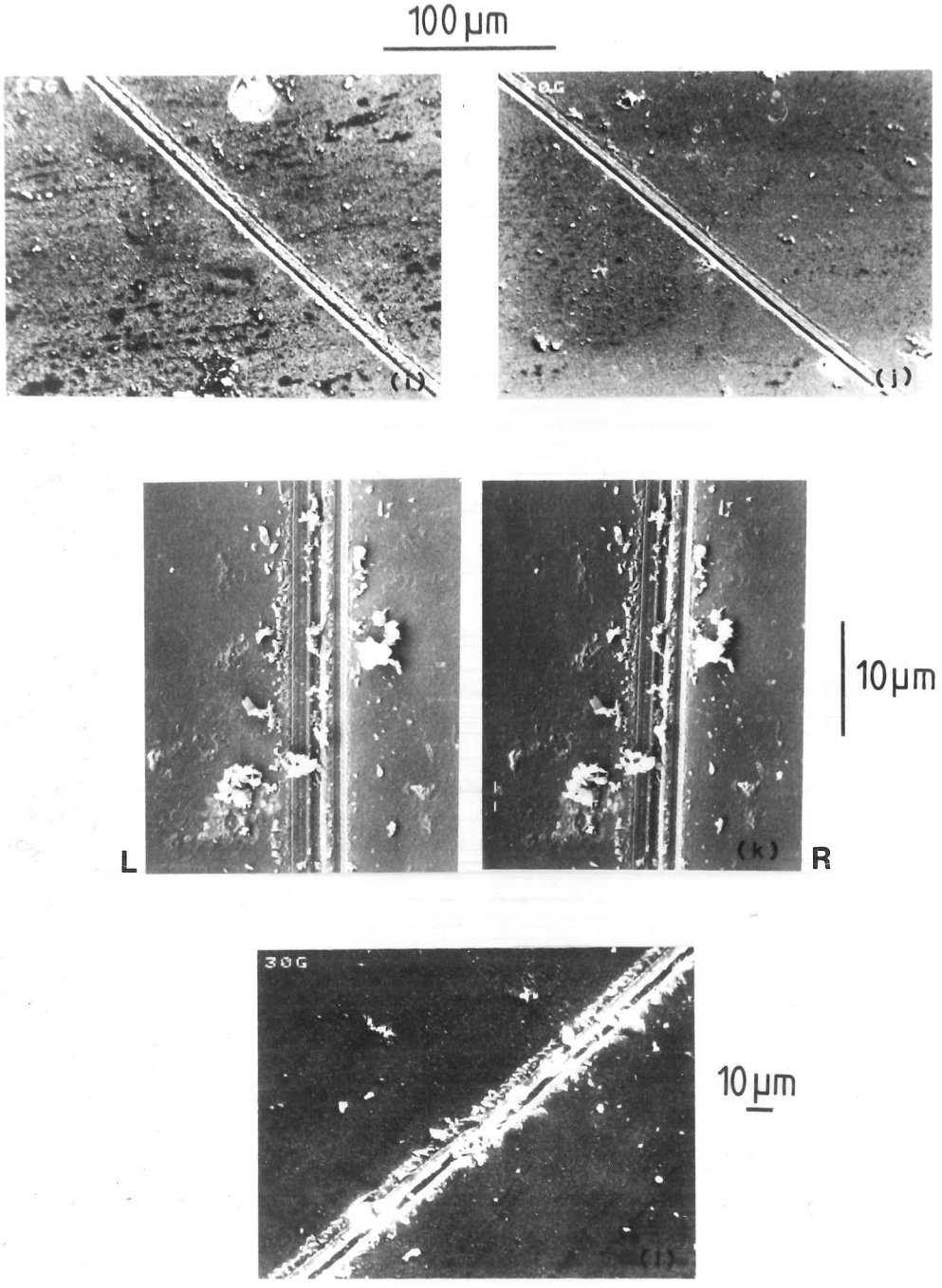

FIGS. 5.1.5.1(i)-(l) Single-point scratch tracks in implanted SiC, dose $6 \times 10^{17} N_2^+ cm^{-2}$. SEM (secondary electron) images: (i) 10g load; (j) 20g load; (k) 20g load, stereo pair (30^o& 40^o tilts); (l) 30g load. Note absence of chipping at all loads and the plastic appearance of the wear tracks and debris.

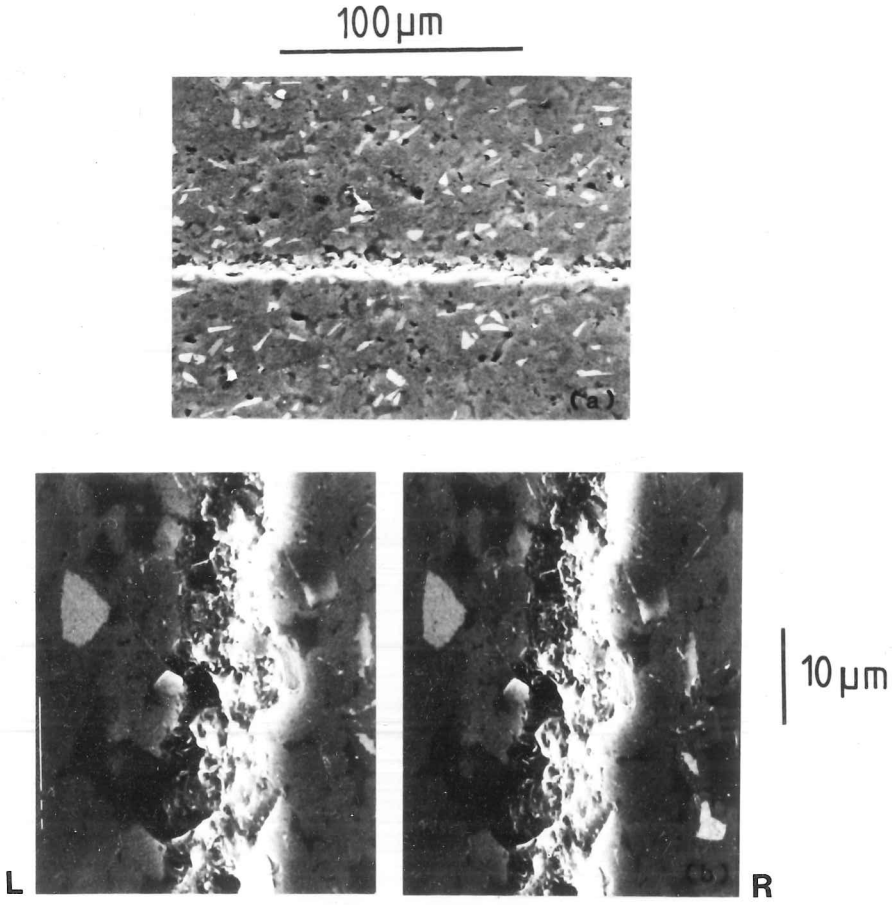

FIGS. 5.1.5.2(a),(b) Single-point scratch track (10g load) in unimplanted REFEL. SEM (secondary electron) images: (b) stereo pair (30° & 40° tilts) of central area of (a). Note trans- and inter-granular chipping.

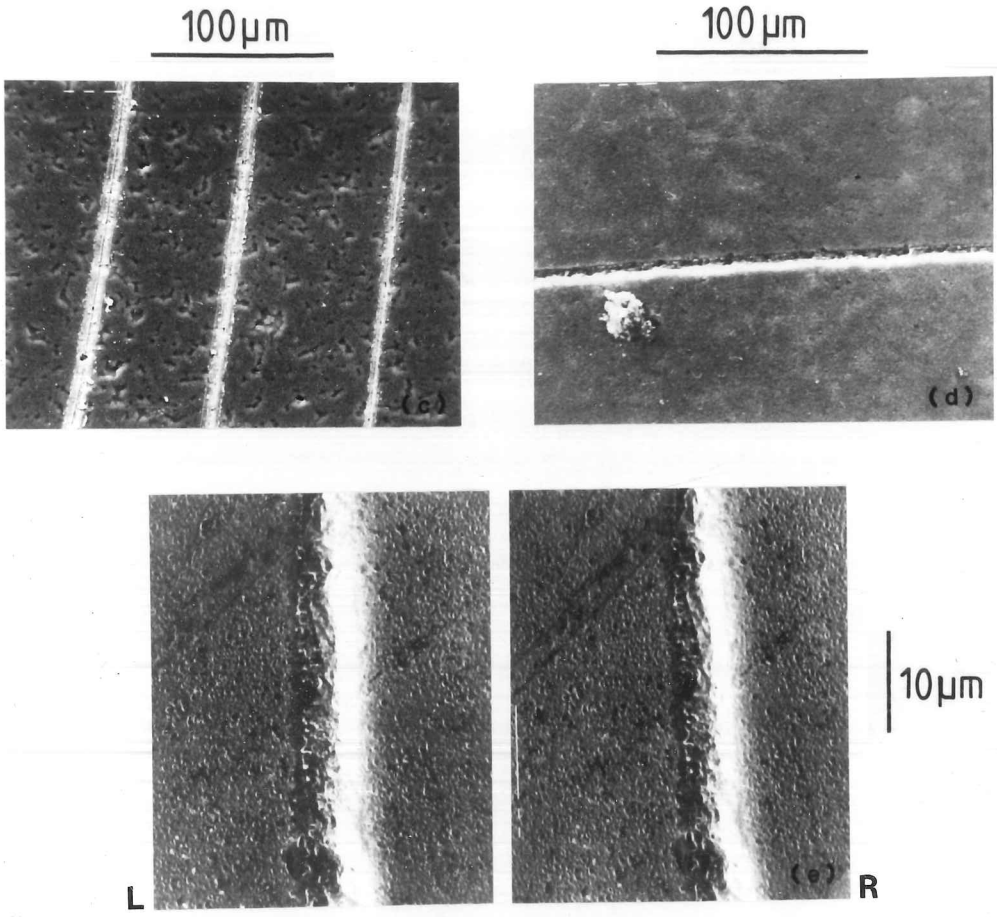

FIGS. 5.1.5.2(c)-(e) Single-point scratch tracks in implanted REFEL. SEM (secondary electron) images: (c) Dose $10^{17} N_2^+$ cm^{-2}, 50g, 20g and 10g loads; (d),(e) Dose $8 \times 10^{17} N_2^+$ cm^{-2}, 10g load. (e) is stereo pair (30^o& 40^o tilts) of central area of (d). Note almost complete suppression of chipping even at low dose and high load.

load, as opposed to ~6μm on the high dose specimen. Since both the implanted specimens behaved similarly as regards near-track fracture, this indicates that the softening caused by implantation is not very significant in altering the fracture behaviour of the material (see also 5.1.6).

5.1.6 Effects of Boron Implantation on SiC

A range of specimens of single crystal SiC was prepared (see 4.1.3) with doses between 2 and $16 \times 10^{17} B^{+} cm^{-2}$. The accelerating voltage used was 40kV, and the ion flux chosen to be the equivalent of that in the nitrogen-implanted samples, ie. $10 \mu A\ cm^{-2}$. If the beam of 80kV N_2^+ is considered as twice the flux of 40kV $N^{0.5+}$, it will be seen that the conditions of implantation are the same in both cases. The N and B atoms differ in atomic number by only 2, and in atomic mass by 3 Daltons. The final characteristics of the implanted layer would therefore be expected to be similar in both cases, the only differences being:

i) N is an n-dopant in SiC and B a p-dopant;

ii) N is thought to stabilise the β, and B the α, form of SiC. (see 5.1.1.i)

The specimens were tested in similar ways to those implanted with nitrogen - ie. by microhardness testing, SEM and optical observation of indentations and scratch tracks, and by TEM examination of scratched specimens.

i) Results of Microhardness Tests

The load range used was 50-500g, as the samples were too thin to withstand 1kg loads. The data were analysed by the program described in section 4.4.1. Results of these analyses are shown in figs. 5.1.6.1. It can be seen that neither the 10μm hardness nor the Meyer index change significantly over the dose range used.

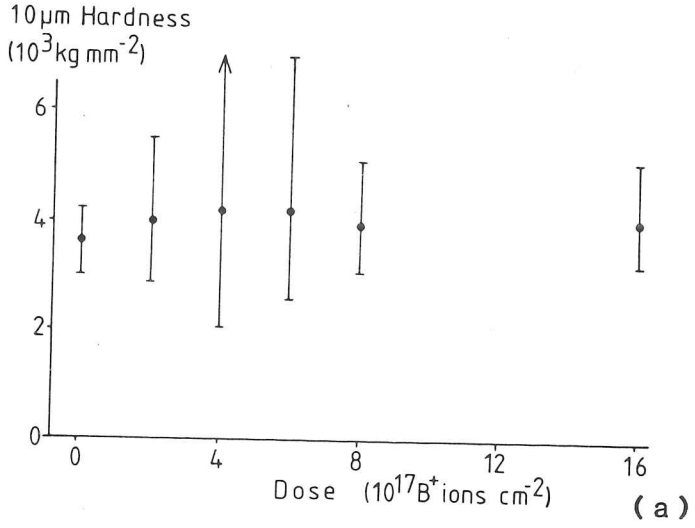

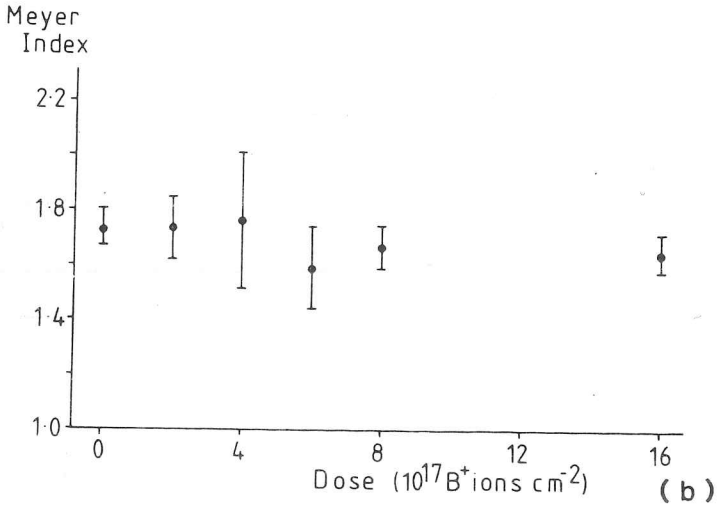

FIGS. 5.1.6.1 ISE behaviour of boron-implanted SiC: (a) Hardness at 10μm diagonal (2σ erorr bars); (b) Meyer index (3σ error bars). No significant change in behaviour occurs with increasing dose.

ii) Optical and SEM examination of Indentations

No lateral breakout was observed in the $16x10^{17}B^{+}cm^{-2}$ specimens, and only a little around indentations on the $8x10^{17}B^{+}cm^{-2}$ specimens (see figs. 5.1.6.2) The appearance of the indentations on the lower dose specimens was not photographed immediately they were performed, and after an interval of about 4 months, a type of corrosive attack of the surface was noticed, which obscured the near-indentation topography. This effect is described at the end of this section.

SEM examination of the high dose specimens showed no pile-up or 'extrusion' of the type noted in the nitrogen-implanted samples. The cracking near to and parallel to the indentation edges appeared somewhat, but not totally, suppressed at these high doses. The indentations appeared slightly 'pin-cushioned' compared to indentations on unimplanted material (see fig. 5.1.6.2c, d). Signs of sputtering were visible on the sample surfaces of roughly the same severity as those on equivalently dosed N_2^+ samples.

In order to investigate the possible existence of subsurface lateral cracks in the high dose specimens, a broken-open specimen of 500g indentations on $16x10^{17}B^{+}cm^{-2}$ material was prepared, and examined in the SEM. Some typical results are shown in figs. 5.1.6.3. It appears that the plane of the specimen's surface was cut slightly inclined to the (0001) plane, since all lateral fractures visible beneath the surface were tilted at about 10^{o} to it. This was quite useful, since it can be seen that the downward arm of the lateral cracks (which were found beneath all indentations) extend to some distance away from the indentations, whereas the upward cracks stop, or in some cases are diverted, as they approach the surface. This indicates that there is some property of the implanted layer which tends to prevent cracks from approaching it. Since the influence seems to be effective ~3μm beneath the surface, it is likely to be associated with the implantation-induced stress field rather than with the surface microstructure.

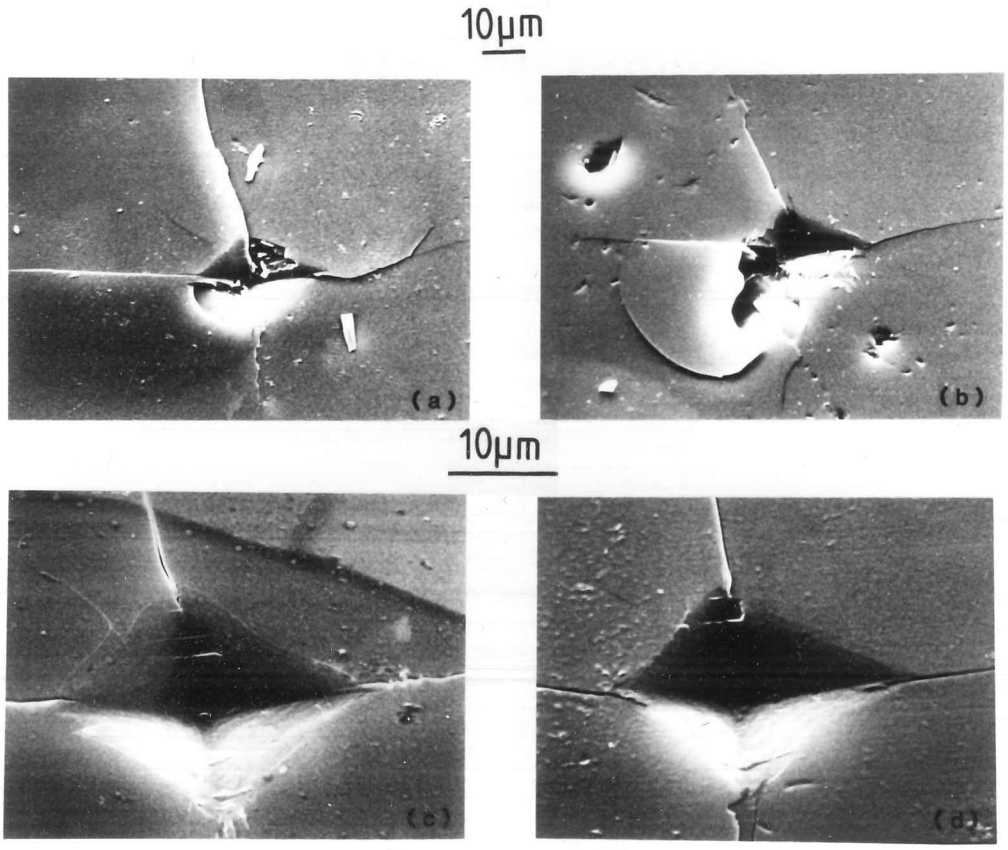

FIGS. 5.1.6.2 1kg indentations on boron-implanted SiC. SEM (secondary electron) images: (a),(b) Dose $8 \times 10^{17} B^{+}$ cm^{-2}; (c),(d) Dose $16 \times 10^{17} B^{+}$ cm^{-2}. Note suppression of lateral fracture at the highest dose.

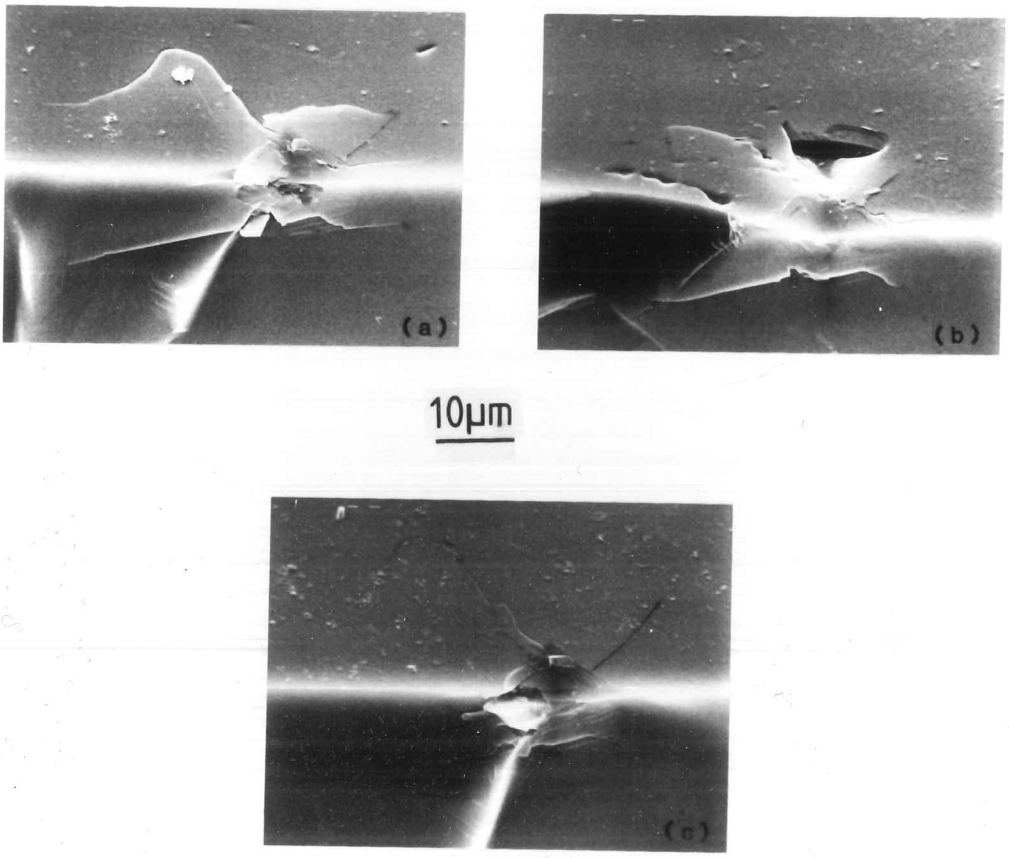

FIGS. 5.1.6.3 Broken-open 500g indentations on boron-implanted SiC, dose $16 \times 10^{17} B^{+}\ cm^{-2}$. The (0001) fracture plane appears to be inclined by $\sim 10^{\circ}$ to the surface. Note the stopping or diversion of the upward arms of the cracks.

iii) Scratch tracks in Boron-implanted SiC

Tracks using 90° diamond cones were made on the high dose specimens, and on a clear area of the $2x10^{17}B^+cm^{-2}$ specimen. Again, an unimplanted sample of SiC was used as a reference to check the sharpness of the cone. Loads of 10, 20 and 50g were used. On all the implanted specimens, all tracks appeared as purely plastic grooves; vitually no chipping was seen at any load or dose. The zero-dose reference sample showed chipped tracks at all stages of the tests. Typical results are shown in figs. 5.1.6.4. These results imply that the softening of the surface for the N_2^+ implanted samples is not responsible for the suppression of chipping fracture. Further investigation of the scratch tracks was carried out by examining a TEM specimen made by back-thinning into a scratch track in a high dose specimen; results are reported in section 5.1.7.

iv) Pitting of Boron-implanted surfaces

This effect was noticed in the low dose ($<6x10^{17}B^+cm^{-2}$) specimens after about 3 months, when the pitting had become rather heavy, and in the high dose specimens only 3 weeks after implantation. The pits were particularly spectacular on the $4x10^{17}B^+cm^{-2}$ specimen, but all the pits on all the specimens showed the same general features. Typical pits are shown in figs. 5.1.6.5. It can be seen that:

a) The pits lie in lines following <11$\bar{2}$0> directions (ie. parallel to the crystal habit planes) (fig. 5.1.6.5a);

b) The pits themselves are crystallographically shaped, appearing most often as 30° 'arrowheads' (figs. 5.1.6.5a and d);

c) The pitting severity varies sharply from one side of a crystallographically oriented boundary to another (figs. 5.1.6.5b and c);

d) Occa sional lumps are visible on the surface, of the same orientation as the pits (fig. 5.1.6.5d). These are possibly an early stage in the formation of the pits;

e) Such pits are not observed on N_2^+ implanted SiC of any dose or age.

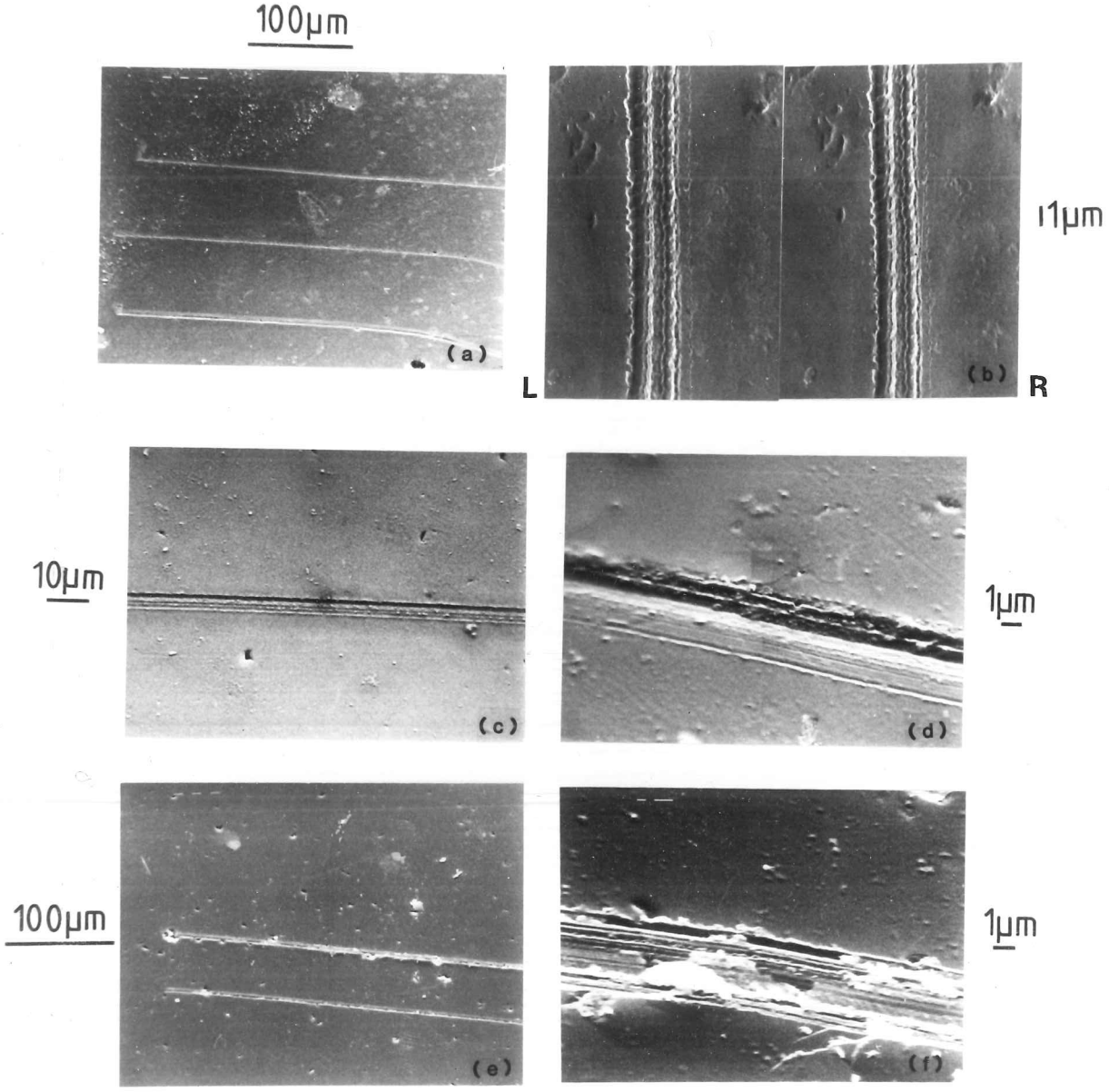

FIGS. 5.1.6.4 Single-point scratch tracks on boron-implanted SiC. SEM (secondary electron) images: (a) Dose $2x10^{17}B^{+}$ cm^{-2}, 10g, 20g and 50g loads; (b) dose $2x10^{17}B^{+}$ cm^{-2}, 10g load (stereo pair (30^{o}& 40^{o} tilts)); (c) Dose $8x10^{17}B^{+}$ cm^{-2}, 10g load; (d) Dose $8x10^{17}B^{+}$ cm^{-2}, 50g load; (e) Dose $16x10^{17}B^{+}$ cm^{-2}, 10g and 20g loads; (f) Dose $16x10^{17}B^{+}$ cm^{-2}, 50g load. Note absence of chipping at all doses and loads. In (a), the pitting shown in figs. 5.1.6.5 can be seen.

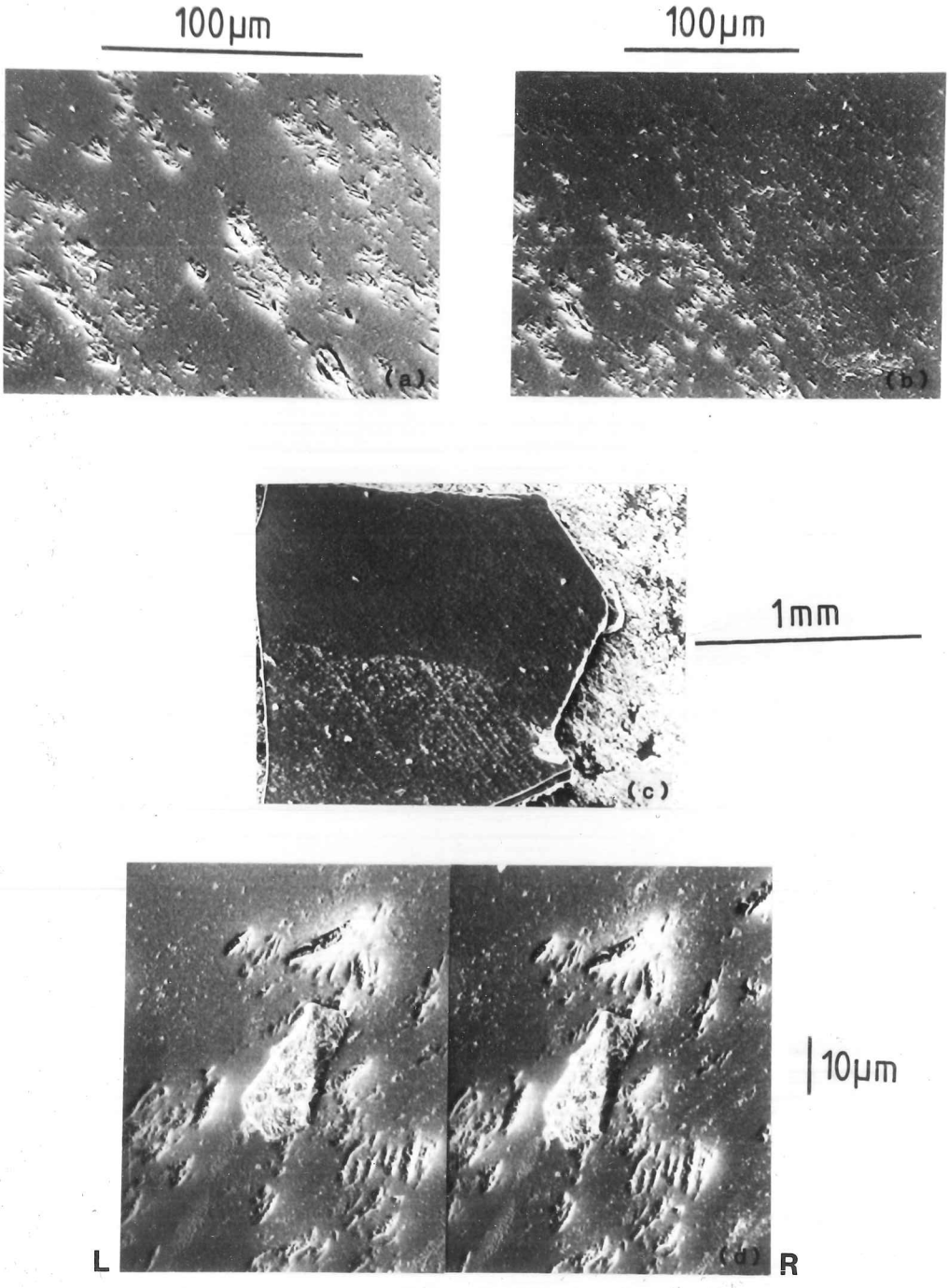

FIGS. 5.1.6.5 Pitting of boron-implanted SiC, dose $4 \times 10^{17} B^{+}$ cm^{-2}. SEM (secondary electron) images: (a) Pits have 'arrowhead' shapes; (b) Severity of pitting varies across a sub-crystal boundary; (c) Pits are crystallographically oriented; (d) Possibly an early stage in pit formation (stereo pair (30^{o}& 40^{o} tilts)).

It is rather surprising that these pits form on boron- rather than nitrogen-implanted surfaces, since p-type dopants (such as boron) have been found to inhibit oxidation [Jepps and Page (1981)], and n-type dopants to enhance it. Possibly the effect is not due to oxidation, but in any case its cause is so far obscure. The pitting does seem to have a strong crystallographic dependency, since the rate varies substantially in the crystal which appears to be divided by a sub-grain boundary ((c) above).

5.1.7 T.E.M. Examination of Implanted SiC

Initially, plan-view specimens of nitrogen-implanted SiC were prepared (see 4.6.1). Within the usable thickness of material, all implanted specimens were found to be microcrystalline, producing diffraction patterns consisting of well-defined rings (see figs. 5.1.7.1.). Dark-field images taken from any of the rings illuminated discrete microcrystals, of ~1000Å diameter. No differences in diffraction patterns were found between specimens above and below the 'critical dose' of ~$4 \times 10^{17} N_2^+$ cm^{-2}.

In order to investigate further the possible differences between implanted and unimplanted SiC samples, in particular in their response to deformation, plan-view specimens were prepared from material scratched as described in sections 4.5.1 and 5.1.5. A blunt diamond was used, at a load of 10g. The thinning of the specimens was stopped when the hole thus produced intercepted the base of the scratch track. Specimens were successfully prepared only of zero and $8 \times 10^{17} N_2^+$ cm^{-2} dose specimens. Results are illustrated in figs. 5.1.7.2 (unimplanted) and 5.1.7.3 ($8 \times 10^{17} N_2^+$ cm^{-2}). For the zero dose specimen note that:

i) Both the sub-track and normal material give diffraction patterns characteristic of hexagonal SiC (figs. 5.1.7.2a and b);

ii) Diffraction patterns taken from material close to the track show spot smearing, due to the high degree of deformation in this region (fig. 5.1.7.2b);

iii) The details of the deformation mechanism beneath the track are not resolvable (fig. 5.1.7.2c). The region appears highly disturbed.

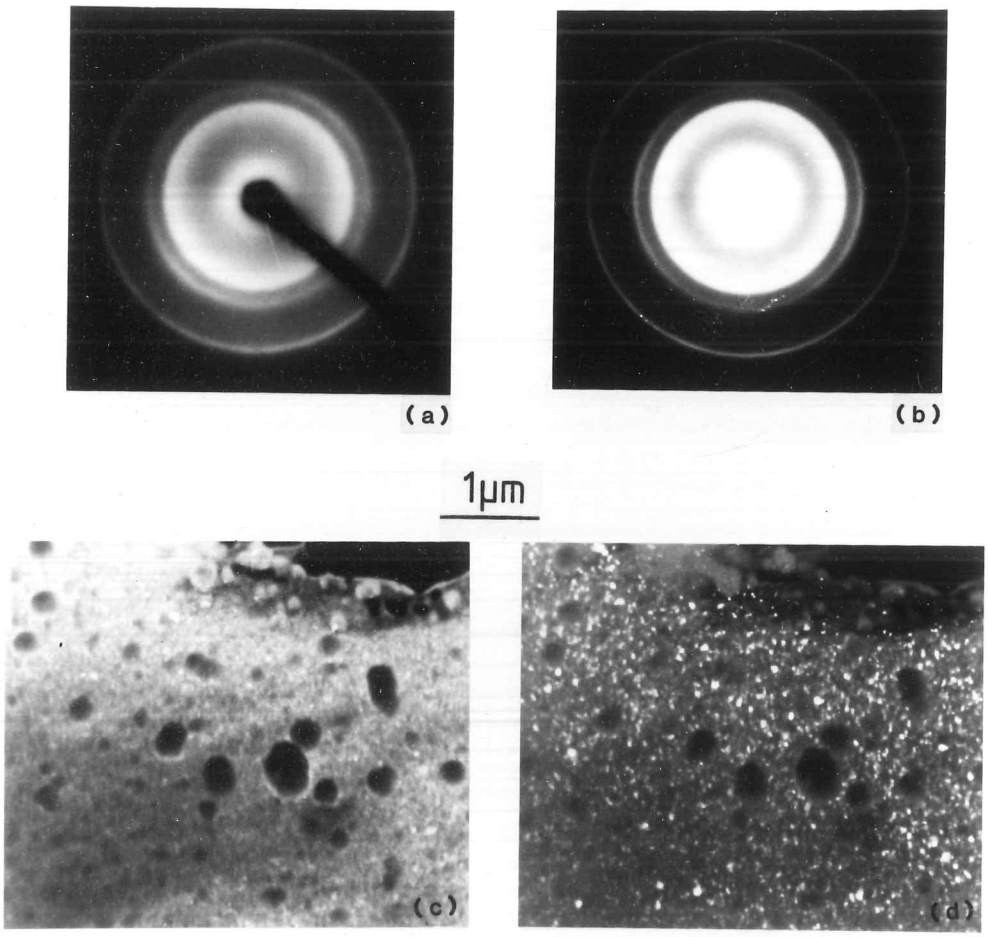

FIGS. 5.1.7.1 Plan-view TEM of nitrogen-implanted SiC: (a) DP from specimen of dose $3x10^{17}N_2^+$ cm^{-2}; (b) DP from specimen of dose $6x10^{17}N_2^+$ cm^{-2}; (c),(d) Dose $6x10^{17}N_2^+$ cm^{-2}, DF images using different parts of the outer ring. Note microcrystalline structure.

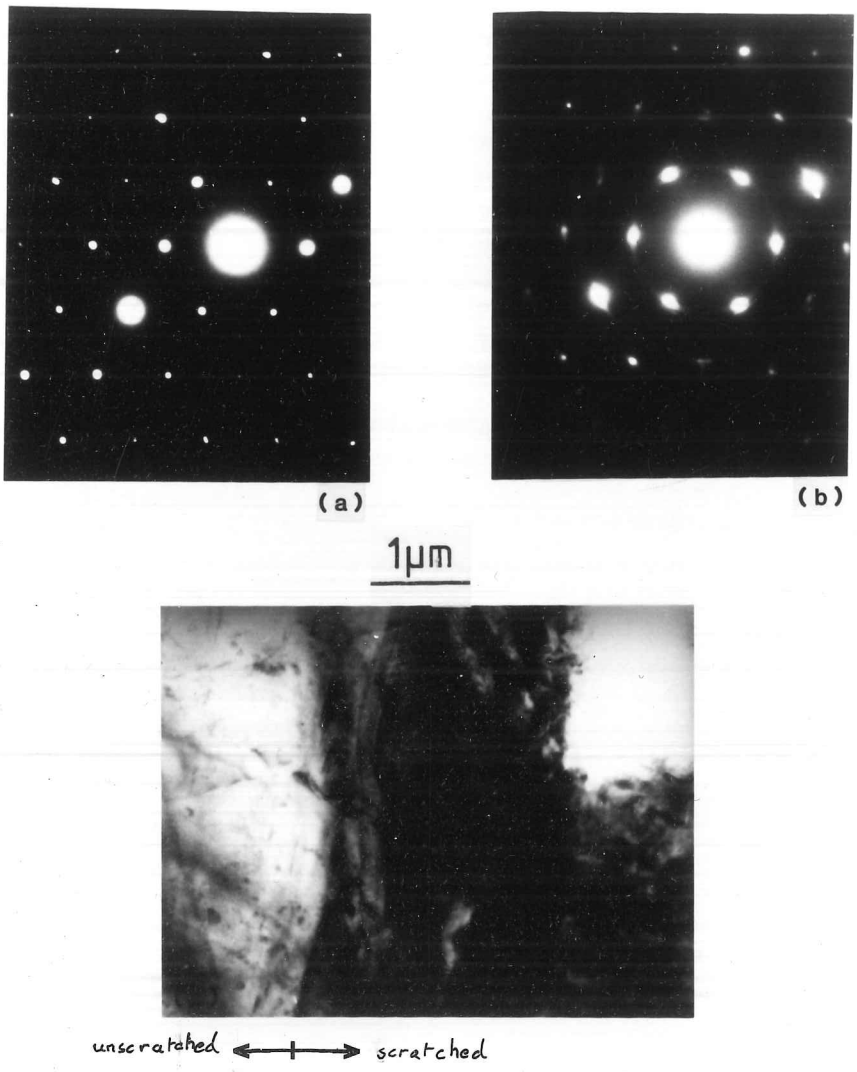

FIGS. 5.1.7.2 Plan-view TEM of scratched (10g) unimplanted SiC: (a) DP from outside the scratched area; (b) Diffraction pattern from the scratched are. Note structure is still hexagonal, and near the original orientation. (c) Edge of the scratch, BF image.

For the high dose specimen, somewhat different results were found, in particular:

iv) Diffraction patterns produced from the sub-track area (the only area on this specimen thin enough to transmit electrons) were characteristic of cubic material (figs. 5.1.7.3a and b);

v) Spot streaking and rotation, similar to that described in (iii) above, can be seen. Use of different 'subspots' to form dark-field images showed small regions of slightly differing orientation (see fig. 5.1.7.3c, d);

vi) The cubic material observed was all close to a single orientation; however, as no diffraction patterns could be obtained from the non-scratched part of the specimen, the orientation relationship between the new cubic phase and the old hexagonal one could not be determined.

It was initially thought that the phase-change was due to the β-stabilising effect of the implanted nitrogen, so that heavy deformation of nitrogen-doped non-crystalline SiC would tend to produce this phase rather than α-SiC. It was also thought that the phase change might act to relieve stress and so account for the softening observed in the microhardness tests (see 5.1.3). To investigate these possibilities, a sample of boron-implanted and scratched SiC was prepared (dose $16 \times 10^{17} B^{+} cm^{-2}$). Since boron-implanted SiC shows no change in its microhardness behaviour with dose, it was expected that the microstructure near the scratch would be similar to that of unimplanted SiC. However, the transformation to the cubic form was also observed in this specimen (see figs. 5.1.7.4).

It therefore appears that the supposed α/β stabilising effects of boron and nitrogen have less effect on the final crystalline form produced by deformation of metastable non-crystalline SiC than simply the low temperature stability of β-SiC compared to α-SiC. The phase change alone does not have any effect on microhardness behaviour, since boron and nitrogen-implanted SiC behave differently in this respect (see 5.1.3, 5.1.6). Although the microstructures of the as-implanted materials were not resolved in these observations, the similarity of the masses of boron and nitrogen, and the equivalence of the implantation conditions used, would imply that the physical effects of implantation on the surface (see 2.1,

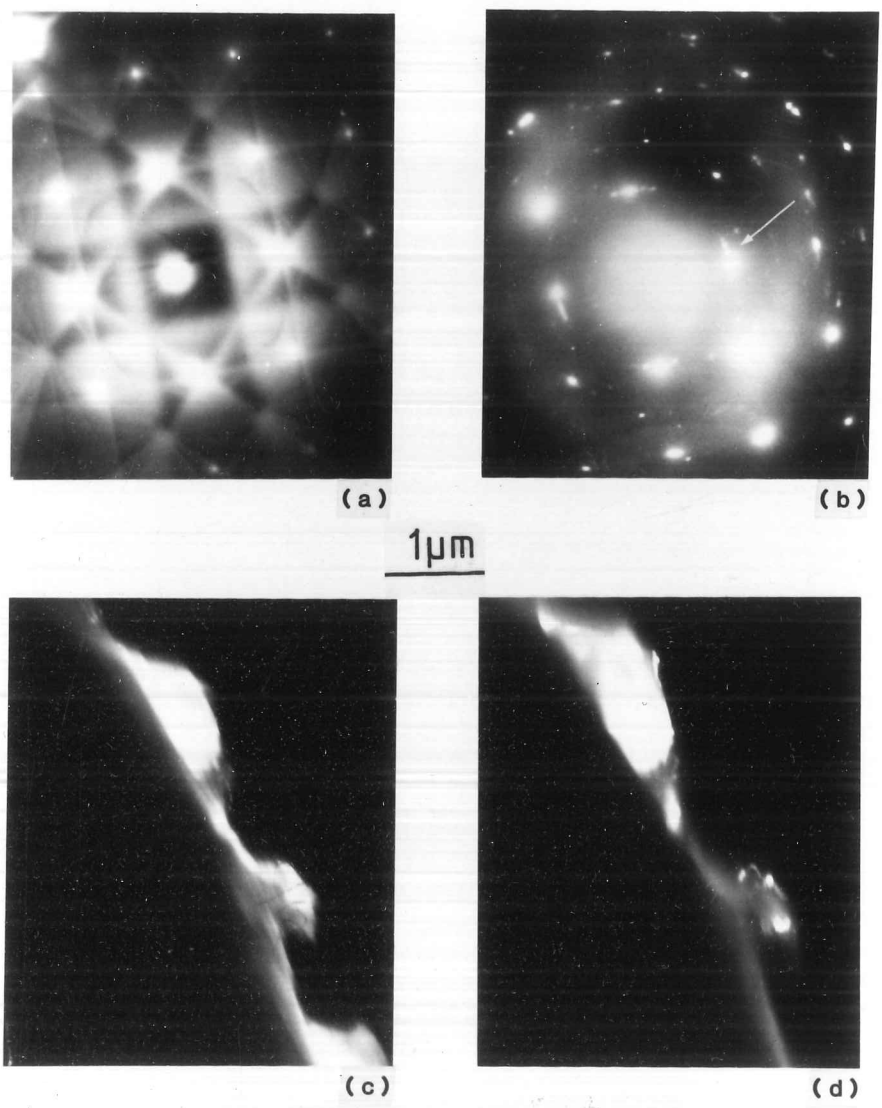

FIGS. 5.1.7.3 Plan-view TEM of scratched (10g) $8x10^{17} N_2^+ cm^{-2}$ SiC: (a) DP and Kikuchi lines from scratched area; (b) DP from different area of scratch; (c) CDF images using different ends of the streaked spot marked in (b). DPs correspond to {100} cubic.

Figs. (c) and (d) indicate that the only electron-transparent parts of the foil edge are cubic, though with slight orientation variations.

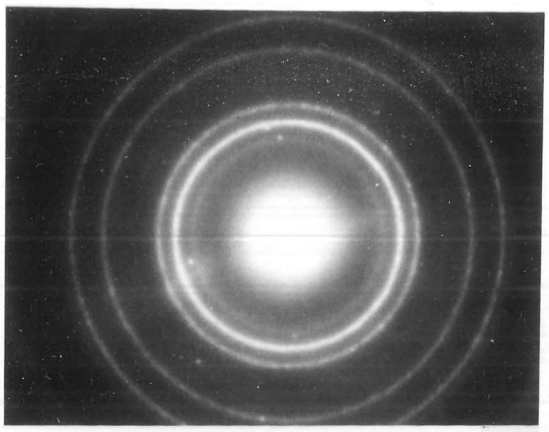

(a)

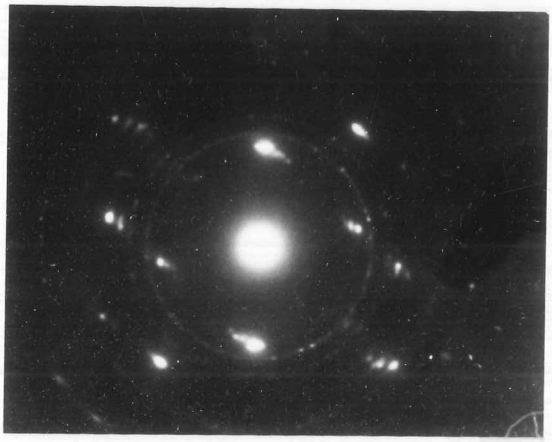

(b)

(c)

FIGS. 5.1.7.4 Plan-view TEM of scratched (10g) $16 \times 10^{17} B^{+}$ cm^{-2} SiC: (a) DP from unscratched area; (b) DP from edge of scratch:- principal spots are {110} cubic; (c) DP from scratch:- pattern is {100} cubic.

2.2) should be nearly identical. However, examination of the diffraction patterns from the two specimens (figs. 5.1.7.3a, b and 5.1.7.4a) shows that the structures are not identical. Measurement of the patterns gives the (approximate) interplanar spacings corresponding to the various rings:

Nitrogen-implanted: 3.08, 2.45, 1.73, 1.40, 1.22, 1.08, 0.99 Å

Boron-implanted: 2.53, 2.18, 1.83, 1.29, 1.09, 0.82 Å

Some of these spacings can be identified with various lengths in the SiC unit tetrahedron (3.08, 2.45/2.53, 1.08/1.09, 1.83 Å) and some with the interplanar spacings of SiC phases (eg. 2.18 Å may be (002) in β-SiC). However, no definite conclusions can be drawn about the polytype mixes in the differently implanted specimens, except that they appear to differ. However, the microstructures of the nitrogen- and boron-implanted SiC after deformation appear identical. It is therefore probable that the differences in the microhardness behaviour of boron-implanted and nitrogen-implanted SiC are probably due to their different characters as electronic dopants, by a mechanism similar to that proposed by Hirsch (1981).

5.1.8 Summary and Discussion of Results on Implanted SiC

A brief summary of the results presented above is given below:

i) Implantation with nitrogen to above a critical dose of $\sim 3\text{-}4 \times 10^{17} N_2^+ \text{ cm}^{-2}$ changes the microhardness behaviour, in that a softening is observed at low loads. Boron-implantation, up to a dose of $16 \times 10^{17} B^+ \text{cm}^{-2}$, does not significantly change the microhardness behaviour.

ii) Lateral fracture is suppressed around indentations in high dose samples (both boron and nitrogen-implanted). In the boron-implanted samples it is only the breakout that is suppressed; in nitrogen-implanted samples the nucleation of the cracks also appears suppressed at the highest doses.

iii) Pile-up and a consequent exfoliation is observed around indentations in high-dose nitrogen-implanted SiC, but is not seen in boron-implanted SiC.

iv) The occurrence of the circumferential cracking observed around unimplanted indentations becomes reduced with increasing dose of boron or nitrogen. In nitrogen-implanted samples the cracking is eliminated, and

effect (iii) above occurs, above the critical dose. Indentations in high dose specimens (both ion species) showed a small amount of pin-cushioning.

v) Even the lowest doses of boron or nitrogen produced marked changes in the form of diamond cone scratch tracks. Chipping fracture was eliminated under all but the most severe scratching conditions, and the tracks appeared as plastically deformed grooves.

vi) TEM examination showed that a transformation to the cubic form (β-SiC) from microcrystalline material occurred beneath scratch tracks in SiC implanted with boron or nitrogen. Similarly scratched unimplanted material remained hexagonal, though highly deformed.

From the above it may be deduced that:

i) The softening observed in nitrogen-implanted SiC cannot be caused by the observed phase change, nor by any purely physical effects of ion 'stuffing'.

ii) The only simple difference between boron and nitrogen is their opposite semiconductor doping effects. Mechanisms such as that due to Hirsch (1981) could therefore be the cause of the softening in the nitrogen-implanted SiC.

iii) The surface stress state (see 2.2.3) is the probable cause of the suppression of lateral breakout on implanted SiC. In nitrogen-implanted SiC, the additional reduced nucleation of the cracks is possibly connected with the softening effect of the implantation, perhaps by aiding blunting of crack nuclei. The surface stresses are also the probable cause of the pin-cushioning of indentations in high-dose specimens, by promoting elastic recovery.

iv) The changes in scratch track topography in implanted SiC are not primarily connected with surface softening, as the effect is the same for both boron- and nitrogen-implanted material. The suppression of chipping by surface stresses, as for indentation fracture, is the likely controlling effect.

v) β-SiC seems to be the low temperature stable state of SiC, and the presence of supposedly α-stablising nitrogen in large amounts does not affect this.

Unexplained observations include:

i) The existence (and magnitude) of the critical dose for microhardness effects in nitrogen-implanted SiC. If the softening effect is due to the influence of semiconductor doping on dislocation mobility, then the very high level of nitrogen implanted at the critical dose (a 30-50% solution, at peak) would imply that either the proportion of electically active nitrogen is very small, or that the nitrogen has to be present in some quantity at a large depth in the sample to have an effect.

ii) The pitting attack observed on boron-implanted SiC.

All these results are discussed in relation to results from other materials in chapter 6.

5.2 Experiments with Nitrogen-implanted Silicon

5.2.1 Materials Description

Silicon is a covalent material with a cubic F lattice (a=5.43Å) and the diamond structure. Large single crystals of dislocation-free material with controlled impurity levels in the ppm range are readily available, because of its widespread use as the matrix for semiconductor devices. Interest in the possibilities of doping silicon by implantation for device use has initiated a great deal of research into the effects of implantation on the electronic properties of silicon and other semiconductors, as outlined in section 2.2.1. Most of this research has been concerned with doses much lower than those used here (typically 10^{14}-10^{15}ions cm^{-2}).

The slip systems in silicon have been found to be {111}<1T0> [Hill and Rowcliffe (1974)]. Dislocation motion in silicon and other diamond structure semiconductors has been reviewed by Alexander and Haasen (1968). At low temperatures their motion is controlled by the nucleation and propagation of kinks; dislocation velocity is known to be greater in n-type and p-type than in intrinsic silicon [George and Champier (1979)].

Mechanisms for such effects have been proposed, by eg. Hirsch (1979),(1981), and their influence on hardness behaviour is the subject of current research [Roberts (1982)]. It has been suggested that non-slip deformation mechanisms may act, at least transiently, beneath a moving indenter in silicon. These include:

i) Pressure-induced transition to a metallic phase [Gridneva et al. (1972)], [Sargent (1979)];

ii) Twinning [Eremenko and Nikitenko (1972)];

iii) Block shear [Sawyer et al. (1980)].

Studies of the motion of dislocations in silicon at high temperatures have been performed by indentation dislocation rosette etching [Hu (1973)], and by TEM observation [eg. Louchet (1981)]. Hu and Schwenker (1978) found a hardening effect after the implantation of boron or arsenic into silicon; however their results were from specimens of much lower doses than those used here ($\sim 10^{16}$ ions cm^{-2}), and were obtained at high temperatures ($\sim 600^{o}C$). The behaviour of silicon under conditions of abrasion and polishing has been studied using TEM by Stickler and Booker (1962). They observed dislocations beneath fine diamond tracks,and sub-track cracking under harsher conditions.

The indentation fracture behaviour of silicon has been studied by Lawn and others [eg. Lawn et al. (1981)], who found the median crack span to be proportional to the applied load to the power 2/3. Naylor (1982) investigated the variation of the indentation fracture behaviour of silicon with temperature up to $1000^{o}C$. In particular, he found the critical load for fracture (P^{*}) of silicon to be 0.005N at room temperature, and K_{Ic} to be 0.5 $MPam^{1/2}$. Silicon is thus an extremely brittle material. The preferred crack planes are {110}, {111} and possibly {100} [Naylor (1982)]. Crack tip microstructures have been investigated by TEM by Lawn et al. (1980); no evidence of crack tip plasticity was found.

The material used here was n-type semiconductor grade silicon, conductivity 4-8 ohm cm. The silicon was supplied in the form of 3 inch diameter {001} wafers, with a good surface polish, by Texas Instruments Ltd. (UK). Specimens were cleaved from the wafers and implanted using the 'Pimento' machine (see 4.1.1). The maximum dose used was $8 \times 10^{17} N_2^{+}$ cm^{-2}.

Implanted specimens showed surface colours, similar to those described by Beanland and Chivers (1978), due to the interference effects between near-surface layers of amorphous and crystalline silicon.

5.2.2 Microhardness tests on Nitrogen-implanted Silicon

The testing technique was that described in section 4.4.1. Indentations were aligned so that the diagonals lay parallel to the <110> cleavage directions. The load range used was 25-1000g, giving a range in indentation diagonal from ~5 to ~50μm. Results are shown in figs. 5.2.2.1, consisting of plots of 1kg hardness, 10μm hardness and Meyer index with dose. It can be seen that there is a surface softening effect above a 'critical dose' of ~$4 \times 10^{17} N_2^+$ cm^{-2}. This is similar to the critical dose in the SiC materials, described in section 5.1.3. Note that in the case of silicon, the Meyer index rises with increasing dose, but does not exceed a value of 2 (unlike the SiC materials). The softening effect of the implantation is a softening relative to an equivalently sized indentation on unimplanted silicon; the combination of this softening with the normal ISE behaviour produces the observed final Meyer index. Typical low load diagonal sizes are:

Load	Diagonal (μm)	
	Zero dose	Dose $8 \times 10^{17} N_2^+$ cm^{-2}
50g	9.4 ±0.4	10.1 ±0.4
25g	6.1 ±0.3	7.0 ±0.3

(errors are $\pm 2\sigma$, as determined by the ISEMH program (see 4.1.1))

Three data sets at the $4 \times 10^{17} N_2^+$ cm^{-2} dose were taken from three different areas on the specimen, which was one implanted before the necessity for specimen rotation for dose uniformity was realised. The variation in the results for these areas implies that the 'step' in hardness behaviour occurs over a dose range less than that of the variation on this specimen.

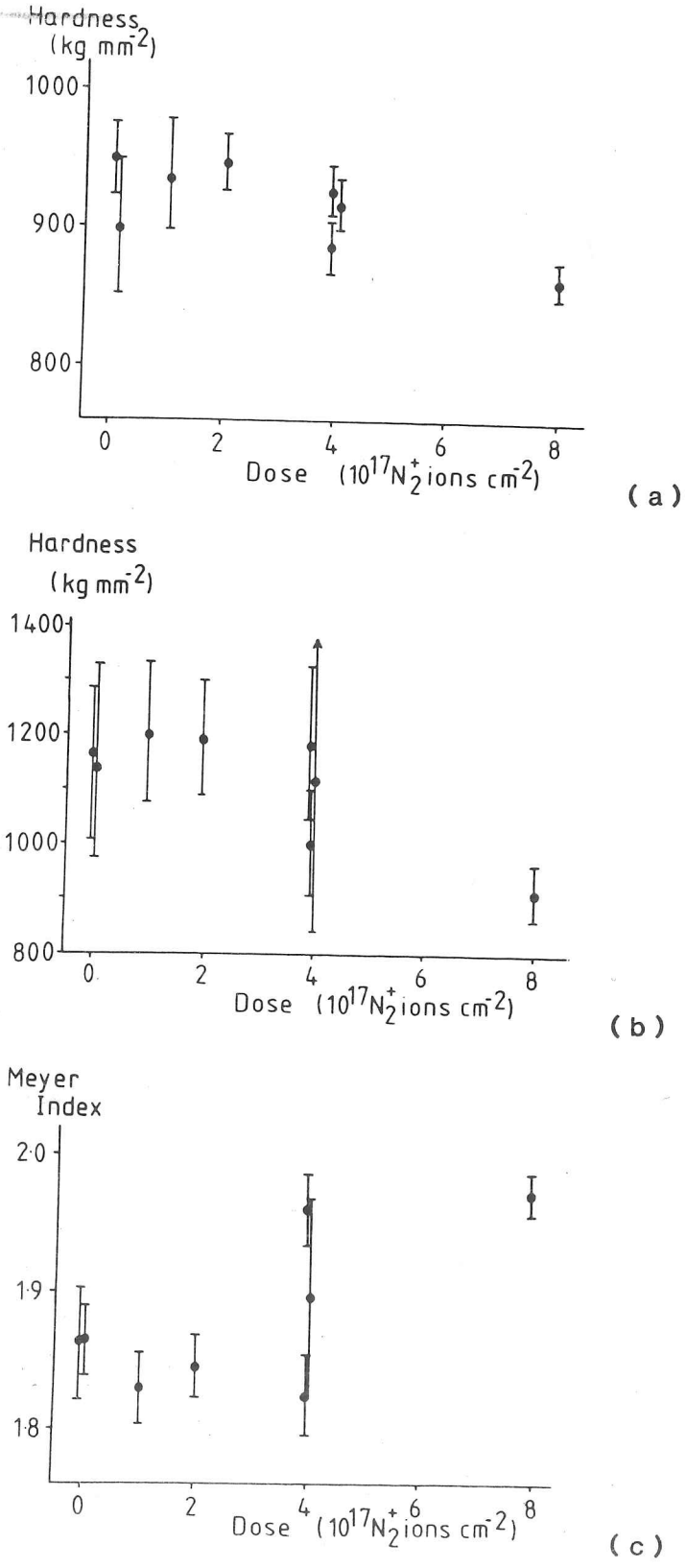

FIGS. 5.2.2.1 ISE behaviour of nitrogen-implanted silicon: (a) Hardness at 1kg load; (b) Hardness at 10μm diagonal; (c) Meyer (ISE) index. Note surface softens at dose ~$4 \times 10^{17} N_2^+$ cm^{-2}. Error bars: (a),(b) $2\bar{\sigma}$; (c) $3\bar{\sigma}$.

5.2.3 Indentation Fracture in Nitrogen-implanted Silicon

Figs. 5.2.3.1 show optical micrographs of high load indentations in silicon specimens of increasing dose up $8x10^{17} N_2^+ cm^{-2}$. It can be seen that the incidence of visible lateral fracture at these loads is progressively reduced with increasing dose; at a dose of $8x10^{17} N_2^+ cm^{-2}$ it is almost completely absent.

Subsurface crack geometry was investigated by breaking open indented specimens (see 4.4.2). Specimens were made using 500g indentations in material of doses zero and $8x10^{17} N_2^+ cm^{-2}$, and were examined in the SEM. Typical results are shown in figs. 5.2.3.2. It can be seen that extensive subsurface lateral cracking is present in both the implanted and the unimplanted material, but that there is less breakout in the implanted case.

The median/radial crack lengths were measured on all specimens. The span of this type of crack was found not to change with dose. The combined data are shown in fig. 5.2.3.3; the crack length was found to vary with indentation load according to the relation:

$$c = AL^{0.77 \pm 0.03}$$

[c = crack span, including indentation diagonal,
L = indenting load, A = a constant]

5.2.4 Scratch Tracks on Nitrogen-implanted Silicon

Tracks were made at 10g and 20g loads along near-<110> directions using a blunt 90° diamond stylus, as described in section 4.5.1. Stylus blunting was checked by making frequent reference tracks on an unimplanted specimen. Results are shown in figs. 5.2.4.1. It can be seen that debris production and sideways chipping fracture are suppressed in all the implanted specimens at both loads. Some fracture occurred around the 20g track on the $4x10^{17} N_2^+ cm^{-2}$ dose specimen; this result seems rather anomalous compared to the overall trend of fracture behaviour with dose.

5.2.3 Indentation Fracture in Nitrogen-implanted Silicon

Figs. 5.2.3.1 show optical micrographs of high load indentations in silicon specimens of increasing dose up $8 \times 10^{17} N_2^+ \text{ cm}^{-2}$. It can be seen that the incidence of visible lateral fracture at these loads is progressively reduced with increasing dose; at a dose of $8 \times 10^{17} N_2^+ \text{ cm}^{-2}$ it is almost completely absent.

Subsurface crack geometry was investigated by breaking open indented specimens (see 4.4.2). Specimens were made using 500g indentations in material of doses zero and $8 \times 10^{17} N_2^+ \text{ cm}^{-2}$, and were examined in the SEM. Typical results are shown in figs. 5.2.3.2. It can be seen that extensive subsurface lateral cracking is present in both the implanted and the unimplanted material, but that there is less breakout in the implanted case.

The median/radial crack lengths were measured on all specimens. The span of this type of crack was found not to change with dose. The combined data are shown in fig. 5.2.3.3; the crack length was found to vary with indentation load according to the relation:

$$c = AL^{0.77 \pm 0.03}$$

[c = crack span, including indentation diagonal,
L = indenting load, A = a constant]

5.2.4 Scratch Tracks on Nitrogen-implanted Silicon

Tracks were made at 10g and 20g loads along near-<110> directions using a blunt 90° diamond stylus, as described in section 4.5.1. Stylus blunting was checked by making frequent reference tracks on an unimplanted specimen. Results are shown in figs. 5.2.4.1. It can be seen that debris production and sideways chipping fracture are suppressed in all the implanted specimens at both loads. Some fracture occurred around the 20g track on the $4 \times 10^{17} N_2^+ \text{ cm}^{-2}$ dose specimen; this result seems rather anomalous compared to the overall trend of fracture behaviour with dose.

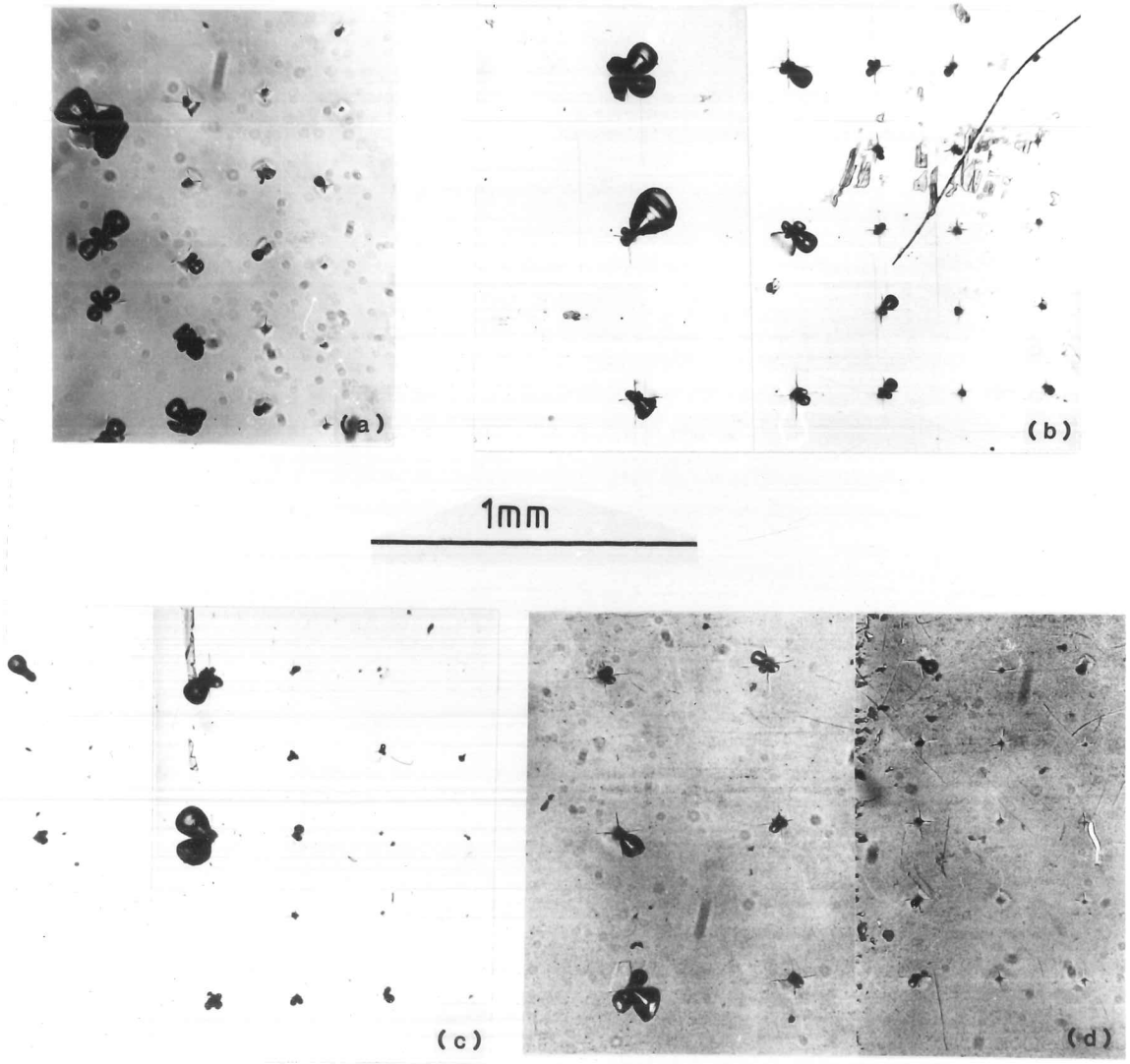

FIGS. 5.2.3.1 Lateral fracture in implanted silicon. Optical micrographs: (a) Unimplanted; (b) $2x10^{17}N_2^+$ cm^{-2}; (c) $4x10^{17}N_2^+$ cm^{-2}; (d) $8x10^{17}N_2^+$ cm^{-2}. Indentations shown are at loads 1kg, 500g, 300g and 200g. Note progressive reduction in visible lateral fracture with increasing dose.

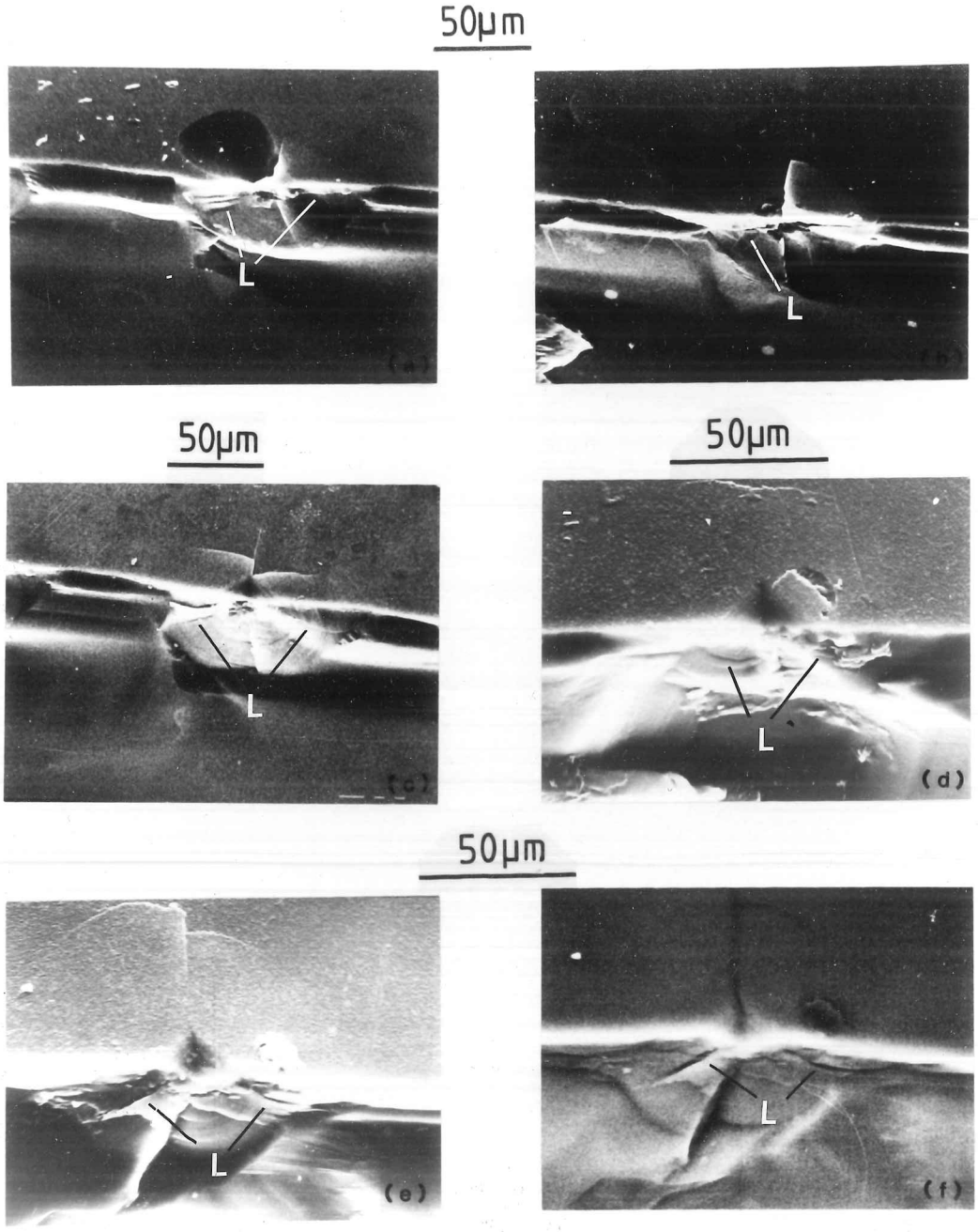

FIGS. 5.2.3.2 Lateral fracture in silicon, broken-open specimens, 500g indentations: (a)-(c) Unimplanted; (d)-(f) dose $8 \times 10^{17} N_2^+$ cm^{-2}. SEM images, all secondary electron except (f), backscattered electron image (annular detector), of same area as (e). Note that in implanted silicon, lateral fracture still extends below the surface, but has a lower tendency to break out.

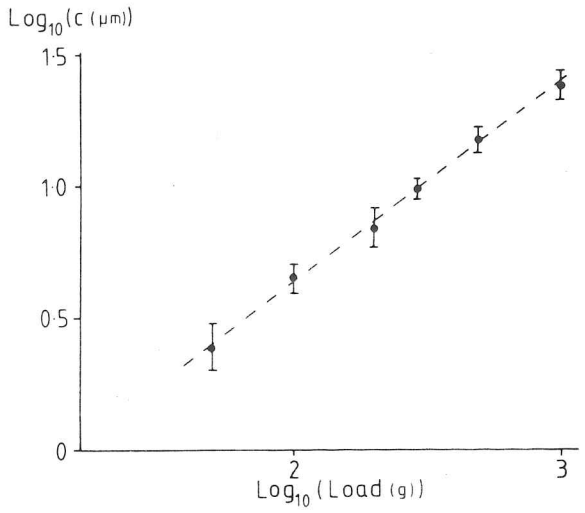

FIG. 5.2.3.3 Median/radial crack length on indented silicon (all doses). Error bars are 2σ. The crack span (c) includes the indentation diagonal.

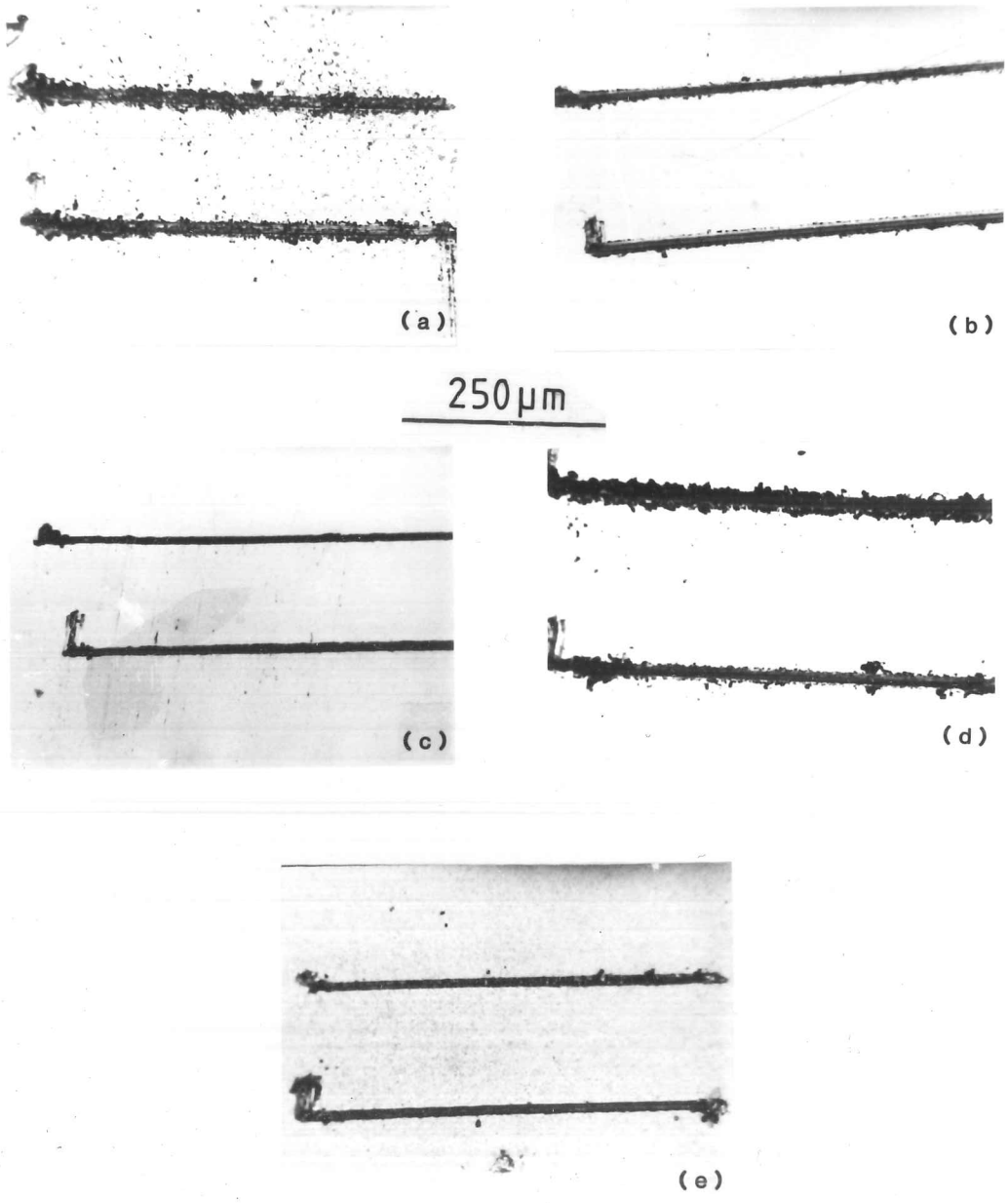

FIGS. 5.2.4.1 Scratch tracks in silicon, 10g and 20g loads. Optical micrographs. Doses: (a) zero; (b) $10^{17}N_2^+$ cm^{-2}; (c) $2x10^{17}N_2^+$ cm^{-2}; (d) $4x10^{17}N_2^+$ cm^{-2}; (e) $8x10^{17}N_2^+$ cm^{-2}. Note the suppression of chipping fracture even at a dose of $10^{17}N_2^+$ cm^{-2}. The tracks in (d) seem rather anomalous.

SEM examination revealed more details of the crack morphologies (see fig. 5.2.4.2). Chipping fracture is evident around all tracks in the unimplanted specimen. Fracture is much reduced around the tracks on implanted silicon, allowing the central plastically formed groove to be easily seen.

A back-thinned TEM specimen was prepared from a 10g scratch track in $8x10^{17} N_2^+ cm^{-2}$ dosed silicon (see 4.6.1). Results are shown in figs. 5.2.4.3. A high density of dislocations can be seen around the base of the track, where the material was crystalline cubic silicon. Several attempts were made to prepare similar specimens from unimplanted silicon, but all specimens produced proved too thick to transmit electrons at the track base, probably because of the steeply sloping track sides.

5.2.5 Laser-annealed Nitrogen-implanted Silicon

Laser annealing is a technique used in semiconductor research to remove implantation damage and electrically activate the implanted dopant (see 2.2.1). It was thought that such annealing of the implanted materials used here, so as to produce heavily doped but crystalline and stress-free surfaces, followed by microhardness testing, etc. would help to elucidate which of the many effects of implantation (see 2.2) produce the changes in mechanical behaviour that are the subject of this thesis. Specimens of $8x10^{17} N_2^+ cm^{-2}$ silicon were laser-annealed by the Engineering Laboratory (Cambridge University) and RSRE Malvern. Examination of the annealed surfaces showed that at the energy densities used to anneal silicon-implanted for semiconductor applications (0.5-1 Jcm^{-2}, pulse length ~30ns), the original surface was removed to a depth of ~1/2μm (see fig. 5.2.5.1). No further experiments of this type were carried out, since insufficient time was available to determine whether suitable annealing conditions could be found.

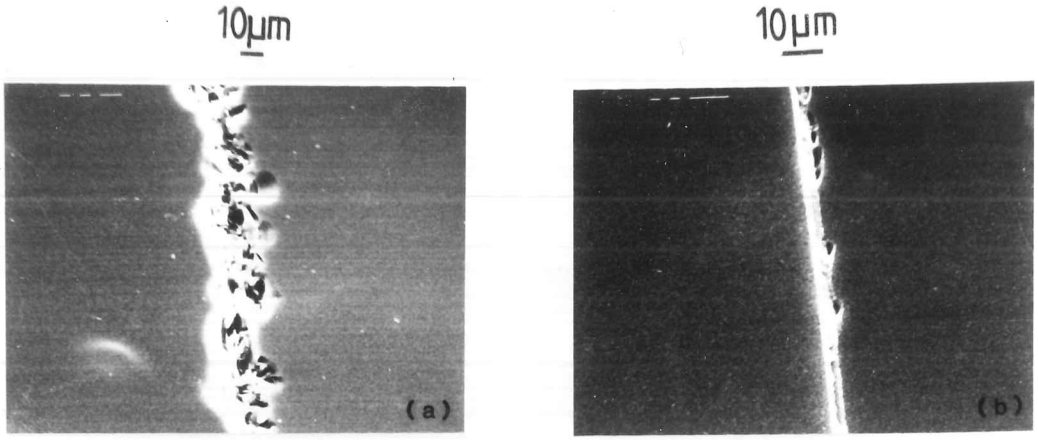

FIGS. 5.2.4.2 10g scratch tracks on silicon: (a) Unimplanted; (b) $8x10^{17}N_2^+$ cm^{-2}. SEM (secondary electron) images. Note extensive chipping around unimplanted track, suppressed in implanted material.

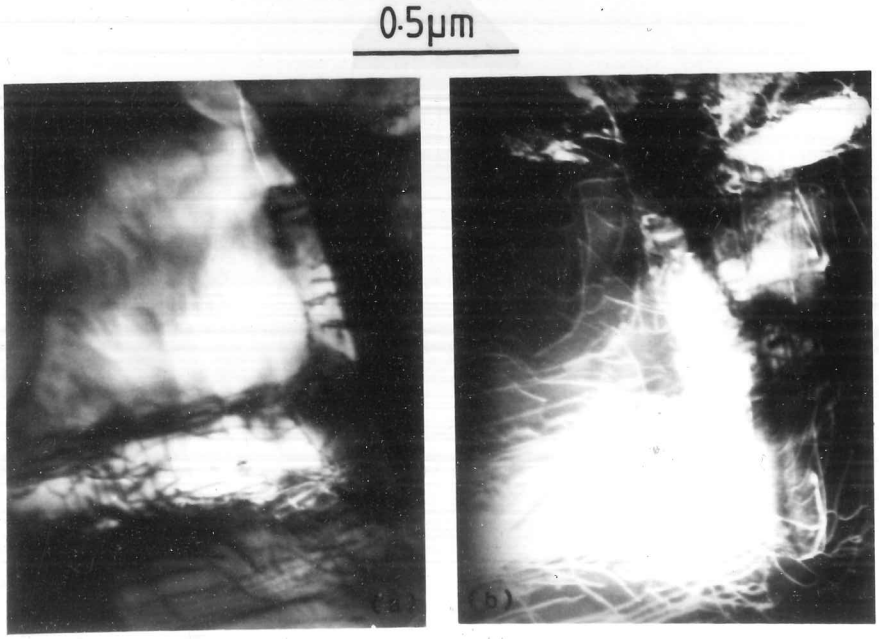

FIGS. 5.2.4.3 TEM images of base of 10g scratch track in unimplanted silicon: (a) BF; (b) WBDF ($\underline{g}$=200, $-\underline{g}$ imaging). Both micrographs show the same area. Note high dislocation densities.

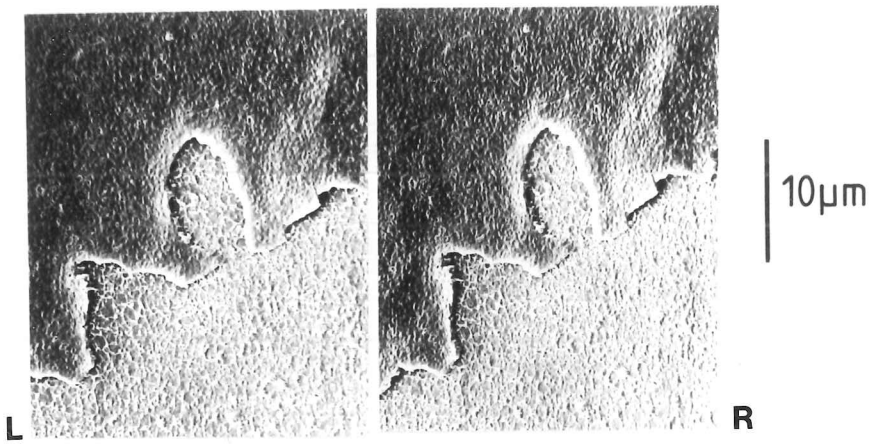

FIG. 5.2.5.1 SEM stereo pair (secondary electron, 30° & 40° tilts) of edge of laser-'annealed' area. The surface has been stripped to a depth of 0.5-1μm. Specimen was originally of dose $8 \times 10^{17} N_2^+ cm^{-2}$.

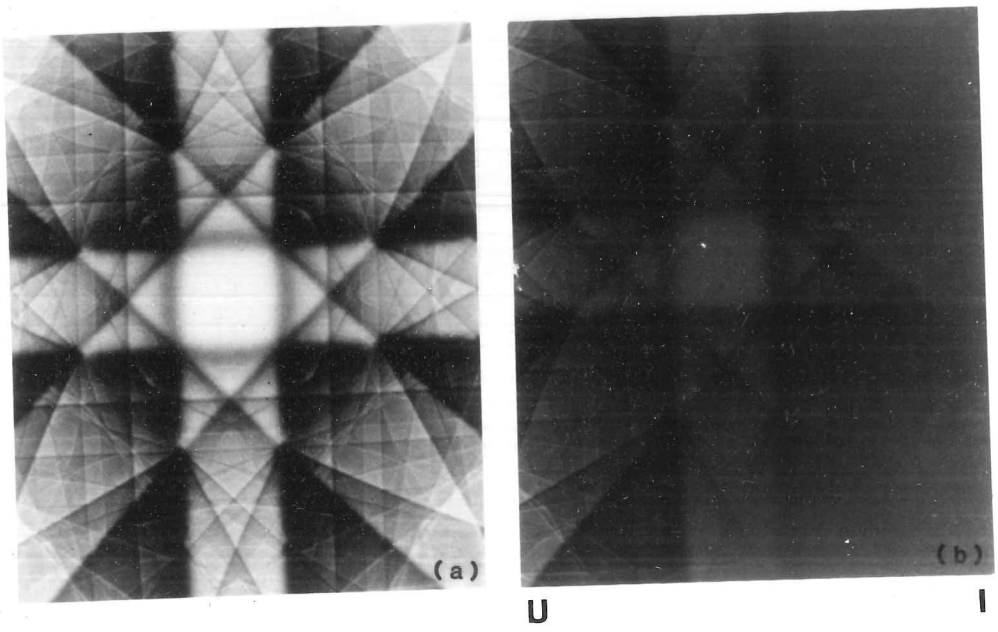

FIGS. 5.2.6.1 SEM selected area chanelling patterns, 40kV, from silicon specimens: (a) Unimplanted silicon, [001] pole; (b) as (a), but at edge of the implanted region (dose 10^{15} ions cm^{-2}). The slight movement of the spot with rocking traverses the boundary between implanted (s) and unimplanted (u) material. The implanted silicon is non-crystalline at the surface.

5.2.6 Electron Channelling Patterns from Implanted Silicon

Attempts were made to obtain electron channelling patterns [Joy and Newbury (1977)], [Schulson and Marsden (1975)] from silicon wafers implanted to doses greater than $10^{17} N_2^+ cm^{-2}$; no patterns could be obtained. A low dose wafer, implanted to doses of zero, 10^{15}, $5x10^{15}$, 10^{16} and $5x10^{16} N_2^+ cm^{-2}$ was prepared, but channelling patterns could be obtained only from the unimplanted section. Results are shown in figs. 5.2.6.1. These results confirm that the surfaces of these samples are made non-crystalline (see 2.2.1) at doses much lower than those at which changes in the mechanical properties occur.

5.2.7 TEM Examination of Abraded Silicon

Specimens covering the dose range $0-8x10^{17} N_2^+ cm^{-2}$ were prepared by abrasion with 6μm diamond paste as described in section 4.5.2. Thin foils were prepared from these, both by back thinning (see 4.6.1) and by the cross-sectioning technique described in section 4.6.2. Foils were examined in a JEM 200 TEM.

Typical results from back thinned foils are shown in figs. 5.2.7.1 and 5.2.7.2. It can be seen that:

i) In the unimplanted material (figs. 5.2.7.1), fairly sparse arrays of dislocations are visible beneath the scratch tracks from individual diamond grits;

ii) In the implanted specimens (figs. 5.2.7.2), areas thin enough to be transparent are amorphous. Scratch tracks lie completely within this amorphous layer and no deformation structures can be seen.

Only a limited number of cross-sectional specimens were successfully prepared, owing to the difficulty of the technique. Useful specimens were made of :

i) unimplanted abraded against implanted abraded;

ii) unimplanted abraded against unimplanted unabraded;

iii) unimplanted/abraded against implanted/abraded;

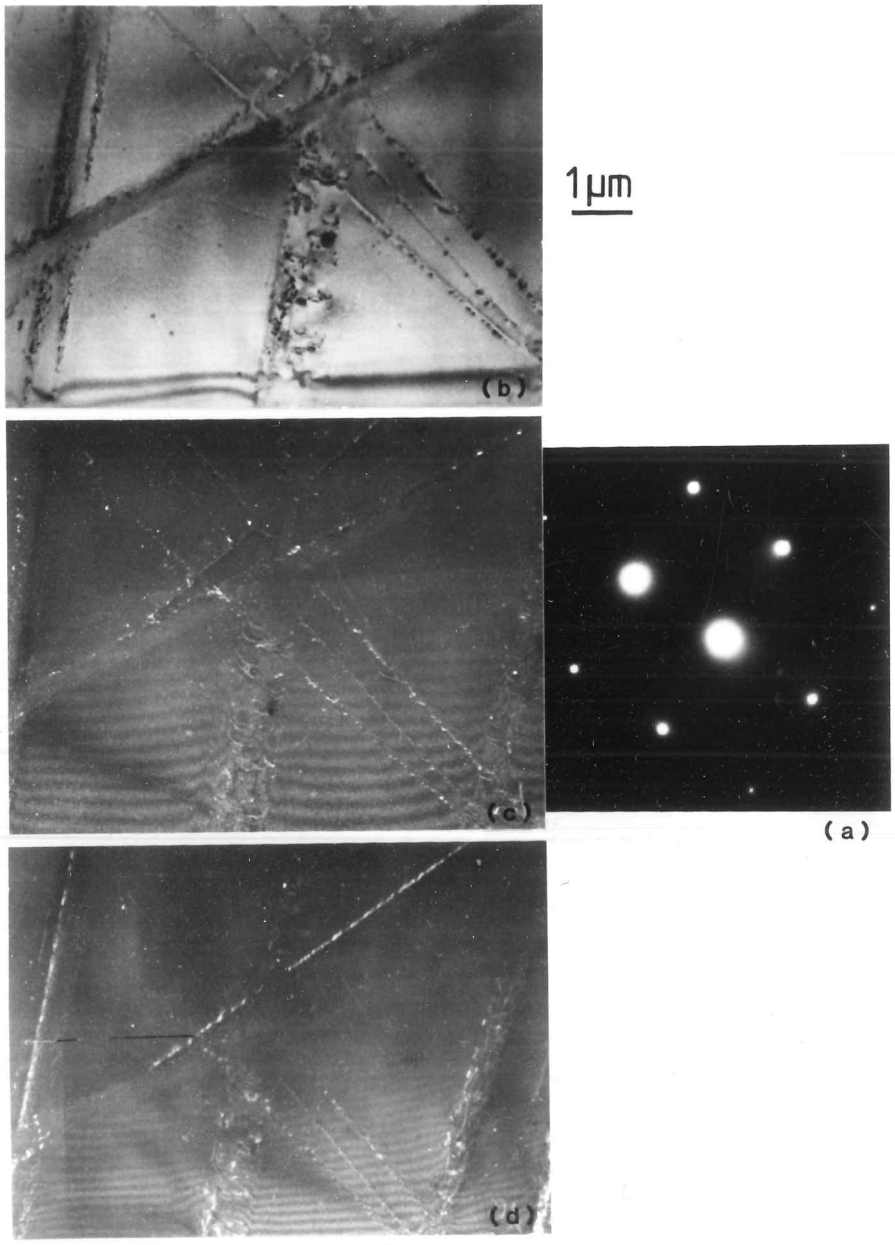

FIGS. 5.2.7.1 · Unimplanted silicon specimen abraded with 6μm diamond paste. TEM micrographs: (a) DP; (b) BF; (c) WBDF ($\underline{g}$=022, -$\underline{g}$ imaging); (d) WBDF ($\underline{g}$=02$\bar{2}$, -$\underline{g}$ imaging).

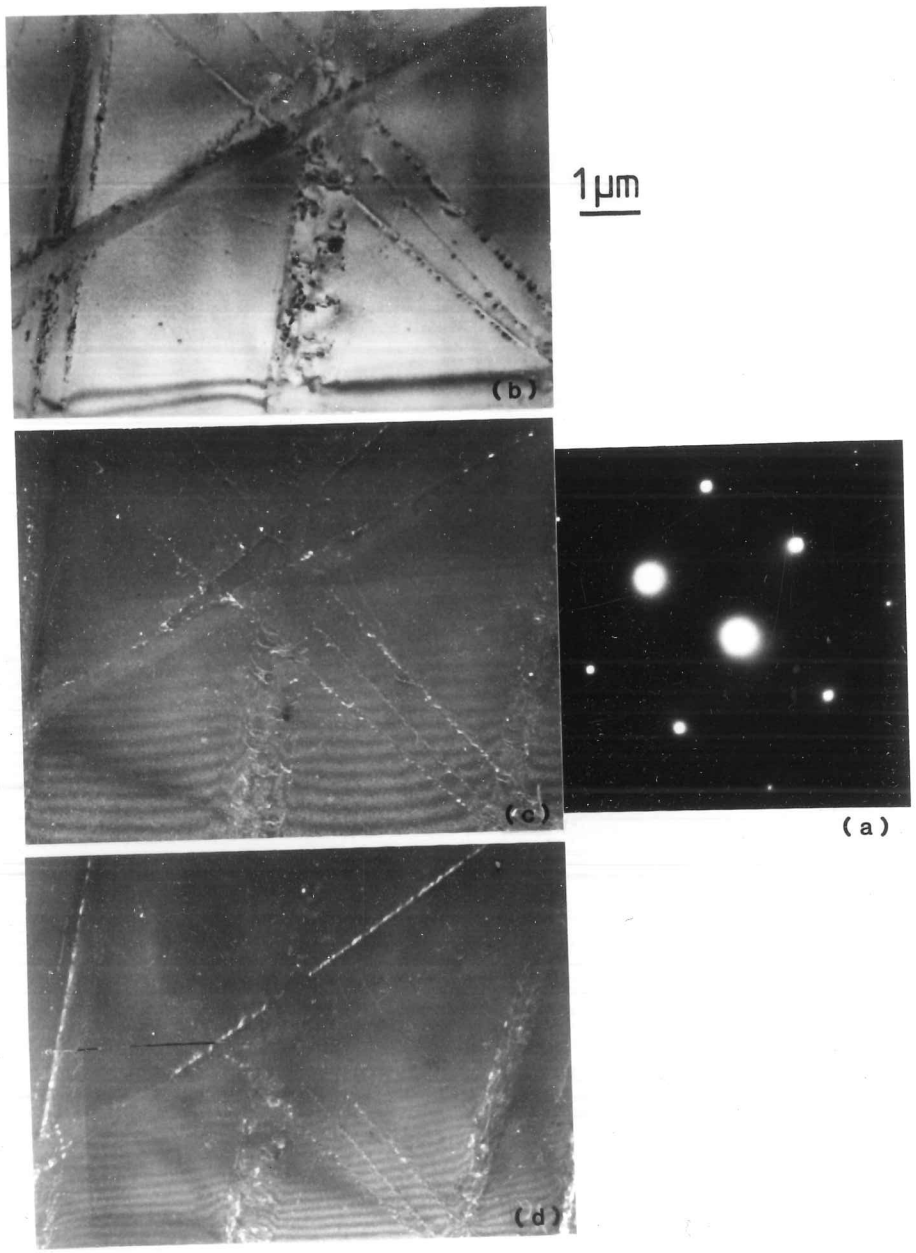

FIGS. 5.2.7.1 Unimplanted silicon specimen abraded with 6μm diamond paste. TEM micrographs: (a) DP; (b) BF; (c) WBDF ($\underline{g}$=022, $-\underline{g}$ imaging); (d) WBDF ($\underline{g}$=02$\bar{2}$, $-\underline{g}$ imaging).

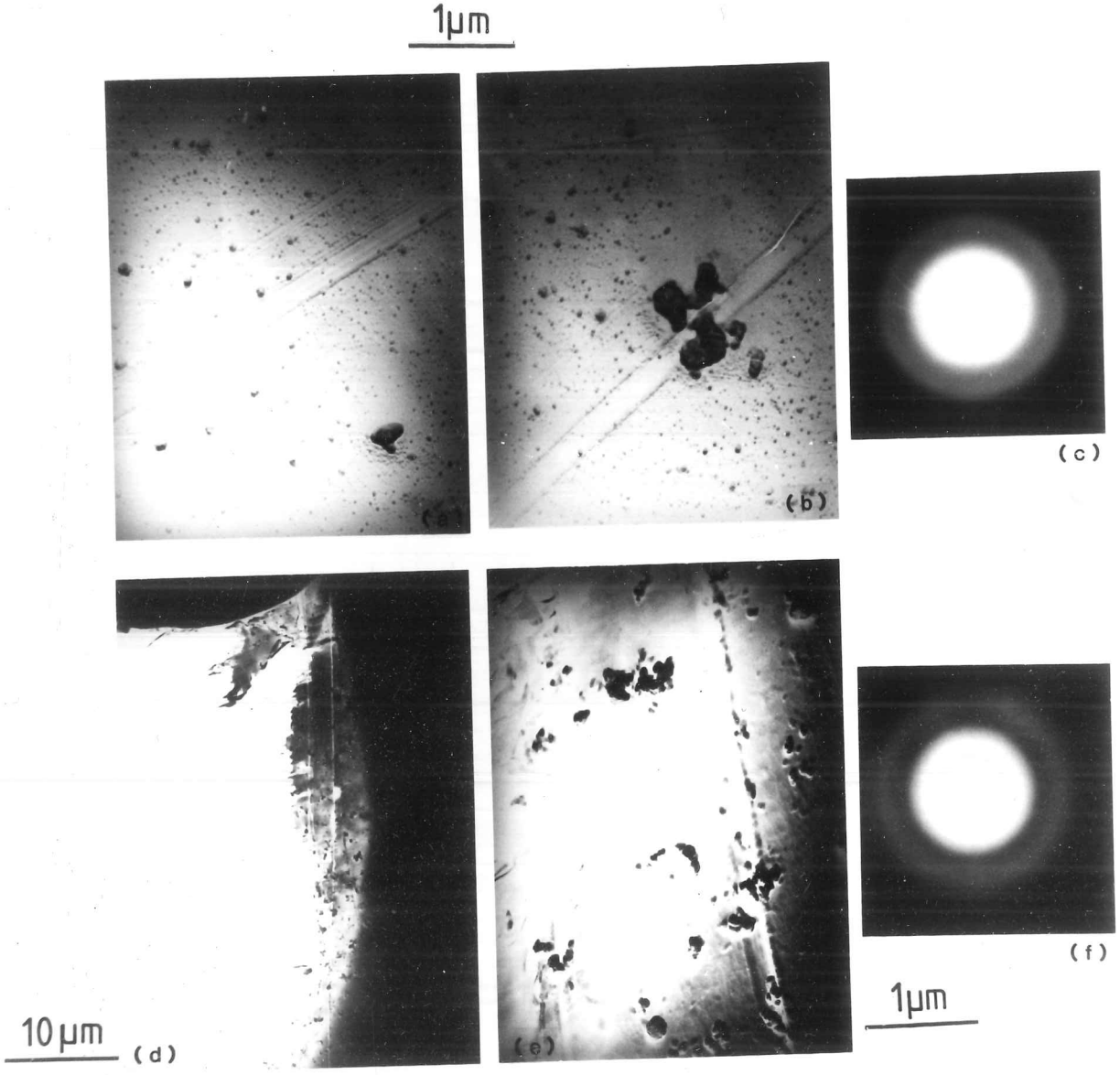

FIGS. 5.2.7.2 Implanted silicon abraded with 6μm diamond paste. TEM micrographs, BF and diffraction patterns: (a)-(c) Dose $4 \times 10^{17} N_2^+ cm^{-2}$; (d)-(f) Dose $8 \times 10^{17} N_2^+ cm^{-2}$. No deformation mechanisms can be seen beneath the grooves, and the material is amorphous.

iv) implanted abraded against implanted unabraded -

in this way the effects of heating, etc. during thinning could always be checked against a reference specimen. 'Implanted' specimens in the list above were to a dose of $8 \times 10^{17} N_2^+$ cm^{-2} (though some specimens at other doses were also prepared).

Typical results from these specimens are shown in figs. 5.2.7.3 and 5.2.7.4. It can be seen that:

i) The dislocation structures extend below scratch tracks to depths of ~0.1-0.2μm in the unimplanted specimens;

ii) The total depth of the implanted layer producing contrast in the TEM is ~0.3-0.4μm;

iii) The implanted layer has several bands of differing contrast;

iv) No deformation structures can be seen anywhere in the implanted abraded specimens.

5.2.8 Nitrogen-implanted Silicon: Summary of Results and Discussion

The results presented in sections 5.2.2 - 5.2.7 may be summarised as follows:

i) The indentation size effect behaviour of silicon is altered by implantation to a dose greater then ~$4 \times 10^{17} N_2^+$ cm^{-2}. The surface becomes softened relative to the surface of low-dose or unimplanted specimens, though the Meyer index is still below 2.

ii) Implantation to very high doses ($8 \times 10^{17} N_2^+$ cm^{-2}) inhibits the break-out of lateral cracks around indentations, though they still extend below the specimen surface. This effect increases in strength progressively over the dose range 2-$8 \times 10^{17} N_2^+$ cm^{-2}.

iii) Chipping fracture around low load (10 and 20g) diamond cone scratch tracks is greatly reduced by implantation to doses as low as $10^{17} N_2^+$ cm^{-2}.

iv) Electron channelling shows that silicon is rendered non-crystalline near the surface by doses of nitrogen less than $10^{15} N_2^+$ cm^{-2}.

v) Fine-scale surface grooving can be produced in both unimplanted and implanted silicon by abrasion with 6μm diamond grit. In the unimplanted silicon, the grooves are associated with dislocations; in the

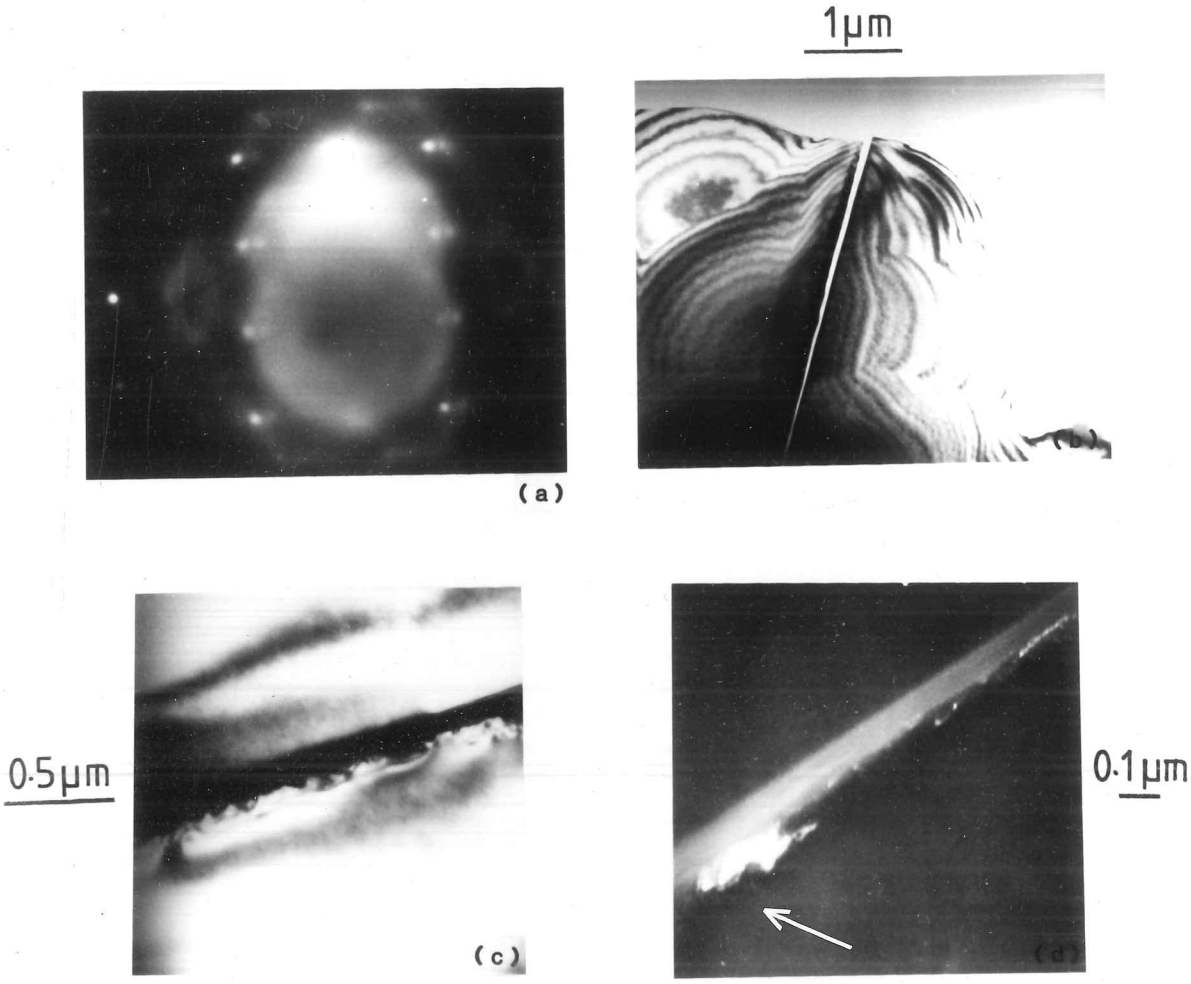

FIGS. 5.2.7.3(a)-(d) Unimplanted silicon, abraded/unabraded, cross-section TEM: (a) DP (spots from both sides of specimen); (b) BF, general view, abraded silicon to the left; (c) BF and (d) WBDF ($\underline{g}$=400, $-\underline{g}$ imaging) of the same area. Note dislocation loops beneath the scratch tracks on the abraded side.

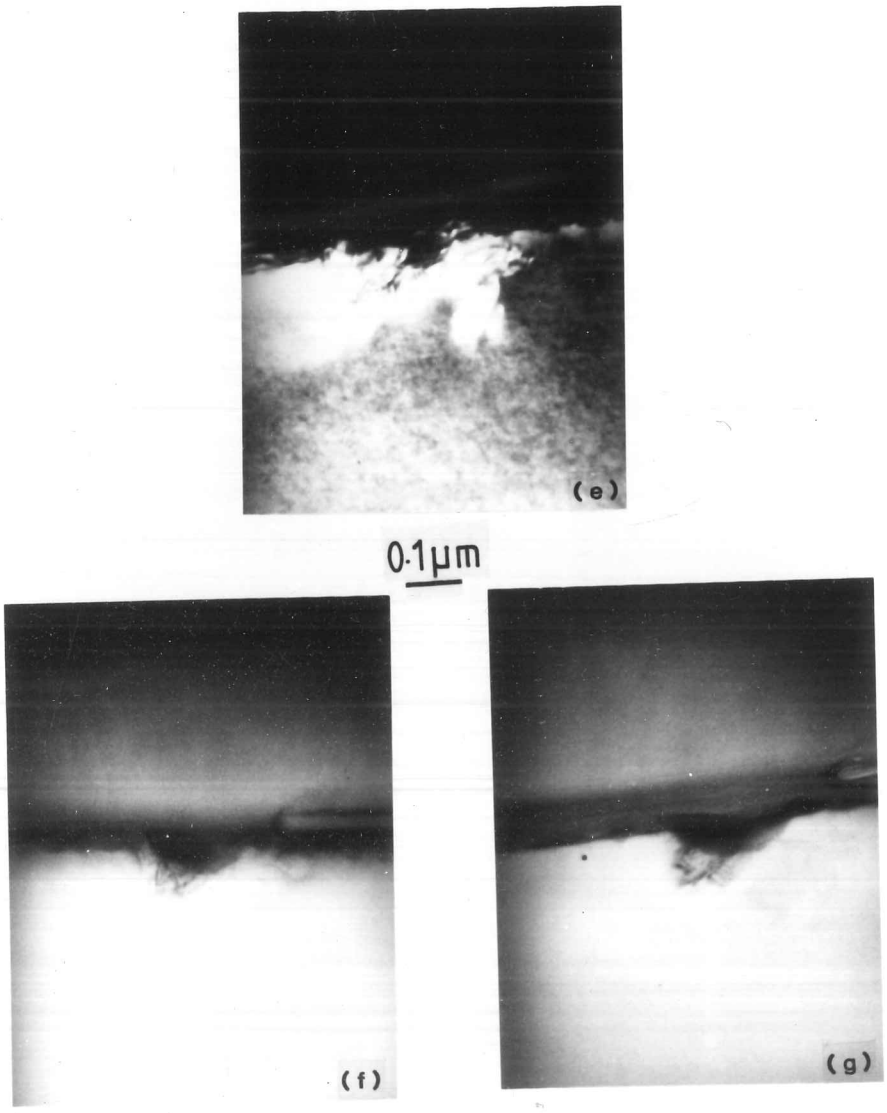

FIGS. 5.2.7.3(e)-(g) Unimplanted abraded silicon, cross-section TEM (DP as 5.2.7.1a). All the same area: (a) BF; (b) CDF ($\underline{g}$=022); (c) CDF ($\underline{g}$=02$\bar{2}$). Note dislocation array beneath the scratch track, to depth ~1µm.

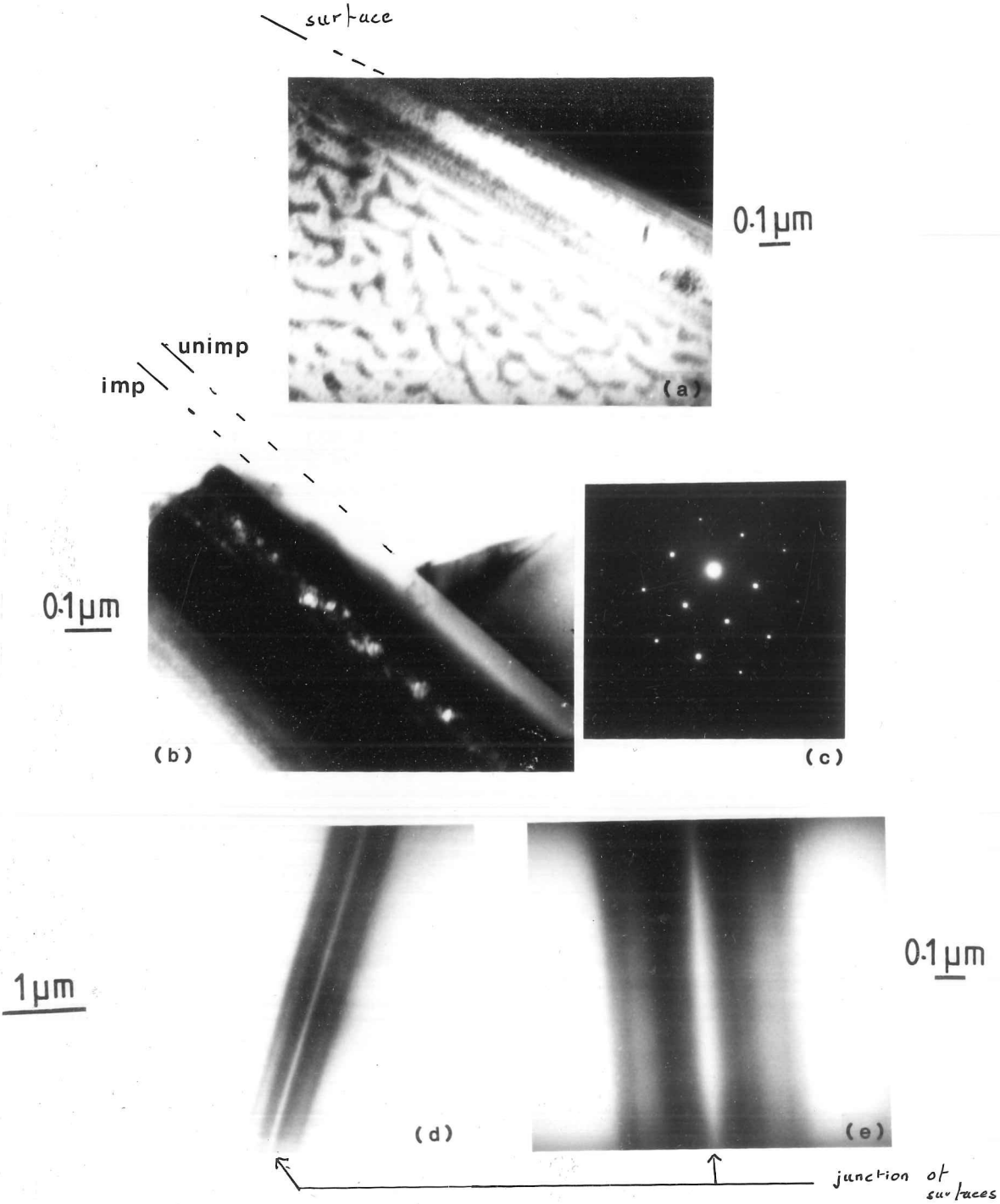

FIGS. 5.2.7.4(a)-(e) Implanted silicon, cross-section TEM: (a) $8x10^{17}N_2^+$ cm^{-2} abraded, BF; (b) $8x10^{17}N_2^+$ cm^{-2} vs. unimplanted, both unabraded, BF; (c) DP from crystalline part of (b); (d),(e) $8x10^{17}N_2^+$ cm^{-2} abraded vs. unabraded, BF. Note the banded appearance of the implanted layers. In (d) and (e), no deformation structures can be seen.

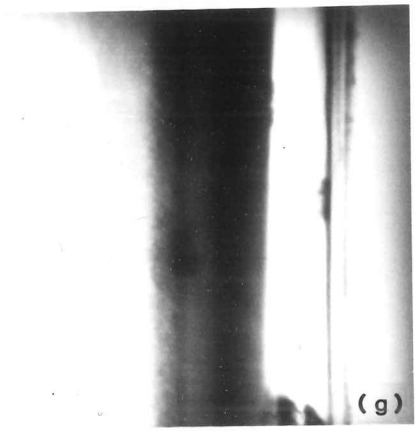

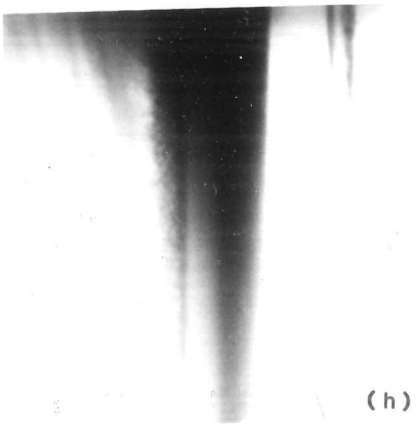

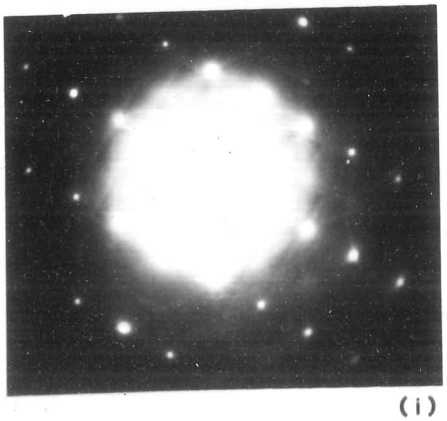

0·5µm

FIGS. 5.2.7.4(f)-(i)
Abraded silicon, $8x10^{17} N_2^+ cm^{-2}$ vs. unimplanted. Cross-section TEM (BF). No deformation structures can be seen on the implanted side, though some grooves can be seen in cross-section. The unimplanted surface shows near-surface dislocations as in 5.1.7.3. (i) DP from unimplanted side.

implanted silicon, no deformation mechanism can be identified beneath the grooves. The dislocation loops produced in the unimplanted silicon extend 0.1-0.2μm beneath the surface. The depth to which implantation affects contrast in the TEM is ~0.3-0.4μm.

vi) The implanted layer appears banded in cross-section in the TEM.

vii) The standard laser-annealing process used for low-dose (~10^{15} ions cm^{-2}) silicon strips the surface from material implanted to doses sufficient to change the surface mechanical behaviour.

A discussion of the above results together with results from other implanted materials is presented in chapter 6. From the silicon results taken in isolation, only a few conclusions can be drawn, these being:

i) The softening effect seen in the microhardness tests cannot be the result of surface amorphisation alone, as this occurs at much lower doses than those required to produce the softening.

ii) The reduction in indentation fracture breakout is probably due to the presence of a compressed surface layer produced by the implantation (see 2.2.3). The shallowly-inclined lateral cracks tend to be deflected by such a layer; the steeply inclined median/radial cracks can penetrate easily to the surface.

iii) The reduction in chipping fracture around the scratch tracks is connected with the reduction in lateral fracture breakout. The effect on chipping becomes noticeable at lower doses than those required to alter indentation fracture behaviour, as the loads in the scratch test are much lower and so fracture would be initiated closer to the surface.

iv) A non-dislocation mechanism, of undetermined form, gives surface plasticity in the implanted layer. Deformation on the same scale in unimplanted silicon occurs by dislocation processes.

5.3 Experiments with Nitrogen-implanted Cemented Carbide and Cobalt

5.3.1 Materials Description

The material used in these experiments was WC-6%Co, supplied by Wimet (UK) Ltd. Its properties as determined by the manufacturers [Lardner (1979)] are:

Wimet 'N' Grade WC-Co	
Mean WC Grain Size	1.4μm
Specific Gravity	14.95
Vickers Hardness	1600 $kgmm^{-2}$
Transverse Rupture Strength	2311 MPa
Compressive Strength	4240 MPa
Youngs Modulus	630 GPa
K_{Ic}	~8 $MPam^{1/2}$ *

The relations between microstructure and mechanical properties, particularly wear behaviour, for this type of material are complicated and not well understood. Reviews (eg. Chermant and Osterstock (1976), (1979), Lee and Gurland (1978), Lardner (1978) and Exner (1979)) give details of some aspects of microstructure/property relations, especially variations with cobalt content. It is thought that at cobalt contents as low as 6%, a continuous 'skeleton' of the carbide material exists. TEM examination of the material used here showed apparently contiguous carbide grains (see figs. 5.3.5.1). The properties of both phases will contribute to the mechanical response of the composite, and the effects of implantation on both must be considered.

Tungsten carbide is a hard ceramic with a hexagonal crystal structure (a = 2.90 Å, c = 2.83 Å [Hibbs and Sinclair (1981)]. The primary slip system has been reported as $\{10\bar{1}0\}\langle 0001\rangle$, with $\{10\bar{1}0\}\langle 11\bar{2}3\rangle$, $\{10\bar{1}0\}\langle 1210\rangle$ and $\{2\bar{1}\bar{1}2\}\langle\bar{2}113\rangle$ as subsiduary slip systems [Bolton and Redington (1980)]. The Vickers hardness has been reported as

---

* [Chermant and Osterstock (1976)]

2100 kgmm^{-2} on (0001) and 1080 kgmm^{-2} on {1$\bar{1}$00} [Takahashi and Friese (1965)]. Large single crystals of this material are difficult to obtain, and so no work could be carried out in this study on the effects of implantation on tungsten carbide alone. Cobalt is a metal with an hcp crystal structure; its properties are described in section 5.3.6.

The specimens of the composite used in this study were cut using a diamond bladed saw, and polished on laps and cloths to a 1/4μm finish, as described in section 4.3. Some specimens, particularly those used by Harwell in the pin-on-disc wear tests (see 4.5.3, 5.3.2, 5.3.4, 5.3.5) had the finish as supplied by the manufacturer. Such specimens had a fairly high density of sub-micron sized surface scratches. Implantation was performed using the 'Pimento' machine, as described in section 4.1.1.

5.3.2 Work at AERE Harwell on Implanted WC-Co

Experiments at Harwell on this material have been of two types:

i) Pin-on-disc and other laboratory tests;

ii) Lifetime studies of industrial components.

The laboratory tests have been summarised by Dearnaley (1981c). Several types of wear test, of varying degrees of severity, were carried out on nitrogen-inplanted WC-Co. No differences between the behaviour of the implanted and the unimplanted materials could be detected in the 'accelerated wear' tests; these included vibratory polishing on alumina slurry, abrading on SiC grit and wear against rapidly rotating metal wheels. Considerable improvements in wear lifetime were, however, found in the pin-on-disc tests (see 4.5.3) under lubricated conditions. Results from the examination of such specimens are presented in sections 5.3.4 and 5.3.5.

Specimens tested by the pin-on-disc method differed in both their frictional behaviour and in their wear rates. Unimplanted specimens showed a gradual drop in friction coefficient from ~0.1 to ~0.07 over ~60km sliding distance (the final friction coefficient is a mean of widely fluctuating values). The implanted discs ($4\times10^{17}N_2^+$ cm^{-2}) rapidly 'ran in' over ~1km sliding distance to a stable state with friction coefficient ~0.03 ~~0.1~~. After the running-in period, nitrogen was found to be present in both

the disc and the originally unimplanted pin, even after a thickness several times greater than the mean ion range had been worn away. Wear rates were greatly altered by implantation:

	Unimplanted disc	Implanted disc ($4x10^{17} N_2^+ cm^{-2}$)
Pin wear rate (cm^3/cm travel)	5.5 ±0.7	1.5 ±0.5
Disc wear rate (cm^3/cm travel)	6.2 ±0.5	0.7 ±0.3

(conditions: 0.5mm pin, speed $2ms^{-1}$, load 100N, white spirit lubricant)

It was suggested that the effects of implantation on the cobalt binder phase are the ones principally responsible for the above changes in behaviour, possibly by altering the stacking fault energy or the hcp-fcc transformation characteristics. It was suggested that the nitrogen was most likely to be transported inwards between the carbide grains during the wear process, either in the binder phase or along the binder/carbide interfaces. It has also been suggested [Dearnaley (1980a)] that displacement damage may create diamond-like regions within the carbide grains. However, all these mechanisms postulate a hardening in either or both phases present. The results of Pethica (1982) suggest that this is not the case for the carbide phase (see 2.4.2) and the results in section 5.3.6 indicate that the binder phase may also be softened by implantation. Possible mechanisms for the wear rate changes in implanted WC-Co are discussed in section 5.3.7.

Though the mechanisms are not well understood, the large reductions in friction and wear produced by implantation have rapidly found industrial applications - WC-Co is used for many components in harsh wear environments. Trials of implanted components in such applications as wire drawing dies [Hartley (1979b)], swageing dies [Dearnaley (1980a)] and slitting knives [Dearnaley (1980b)] have shown component lifetime increases of 2-10x normal.

5.3.3 Microhardness Tests on Nitrogen-implanted WC-Co

Microhardness testing was performed and the results analysed as described in section 4.4.1, using a load range of 50g-1kg. No significant changes in the microhardness behaviour were observed over the dose range $0\text{-}16\text{x}10^{17} N_2^+ \text{ cm}^{-2}$. The material was, however, quite variable in its response to hardness testing from sample to sample. In particular, the three samples of unimplanted material each behaved very differently. These were examined in the SEM, and found to be of an Fe-Cr alloy rather than WC-Co. In order to obtain representative data for unimplanted material, a section of each of the implanted samples, taken from close to the indentation array, was repolished so as to expose unimplanted material. Microhardness testing was then performed on these repolished specimens. Figs. 5.3.3.1 show the results from implanted (I) and unimplanted (U) sections of each sample. It can be seen that all samples, whether implanted or not, behaved identically to each other within the limits of experimental error.

These results should be compared with those of Pethica (1982). Using an ultra-low-load microhardness tester, with penetration depths of the order of 10-100nm, he found a significant hardness decrease was produced by nitrogen ion implantation to doses of 10^{17} to 10^{18} ions cm^{-2}. No distinction was made between indentations in the cobalt and the carbide phases. The discrepancy between Pethica's results and those presented here can be resolved if it is the case that in this composite material, the normal type of plastic zone geometry beneath the indenter (see 3.1.2) is not present. Indentation within the load range 50-1000g appears to deform the surface by re-arrangement of the carbide grains, without greatly deforming the grains themselves (see figs. 5.3.3.2). Since the ion range is rather less than the carbide grain size, implantation would not be expected to have much effect in the results of this type of test. However, the ultra-low load type of microhardness testing would be expected to cause yielding within the grains, without moving them bodily, and so could detect changes in the plastic response of the carbide.

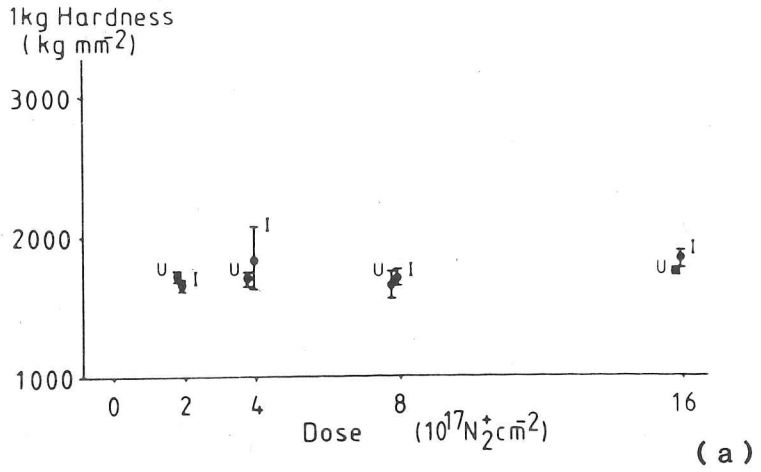

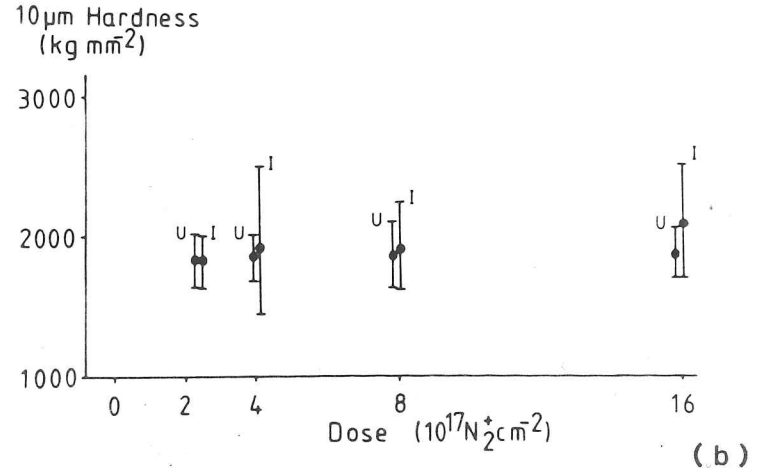

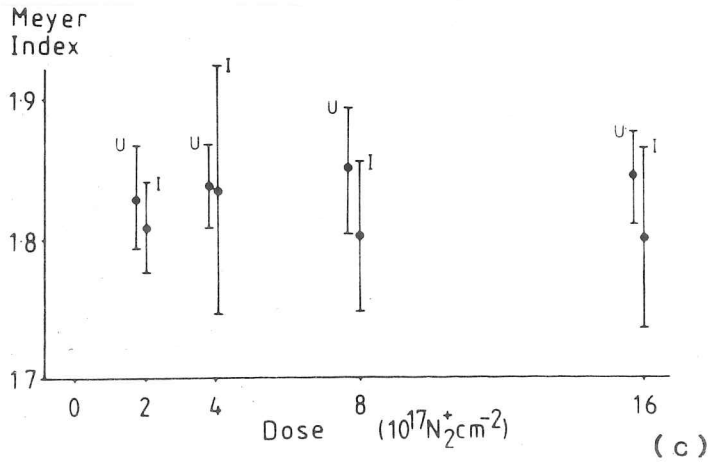

FIGS. 5.3.3.1 ISE behaviour of nitrogen-implanted WC-Co: (a) Hardness at 1kg load; (b) Hardness at 10μm diagonal; (c) Meyer (ISE) index. 'U' indicates a repolished, unimplanted section of the adjacent implanted 'I' material. The ISE behaviour is not significantly changed by implantation. Error bars: (a),(b) 2σ; (c) 3σ.

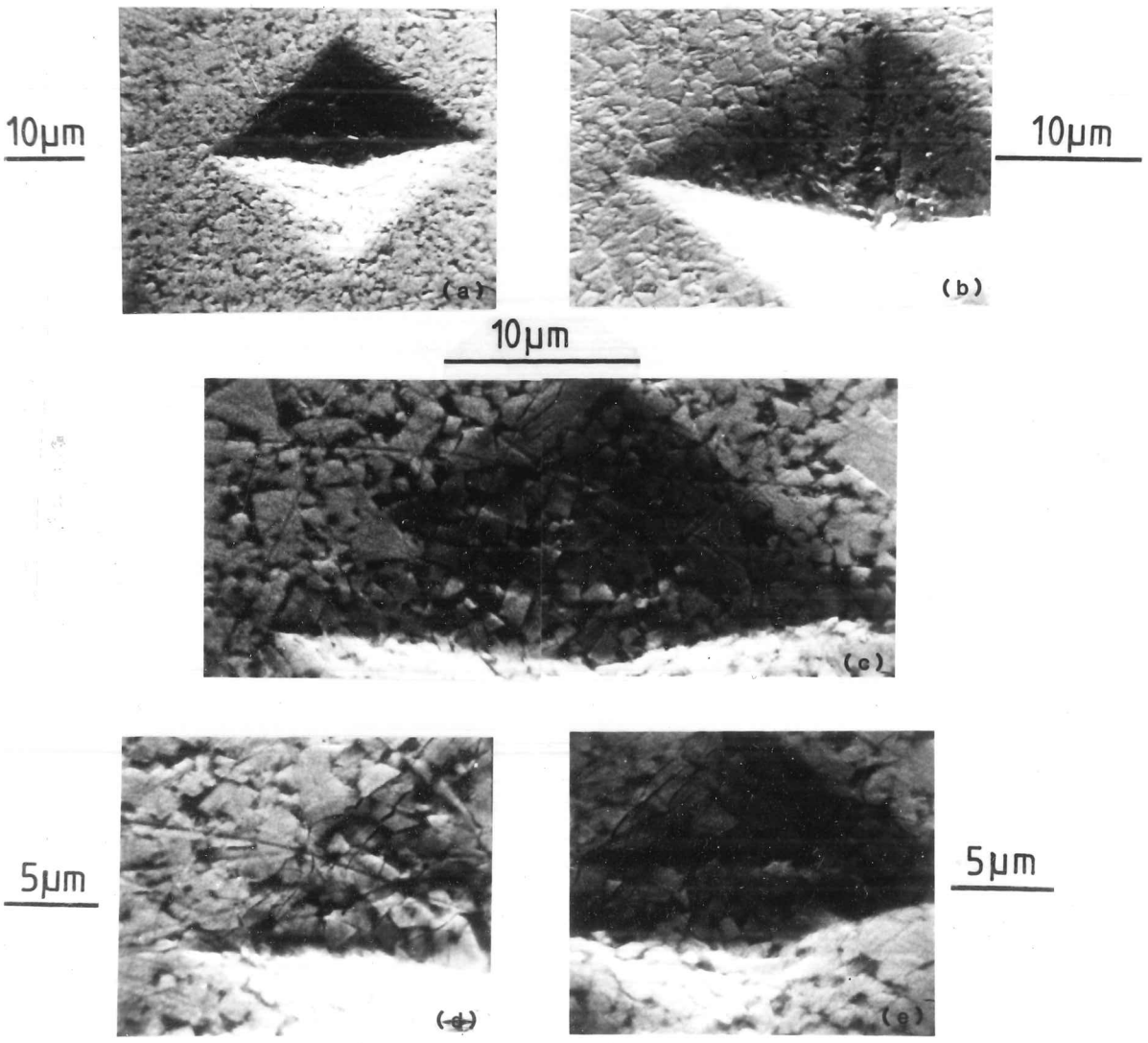

FIGS. 5.3.3.2 Microstructures around 1kg indentations in WC-Co. SEM (secondary electron) images: (a)-(c) Unimplanted WC-Co; (d)-(e) Dose $4 \times 10^{17} N_2^+$ cm^{-2} ((e) is 500g indentation). Note accentuated cracking of WC grains inside the indentation edge in implanted material.

Figs. 5.3.3.2 show the microstructure around typical indentations. It can be seen that the carbide grains appear deformed only at the extreme edges of the indentations. No pile-up is evident at any load. All indentations appear square, with no pincushioning or barrelling visible at any dose. Slight differences in crack morphology are evident between implanted and unimplanted specimens. Indentations in unimplanted WC-Co show almost no cracking of any kind up to the maximum load used, but some high load indentations in implanted material show fine cracking just inside and parallel to the indentation edges. This may be due to an implantation-induced reduction in fracture toughness of the carbide, or to a change in indenter-surface friction, or possibly to the implantation-induced surface stresses. This last is unlikely as it is most probable that any such stresses would be compressive (see 2.2.3), and thus tend to reduce this type of fracture rather than encourage it.

The high-dose specimens also show signs of sputtering, especially in the cobalt phase. As the dose increases the carbide/carbide boundaries and the cobalt areas become more visible in the optical microscope due to preferential ion-etching (see figs. 5.3.3.3).

5.3.4 SEM Examination of Pin-on-Disc Specimens

The microhardness results described in the previous section prompted a study of WC-Co actually worn in the tests for which implantation had been reported to have brought about improvements. Two specimens, in the form of 25mm diameter discs with several wear tracks on each, were obtained from AERE Harwell. One specimen was unimplanted, the other implanted to a dose of $4 \times 10^{17} N_2^+ \text{ cm}^{-2}$. Wear conditions were (see also 4.5.3):

Pin diameter	0.5 mm (cylindrical pin)
Pin material	WC-6%Co
Load on pin	100N
Speed	2000 rpm
Lubrication	Recirculated white spirit

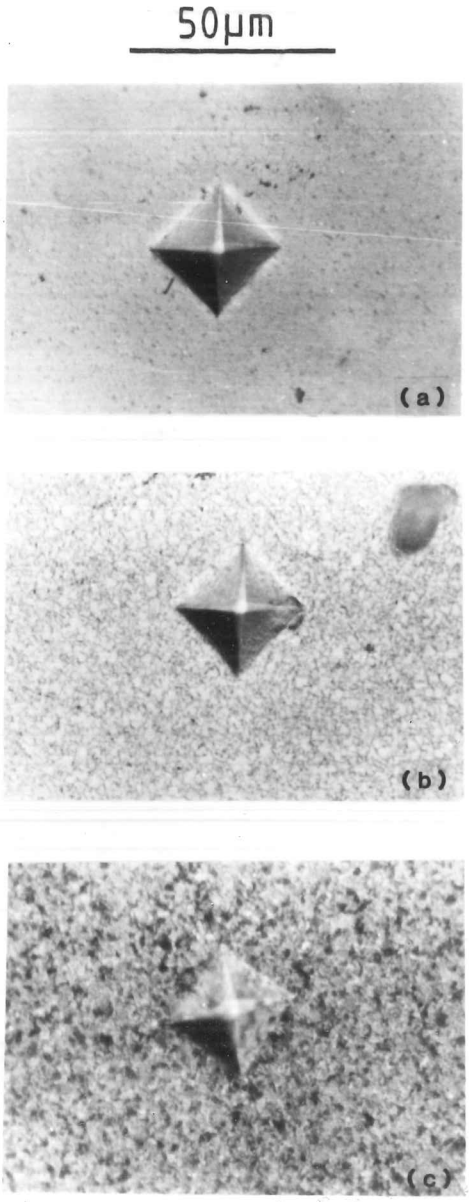

FIGS. 5.3.3.3 Optical micrographs of 1kg indentations in implanted WC-Co: (a) Dose $2x10^{17}N_2^+$ cm^{-2}; (b) Dose $4x10^{17}N_2^+$ cm^{-2}; (c) Dose $8x10^{17}N_2^+$ cm^{-2}. Note prefential ion-etching of boundaries and cobalt.

The run times for the various wear tests were not recorded by the machine operator, as the specimens were used to test the reproducability of the effects described in section 5.3.2. Tracks varied considerably in the amount of visible wear, particularly on the implanted specimen. It was found [Dearnaley (1981e)] that the pin drag force was 10-12N for the implanted specimen and 21-22N for the unimplanted specimen. Post-wear nuclear reaction analysis (see 4.2) showed that large amounts of the implanted nitrogen had been transferred to the pin. Volumetric wear rates of the pin and the disc material were roughly equal in both implanted and unimplanted cases.

Optical examination of the discs, both by eye and by microscope, showed differences in track visibility between the two specimens. The tracks on the unimplanted specimen were all easily visible, being deeply cut into the disc surface and markedly grooved within the tracks. Tracks on the implanted specimen were much less visible, particularly under the microscope, though use of oblique illumination improved contrast. This lack of contrast is probably due to the much lower wear rates, which give less of a step in the surface at the edge of the track.

Examination of the pin-on-disc specimens in the SEM showed more details of the structure of the tracks (see figs. 5.3.4.1 (unimplanted) and 5.3.4.2 (implanted)):

i) Tracks on the unimplanted specimen were easily visible even at high magnifications; those on the implanted specimen could only be readily distinguished at low magnifications and with high beam currents. In this latter condition, contamination lines were used to mark the postion of track edges, etc.

ii) Tracks on the unimplanted disc appeared darker than their surroundings, whereas those on the implanted specimen appeared slightly lighter (using SEM secondary electron imageing).

iii) Patches of material within the tracks in both specimens appeared much darker than than any other part. These patches were streaked along the rotation direction; close examination did not show any topographical change in these regions. It is possible that they might be due to local surface contamination, perhaps from breakdown of the lubricant. On the implanted specimen the patches were visible only on the most heavily worn

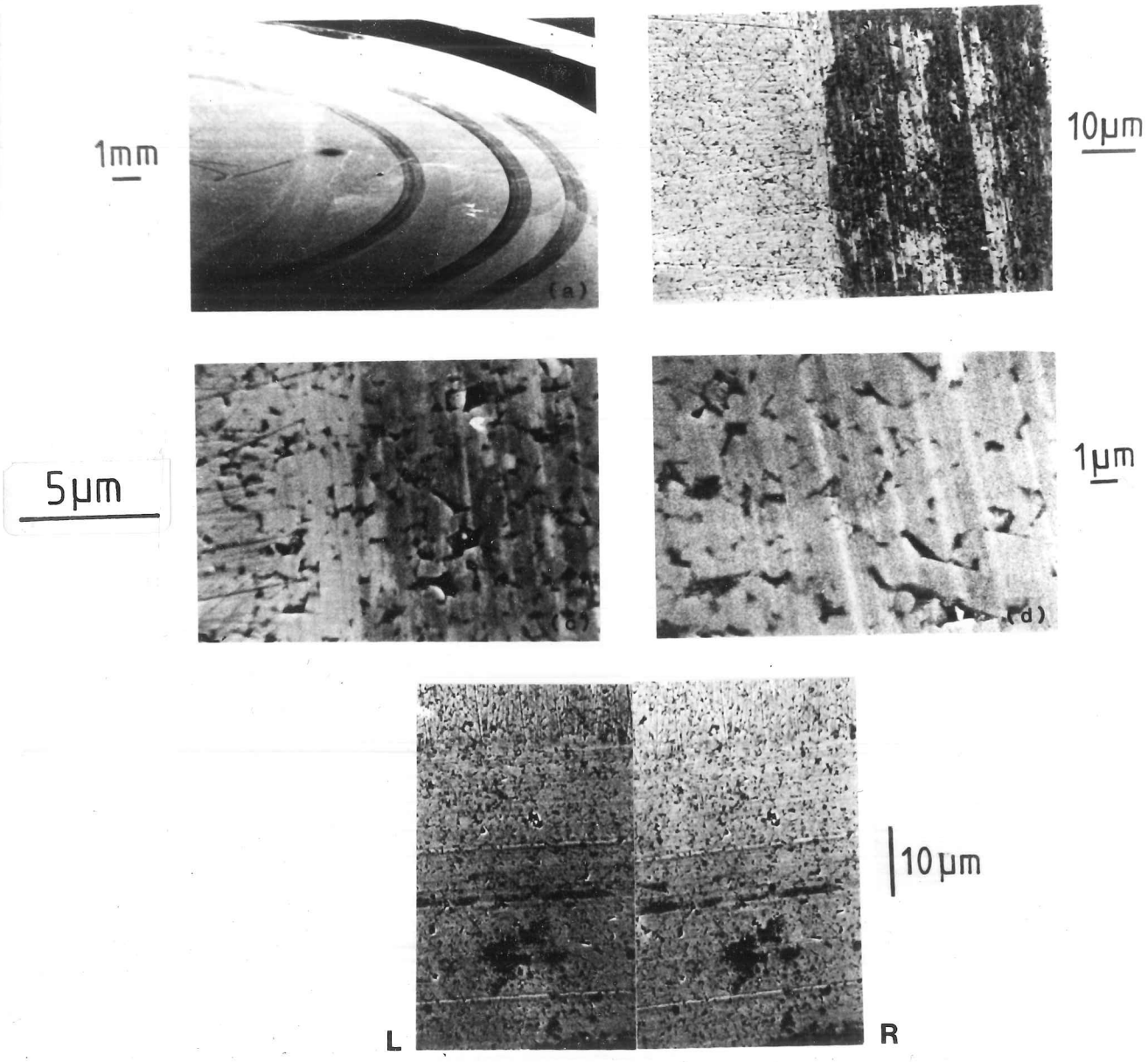

FIGS. 5.3.4.1 Unimplanted WC-Co pin-on-disc wear test specimen. SEM (secondary electron) images: (a) General view (70° tilt) showing three wear tracks; (b),(c) Edge of track; (d) Inside track; (e) Stereo pair (30°& 40° tilts) of track edge. Note surface grooves within tracks, obscuring the original surface finish, and the surface contamination within the tracks. Some grain pull-out is visible.

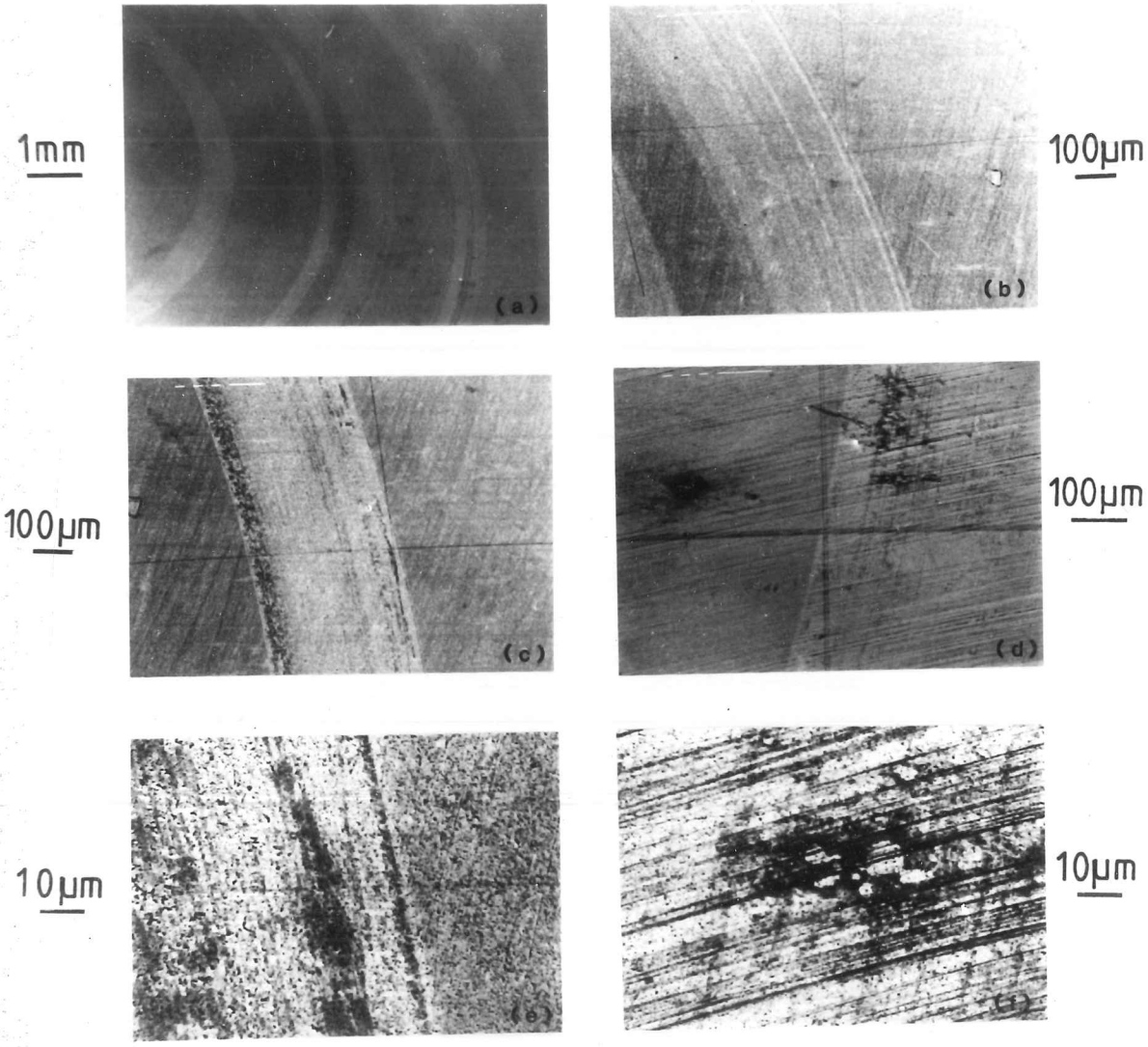

FIGS. 5.3.4.2 Implanted ($4x10^{17} N_2^+ cm^{-2}$) WC-Co pin-on-disc wear test specimen. SEM (secondary electron) images: (a) General view (60^o tilt); (b)-(f) Edges of wear tracks. Note the wear tracks are lighter than their surroundings, apart from a few contaminated areas, and that wear is much lighter on this specimen, compared to 5.3.4.1. The original surface finish is obscured only on the most heavily worn tracks.

tracks.

iv) The bases of the tracks showed grooving in the rotation direction. The grooves were approximately micron sized, and appeared as surface deformation of, rather than displacement of, the carbide grains. For most of the tracks on the implanted specimen, the grooves did not totally obscure the original surface scratches. On this specimen the grooves were also wider and shallower than those on the unimplanted specimen. On all the tracks on the unimplanted specimen, the track base was well below the original surface level, indicating a high wear rate. Without knowledge of the wear test durations, however, a direct comparison of the wear rates of the two specimens is not possible.

v) The carbide grains appear less contiguous in the track bases. In a few cases, whole grains seem to have been removed. Nonetheless, the granular microstructure visible in the track bases did not appear to have been directionally distorted by the frictional dragging of the pin.

Specimens of implanted and unimplanted material were also cut so that a track could be examined in longitudinal and transverse cross section. The specimens were mounted in bakelite, polished as described in section 4.3.2, then removed from the bakelite and examined in the SEM. These specimens were prepared to check the possiblity that near-surface material might have been dragged forward by the pin, in which case the differences in coefficients of friction between the two specimens might have a direct bearing on their wear rates. As can be seen in figs. 5.3.4.3, no such effects were found for either the unimplanted or the implanted specimen. The microstructure appears unchanged right up to the surface, with no friction-induced directionality visible.

From the above observations, it appears that the main wear mechanism under these conditions involves material loss at the sub-grain level. Grain pull-out, though occasionally observed, is probably not a major loss mechanism, as the grain stucture does not appear to be disturbed beneath the worn surfaces. Within the grooves, the surface appears plastically deformed on a scale finer than the grain size. This may be connected with the light contrast of the wear tracks in the implanted specimen; Sawyer (1979) observed a similar phenomenon on heavily worn SiC surfaces, and attributed this to an increase in dislocation density. However, the

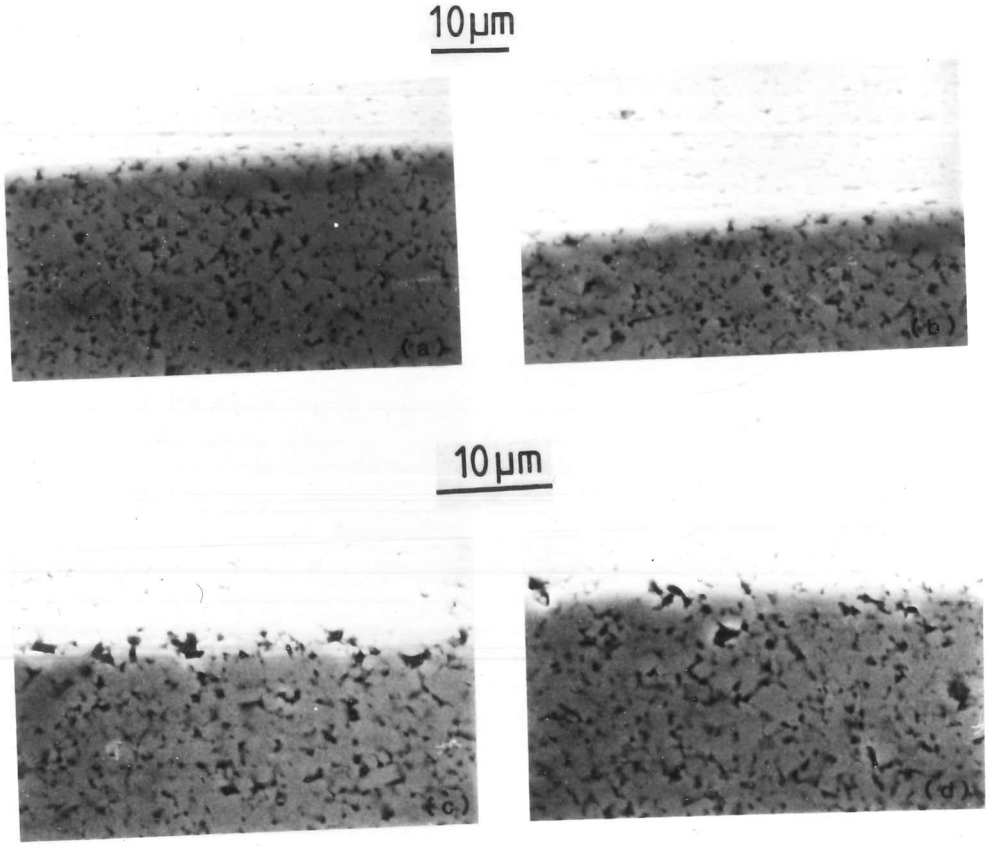

FIGS. 5.3.4.3 Cross-sectioned pin-on-disc specimens. SEM (secondary electron) images. Wear direction was horizontally on the top surface: (a),(b) Unimplanted; (c),(d) Implanted, dose $4 \times 10^{17} N_2^+ cm^{-2}$. The microstructure appears unchanged right up to the surface in each case.

reverse contrast on the unimplanted specimen is not explicable in this way.

Further investigation of the pin-on-disc specimens was carried out by examination of TEM specimens. Results from such specimens are described in the next section.

5.3.5 TEM Examination of Pin-on-Disc Specimens

Results from plan-view specimens only are presented here. Attempts were made to prepare profile-view specimens of worn and/or implanted surfaces,but these proved unsuccessful. The techniques described in section 4.6.2 failed as the glued joint was not strong enough to withstand the stresses involved in lapping and polishing the specimens. A method successfully used by Gibbs (1982), to examine worn ceramic fibreguide surfaces, was also attempted; this method involved the preparation and thinning of a semi-disc of the material, with the surface of interest as the diameter. This method also proved unsuccessful for WC-Co specimens.

The plan view specimens were prepared in the way described in section 4.6.1. Specimens were made from the pin-on-disc specimens used for the experiments described in section 5.3.4 (ie. unimplanted and dose $4x10^{17}N_2^+$ cm^{-2}). 3mm discs were cut so that a track edge crossed the centre of the disc; careful thinning produced usably thin areas in both the worn and the unworn material. A specimen of high dose WC-Co ($16x10^{17}N_2^+$ cm^{-2}) was also prepared. Results from each of these specimens are described below:

i) Unimplanted pin-on-disc specimen (see figs. 5.3.5.1)

The tungsten carbide grains, roughly equiaxed and of ~1μm diameter, are easily visible; the cobalt binder is less readily identifiable. In the unworn region, some dislocations, often in well-formed networks, are visible in the carbide phase. The dislocation density is noticeably higher in the worn areas; dense tangles can often be seen. This indicates that the wear mechanism involves at least some plastic deformation. No cracks can

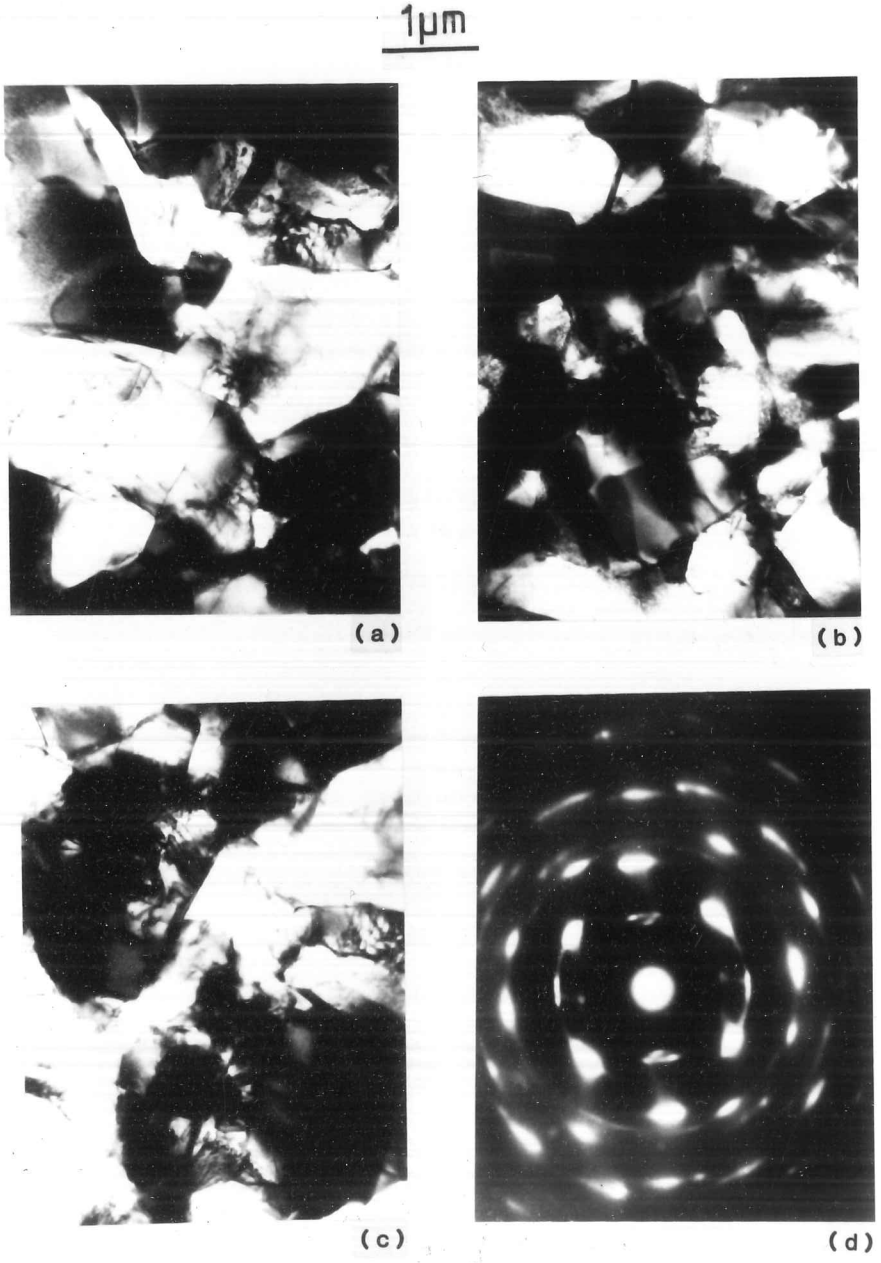

FIGS. 5.3.5.1(a)-(d) TEM examination of unimplanted pin-on-disc specimen:- unworn areas: (a)-(c) BF; (d) DP, from several grains.

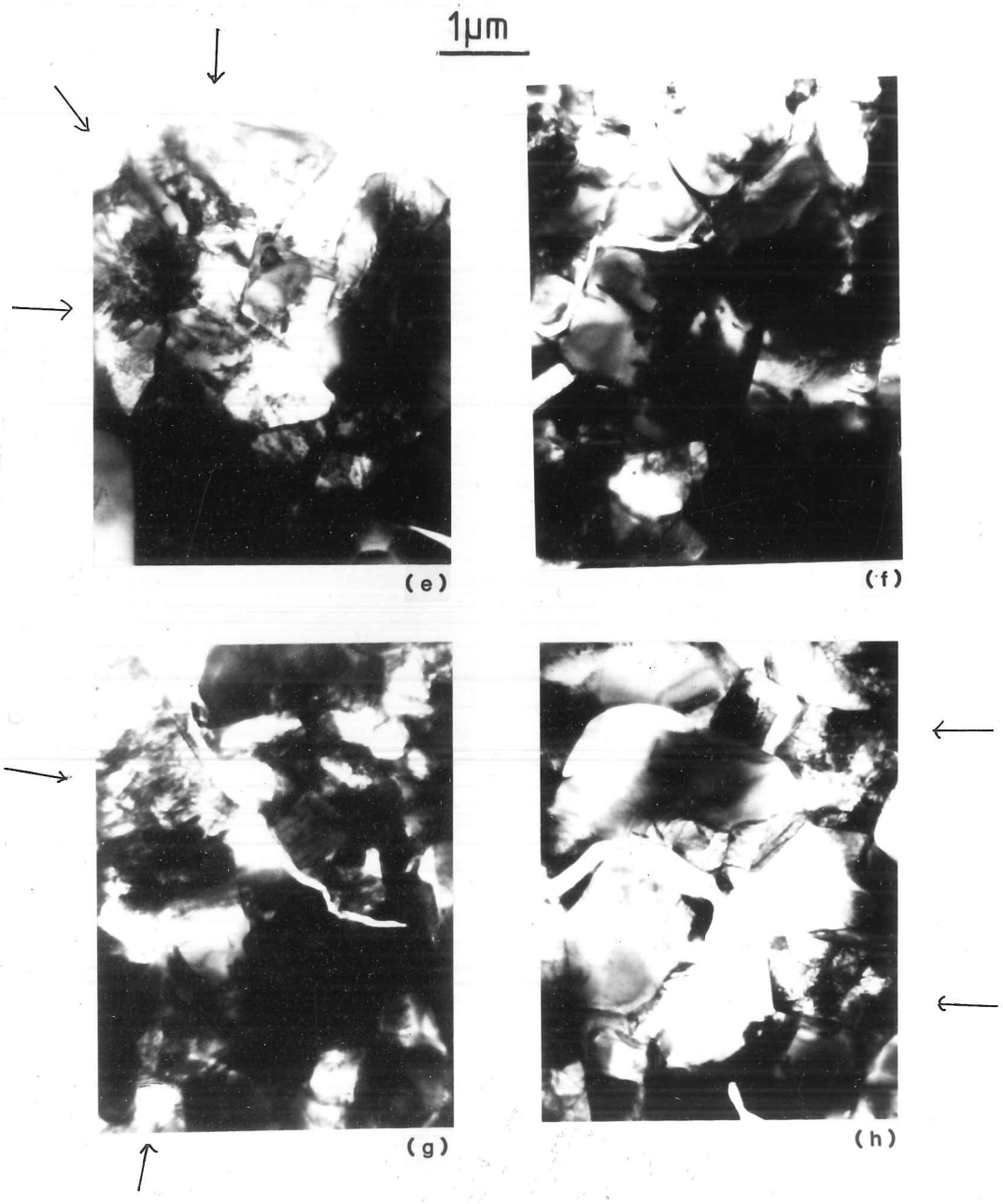

FIGS. 5.3.5.1(e)-(h) TEM examination of unimplanted pin-on-disc specimen:- worn areas. BF images. Note higher dislocation densities than in areas of (a)-(d). (arrowed)

be seen in the carbide grains in either the worn or the unworn regions. Some intergranular cracks can be seen in both the worn and the unworn areas, and are most likely an artefact of the thinning process.

ii) Implanted pin-on-disc specimen (Dose $4 \times 10^{17} N_2^+ cm^{-2}$) (see figs. 5.3.5.2)

The microstructures in the worn and the unworn areas appear identical, though the worn area can be identified by the surface grooving (see 5.3.4). The carbide grains are still easily visible and retain their original shapes, but have internally recrystallised on a fine scale. Within single grains, bands or regions of one predominant microcrystal orientation are present; these could be identified by dark field imageing, and were aligned with the track grooving direction. The microstructure of the cobalt in any region could not be determined.

iii) High-dose ($16 \times 10^{17} N_2^+ cm^{-2}$) specimen (see figs. 5.3.5.3)

This specimen was prepared so that the possible effects of specimen heating in the pin-on-disc test could be assessed. The final microstructure observed consists of finely recrystallised material, similar to that described in (ii) above, though with no bands of preferred orientation. This result differs from that of Greggi and Kossowsky (1981) who found only higher dislocation densities in implanted tungsten carbide. However, their highest dose was $5 \times 10^{16} N_2^+ cm^{-2}$, so it may be that the recrystallisation occurs at the $10^{17} N_2^+ cm^{-2}$ dose level (ie. that required for an effect on the pin-on-disc test).

It can therefore be seen that implantation with nitrogen to high doses ($\geq 10^{17} N_2^+ cm^{-2}$) produces fine scale recrystallisation near the surface. The possible effects of this on wear rates, etc. are discussed in section 5.3.7.

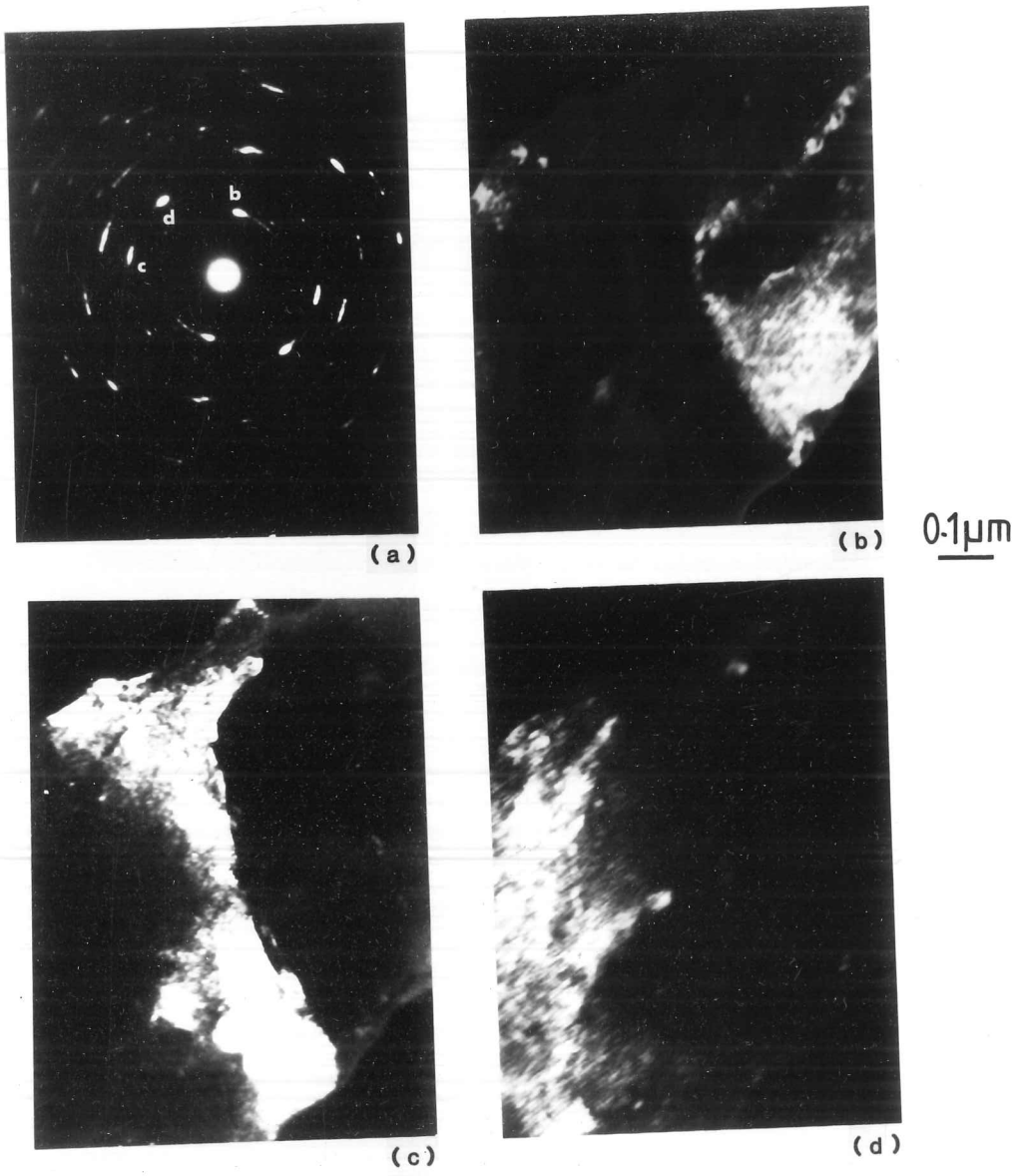

FIGS. 5.3.5.2(a)-(d) TEM examination of implanted pin-on-disc specimen:- unworn area: (a) DP from area shown in (b)-(d); (b)-(d) CDF images, using spots indicated on (a). The area seems to have split into subgrains of preferred orientation.

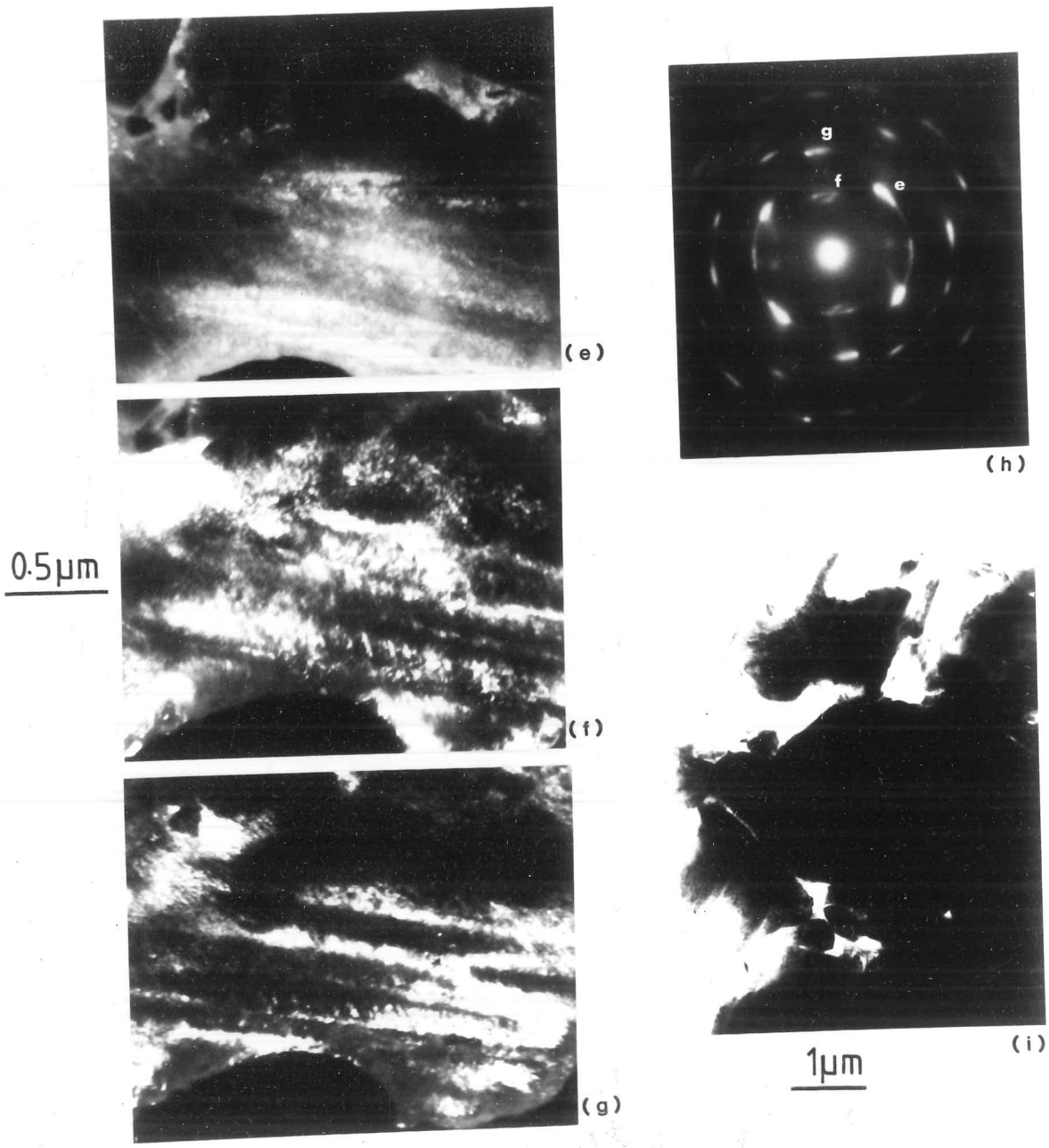

FIGS. 5.3.5.2(e)-(i) TEM examination of implanted pin-on-disc specimen:- worn area: (e)-(g) CDF images of same area, using spots indicated in (h); (i) General view, showing grooving in the track base. The subgrain domains in (e)-(g) are aligned with the grooves.

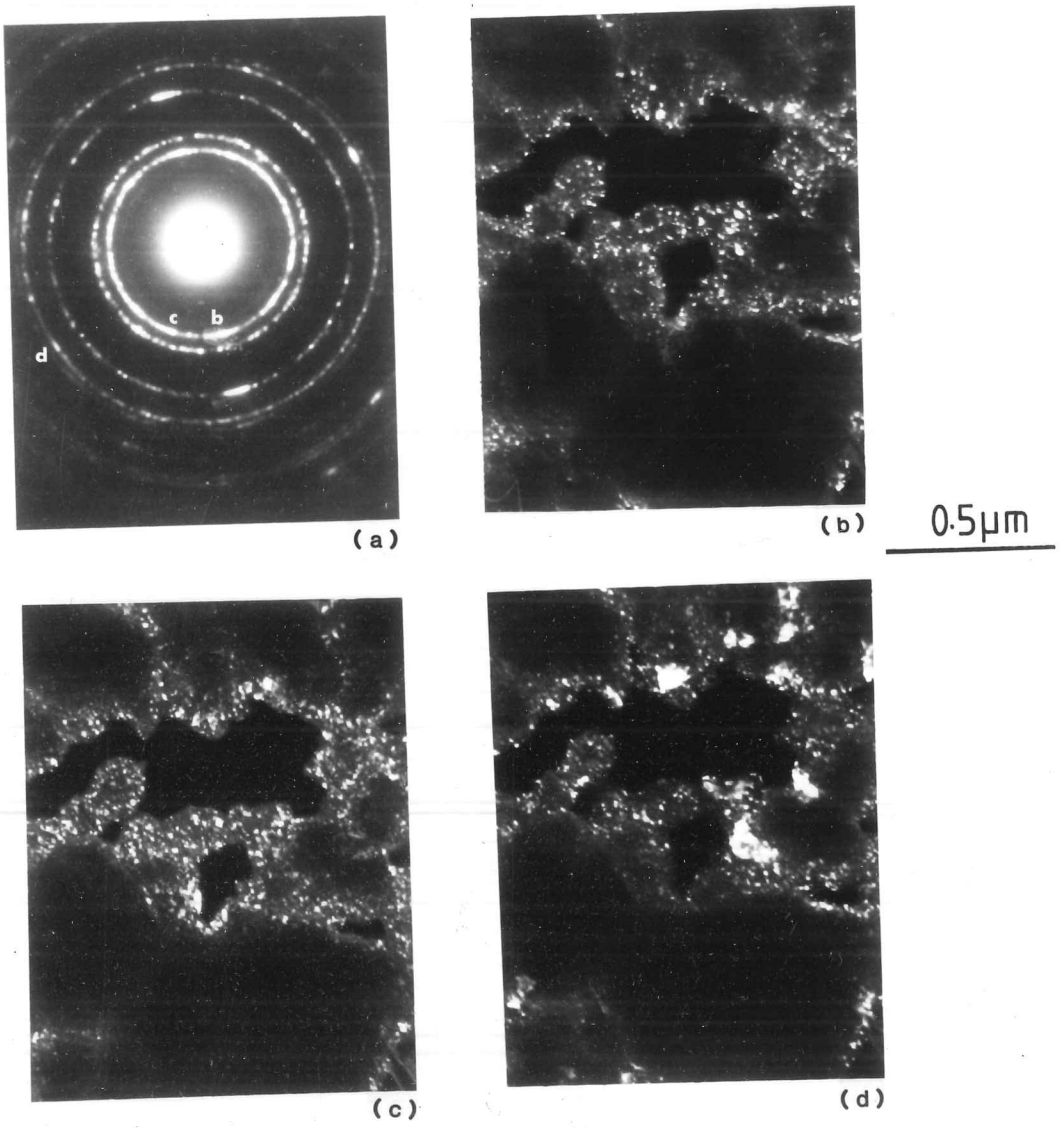

FIGS. 5.3.5.3 TEM examination of high dose ($16 \times 10^{17} N_2^+ cm^{-2}$) implanted WC-Co specimen: (a) DP from area shown in (b)-(d); (b)-(d) CDF images, using the spots indicated in (a). Note fine scale recrystallisation of WC grains.

5.3.6 Microhardness Testing of Nitrogen-implanted Cobalt

i) Materials Description

Since the experiments performed on the composite WC-Co could not easily detect implantation-induced changes in the cobalt phase, this material was implanted and examined separately. It should, however, be noted that the cobalt phase in the composite is certainly very impure compared with the material used here, and that any impurities present (eg. carbon, tungsten), may interact with the implanted nitrogen in unpredictable ways.

Cobalt is a metal with two crystal structures, α (hcp), a=2.51Å, c=4.07Å, which is stable below 417°C, and β (fcc), a=3.54Å [ASM, Metals Handbook, (1975)]. The stacking fault energy in cobalt is very low, and the transformations between the two crystal forms are sluggish. Samples of cobalt usually contain stable amounts of the fcc phase, even at room temperature. The hcp-fcc transformation temperature has been shown to be lowered by ~50°C by the presence of nitrogen [Hansen (1958)]. The atomic volume of the fcc phase is ~0.5% geater than that of the hcp phase, so it might be expected that under high pressures (eg. beneath a hardness indenter) the transformation of residual fcc material to hcp would be encouraged. The yield stress for cobalt has been reported as 345-385 MPa (annealed material), and the hardness as 170 $kgmm^{-2}$ (annealed) and 320 $kgmm^{-2}$ (worked) [Smithells (1976)] (see also results below).

The material used in these experiments was 99.9% pure annealed cobalt foil of 250μm thickness, supplied by Goodfellow Metals. The grain size was 50-100μm, as could be seen from ion etching during implantation. The metal was polished to a 1/4μm finish using diamond paste on laps and cloths, as described in section 4.3.2. Electropolishing was attempted, but no success was achieved in the limited time available (the work carried out in this section was combined with an undergraduate research project). The specimens were implanted to doses up to $6x10^{17} N_2^+ cm^{-2}$ as using the 'Pimento' machine, as described in section 4.1.1. Post-implantation

analysis, (see 4.2) showed that the doses estimated from the implantation times etc. were in error, because of machine miscalibration after a major service. Actual doses were ~40% of those estimated [Turner (1980)]. The maximum dose was therefore $2.4 \times 10^{17} N_2^+ \text{ cm}^{-2}$

ii) Microhardness Testing

Microhardness testing was carried out as described in section 4.4.1, using a load range of 5-200g. Independent indentations and analyses were carried out by the author and the project student (T.C. Jones), so that the variability of results due to operator error could be assessed. Results are shown in figs. 5.3.6.1. At all doses the Meyer index was less than 2, so that the surface hardness was greater than that of the bulk material, but for the implanted specimens this tendency was reduced, and the Meyer index approached 2. The implanted near-surface cobalt was softer than its unimplanted counterpart. Typical diagonal measurements were:

Dose	Diagonal (μm) at	
	10g	5g
zero	6.0 ±0.3	3.8 ±0.2
$2.4 \times 10^{17} N_2^+ \text{ cm}^{-2}$	7.7 ±0.4	5.2 ±0.3

The appearance of the indentations, as seen by light and scanning electron microscopy, did not vary significantly with dose (see figs. 5.3.6.2). All indentations showed pile-up and no fracture was observed. The heavily implanted specimens showed some signs of etching, particularly at grain boundaries.

Attempts were made to prepare TEM specimens from implanted and unimplanted cobalt, but these were unsuccessful, because of excessive foil oxidation. The metal had been kept under dry toluene after the initial polishing, but this is obviously insufficient. Mazey (quoted by Dearnaley and Hartley (1978)), has reported a martensitic fcc to hcp transformation in nitrogen-implanted cobalt and it is possible that strain could be accommodated by such a transformation, as the hcp phase is slightly denser than the fcc phase; such a transformation could account for the observed softening. Further, if the presence of nitrogen stabilises the fcc phase,

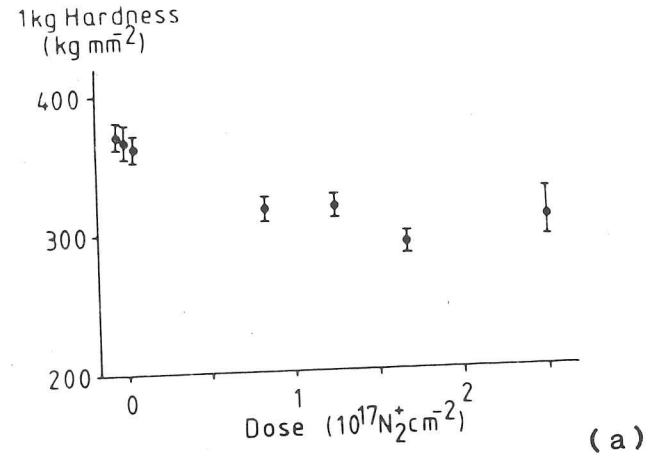

(a)

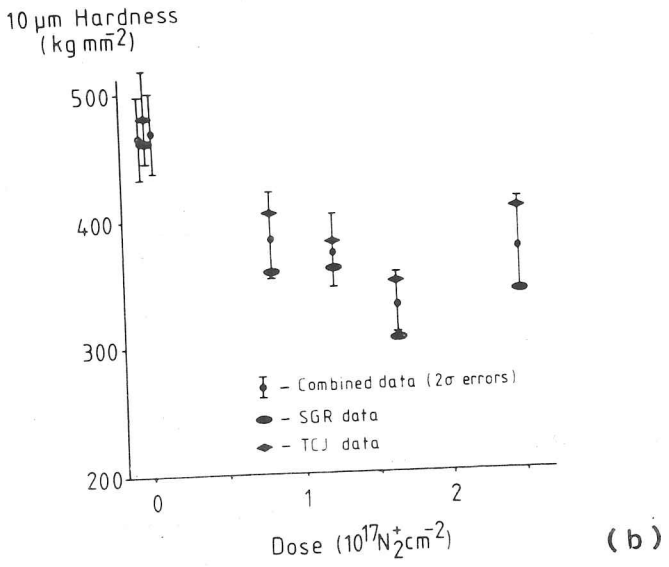

(b)

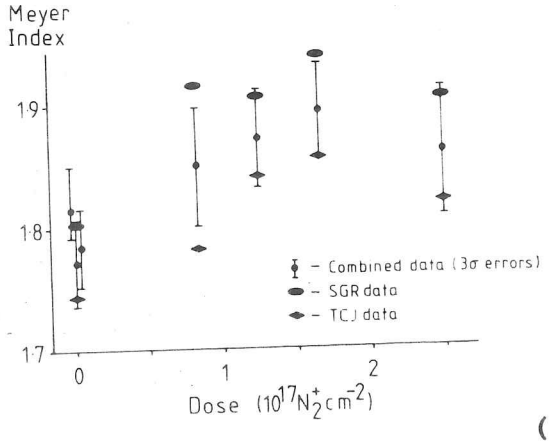

(c)

FIGS. 5.3.6.1 ISE behaviour of nitrogen-implanted cobalt: (a) Hardness at 1kg load; (b) Hardness at 10μm diagonal; (c) Meyer (ISE) index. The surface is softened at all implanted doses. Error bars: (a),(b) 2σ; (c) 3σ.

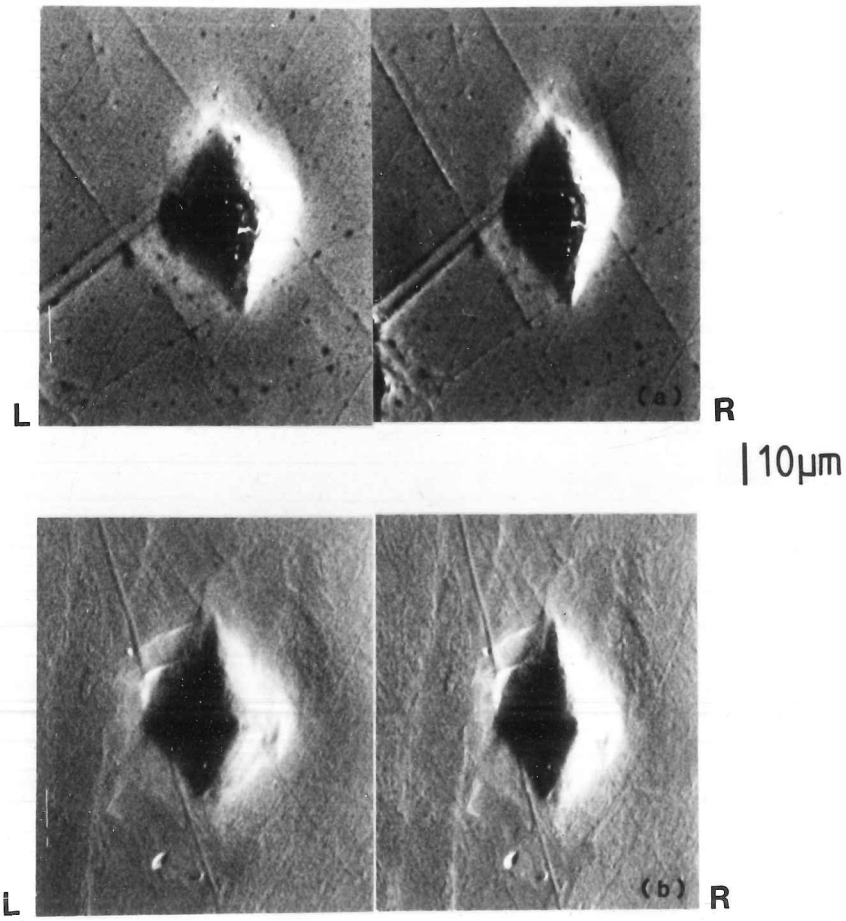

FIGS. 5.3.6.2 200g indentations in cobalt, SEM stereo pairs (30° & 40° tilts): (a) Unimplanted; (b) Dose $2.4 \times 10^{17} N_2^+ cm^{-2}$. No significant change can be seen in the shape of the indentations. The surface of the implanted specimen is roughened by sputtering.

as suggested by Hansen (1958), then more of this metastable phase might be available for such a pressure-induced tranformation after implantation, thus giving rise to the observed softening.

5.3.7 Summary and Discussion of Results for WC-CO and Co

The results given in more detail in sections 5.3.3 to 5.3.6 may be summarised as follows:

i) The hardness behaviour of WC-6%Co is not altered by nitrogen-implantation to doses of $16 \times 10^{17} N_2^+ \text{ cm}^{-2}$, using test loads between 50g and 1kg.

ii) The incidence of fracture at the edges of indentations is increased by nitrogen-implantation. No other type of fracture (eg. lateral, radial/median) was observed.

iii) Examination of pin-on-disc wear tracks in the SEM reveals a contrast reversal between unimplanted and implanted specimens, the tracks on the implanted specimen appearing slightly lighter than their surroundings. No other differences could be seen apart from the greatly reduced amount of wear on the implanted specimen.

iv) Pin-on-disc wear tracks show a small amount of grain pull-out, but this does not seem to be the major material loss process. Cross-sectioning of wear tracks shows no gross structure deformation by pin friction. The bases of wear scars show fine grooving on a scale slightly smaller than that of the carbide grains.

v) TEM observation shows that worn unimplanted WC-Co has a greater dislocation density in the worn area than in the unworn area.

vi) TEM observation of implanted WC-Co shows that the carbide phase has recrystallised on a fine scale. This recrystallisation appears similar in both the worn and the unworn areas of pin-on-disc specimens, apart from the directionality of agglomerations of microcrystals in the worn area.

vi) Cobalt is softened by implantation with nitrogen. This effect occurs at doses lower than $5 \times 10^{16} N_2^+ \text{ cm}^{-2}$.

It seems clear from the results described above that the wear and implantation phenomena occur on a scale finer than the carbide grain size. The wear mechanism seems to involve plastic deformation of the surfaces of

the carbide grains. The fine scale recrystallisation observed in the carbide grains after implantation might hinder such plastic flow by a 'Hall-Petch' type of effect. This would not, however, explain the observations that implantation-induced improvements in the wear rate of WC-Co can continue well after the original implanted layer has been worn away (see 5.3.2). A mechanism such as that proposed by Dearnaley and Hartley (1978), whereby 'Cottrell atmosphere drag' both transports nitrogen into the body of the specimen and reduces plastic flow, might be the cause of this type of behaviour.

5.4 Implantation of Amorphous Materials

The effects of ion implantation on two amorphous materials were studied in order that possible changes in mechanical properties due to implantation-induced amorphisation could be more clearly distinguished from the doping, stressing etc. effects of implantation. The two materials were:

i) A metallic glass, Metglas 2826A, composition $Ni_{36}Fe_{32}Cr_{19}P_{12}B_6$, supplied by J. Patterson and manufactured by the Allied Chemical Corporation, USA.

ii) Pure silica glass, 'Spectrosil', supplied by UGC, Comberton, Cambs. and manufactured by Thermal Syndicate Ltd, UK. Each material is more fully discussed and the results of microhardness testing, etc. are detailed in sections 5.4.1 – 5.4.4.

5.4.1 Microhardness Testing of Nitrogen-implanted Metglas 2826A

The mechanisms of plastic deformation of metallic glasses are not well understood. Deformation at low temperatures (room temperature for 2826A) is concentrated into highly localised shear bands, of thickness up to 200nm, typically 10nm [Donovan and Stobbs (1981)], [Patterson et al. (1978)]. Neither the radially-directed displacement nor the surface-directed flow models of indentation plasticity fit the measured values of E, H, Y and ν and this has been attributed to the peculiarities

of the shear band deformation mechanism [Sargent and Donovan (1982)]. The hardness behaviour is very sensitive to the material's crystallinity. The hardness of Metglas 2826A was investigated by Patterson et al. (1978), who found a substantial rise in the hardness of crystallising metglass before any change could be detected by differential scanning calorimetry. At the same stage of annealing the near-indentation surface pile-up normally seen in the non-crystalline material ceased to occur.

Specimens of this material (supplied as ribbon, 1.8mm x 50μm) were prepared by cutting 10 pieces approximately 30mm long, which were fixed using epoxy resin to an aluminium stub. Polishing was performed by hand on 14μm and 6μm diamond paste laps, followed by polishing on 6μm and 1μm paste on cloths (see 4.3.2). The final stage of polishing was performed using 0.05μm alumina slurry in a vibratory polishing machine for 12 hours. This procedure was found by Patterson (1980) to give a virtually undeformed surface for subsequent microhardness testing.

The specimens were implanted with nitrogen, using the 'Pimento' machine (see 4.1.1), to doses of 2, 4, 6 and $8 \times 10^{17} N_2^+ cm^{-2}$. Microhardness testing was carried out using loads of 10-200g, and the results analysed by the program described in section 4.4.1. The range in the sizes of the indentations thus produced was from ~4μm to ~25μm. Results are shown in figs. 5.4.1.1. It can be seen that no change occurs in the hardness behaviour over the dose range used. The surface topography near the indentation does not change with dose, as shown in figs. 5.4.1.2; pile-up is visible at all loads, and is similar in form and extent at all doses.

These results indicate that:

i) The operative deformation mechanism is still by shear bands;

ii) The surface (non)crystallinity has not been changed, either by the displacement damage involved in implantation (see 2.1.1), or by thermal effects (the max. temperature during implantation was estimated to be ~300°C (see 4.1.1));

iii) The large surface stresses probably introduced by the implantation, and the high concentrations of nitrogen certainly present (down to ~0.5μm depth) do not alter the yielding and flow characteristics of the material enough to change the microhardness behaviour.

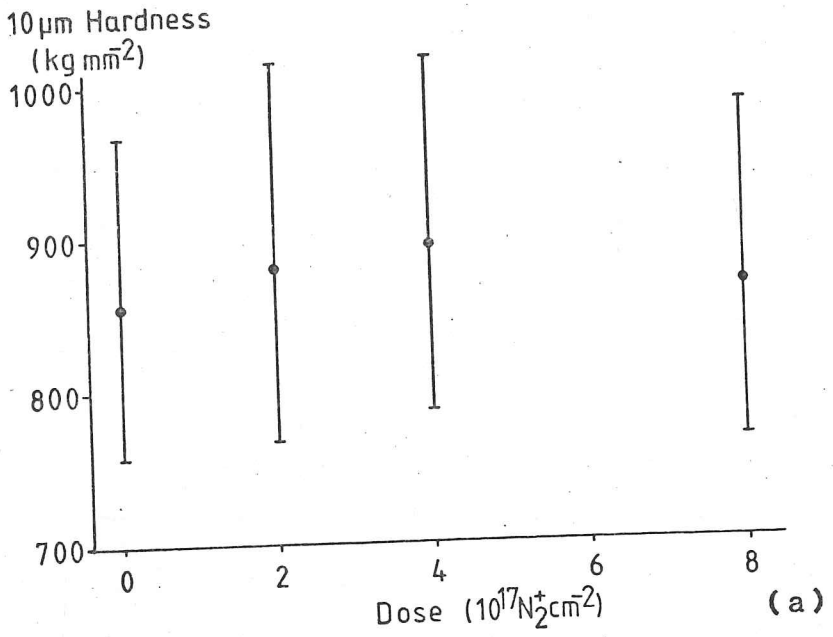

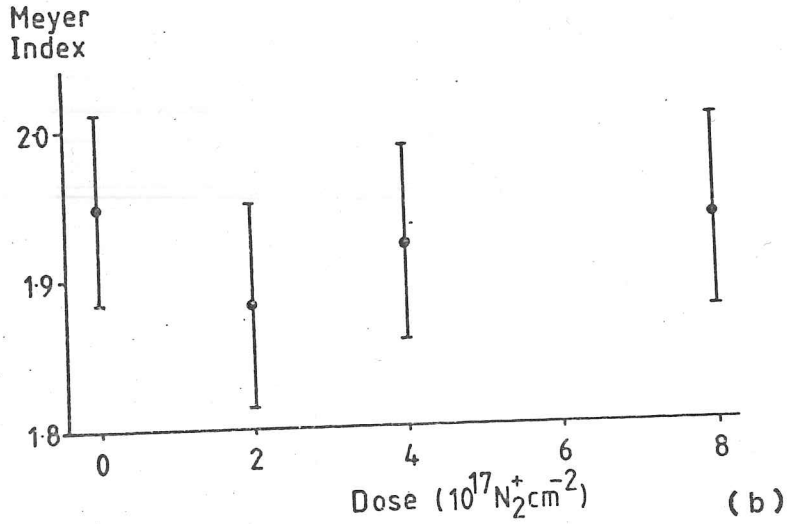

FIGS. 5.4.1.1 ISE behaviour of nitrogen-implanted Metglas 2826A: (a) Hardness at 10μm diagonal (2σ error bars); (b) Hardness at 10μm diagonal (3σ error bars). No significant change in behaviour occurs with increasing dose.

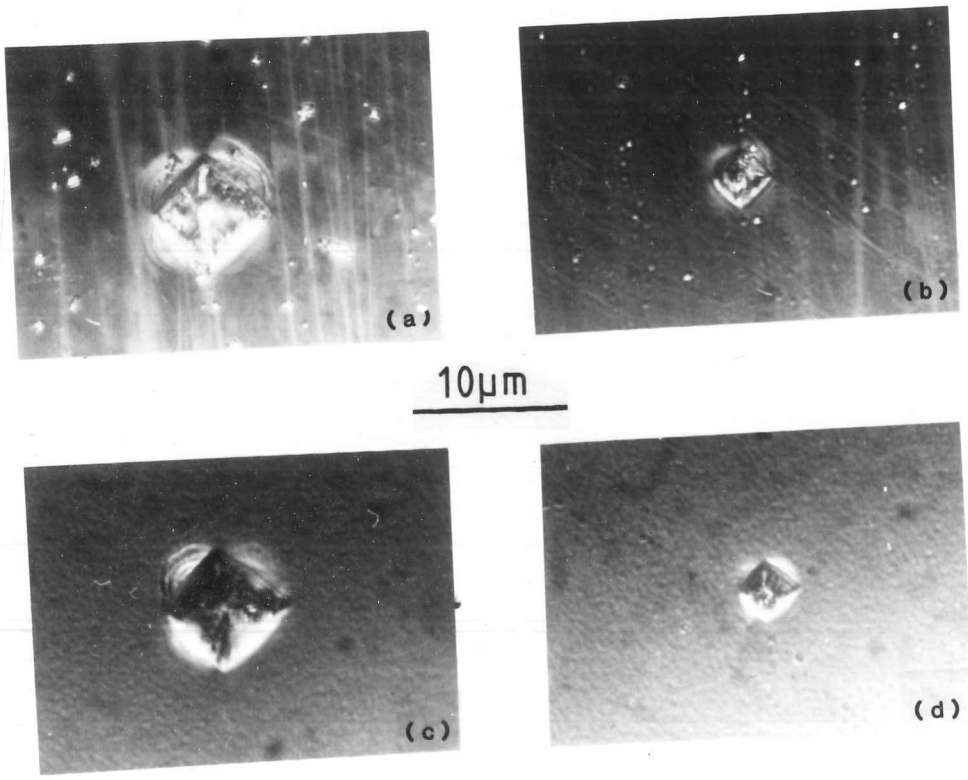

FIGS. 5.4.1.2 Indentations on Metglas 2826A. Optical micrographs: (a),(b) 100g load; (c),(d) 25g load; (a),(c) Unimplanted; (b),(d) Dose $8 \times 10^{17} N_2^+ \text{ cm}^{-2}$. The morphology of the indentations does not change with dose.

5.4.2 Silica Glass- Materials Characteristics

This material was claimed by the manufacturers to be a pure, annealed silica glass, with no crystallinity. A sample was chemically analysed and found to have no contaminants even at the ppm level [Sturton (1981)]. The crystallinity and the annealing state were not checked. The specimens were supplied in a good state of polish, in the form of 10mm diameter x 2mm thick discs.

The deformation mechanisms in this type of material are not well understood. Marsh (1964) notes that for both pure and modified (ie. alkali metal ions added) glasses, the flow stress is much lower than that required for fracture. He also points out that neither compaction and relaxation of the material, nor viscous flow alone as yielding mechanisms adequately account for the observed behaviour on indentation. Hagan (1980) has shown that beneath high load (1-10kg) indentations in soda-lime glass flow occurs in narrow shear bands, although the nature of the flow mechanism is unclear. Intersection of such bands can lead to crack nucleation.

Silica glass materials, usually of the modified type (soda-lime glass), have been widely used as model isotropic brittle materials in studies of indentation fracture mechanics. Fracture data for this type of material are [Lawn (1979)]:

Hardness	610 $kgmm^{-2}$
K_{Ic}	0.7 $MNm^{1/2}$
P^*	0.02N
c^*	1.5μm
E	73 GPa*

Fracture would therefore be expected at all loads within the 25-1000g range used in the microhardness tests decribed in section 5.4.3. However the cracks observed (see 5.4.4) were in the form of Hertzian-type cone cracks (see 3.2.2) and median/radial cracks, rather than the lateral and median/radial cracks seen by eg. Lawn and Wilshaw (1975b) in soda-lima

---

* [EerNisse (1973)]

glass. Hagan (1979) has observed similar Hertzian-type fracture in pure silica glass. Presumably this difference in fracture behaviour is due to some intrinsic difference between the mechanical properties of the two types of glass. Marsh (1964) and Yoffe (1982) have suggested that the difference lies in the available free space in the glasses for compaction on indentation (this would also be expected to alter the flow properties).

Silica glass is also of interest for implantation studies as EerNisse (1974) has shown that the material undergoes a compaction, leading to an in-surface tensile stress, on implantation. For ions of mass 10-20 Daltons, the effect peaks at a dose of $\sim 10^{14}$ ions cm^{-2}; beyond this dose, the tensile stress rapidly decreases (see fig. 5.4.2.1). Results given in section 5.4.4 indicate that compressive stresses are produced at the higher doses used in this study.

Specimens were implanted using the 'Pimento' machine (see 4.1.1) to doses of 1, 2, 3 and $4 \times 10^{17} N_2^+$ cm^{-2}. The specimen implanted to $4 \times 10^{17} N_2^+$ cm^{-2} had previously been indented, using loads in the range 25-1000g.

5.4.3 Microhardness Testing of Nitrogen-implanted Silica Glass

Specimens were indented using a load range of 25-1000g, and were examined by light and scanning electron microscopy. It was found that the cracking produced at all loads made measurement of indentation sizes by the normal method impossible, even after the application of a sputtered gold coating. Microhardness values were therefore calculated from measurements made from SEM images (see 4.4.1). Only indentations at loads of 25g, 50g and 100g could be measured, because of the extent of cracking at higher loads. Results are shown in table 5.4.3a. It can be seen that there is no significant change in the microhardness behaviour with dose. Measurements on the SP1 specimen were made after a 1 minute vibropolish (so as to enhance crack visibility); here both the pre-implantation indentations and the post-implantation indentations are the same sizes, and are smaller than the indentations on the other specimens by an amount consistent with the removal of $\sim 1/4 \mu m$ of the surface by vibropolishing.

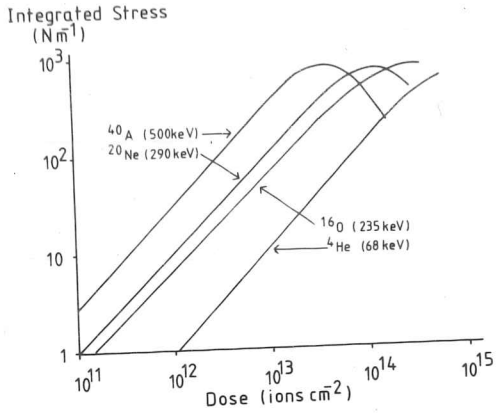

FIG. 5.4.2.1 Data of Eernisse (1974) for stresses produced by low-dose implantation into silica glass. Stresses are tensile in the plane of the surface. Note peaking and decrease of the stresses at high doses.

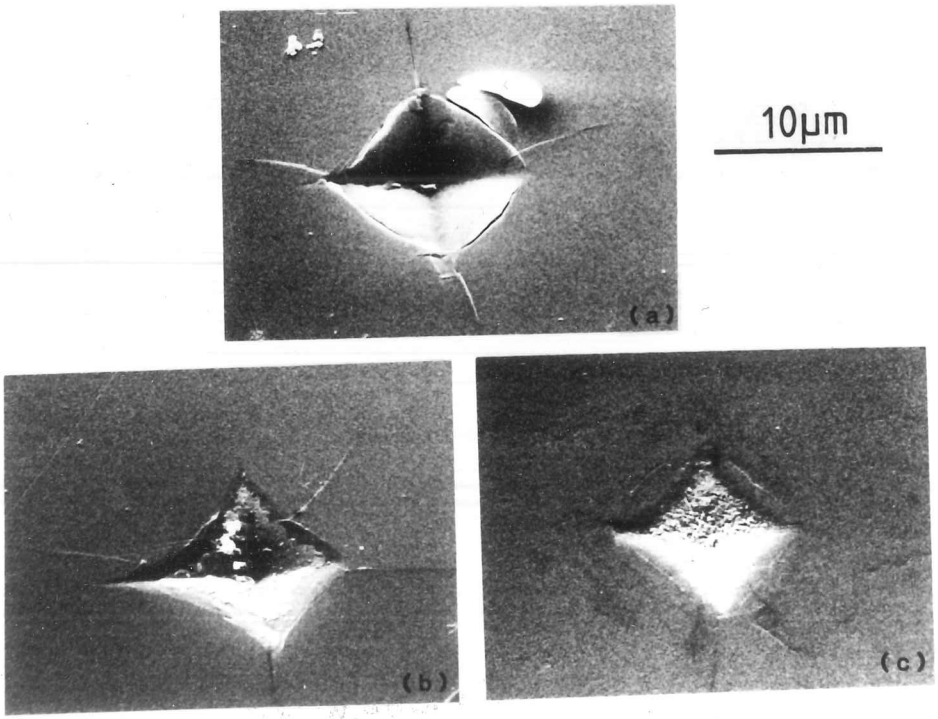

FIGS. 5.4.3.1 100g indentations on silica glass, SEM (secondary electron) images: (a) SPU5 (unimplanted); (b) SPI1, indented before implantation to $4 \times 10^{17} N_2^+ cm^{-2}$; (c) SPI3, dose $2 \times 10^{17} N_2^+ cm^{-2}$. Note 'pincushioning' of indentations as dose increases.

TABLE 5.4.3a

Microhardness Results for Silica Glass

Specimen code	Dose ($\times 10^{17} N_2^+ cm^{-2}$)	Diagonal (μm) at load: 100g	50g	25g
SPU5	zero	13.6	8.7	6.6
SPU1*	zero, subsequently implanted (SPI1)	10.8	6.0	4.0
SPI4	1	13.8	8.0	5.4
SPI3	2	12.5	7.5	5.1
SPI2	3	13.1	8.6	6.2
SPI1*	4	11.2	7.5	4.6
MEAN	-	13.3	8.2	5.8
Mean Hardness ($kgmm^{-2}$)	-	1045	1380	1380

Errors in diagonal measurement $\pm \sim 1 \mu m$.
* measured after 1 min. vibropolish (not included in mean)

The shapes of the hardness indentations vary with dose as shown in figs. 5.4.3.1. Those on SPU5 (unimplanted at any stage) are square, or even slightly barrelled in some cases. As the implantation dose increases, indentations appear increasingly pincushioned, whether the indentations were made before or after implantation. This is explicable in terms of an in-surface compressive stress, leading to increased elastic recovery.

5.4.4 Indentation Fracture in Nitrogen-implanted Silica Glass

Figs. 5.4.4.1 show typical fracture patterns around indentations. At high loads (300-1000g), spectacular Hertzian-type cone fracture is seen. This type of fracture is unaffected in incidence or extent by implantation up to the maximum dose used here. At lower loads, the cracks appear only as rings on the surface of the specimens. Incidence of such cracks is reduced with increasing implantation dose. Another form of cracking is seen at low loads, where the cracks lie close to and parallel to the indentation edges (similar to those seen in silicon carbide (see 5.1.4)). This type of cracking is eliminated by implantation to a dose of $4 \times 10^{17} N_2^+$ cm^{-2}. All these types of fracture are initiated on the surface by tensile components of the stress field around the indentation (see 3.2.2). Their reduction by implantation is consistent with the existence of an in-surface compressive stress, as is the elastic recovery in indentation shape noted in section 5.4.3. EerNisse (1974) found that a tensile surface stress was produced in silica glass by implantation to doses $\sim 10^{14}$ ions cm^{-2}. The most likely structural explanation for these apparently conflicting results is that the initial effect of implantation is partial structural collapse, leading to a compaction; at higher doses, the 'stuffing' effect of the large number of implanted atoms gives a surface expansion and thus a compressive stress.

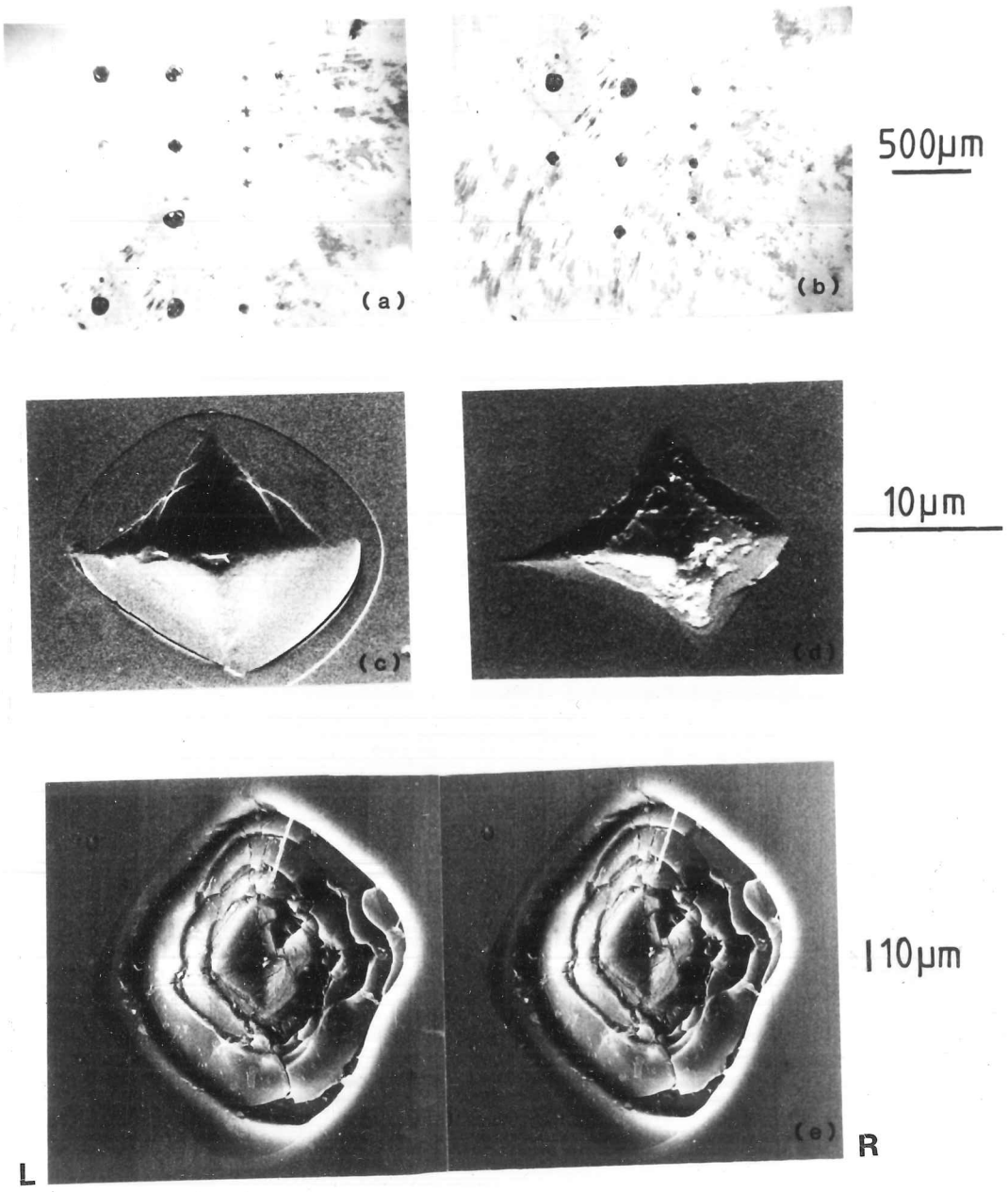

FIGS. 5.4.4.1 Indentation fracture in silica glass: (a),(b) Optical micrographs of 1kg, 500g, 300g, 200g and 100g indentations on (a) Unimplanted; (b) Implanted, dose $4x10^{17}N_2^+$ cm^{-2}, material. (c),(d) SEM (secondary electron) images, 100g indentations on (c) Unimplanted; (d) Implanted, dose $4x10^{17}N_2^+$ cm^{-2}, material. (e) SEM stereo pair (30^o& 40^o tilts) of Hertzian-type fracture around 1kg indentation in unimplanted silica glass. Indentation-edge and surface ring fracture is suppressed around low-load indentations by high-dose implantation.

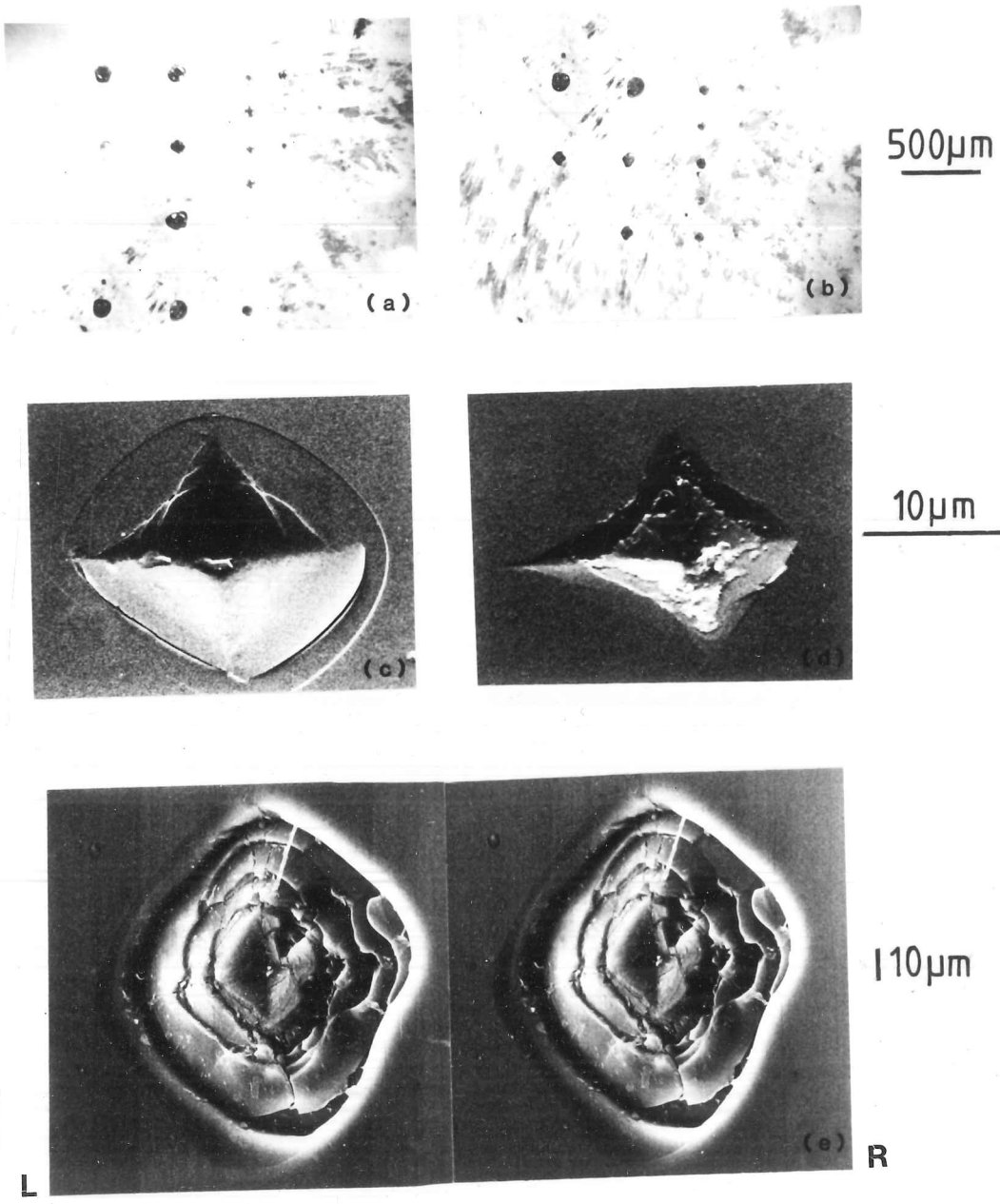

FIGS. 5.4.4.1 Indentation fracture in silica glass: (a),(b) Optical micrographs of 1kg, 500g, 300g, 200g and 100g indentations on (a) Unimplanted; (b) Implanted, dose $4x10^{17}N_2^+$ cm^{-2}, material. (c),(d) SEM (secondary electron) images, 100g indentations on (c) Unimplanted; (d) Implanted, dose $4x10^{17}N_2^+$ cm^{-2}, material. (e) SEM stereo pair (30^o& 40^o tilts) of Hertzian-type fracture around 1kg indentation in unimplanted silica glass. Indentation-edge and surface ring fracture is suppressed around low-load indentations by high-dose implantation.

5.5 Experiments with Nitrogen-implanted Lithium Fluoride

5.5.1 Materials Description

Lithium Fluoride (LiF) is an ionic solid with the sodium chloride crystal structure. It cleaves readily on {100} and less easily on {110}; large single crystals of known orientation can be easily prepared. Since the initial study of Gilman and Johnston (1957), who showed how etching could reveal the positions of dislocations, the relationships between dislocation behaviour and macroscopic mechanical properties of LiF have been extensively researched. The principle slip systems are {110}<1T0>. Microhardness indentations produce large dislocation loops on {110} planes, which can be revealed by suitable etching as 'rosettes', as reviewed by Hockey (1973). The geometry of such a rosette is shown in fig. 5.5.1.1. and a typical rosette is shown in fig. 5.5.2.1a. Rosette diameters for indentations in the load range used here (5-200g) ranged from 20 to 200μm (see 5.5.2).

Plastic flow in LiF is known to be affected by ionising radiation, which produces 'colour centres'. These are localised electrically charged defects of various configurations [eg. Kittel (1976)]. Dislocations in ionic materials have electrically complicated core structures; in particular, kinks and jogs have an associated charge. Dislocations can therefore be strongly pinned by charged defects, and so lithium fluoride can be hardened by X-irradiation [Whapham (1957)], [Catlow et al. (1980)].

By contrast with X-radiation, ion implantation would be expected to produce displacement damage rather than ionisation. The affected layer would also be very thin compared with the penetration of X-rays; the intensity is proportional to $e^{-depth/0.3mm}$ in LiF for $Cr_{K\alpha}$ [MacGillavry and Rieck (1962)]). In this study, the effects of implantation alone and of implantation combined with X-irradiation were examined by microhardness testing and etching.

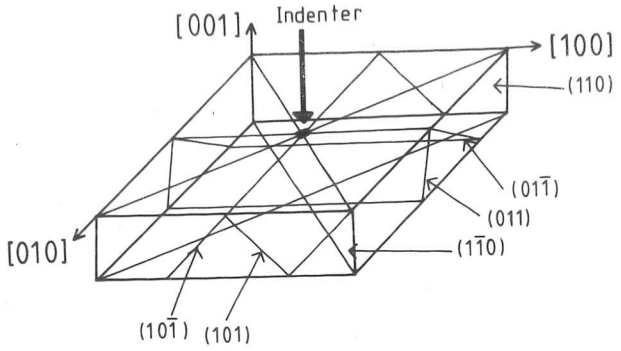

FIG. 5.5.1.1 Slip planes in LiF, intersecting at an indenter. Dislocation loops on these planes can be etched on the indented surface to form a 'rosette'.

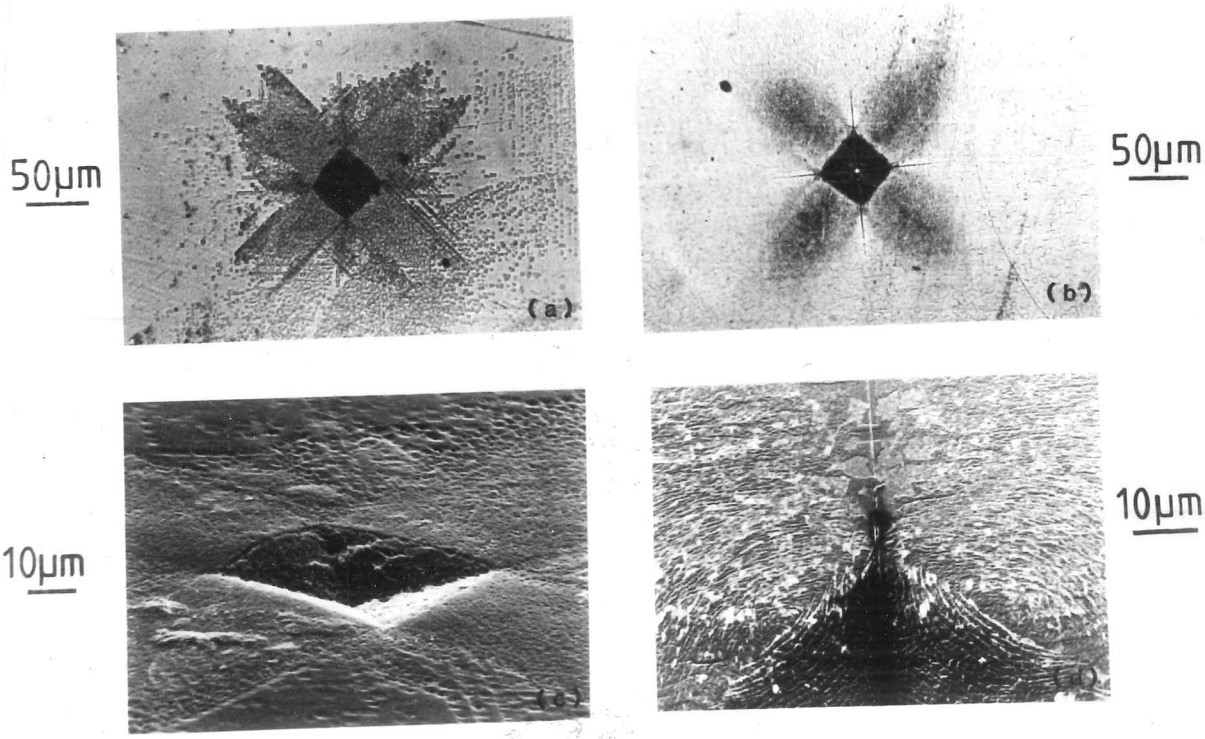

FIGS. 5.5.2.1 Rosettes around 200g indentations in LiF: (a),(b) Optical micrographs; (c),(d) SEM (secondary electron) images; (a),(c) Unimplanted LiF; (b),(d) Dose $6 \times 10^{17} N_2^+ cm^{-2}$. Note radial cracks in implanted LiF, and the different etching behaviour of the rosette arms.

Specimens were prepared by cleavage from larger crystals. The implanted specimens were cleaved immediately before implantation in the 'Pimento' machine (see 4.1.1) and subsequently kept in a well-sealed box containing absorbent silica gel. This was to avoid contamination of the active surfaces by water vapour, which degrades the surface finish and can alter the hardness behaviour [Sargent (1979)]. Etching was performed in saturated FeF_3 solution at 70°C; production of good etch pit rosettes took 2-10 mins, the implanted specimens in particular needing longer etching times. The specimens were examined by light microscopy and SEM. For the latter, a sputtered coating of gold was applied, and this was found also to improve contrast in the optical microscope.

5.5.2 Microhardness Testing of Nitrogen-implanted LiF

Tests were performed on freshly-cleaved, unimplanted lithium fluoride and on material implanted to a dose of $6\times10^{17} N_2^+ cm^{-2}$. A load range of 5-200g was used; the indentation diagonals were aligned parallel to <100>. Results are shown below:

Dose	Meyer index	$H_{10\mu m}$	H_{200g}
zero	1.99 ±0.05	112 ±8	112 ±4
$6\times10^{17} N_2^+ cm^{-2}$	1.99 ±0.06	110 ±9	107 ±3

It can be seen that no changes in the microhardness behaviour are produced by implantation.

It was thought that this null result might be due to the difference in scale between the dislocation loops produced by the indentation process and the implantation-affected layer. Whatever the mechanical properties of a disordered ionic solid, a layer less than a micron deep would not be expected to change the motion of large (10-100μm deep) dislocation loops. This is particularly the case if, as has been proposed by Swain and Lawn (1969), the dislocation loops are nucleated some distance beneath the surface. In order to check this possibility, the samples were etched as described in section 5.5.1 and the resultant rosettes examined (see figs.

5.5.2.1). The rosettes on the unimplanted specimens were well-formed with individual dislocation etch pits easily visible. Those on the implanted specimen were rather ill-defined. The etched area appeared to have linear, rather than point, features. The short rosette arms in the <100> directions, present on the unimplanted specimens, were not visible on the implanted specimens. SEM examination showed these differences in etching behaviour more clearly; the action of the etchant inside the indentations could also be observed (see figs. 5.5.2.1c,d). The rosettes on the implanted specimen seem to consist of ripples, roughly parallel to the indentation edges. Similar rosette structures were produced on specimens implanted to doses of 2 and $4 \times 10^{17} N_2^+ \text{ cm}^{-2}$. These surface rippples are probably caused by a large number of dislocation loops ending in the disordered layer, just below the surface; however, their linear nature is not easy to explain.

Comparison of rosette sizes showed that the rosettes in the implanted specimens were slightly smaller than those on the implanted specimens. However, the rosette ends in the implanted material were very poorly defined, and the difference could easily be due to measuring difficulties. Attempts were made to measure the rosette size beneath the implanted layer by vibropolishing the specimens so as to remove ~1/2μm of the surface. However, even this relatively gentle polishing treatment introduced enough surface damage to affect the etching behaviour severely, and measurement of the rosette sizes was impossible because of the high etch pit density over the whole surface. The unimplanted and the implanted specimens appeared identical after such treatment.

Differences could be seen in the indentation fracture behaviour of implanted and unimplanted specimens. Indentations in the unimplanted material showed no fracture, even at the highest loads. Indentations in the implanted material, even at the minimum load (5g), and dose ($2 \times 10^{17} N_2^+ \text{ cm}^{-2}$) used, showed radial cracking. The cracks extended in the <100> directions from indentation corners; some low-load indentations also showed cracking along <110>. The crack lengths were measured and the results are shown in table 5.5.2a. It is unlikely that implantation affects simply the crack growth, since no cracks were observed even at the highest load on the unimplanted material. Implantation must alter the crack

TABLE 5.5.2a

Crack Lengths in Implanted LiF

Indenting Load (g)	Indentation Diagonal (μm)	Crack Length (μm)
200	59 ±2	140 ±20
100	40 ±2	90 ±10
50	30 ±1	50 ±5
25	20 ±1	41 ±5

Crack lengths are total end-to-end lengths, including the indentation diagonal.

nucleation. Two possibilities exist:

i) Cracks nucleate beneath the surface, in normal material; the stress field associated with implantation facilitates crack nucleation (the stress field is compressive at the surface, but may have tensile and shear components at greater depths).

ii) Cracks nucleate at the surface; the implanted material has a lower fracture toughness than normal LiF.

So as to distinguish between these two possibilities, attempts were made to prepare specimens cross-sectioned through indentations, as described in section 4.4.2. However, there was a strong tendency for specimens to cleave along random <100> planes rather than those through the indentations, and so only one specimen (of dose $2 \times 10^{17} N_2^+ \text{ cm}^{-2}$) was successfully prepared. Examination of the specimen (see figs. 5.5.2.2) suggested that surface nucleation of the cracks had occurred, on each side of the indentation separately, and so that implanted LiF has a lower fracture toughness than unimplanted LiF. Etching of the specimen showed the penetration of dislocation loops into the material.

5.5.3 Implanted and X-irradiated Lithium Fluoride

As ion implantation would be expected to produce some displacement damage even at depths large compared with the mean ion range, some implanted specimens (dose $6 \times 10^{17} N_2^+ \text{ cm}^{-2}$) were subsequently X-irradiated so as to investigate the interactions of displacement and ionisation damage. Unimplanted specimens were also X-irradiated.

The specimens were mounted on a slotted lead sheet so that a region approximately 3mm in width in the centre of each specimen was exposed to the X-rays. The implanted specimens were oriented with the implanted surface facing the beam. The radiation used was $Cr_{K\alpha}$ (λ = 2.291 Å) from a Siemens Sequential X-ray Spectrometer, using a Kristalloflex 4 source operating at 50kV and 40mA. Exposure was for 7 hours.

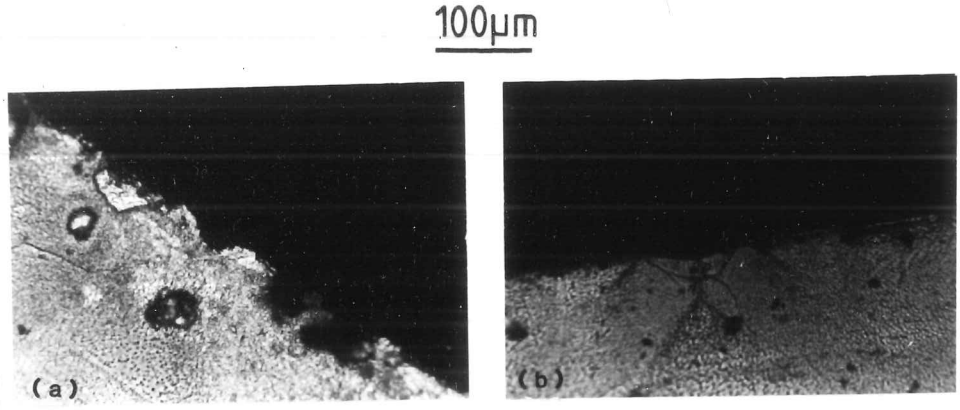

FIGS. 5.5.2.2 Broken-open 200g indentations in LiF, dose $2x10^{17}N_2^+$ cm^{-2}, after etching. Optical micrographs. Cracks appear to be close to the surface, and to have nucleated seperately on ech side of the indentation.

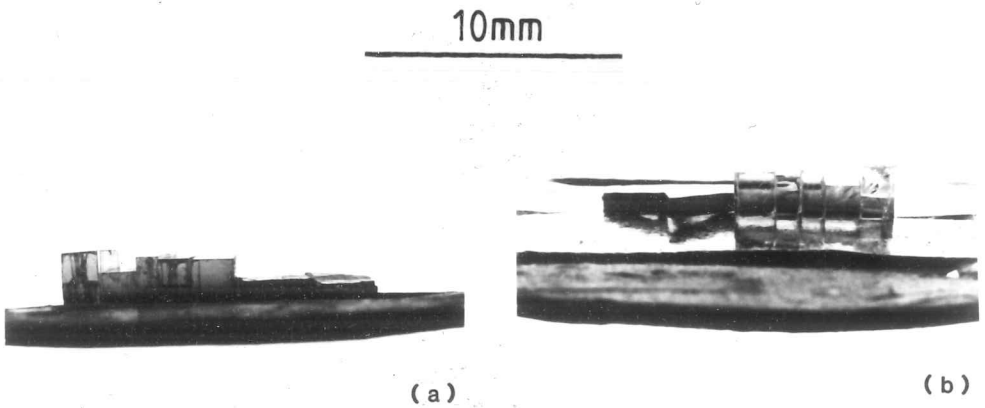

FIGS. 5.5.3.1 X-irradiated LiF. The thinnest two specimens (rightmost in (a)) were pre-implanted to $6x10^{17}N_2^+$ cm^{-2}. These specimens are dark throughout. The unimplanted LiF specimens show a rapid decrease in colour density with depth.

Initial examination of the samples showed a surprising difference between the pre-implanted and the normal LiF (see figs. 5.5.3.1). The unimplanted specimens were dark brown in colour near to the exposed surface, fading rapidly to yellow over a depth of ~1mm. The implanted specimens were dark right through their thickness, with only a slight attenuation in colour with depth. This can only be attributed to the effects of ion channelling (see 2.1.2). Only a very small fraction of the incident nitrogen could be channelled to any depth along the <100> direction, but enough seem to do so, producing displacement damage when finally dechannelled, to produce the vacancies required to form colour centres on X-irradiation. It is quite remarkable how effective the process is, producing a deep colour even at 1-2mm depth.

Since such strong colour effects were produced, it was decided to investigate the hardness of implanted/irradiated crystals in cross-section. Rosette sizes could then be easily measured as all tests would be carried out on crystalline material. Crystals were cleaved normal to the implanted and/or irradiated surface. Indentations were made at a load of 25g in a line that traversed the irradiated zone at constant depth (75μm), and in a line going into the depth of the crystal. Results of the hardness measurements are shown in fig. 5.5.3.2. It can be seen that pre-implanted and unimplanted specimens are indistinguishable in their hardness behaviour.

The specimens were then etched and the rosette sizes measured. Data from indentations to a depth of 1mm are shown in fig. 5.5.3.3. It can be seen that the rosettes in the pre-implanted specimens are consistently smaller than those in the unimplanted specimen, but that the difference is small except within the ~150μm nearest to the irradiated surface. This depth is still ~300x that of the peak ion range. The small reduction in the size of rosettes in the preimplanted specimen at depths greater than 150μm might be dismissed as being within experimental error were it not that the direction of the change is consistent with that seen near the surface, and that the unimplanted crystal is slightly harder than the implanted crystal in the unirradiated region (see fig. 5.5.3.2).

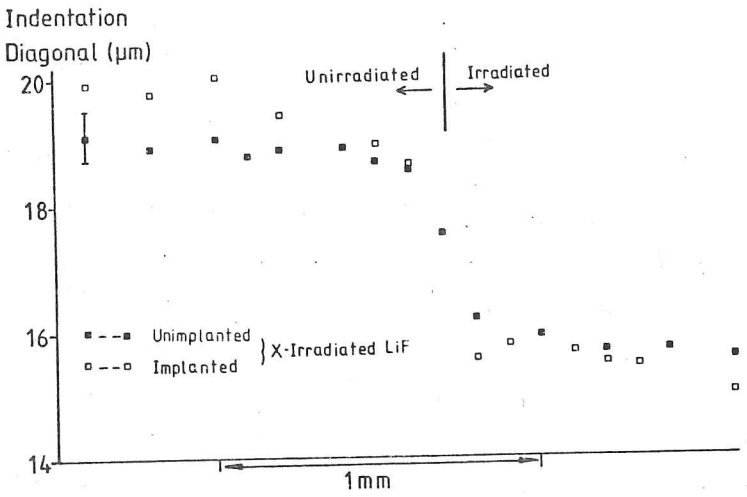

FIG. 5.5.3.2 50g indentations at 75μm depth, crossing the irradiated/unirradiated boundary. The pre-implanted and the unimplanted specimens are indistinguishable in their hardness behaviour.

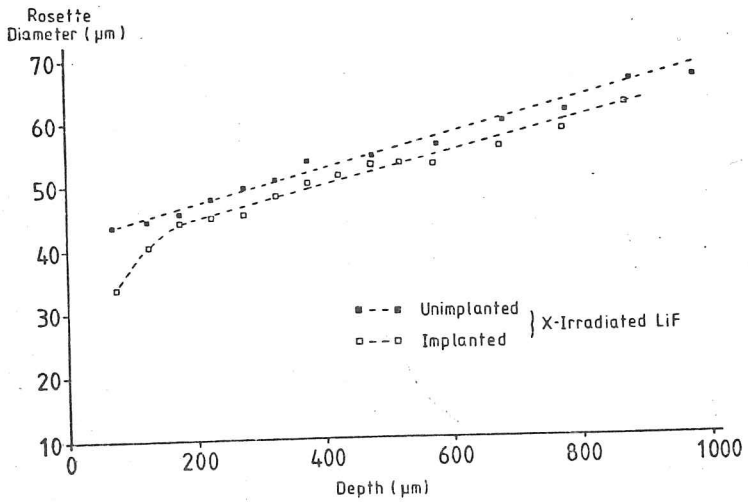

FIG. 5.5.3.3 Rosette diameter (50g indentations) variation with depth on pre-implanted and unimplanted LiF, after X-irradiation. The pre-implanted LiF show a consistently smaller rosette size, particularly within ~200μm of the surface.

The changes in rosette size at depths up to 1mm in the pre-implanted specimens were much less marked than the changes in colour, thus indicating that the colour centres inhibiting dislocation motion are not exclusively those causing the colour change. Also, the centre producing the yellow colour (by absorption of blue light at ~3.5 eV) must have a more complex structure than the simple F-centre of energy ~5.0 eV [Kittel (1976)]. It is probable that more simple than complex colour centres exist, and thus that these are the ones most contributing to the restriction of dislocation motion.

5.5.4 Summary of Results for Lithium Fluoride

The results given in more detail and discussed in sections 5.5.2 and 5.5.3 may be summarised as follows:

i) Ion implantation alone does not affect the hardness or rosette sizes on the implanted surface, up to a dose of $6 \times 10^{17} N_2^+$ cm^{-2};

ii) Implantation produces microstructural change in the surface that alters the etching behaviour;

iii) The implanted surface has a lower fracture toughness than the unimplanted material;

iv) Pre-implanted X-irradiated specimens show an accentuated rosette size reduction in the irradiated zone compared with unimplanted irradiated samples. The effect persists significantly to a depth of ~150μm;

v) Colour changes in the X-irradiated zone persist to a far greater depth in the pre-implanted specimens. This effect is probably due to channelling of a small fraction of the implanted ions.

The changes in rosette size at depths up to 1mm in the pre-implanted specimens were much less marked than the changes in colour, thus indicating that the colour centres inhibiting dislocation motion are not exclusively those causing the colour change. Also, the centre producing the yellow colour (by absorption of blue light at ~3.5 eV) must have a more complex structure than the simple F-centre of energy ~5.0 eV [Kittel (1976)]. It is probable that more simple than complex colour centres exist, and thus that these are the ones most contributing to the restriction of dislocation motion.

5.5.4 Summary of Results for Lithium Fluoride

The results given in more detail and discussed in sections 5.5.2 and 5.5.3 may be summarised as follows:

i) Ion implantation alone does not affect the hardness or rosette sizes on the implanted surface, up to a dose of $6 \times 10^{17} N_2^+$ cm^{-2};

ii) Implantation produces microstructural change in the surface that alters the etching behaviour;

iii) The implanted surface has a lower fracture toughness than the unimplanted material;

iv) Pre-implanted X-irradiated specimens show an accentuated rosette size reduction in the irradiated zone compared with unimplanted irradiated samples. The effect persists significantly to a depth of ~150μm;

v) Colour changes in the X-irradiated zone persist to a far greater depth in the pre-implanted specimens. This effect is probably due to channelling of a small fraction of the implanted ions.

CHAPTER 6

SUMMARY, DISCUSSION, CONCLUSIONS, AND SUGGESTIONS FOR FURTHER WORK

6.1 Summary of Results

The results given in detail in chapter 5 may be classified as follows:

i) Microstructural observations;

ii) Effects of ion implantation on plastic flow;

iii) Effects of ion implantation on fracture behaviour;

iv) Miscellaneous.

6.1.1 Microstructural Effects of Ion Implantation

i) Both boron- and nitrogen-implanted silicon carbide (originally hexagonal) have microcrystalline near-surface microstructures. These changes occur at the lowest dose used for nitrogen implantation ($10^{17} N_2^+$ cm^{-2}), and probably also at the lowest dose for boron implantation. Diffraction patterns from the differently doped surfaces indicate that the polytype mixtures present in the B-implanted and the N-implanted materials are not identical (see 5.1.7).

ii) After deformation by a diamond scriber, both nitrogen- and boron-implanted silicon carbide transform to a cubic phase (see 5.1.7).

iii) Silicon is rendered non-crystalline at the surface by doses of nitrogen as low as $10^{15} N_2^+$ cm^{-2} (see 5.2.6). TEM examination shows no change

in the diffraction patterns (characteristic of amorphous material) over the dose range 10^{17}-$8x10^{17}N_2^+$ cm^{-2}(see 5.2.7).

iv) Tungsten carbide is rendered microcrystalline at the surface by implantation to doses $4x10^{17}N_2^+$ $cm^{-2}$and above. The microcrystals are grouped together in regions of one preferred orientation within the original grains. In pin-on-disc specimens, these regions are oriented along the wear direction (see 5.3.5).

6.1.2 Effects of Ion Implantation on Plastic Flow

i) Nitrogen implantation into silicon carbide produces an appreciable surface softening. This softening becomes effective at doses greater than ~$4x10^{17}N_2^+$ cm^{-2}. The effect is the same in both single crystal and reaction bonded (REFEL) silicon carbide (see 5.1.3).

ii) Boron implantation into single crystal silicon carbide up to a dose of $16x10^{17}B^+$ cm^{-2}produces no significant changes in the microhardness behaviour (see 5.1.6).

iii) Nitrogen implantation into silicon produces a surface softening at doses greater than ~$4x10^{17}N_2^+$ cm^{-2}. The effect is not as large as in nitrogen-implanted silicon carbide (see 5.2.2).

iv) Dislocations are visible beneath abrasion tracks (plastic grooves) made by diamond paste abrasion in unimplanted silicon. In the implanted material (all doses in the range 10^{17}-$8x10^{17}N_2^+$ cm^{-2}), a non-dislocation process operates; the abrasion grooves lie entirely within non-crystalline material (see 5.2.7).

v) Nitrogen implantation into cobalt produces a softened surface layer at doses in the range $4x10^{16}$-$2.4x10^{17}N_2^+$ cm^{-2}(see 5.3.6).

vi) The microhardness behaviour of WC-Co composite, silica glass and Metglas 2826A is not noticeably changed by implantation with nitrogen up to doses of 6-$8x10^{17}N_2^+$ cm^{-2}(see 5.3.3, 5.4.3, 5.4.1).

vii) The microhardness behaviour of LiF is not changed by implantation up to a dose of $6x10^{17}N_2^+$ cm^{-2}. However, dislocation rosettes are reduced in size in implanted and X-irradiated material within ~150μm of the surface (see 5.5.2, 5.5.3).

6.1.3 Effects of Ion Implantation on Fracture Behaviour

i) The surface breakout, and possibly the nucleation, of lateral cracks around indentations in silicon carbide is reduced by nitrogen implantation. The effect increases progressively over the dose range 10^{17}-$8\times10^{17} N_2^+$ cm^{-2} (see 5.1.4).

ii) Boron implantation into single crystal silicon carbide reduces lateral fracture breakout, but not its nucleation or extent. Cracks approaching the surface are deflected at a depth of ~3μm (see 5.1.6).

iii) Lateral chipping fracture around low-load (10-50g) single-point scratch tracks in silicon carbide is almost completely suppressed by implantation with boron or nitrogen. This suppression is effective even at the lowest doses used (2×10^{17} ions cm^{-2}) (see 5.1.5, 5.1.6).

iv) Lateral fracture breakout around indentations is suppressed in silicon by nitrogen implantation. The effect increases in strength progressively with increasing dose over the range 10^{17}-$8\times10^{17} N_2^+$ cm^{-2}. The cracks still extend beneath the surface even in heavily implanted material (see 5.2.3).

v) Median/radial fracture is not affected in silicon in occurrence and extent up to a dose of $8\times10^{17} N_2^+$ cm^{-2} (see 5.2.3).

vi) In WC-Co, the incidence of fracture within indentations, parallel to and close to the indentation edge, is increased by nitrogen implantation to a dose of $4\times10^{17} N_2^+$ cm^{-2} (see 5.3.3).

vii) In silica glass, near-indentation fracture, both of the incipient cone-crack type and at the indentation edges, is reduced in occurrence by implantation to a dose of $4\times10^{17} N_2^+$ cm^{-2}. This effect is only noticeable around low-load indentations; at high loads (>200g) Hertzian cone-type fracture is seen at all doses (see 5.4.4).

viii) Lithium fluoride, implanted to $2\times10^{17} N_2^+$ cm^{-2} and above, showed radial fracture around indentations made with loads as low as 5g. No such fracture was visible on unimplanted material, even at loads of 500g. Examination of a cross-sectioned specimen indicated that the cracks form and grow close to the surface (see 5.5.2).

6.1.4 Miscellaneous Results

i) All heavily implanted ($\geq 4 \times 10^{17}$ ions cm^{-2}) specimens showed signs of surface sputtering, in the form of fine-scale surface roughness and etching. In REFEL, it was estimated that ~0.3μm of material had been removed at a dose of $8 \times 10^{17} N_2^+$ cm^{-2}. Such sputtering reduces the amount of dopant retained in the surface (see 5.1.2).

ii) Implantation to the lowest dose used in REFEL ($10^{17} N_2^+$ cm^{-2}) suppressed the SEM secondary electron contrast normally seen between original and epitaxial SiC (see 5.1.2).

iii) Boron-implanted silicon carbide developed crystallographically oriented pits over a period of a few months (see 5.1.6).

iv) Laser 'annealing' of high-dose nitrogen-implanted silicon removed the surface to a depth of ~0.5μm (see 5.2.5).

v) SEM examination of implanted and unimplanted WC-Co pin-on-disc specimens showed very few differences between them, apart from the depths of the wear tracks. Within the tracks, fine scale grooving along the wear direction could be seen. However, tracks on the implanted material appeared lighter than their surroundings; those on the implanted material appeared darker (see 5.3.4).

vi) Implantation affected the etching behaviour of lithium fluoride. Arrays of linear features, rather than the normal etch pit rosettes, were produced by etching indented specimens (see 5.5.2).

vii) X-irradiation of pre-implanted LiF produced greatly enhanced colouring; crystals appeared dark to a depth of ~1.5mm (see 5.5.3).

6.2 Discussion and Conclusions

The major results of this study are discussed below. Where possible, results from different materials are correlated with one another. In some cases, more detailed discussions of the results for individual materials are to be found in the appropriate section of chapter 5.

6.2.1 Plastic Flow in Silicon and Silicon Carbide

The key result here is the different ISE behaviour of nitrogen- and boron-implanted silicon carbide. These dopants are so similar in atomic mass and size that the physical characteristics of the implanted layers is probably nearly identical, and so the different semiconductor doping properties of these dopants must be the most significant factor. It is known that doping affects dislocation mobility in silicon, with both p- and n-type dopants tending to increase dislocation mobility; however, in germanium, p- and n-dopants have opposite effects on dislocation mobility [Hirsch (1981)]. It is possible that the situation in silicon carbide is similar to that in germanium, with n-doping (nitrogen) having a strong effect, and p-doping (boron) only a very small effect on dislocation mobility. Such a mechanism would also fit the observation that the effect of nitrogen implantation on the ISE behaviour of silicon is smaller than the effect in silicon carbide. The band gap in SiC (2-3eV) is larger than that in silicon (1.1eV) and the strength of the doping effect on the dislocation mobilities depends on the relative positions of the Fermi level and energy levels associated with dislocations and kinks, etc., in the band gap. However, the observation by Burnett (1982) that silicon-implanted silicon also has a higher Meyer index than unimplanted silicon indicates that such a doping effect may not be the only one acting, and that (at least in silicon) amorphous or microcrystalline solids may have lower flow stresses than their crystalline counterparts.

The processes by which near-surface plastic flow occurs in implanted silicon and silicon carbide are obscure. It is possible that flow occurs by a shear-band mechanism, similar to those known to exist in metallic and inorganic glasses, but the TEM observations performed in this study did not reveal any such deformation structures. The microcrystalline to cubic phase change observed in boron- and nitrogen-implanted SiC after deformation indicates that the cubic polytype is the low-temperature stable form of SiC, whatever the doping, and that the phase change has no significant effect on the microhardness behaviour.

The existence and magnitude of the 'critical dose' ($\sim 4 \times 10^{17} N_2^+ \ cm^{-2}$) for changes in the ISE behaviour of silicon and silicon carbide is difficult to explain. The behaviour of silicon has been attributed by Burnett (1982) to an interaction between the size of the indentation plastic zone and the amorphous layer thickness. However, such an explanation cannot account for the observed behaviour of nitrogen-implanted SiC, where the change in morphology of the indentations is very marked at the critical dose. Below this dose, cracks occur at the indentation edges, whereas above it, a thin, highly plastic layer is visible. The critical dose in nitrogen-implanted SiC cannot be connected with amorphisation of the surface, as this is observed to occur at much lower doses, and also in boron-implanted material.

6.2.2 Microhardness Behaviour of Cobalt and Wear of WC-Co

The results of microhardness tests on cobalt were unexpected, as implantation has generally been found to produce surface hardening in a wide variety of metals (see 2.4, 3.1.1). It is probable that this behaviour is connected with the unusual crystallography of cobalt, which has a very low stacking fault energy and exists in two polymorphic forms, the metastable one of which (fcc) can persist in large quantities at room temperature. Based on this , there are two possible mechanisms for the observed softening:

i) Nitrogen implantation might increase the stacking fault energy of cobalt. The lower the stacking fault energy of a material, the greater the tendency to work-harden, as cross-slip is restricted. If cobalt were to

work-harden less rapidly in the implanted layer, this could account for the observed ISE behaviour

ii) Nitrogen implantation might alter the balance of metastable fcc: stable hcp material present (dissolved nitrogen is known to stabilise the fcc phase) in favour of the fcc phase, so that an fcc-hcp transformation could act as an additional yielding mechanism on indentation.

In the absence of microstructural evidence, however, no definite conclusions can be drawn. Also, the cobalt actually present as binder material in the WC-Co composite is highly impure, with high concentrations of carbon and tungsten, at least. It might be that the results of implantation on the binder material might be different from those in pure cobalt. Furthermore, the results from examination of pin-on-disc specimens (see 5.3.5, 5.3.6) indicate that the wear processes in WC-Co discs operate on a scale much finer than the carbide grain size, and involve plastic deformation of the surface of the carbide grains in both implanted and unimplanted material. It is therefore probable that the observed microcrystalline microstructure of implanted WC controls the wear reponse in pin-on-disc tests, especially considering the observed alignment of the the bands of similarly oriented microcrystals with the wear direction. However, it appears difficult to fit in with such a scheme the results of Pethica (1982), who found that the surfaces of WC grains were softened by nitrogen implantation, and the results of Dearnaley and Hartley (1978), who found that the wear rate reduction persisted even after the implanted layer had been worn away.

6.2.3 Microhardness Behaviour of Amorphous Materials

The hardness behaviour of both the silica glass and the metallic glass (Metglas 2826A) was not changed by implantation to high doses. The result for the metallic glass indicates that the implantation has not altered the (non-) crystalline structure of the material, as the formation of pile-up near the indentation is very sensitive to this [Patterson et al. (1978)]. Further, Sargent and Donovan (1982) suggest that pile-up occurs because of the relative ease of shear-band formation near the free surface; it was proposed that local dilation associated with the shear

band formation would be easier here, as tensile stresses exist from the indentation stress field. If, as is likely, ion implantation introduces compressive stresses into the surface, then this model would indicate that pile-up should not be produced in implanted material. It is unlikely that the metallic glass could spontaneously reduce the implantation stresses without changing its crystallinity, in which case pile-up would also not be observed. Thus, while the presence of surface compressive stresses is not certain, it appears that neither these nor the high concentrations of nitrogen present affect the yielding/flow behaviour.

The same appears to be the case for the silica glasses, though here the fracture behaviour (see below) indicates that compressive stresses exist in the surface. However, the mechanism of plastic flow in this material is even more obscure than in metallic glasses. It may be that compaction occurs during flow beneath hardness indenters; if so, the influence of displacement damage and 'ion stuffing' on such processes appears to be negligible.

6.2.5 Microhardness Behaviour of Lithium Fluoride

A fuller discussion of these results is presented in section 5.5. The conclusions may be summarised as:

i) Ion implantation does not noticably affect the microhardness behaviour. The yield volume (as seen in the size of dislocation loops around indentations) is very large compared to the implanted layer thickness, so that even if plastic flow was different in the implanted layer, it would be unlikely to be detectable by microhardness testing.

ii) Ion implantation followed by X-irradiation forms more colour centres than X-irradiation alone, because of the displacement damage produced by implantation. Channelling can enhance the depth range over which this occurs. The colour centres restrict dislocation motion in the rosettes around indentations. The variation with depth of rosette size and colour density do not match, the effect on rosette size being much shallower, indicating that the defects producing the observed colour are not exclusively those restricting the dislocation motion.

6.2.6 Effects of Ion Implantatation on Fracture Behaviour

With two exceptions (in WC-Co (see 5.3.3) and LiF (see 5.5.2)), the changes produced in fracture around indentations or scratch tracks were always in the reduction of broken-out lateral type fracture. A variety of effects seem to be operating:

i) The surface stress field produced by implantation prevents breakout of lateral fracture (see 5.1.4, 5.1.5, 5.1.6, 5.2.3, 5.2.4). This is particularly well evidenced by the broken-open boron-implanted SiC specimens (see 5.1.6). Also, these stresses appear to reduce the incidence of ring cracks around low-load indentations in silica glass (see 5.4.4).

ii) It appears that the nucleation of lateral fracture in SiC may be reduced by nitrogen implantation, but not by boron implantation. This is possibly connected with increased plasticity in the surface of the nitrogen-implanted SiC (see 5.1.4, 5.1.6).

iii) The reduction in the occurrence of broken-out lateral fracture increases steadily with dose over the ranges used in both silicon and silicon carbide (also for ring cracks in silica glass). Suppression of lateral chipping around scratch tracks generally occurs at lower doses (10^{17} ions cm^{-2}). This is probably because of the relatively low loads used in the scratch tests; any lateral fracture would be nucleated much closer to the surface than in the indentation tests. Since both boron- and nitrogen-implanted SiC show similar reductions in chipping, such reductions cannot be due exclusively or even predominantly to the surface softening observed in nitrogen-implanted Si and SiC (see 5.15, 5.1.6, 5.2.4).

6.3 Suggestions for Further Work

Since all the work described in this thesis consists of preliminary studies of the effects of ion implantation on the mechanical properties of a wide range of materials, the possibilities for further work are very large. Nonetheless, there are some obvious areas of further study, leading more or less directly from the work described here, which appear particularly interesting:

i) The connections between doping and mechanical properties of semiconducting materials could be further investigated by implantation of a wide variety of p- and n-type dopants, particularly into materials with with large band gaps (eg. SiC, diamond).

ii) Studies of the effects of self- and neutral-ion implantation into brittle materials would be useful in the investigation of the influence of the stress state alone on the near-surface fracture behaviour, and also the effect of displacement damage alone on plastic flow.

iii) More extensive TEM studies would be required to elucidate the mechanisms of plastic flow within the implanted layer.

iv) A good deal more work would be required to determine the wear mechanisms operating in WC-Co, and the effect of nitrogen implantation on these. Experiments of the types (i)-(iii) above on WC single crystals would be particularly useful here.

v) Study of the variation of microhardness, scratch behaviour and microstructure with annealing time and temperature might yield interesting results, particularly if coupled with the use of analytical techniques such as RBS. In this way, the influences of dopant and of microstructural damage on the behaviour of implanted surfaces might be better distinguished.

vi) Study of the microhardness behaviour of implanted surfaces would be more complete if data from lower load indentations could be included (ie. at indentation depths of less than ~0.1μm). The use of a displacement-controlled, rather than the normal load-controlled, type of microhardness machine would be useful here. Such data could possibly be used, in combination with cross-section TEM, RBS, etc., to gain information about the layered structure of the implanted surface seen in this study.

The work described in this thesis has shown that high-dose implantation into a variety of material types can produce measurable, and sometimes large, changes in their surface mechanical properties. Study of the mechanical response of ion implanted surfaces can give insights into the factors controlling indentation behaviour, etc. In addition to being scientifically interesting, the possibility of influencing the surface reponses of hard, brittle materials by implantation could have important industrial applications. The work described here has indicated a few areas of interest, but the possibilities for further research in this general area are virtually limitless.

REFERENCES

ION IMPLANTATION CONFERENCES

International Conferences on Ion Implantation into Semiconductors:

1970 Thousand Oaks, California.
Eds. F.H. Eisen, L.T. Chadderton,
Gordon and Breach, 1970.

1971 Garnish-Partenkirchen, Bavaria, Germany.
Eds. I Ruge, J. Graul.
Springer-Verlag, 1971.

1972 Yorktown Heights, New York.
Ed. B.L. Crowder,
Plenum Press, New York, USA, 1973.

1974 Osaka, Japan.
Ed. S. Namba.
Plenum Press, New York, USA, 1974.

1976 Boulder, Colorado.
Eds. J.A. Borders, D.K. Bruce,
Plenum Press, New York, USA, 1977.

'Applications of Ion Beams to Materials 1975'
Inst. Physics Conf. Series no. 28,
Eds. G. Carter, J.S. Colligon, W.H. Grant.
Inst. Physics, London, 1976.

'Ion Implantation Metallurgy'
Proc. ~~Metals.~~ Materials Res. Soc. Symposium, Cambridge, Mass. 1979,
Eds. C.M. Preece, J.K. Hirvonen,
Met. Soc. AIME, New York, 1980.

'Metastable Alloy Formation by Ion Implantation'
Proc. ~~Metals.~~ Materials Res. Soc. Symposium, Boston 1981,
Eds. S.T. Picraux, W.J. Choyke,
North-Holland, New York, 1982.

'Modification of Surface Properties of Metals by Ion Implantation'
UMIST, Manchester, UK, 1981.
published as 'Ion Implantation into Metals',
Eds. V. Ashworth, W.A. Grant, R.P.M. Procter,
Pergamon Press, Oxford, 1982.

ALPHABETICAL

ADEWOYE O.O. and PAGE T.F. (1976)
J. Mat. Sci. 11, 981.

AKIMCHENKO I.P, KISSELEVA K.V, KRASNOPEVTSEV V.V, MILYUTIN Yu.V, TOURYANSKY A.G and VAVILOV V.S. (1977)
Radn. Effects 33, 75.

ALEXANDER H. and HAASEN P. (1968)
Solid State Physics 22, 27.

ALI A, GRANT W.A. and GRUNDY P.J. (1978)
Phil. Mag. 37B, 353.

ALSTRUP O. (1979)
Phys. Stat. Sol. 51A, 407.

AMERICAN SOCIETY for METALS (1975)
'Metals Handbook'
ASM, Ohio.

ARCHARD J.F. (1953)
J. Appl. Phys. 24, 981.

ARNOLD G.W. (1975)
J. Appl. Phys. 46, 4466.

ARNOLD G.W. (1980)
Radn. Effects 47, 15.

ARNOLD G.W. and PEERCY P.S. (1980)
J. Non-Cryst. Solids 41, 359.

ASHBY M.F. and JONES D.R.H. (1980)
'Engineering Materials'
Pergamon Press, Oxford.

ASHWORTH V, GRANT W.A. and PROCTER R.P.M. (1976)
Corros. Sci. 16, 661.

ASHWORTH V, BAXTER D, GRANT W.A. and PROCTER R.P.M. (1977)
Corros. Sci. 17, 947.

ASHWORTH V, GRANT W.A, PROCTER R.P.M. and WRIGHT E.J. (1978)
Corros. Sci. 18, 681.

BACH K. and MUHLE R. (1976)
Exp. Tech. Phys. 24, 255.

BAKRU H, SEN S, GIBSON W, BURR C, MACCRONE R.K, LYONS W,
ST. JAMES A. and WELSCH G.E. (1981)
Paper presented at 'Modification of Surface Properties of Metals
by Ion Implantation', UMIST, 1981.
Unpublished.

BEANLAND D.G. and CHIVERS D.J. (1978)
J. Electrochem. Soc. 125, 1331.

BEELER J.R. (1964)
J. Appl. Phys. 35, 2226.

BENTINI G.G, BERTI M, CARNERA A, DELLAMEA G, DRIGO A.V,
LORUSSO S, MAZZOLDI P. and DEARNALEY G. (1980)
Corros. Sci. 20, 27.

BOLTON J.D. and REDINGTON M. (1980)
J. Mat. Sci. 15, 3150.

BOWDEN F.P. and TABOR D. (1950)
'The Friction and Lubrication of Solids'
Clarendon Press, Oxford.

BOWDEN F.P. and TABOR D. (1967)
'Friction and Lubrication'
Methuen, London.

BOWDEN F.P. and TABOR D. (1974)
'Friction - an Introduction to Tribology'
Heinemann, London.

BRIMHALL J, CHARLOT L.A. and WANG R. (1979)
Scr. Met. 13, 217.

BRINKMAN J.A. (1954)
J. Appl. Phys. 25, 961.

BROESE VAN GROENOU A, MAAN N. and VELDKAMP J.D.B. (1975)
Phillips Res. Rpts. 30, 320.

BROOKES C.A, O'NEIL J.B. and REDFERN B.A.W. (1971)
Proc. Roy. Soc. A322, 73.

BROOKES C.A, BURNAND R.P. and MORGAN J.E. (1975)
J. Mat. Sci. 10, 2171.

BURKE J.J, GORUM A.E. and KATZ R.N. (Eds.) (1974)
'Ceramics for High Performance Applications'
(Army materials technology conference series)
Brook Hill, Chestnut Hill, Mass.

BURNETT P. (1982)
Unpublished work.

BURR C.R, BAKRU H. and GIBSON W. (1980)
in 'Ion Implantation Metallurgy'
Proc. Metals Res. Soc. Symposium, Cambridge, Mass. 1979,
Eds. C.M. Preece, J.K. Hirvonen.
Met. Soc. AIME, New York.
p126.

BYKOV V.N, TROYAN V.A, ZDOROVTSEVA G.G. and KHAIMOVITCH V.S. (1975)
Phys. Stat. Sol. 32A, 53.

CAMPBELL A.B, MITCHELL J.B, SHEWCHUN J, THOMPSON D.A.
and DAVIES J.A. (1974)
in 'Silicon Carbide 1973'
Proc. Int. Conf. on Silicon Carbide, Miami Beach, Florida, 1973,
Eds. R.C. Marshall, J.W. Faust, C.E. Ryan.
Univ. Sth. Carolina Press, Columbia, 1974.
p486.

CAROSELLA C.A, SINGER I.L, BOWERS R.C. and GOSSETT C.R. (1980)
in 'Ion Implantation Metallurgy'
Proc. Metals Res. Soc. Symposium, Cambridge, Mass. 1979,
Eds. C.M. Preece, J.K. Hirvonen.
Met. Soc. AIME, New York.
p103.

CARTER G. and GRANT W.S. (1976)
'Ion Implantation of Semiconductors'
Edward Arnold, London.

CARTER G, WEBB R. and COLLINS R. (1978)
Radn. Effects 37, 21.

CATLOW C.R.A, DILLER K.M. and HOBBS L.W. (1980)
Phil. Mag. 42A, 123.

CHADDERTON L.T. (1965)
'Radiation Damage in Crystals'
Methuen, London.

CHAKRABORTTY S.B, KUJORE A. and STARKE E.A. (1980)
Thin Solid Films 73, 209.

CHAKRABORTTY S.B, SPOONER S. and STARKE E.A. (1980)
Georgia Inst. Tech. Publ. AO-A083643, 59.

CHANNING D.A. and TURNBULL J.A. (1968),(1969)
Berkeley Nuclear Labs Rpts. RD/B/N1114 and RD/B/N1484.

CHERMANT J.L. and OSTERSTOCK F. (1976)
J. Mat. Sci. 11, 1939.

CHERMANT J.L. and OSTERSTOCK F. (1979)
Powder Met. Intll. 11, 106.

CHIANG S.S, MARSHALL D.B. and EVANS A.G. (1982)
J. Appl. Phys. 53, 312.

CHRISTEL L.A, GIBBONS J.F. and SIGMON T.W. (1981)
J. Appl. Phys. 52, 7143.

CLAYTON C.R, DOSS K.G.K, HERMAN H, PRASAD S, WANG Y-F,
HIRVONEN J.K. and HUBLER G.K. (1980)
in 'Ion Implantation Metallurgy'
Proc. Metals Res. Soc. Symposium, Cambridge, Mass. 1979,
Eds. C.M. Preece, J.K. Hirvonen.
Met. Soc. AIME, New York.
p65.

CULLIS A.G, SEIDEL T.E. and MEEK R.L. (1978)
J. Appl. Phys. 49, 5188.

CULLIS A.G. (1980)
Private Comm.

CULLIS A.G, WEBBER H.C, POATE J.M. and CHEW N.G. (1980)
J. Micros. 118, 41.

CULLIS A.G, WEBBER H.C. and CHEW N.G. (1980)
Appl. Phys. Letts. 36, 547.

DAVIDSON S.M. and BOOKER G.R. (1970)
Radn. Effects 6, 33.

DAVIDGE R.W. (1979)
'Mechanical Behaviour of Ceramics'
Cambridge University Press.

DEARNALEY G. (1978a)
Trans. Inst. Metal Finishing 56, 25.

DEARNALEY G. (1978b)
Mats. in Eng. Applics. 1, 28.

DEARNALEY G. (1980a)
Metal Powder Report 35, 64.

DEARNALEY G. (1980b)
in 'Ion Implantation Metallurgy'
Proc. Metals Res. Soc. Symposium, Cambridge, Mass. 1979,
Eds. C.M. Preece, J.K. Hirvonen.
Met. Soc. AIME, New York.
p1.

DEARNALEY G. (1981a)
IEEE Trans. Nucl. Sci. NS28, 1808.

DEARNALEY G. (1981b)
Nucl. Insts. Methods 182/183, 899.

DEARNALEY G. (1981c)
Paper presented at Conf. on Science of Hard Materials,
Jackson Lake Lodge, Wyoming.

DEARNALEY G. (1981d)
Harwell Mat. Dev. News no. 23.

DEARNALEY G. (1981e)
Private Comm.

DEARNALEY G. (1982)
in 'Ion Implantation of Metals',
Proc. Conf. UMIST, 1981,
Eds. V. Ashworth, W.A. Grant, R.P.M. Procter,
Pergamon Press, Oxford.
p180.

DEARNALEY G. and DELVES B.G. (1980)
Paper presented at 'Mould Making 80',
conference of the Plastics and Rubber Institute, Solihull.

DEARNALEY G. and GOODE P.D. (1980)
Inst. Phys. Conf. Ser. no. 54, 26.

DEARNALEY G, FREEMAN J.H, NELSON R.S. and STEPHEN J. (1973)
'Ion Implantation'
North-Holland, Amsterdam.

DEARNALEY G. and HARTLEY N.E.W. (1977)
Proc. 4th conf. on 'Scientific and Industrial
Applications of Small Accelerators',
N. Texas State Univ.
IEEE, New York.
p20.

DEARNALEY G. and HARTLEY N.E.W. (1978)
Thin Solid Films 54, 215.

DECONNINCK G. (1978)
'Introduction to Radioanalytical Analysis'
Elsevier, Amsterdam.

DELVES B.G. (1982)
in 'Ion Implantation of Metals',
Proc. Conf. UMIST, 1981,
Eds. V. Ashworth, W.A. Grant, R.P.M. Procter,
Pergamon Press, Oxford.
p126.

DENNIS J.R. and HALE E.B. (1976)
Appl. Phys. Letts. 29, 523.

DEROODE W.H. and SMITS J.W. (1981)
J. Appl Phys. 52, 3969.

DONOVAN P. and STOBBS W.M. (1981)
Acta. Met. 29, 1419.

DUBOVITSKAYA N.V, ZAHAROV S.M, LARIKOV J.N,
PORITSKII V.Ya. and PROTSENKO I.M. (1979)
Ukr. Fiz. Zh. 24, 1579.

EDELMAN F.L, KUZNETSOV O.N, LEZHEIKO L.V and LUBOPYTOVA E.V. (1976)
Radn. Effects 29, 13.

EDINGTON J.W, ROWCLIFFE D.J. and HENSHALL J.L. (1975a)
Powder Met. Intll. 7, 82.

EDINGTON J.W, ROWCLIFFE D.J. and HENSHALL J.L. (1975b)
Powder Met. Intll. 7, 136.

EERNISSE E.P. (1971a)
Appl. Phys. Letts. 18, 581.

EERNISSE E.P. (1971b)
2nd Int. Conf. on Ion Implantation in Semiconductors,
p17.

EERNISSE E.P. (1973)
3rd Int. Conf. on Ion Implantation in Semiconductors,
p531.

EERNISSE E.P. (1974)
J. Appl. Phys. 45, 167.

EERNISSE E.P. (1977a)
Proc. 4th Int. Conf. on 'Scientific and Industrial Applications of Small Accelerators',
N. Texas State Univ.
IEEE, New York.
p598.

EERNISSE E.P. (1977b)
J. Appl. Phys. 48, 3337.

EREMENKO V.G. and NIKITENKO V.I. (1972)
Phys. Stat. Sol. 14a, 317.

ESKILDSEN S.S. (1982)
in 'Ion Implantation of Metals',
Proc. Conf. UMIST, 1981,
Eds. V. Ashworth, W.A. Grant, R.P.M. Procter,
Pergamon Press, Oxford.
p315.

EVANS A.G. (1979)
U.S. Dept. Energy Publ. LBL 8608.

EVANS A.G. (1980)
Am. Soc. Test. Mats. Spec. Tech. Publ. no. 678.

EVDOKIMOV I.N. and FISCHER G. (1980)
J. Mat Sci. 15, 854.

EXNER H.E. (1979)
Intll. Mets. Revs. no. 4, 149.

FAIRBANKS C.J, POLVANI R.S, WEIDERHORN S.M,
HOCKEY B.J. and LAWN B.R. (1982).
J. Mat. Sci. Letts. 1, 391.

FAUST J.W, TUNG Y. and LIAU H.L. (1974)
in 'Silicon Carbide 1973'
Proc. Int. Conf. on Silicon Carbide, Miami Beach, Florida, 1973,
Eds. R.C. Marshall, J.W. Faust, C.E. Ryan.
Univ. Sth. Carolina Press, Columbia, 1974.
p215.

FINKIN E.F. (1979)
Mats. in Eng. Applics. 1, 154.

FITCH R, MULVEY T, THATCHER W. and MCILRAITH A. (1970)
J. Phys. D 3, 1399.

FLETCHER J. (1973)
Mets. and Mats. 7, 530.

FOLLSTAEDT D.M, KNAPP J.A. and PICRAUX S.T. (1980)
Appl. Phys. Letts. 37, 330.

FORREST C.W, KENNEDY P. and SHENNAN J.V. (1972)
in 'Special Ceramics 5', Ed. P. Popper,
British Ceramics Research Assoc.
p99.

FREEMAN J.H. (1969)
AERE Publ. R-6138
HMSO.

FREEMAN J.H, CHIVERS D.J, GARD G.A. and TEMPLE W. (1977)
AERE Publ. R-8748
HMSO.

FROST N.E, MARSH K.J. and POOK L.D. (1974)
'Metal Fatigue'
Clarendon Press, Oxford.

FROST M.A. and ASHBY M.F. (1982)
'Deformation Maps'
Pergamon Press, Oxford.

GEORGE A. and CHAMPIER G. (1979)
Phys. Stat. Sol. 53a, 529.

GERWARD L. (1978)
Phil. Mag. 37A, 95.

GIBBS N.K. (1982)
PhD. Thesis, University of Cambridge.

GIECZY I.I, NESTEROV A. and SMIRNOV L.S. (1967)
Sov. Phys. Semicond. Bull. 5, 439.

GILMAN J.J. and JOHNSTON W.J. (1957)
in 'Dislocations and Mechanical Properties of Crystals'
Eds. J.C. Fisher, W.G. Johnston, R. Thomson and T. Vreeland
John Wiley and Sons, New York.
p116.

GOODE P.D. (1971)
Nucl. Insts. and Methods 92, 447.

GRANT W.A. (1978)
J. Vac. Sci. and Tech. 15, 1644.

GREGGI J. and KOSSOWSKY R. (1981)
paper presented at Conf. on Science of Hard Materials,
Jackson Lake Lodge, Wyoming.

GRIDNEVA I.V, MILMAN Yu. V. and TREFILOV V.I. (1972)
Phys. Stat. Sol. 14a, 317.

HAGAN J.T. (1979)
J. Mat. Sci. 14, 462.

HAGAN J.T. (1980)
J. Mat. Sci. 15, 1417.

HALE E.B, KAISER T.H, MENG C.P. and KOHSER R.A. (1982)
in 'Ion Implantation of Metals',
Proc. Conf. UMIST, 1981,
Eds. V. Ashworth, W.A. Grant, R.P.M. Procter,
Pergamon Press, Oxford.
p111.

HANSEN M. (1958)
'Constitution of Binary Alloys'
McGraw-Hill, New York.

HARTLEY N.E.W. (1975a)
J. Vac. Sci. and Tech. 12, 485.

HARTLEY N.E.W. (1975b)
Wear 34, 427.

HARTLEY N.E.W. (1978)
in 'Surface Treatments for Protection'
Inst. Metall. Publ. 1101-78-Y.
p197.

HARTLEY N.E.W. (1979a)
Thin Solid Films 64, 177.

HARTLEY N.E.W. (1979b)
Radn. Effects 44, 19.

HARTLEY N.E.W. (1982)
in 'Metastable Alloy Formation by Ion Implantation'
Eds. S.T. Picraux, W.J. Choyke,
North-Holland, New York.
p295.

HARTLEY N.E.W, DEARNALEY G. and TURNER J.F. (1973)
AERE Publ. R-7441.
HMSO.

HAUSER J.J, PATEL J.R. and RODGERS J.W. (1977)
Appl. Phys. Letts. 30, 129.

HERMAN H. (1982)
in 'Ion Implantation of Metals',
Proc. Conf. UMIST, 1981,
Eds. V. Ashworth, W.A. Grant, R.P.M. Procter,
Pergamon Press, Oxford.
p102.

HEYDARI P, STARKE E.A, CHAKRABORTTY S.B. and LEGG K.O.(1982)
in 'Ion Implantation of Metals',
Proc. Conf. UMIST, 1981,
Eds. V. Ashworth, W.A. Grant, R.P.M. Procter,
Pergamon Press, Oxford.
p172.

HIBBS M.K. and SINCLAIR R. (1981)
Acta Met. 29, 1645.

HILL M.J. and ROWCLIFFE D.J. (1974)
J. Mat. Sci. 9, 1569.

HIRSCH P.B. (1979)
J. de Physique, Colloque C6, Supplem. 6, 40, C6.

HIRSCH P.B. (1981)
in Proc. Symposium on Defects in Semiconductors
Boston, Mass. USA.
Eds. J. Narayan and T.Y. Tan,
Elsevier, North Holland.
p257.

HIRVONEN J.K. (1978)
J. Vac. Sci. and Tech. 15, 1662.

HIRVONEN J.K. (1981)
Private Comm.

HIRVONEN J.K, CAROSELLA C.A, KANT R.A, SINGER I.L,
VARDIMAN R and RATH B.B. (1979)
Thin Solid Films 63, 5.

HIRVONEN J.K, BUTLER J.W, SMITH T.P,
KANT R.A. and WESTCOTT V.C. (1980)
Radn. Effects 49, 73.

HARTLEY N.E.W, DEARNALEY G. and TURNER J.F. (1973)
AERE Publ. R-7441.
HMSO.

HAUSER J.J, PATEL J.R. and RODGERS J.W. (1977)
Appl. Phys. Letts. 30, 129.

HERMAN H. (1982)
in 'Ion Implantation of Metals',
Proc. Conf. UMIST, 1981,
Eds. V. Ashworth, W.A. Grant, R.P.M. Procter,
Pergamon Press, Oxford.
p102.

HEYDARI P, STARKE E.A, CHAKRABORTTY S.B. and LEGG K.O.(1982)
in 'Ion Implantation of Metals',
Proc. Conf. UMIST, 1981,
Eds. V. Ashworth, W.A. Grant, R.P.M. Procter,
Pergamon Press, Oxford.
p172.

HIBBS M.K. and SINCLAIR R. (1981)
Acta Met. 29, 1645.

HILL M.J. and ROWCLIFFE D.J. (1974)
J. Mat. Sci. 9, 1569.

HIRSCH P.B. (1979)
J. de Physique, Colloque C6, Supplem. 6, 40, C6.

HIRSCH P.B. (1981)
in Proc. Symposium on Defects in Semiconductors
Boston, Mass. USA.
Eds. J. Narayan and T.Y. Tan,
Elsevier, North Holland.
p257.

HIRVONEN J.K. (1978)
J. Vac. Sci. and Tech. 15, 1662.

HIRVONEN J.K. (1981)
Private Comm.

HIRVONEN J.K, CAROSELLA C.A, KANT R.A, SINGER I.L,
VARDIMAN R and RATH B.B. (1979)
Thin Solid Films 63, 5.

HIRVONEN J.K, BUTLER J.W, SMITH T.P,
KANT R.A. and WESTCOTT V.C. (1980)
Radn. Effects 49, 73.

HOCKEY B.J. (1973)
in 'The Science of Hardness Testing and its Research Applications'
Eds. J.H. Westbrook, H. Conrad,
Am. Soc. for Metals, Ohio, 1973.
p21.

HOFFMAN D.W. and GAERTTNER M.R. (1980)
J. Vac. Sci. and Tech. 17, 425.

HØNSTVET I.A, SMALLMAN R.E. and MARQUIS P.M. (1980)
Phil. Mag. 41A, 201.

HU S.M. (1973)
J. Appl. Phys. 46, 1470.

HU S.M. and SCHWENKER R.O. (1978)
J. Appl. Phys. 49, 3259.

HU W.W, CLAYTON C.R, HERMAN H, HIRVONEN J.K. and KANT R.A. (1980)
Radn. Effects 49, 71.

HU W.W, HERMAN H, CLAYTON C.R, KOZUBOWSKI J, KANT R.A,
HIRVONEN J.K. and MACCRONE R.K. (1980)
in 'Ion Implantation Metallurgy'
Proc. Metals Res. Soc. Symposium, Cambridge, Mass. 1979,
Eds. C.M. Preece, J.K. Hirvonen.
Met. Soc. AIME, New York.
p92.

HUDSON B, SHELDON B.E. (1973)
J. Micros. 97, 113.

HUTCHINGS I.M. (1979)
ASTM Special Tech. Publ. 664,
Ed. W.F. Adler.
p59.

ITOH N, NAKAU T, MORIKAWA Y. and NAGAMI K. (1978)
Jap. J. Appl. Phys. 17, 1003.

JAHANMIR S. (1980)
in 'Fundamentals of Tribology',
Proc. Conf. Cambridge, Mass. 1978,
Eds. N.P. Suh, N. Saka,
MIT Press, Cambridge, Mass.
p455.

JENSEN T, LAWN B.R, DALGLISH R.L. and KELLY J.C. (1976)
Radn. Effects 28, 245.

JEPPS N.W. (1980)
PhD. Thesis, University of Cambridge.

JEPPS N.W. and PAGE T.F. (1979)
J. Micros. 116, 159.

JEPPS N.W. and PAGE T.F. (1980)
J. Micros. 119, 177.

JEPPS N.W. and PAGE T.F. (1981)
J. Micros. 124, 227.

JOHNSON E, WOHLENBURG T, GRANT R.A, HANSEN P and CHADDERTON L.T. (1979)
J. Micros. 116, 77.

JOY D.C. and NEWBURY D.E. (1977)
in 'Scanning Electron Microscopy 1977', Vol. 1,
IITRI, Chicago.
p445.

KANAYA K, KOGA K. and TOKI K. (1972)
J. Phys. E 5, 641.

KANG S.T, SHIMIZU R. and OKUTANI T. (1979)
Jap. J. Appl. Phys. 18, 1717.

KANT R.A, HIRVONEN J.K, KNUDSON A.R. and WOLLAM J.S. (1979)
Thin Solid Films 63, 27.

KIEFFER A.R, ETTMAYER P, GUGEL E. and SCHMIDT A. (1969)
Mat. Res. Bull. 4, S153.

KITTEL C. (1976)
'Introduction to Solid State Physics'
John Wiley and Sons, New York.

KOMENOU K, HIRAI I, ASAMA K. and SAKAI M. (1978)
J. Appl. Phys. 49, 5816.

KUJORE A, CHAKRABORTTY S.B, STARKE E.A. and LEGG K.O. (1980)
in 'Ion Implantation Metallurgy'
Proc. Metals Res. Soc. Symposium, Cambridge, Mass. 1979,
Eds. C.M. Preece, J.K. Hirvonen.
Met. Soc. AIME, New York.
p132.

KYUTT R.N, PETRASHEN P.V. and SOROKIN L.M. (1980)
Phys. Stat. Sol. 60A, 381.

LANGE F.F. (1975)
J. Mat. Sci. 10, 314.

LANKFORD J. and DAVIDSON D.L. (1979)
J. Mat. Sci. 14, 1669.

LARDNER E. (1978)
Powder Met. 2, 65.

LARDNER E. (1979)
Private Comm.

LARSON B.C. and BARHOST J.F. (1980)
J. Appl. Phys. 51, 3181.

LAWN B.R. (1979)
J. Am. Ceram. Soc. 62, 347.

LAWN B.R, HOCKEY B.J. and WIEDERHORN S.M. (1980)
J. Mat. Sci. 15, 1207.

LAWN B.R. and MARSHALL D.B. (1977)
Phys. and Chem. Glasses 18, 7.

LAWN B.R. and MARSHALL D.B. (1978)
in 'Fracture Mechanics of Ceramics', vol 3,
Plenum Press, New York.
p205.

LAWN B.R. and MARSHALL D.B. (1979)
J. Am. Ceram. Soc. 62, 347.

LAWN B.R, MARSHALL D.B. and CHANTIKUL P. (1981)
J. Mat. Sci. 16, 1769.

LAWN B.R. and SWAIN M.V. (1975)
J. Mat. Sci. 10, 113.

LAWN B.R. and WILSHAW T.R. (1975a)
'Fracture of Brittle Solids'
Cambridge University Press.

LAWN B.R. and WILSHAW T.R. (1975b)
J. Mat. Sci. 10, 1049.

LECROSNIER D.P, PELOUS G.P. and BURGEAT J. (1977)
Appl. Phys. Letts. 30, 141.

LEE H.C. and GURLAND J. (1978)
Mat. Sci. and Eng. 33, 125.

LIAU Z.L. and MAYER J.W. (1978)
J. Vac. Sci. and Tech. 15, 1629.

LINDHARD J, SCHARFF M. and SCHIØTT H.E. (1963)
Matt. Fys. Medd. Kyl. Danske Videnskab Selskab 33, no. 14.

LONGWORTH G. and HARTLEY N.E.W. (1978)
Thin Solid Films 48, 95.

LORUSSO S, MAZZOLDI P, SCOTONI I, TOSELLO C. and TOSTO S. (1979)
Appl. Phys. Letts. 34, 627.

LORUSSO S, MAZZOLDI P, SCOTONI I, TOSELLO C. and TOSTO S. (1980)
Appl. Phys. Letts. 36, 822.

LOUBSER J.H.N, DESOUSA BOLONAI J.A. and VAN RYNEVELD W.P. (1969)
Mat. Res. Bull. 4, 249.

LOUCHET F. (1981)
Phil. Mag. 43A, 1289.

MABY E.W, MAGEE C.W. and MOREWOOD J.H. (1981)
Appl. Phys. Letts. 39, 157.

MACGILLAVRY C.H. and RIECK G.D. (Eds.) (1962)
'International Tables for X-ray Crystallography', vol. III,
Kynoch Press, Birmingham.

MACNEAL B.E. and SPERIOSU V.S. (1981)
J. Appl. Phys. 52, 3985.

MAKAROV V.V, TUOMI T, NAUKKARINEN K,
LUOMAJARVI M. and RIIHONEN M. (1979)
Appl. Phys. Letts. 35, 922.

MARSH D.M. (1964)
Proc. Roy. Soc. 279A, 420.

MARSH O.J. (1974)
in 'Silicon Carbide 1973'
Proc. Int. Conf. on Silicon Carbide, Miami Beach, Florida, 1973,
Eds. R.C. Marshall, J.W. Faust, C.E. Ryan.
Univ. Sth. Carolina Press, Columbia, 1974.
p471.

MARSH O.J. and DUNLAP H.L. (1970)
Radn. Effects 6, 301.

MARSHALL D.B. and LAWN B.R. (1977)
J. Am. Ceram. Soc. 60, 86.

MARSHALL R.C, FAUST J.W. and RYAN C.E. (Eds.) (1974)
'Silicon Carbide 1973'
Proc. Int. Conf. on Silicon Carbide, Miami Beach, Florida, 1973,
Univ. Sth. Carolina Press, Columbia, 1974.

MASTERS B.J, FAIRFIELD J.M. and CROWDER B.L. (1970)
Radn. Effects 6, 57.

MAZEY D.J, NELSON R.S. and BARNES R.S. (1968)
Phil. Mag. 17, 1145.

MCHARGUE C.J. and WILLIAMS J.M. (1982)
in 'Metastable Material Formation by Ion Implantation'
Eds. S.T. Picraux, W.J. Choyke,
North-Holland, New York.
p295.

MCILRAITH A. (1966)
Nature 212, 1422.

MISRA A. and FINNIE I. (1979)
J. Mat. Sci. 14, 2567.

MOORE M.A. (1978)
Mats. in Eng. Applics. 1, 97.

MOOREHEAD F.F. and CROWDER B.L. (1970)
Radn. Effects 6, 27.

MORRIS J.J, COLLINS R.A. and DEARNALEY G. (1978)
J. Phys. F 8, 1333.

MULLER G. and KALBITZER S. (1980)
Phil. Mag. 41B, 307.

MYERS S.M. (1978)
J. Vac. Sci. and Tech. 15, 1650.

NAQUIB H.M, KRIEGLER R.J, DAVIES J.A. and MITCHELL J.B (1976)
J. Vac. Sci. and Tech. 13, 396.

NAYLOR M.G.S. (1982)
PhD Thesis, University of Cambridge.

NAYLOR M.G.S. and PAGE T.F. (1979),(1980)
Tech. Rpts. to US Army, European Research Office,
Grant no. DA-ERO-78-G-010.

NELSON R.S. and MAZEY D.J. (1967)
AERE Publ. R-5394,
HMSO.

NEWEY D, POLLOCK H.M. and WILKINS M.A. (1982)
in 'Ion Implantation of Metals',
Proc. Conf. UMIST, 1981,
Eds. V. Ashworth, W.A. Grant, R.P.M. Procter,
Pergamon Press, Oxford.
p157.

NORTH J.C, WOLFE R. and NELSON T.J. (1978)
J. Vac. Sci. and Tech. 15, 1675.

PADMANABHAN K.R. and SØRENSEN G. (1982)
in 'Ion Implantation of Metals',
Proc. Conf. UMIST, 1981,
Eds. V. Ashworth, W.A. Grant, R.P.M. Procter,
Pergamon Press, Oxford.
p341.

PAGE T.F, SAWYER G.R, ADEWOYE O.O. and WERT J.J. (1978)
Proc. Brit. Ceram. Soc. 26, 193.

PANKOVE J.I, MCGINN J.T. and WU C.P. (1981)
Appl. Phys. Letts. 39, 119.

PARCHE M.C. (1964)
in 'Kirk-Olmer Encyclopaedia of Chemical Technology', vol. 4,
John Wiley and Sons, New York.
p114.

PATTERSON J. (1980)
Private Comm.

PATTERSON J, GREER A.L, LEAKE J.A. and JONES D.R.H. (1978)
in Proc. 3rd Int. Conf. on Rapidly Quenched Metals, Brighton,
Ed. B. Cantor,
Metals Society, London.

PAVLOV P.V, KRUSE T.A, TETELBAUM D.I, ZORIN E.I,
SHITOVA E.V. and GUDKOVA N.V. (1976)
Phys. Stat. Sol. 36A, 81.

PETHICA J.B. (1982)
in 'Ion Implantation of Metals',
Proc. Conf. UMIST, 1981,
Eds. V. Ashworth, W.A. Grant, R.P.M. Procter,
Pergamon Press, Oxford.
p147.

POATE J.M. (1978)
J. Vac. Sci. and Tech. 15, 1636.

POATE J.M. (1979)
Thin Solid Films 63, 3.

POATE J.M. and CULLIS A.G. (1980)
in 'Ion Implantation in Materials Science and Technology'
Ed. J.K. Hirvonen,
Academic Press.

POPPER P. (1960)
in 'Special Ceramics',
Ed. P. Popper,
Heywood, London.
p209.

POSEN H. and BRUCE J.A. (1974)
in 'Silicon Carbide 1973'
Proc. Int. Conf. on Silicon Carbide, Miami Beach, Florida, 1973,
Eds. R.C. Marshall, J.W. Faust, C.E. Ryan.
Univ. Sth. Carolina Press, Columbia, 1974.
p238.

RABINOWICZ E. (1965)
'Friction and Wear of Materials',
John Wiley and Sons, New York.

RAMIN M, RYSSEL H. and KRANZ H. (1980)
Appl. Phys. 22, 393.

RECHTIN M.D, BALDO P.M. and VANDERSANDE J. (1978)
Scr. Met. 12, 639.

ROBERTS S.G. (1982)
Unpublished work.

ROBINSON M.T. and OEN O.S. (1963)
Phys. Rev. 162, 2385.

ROY CHOWDHURY S.K, HARTLEY N.E.W, POLLOCK H.M. and WILKINS M.A. (1980)
J. Phys. D 13, 1761.

SADANA D.K, STRATHAM M, WASHBURN J. and BOOKER G.R. (1980)
J. Appl. Phys. 51, 5718.

SARGENT P.M. (1979)
PhD. Thesis, University of Cambridge.

SARGENT P.M. (1982)
Private Comm.

SARGENT P.M. and DONOVAN P. (1982)
Scr. Met., in press.

SARTWELL B.D. (1978)
Thin Solid Films 54, 233.

SAWYER G.R. (1979)
PhD Thesis, University of Cambridge.

SAWYER G.R. and PAGE T.F. (1978)
J. Mat. Sci. 13, 885.

SAWYER G.R, SARGENT P.M. and PAGE T.F. (1980)
J. Mat. Sci. 15, 1001.

SCHULSON E.M. and MARSDEN D.A. (1975)
Radn. Effects 24, 195.

SEIDEL T.E, PASTEUR G.A. and TSAI J.C.C. (1976)
Appl. Phys. Letts. 29, 648.

SHAFFER P.T.B. (1964)
J. Am. Ceram. Soc. 47, 466.

SHAFFER P.T.B. (1965)
J. Am. Ceram. Soc. 48, 601.

SINGER I.L. and BOLSTER R.N. (1980)
in 'Ion Implantation Metallurgy'
Proc. Metals Res. Soc. Symposium, Cambridge, Mass. 1979,
Eds. C.M. Preece, J.K. Hirvonen.
Met. Soc. AIME, New York.
p116.

SINGER I.L, BOLSTER R.N. and CAROSELLA C.A. (1980)
Thin Solid Films 73, 283.

SINGER I.L. and MURDAY J.S. (1980)
J. Vac. Sci. and Tech. 17, 327.

SADANA D.K, STRATHAM M, WASHBURN J. and BOOKER G.R. (1980)
J. Appl. Phys. 51, 5718.

SARGENT P.M. (1979)
PhD. Thesis, University of Cambridge.

SARGENT P.M. (1982)
Private Comm.

SARGENT P.M. and DONOVAN P. (1982)
Scr. Met., in press.

SARTWELL B.D. (1978)
Thin Solid Films 54, 233.

SAWYER G.R. (1979)
PhD Thesis, University of Cambridge.

SAWYER G.R. and PAGE T.F. (1978)
J. Mat. Sci. 13, 885.

SAWYER G.R, SARGENT P.M. and PAGE T.F. (1980)
J. Mat. Sci. 15, 1001.

SCHULSON E.M. and MARSDEN D.A. (1975)
Radn. Effects 24, 195.

SEIDEL T.E, PASTEUR G.A. and TSAI J.C.C. (1976)
Appl. Phys. Letts. 29, 648.

SHAFFER P.T.B. (1964)
J. Am. Ceram. Soc. 47, 466.

SHAFFER P.T.B. (1965)
J. Am. Ceram. Soc. 48, 601.

SINGER I.L. and BOLSTER R.N. (1980)
in 'Ion Implantation Metallurgy'
Proc. Metals Res. Soc. Symposium, Cambridge, Mass. 1979,
Eds. C.M. Preece, J.K. Hirvonen.
Met. Soc. AIME, New York.
p116.

SINGER I.L, BOLSTER R.N. and CAROSELLA C.A. (1980)
Thin Solid Films 73, 283.

SINGER I.L. and MURDAY J.S. (1980)
J. Vac. Sci. and Tech. 17, 327.

SLEESWYK A.W, KOK H.J.G. and BOOM G. (1980)
Scr. Met. 14, 919.

SMITH R, VALKERING T.P. and WALLS J.M. (1981)
Phil. Mag. 44A, 879.

SMITHELLS C.J. (1976)
'Metals Reference Book',
Butterworths, London.

SMUGERESKY J.E. and MYERS S.M. (1978)
in 'Applications of Phase Diagrams in Metallurgy and Ceramics',
Nat. Bureau Standards, Washington DC.
p516.

SOOD D.K. (1978)
Phys. Letts. 68A, 469.

SOOD D.K. and DEARNALEY G. (1978)
Radn. Effects 39, 157.

STEVENS R. (1970)
J. Mat. Sci. 5, 474.

STICKLER R. and BOOKER G.R. (1962)
Phil. Mag. 8, 859.

STROCKA B, BARTELS G. and SPOHR R. (1980)
Appl. Phys. 21, 141.

STUDMAN C.J, MOORE M.A. and JONES S.E. (1977)
J. Phys. D 10, 949.

STURTON J. (1981)
Private Comm.

SUH N.P. (1973)
Wear 25, 111.

SURI N.P, NIMMAGADDA R. and BUNSHAH R.F. (1979)
Thin Solid Films 64, 191.

SWAIN M.V. (1978)
in 'Fracture Mechanics of Ceramics', vol. 3,
Eds. R.C. Bradt, D.P.H. Hasselman, F.F. Lange,
Plenum Press, New York.
p257.

SWAIN M.V. and LAWN B.R. (1969)
Phys. Stat. Sol. 35, 909.

TAKAHASHI T. and FREISE E.J. (1965)
Phil. Mag. 12, 1.

THOMPSON M.W. (1969)
'Defects and Radiation Damage in Metals',
Cambridge University Press.

TOKUYAMA T, MIYAO M. and YOSHIHIRO N. (1978)
Jap. J. Appl. Phys. 17, 1301.

TOWNSEND P.D. (1977)
J. Phys. E 10, 197.

TSUJIDE T, NOJIRI M. and KITAGAWA H. (1980)
J. Appl. Phys. 51, 1605.

TUNG Y. and FAUST J.W. (1974)
in 'Silicon Carbide 1973'
Proc. Int. Conf. on Silicon Carbide, Miami Beach, Florida, 1973,
Eds. R.C. Marshall, J.W. Faust, C.E. Ryan.
Univ. Sth. Carolina Press, Columbia, 1974.
p246.

TURNER J. (1980)
Private Comm.

VARJORANTA T, HIRVONEN J.K. and ANTTILA A. (1981)
Thin Solid Films 75, 241.

VELDKAMP J.D.B, HATTU N. and SNYDERS V.A.C. (1978)
in 'Fracture Mechanics of Ceramics', vol. 3,
Eds. R.C. Bradt, D.P.H. Hasselman, F.F. Lange,
Plenum Press, New York.
p273.

VERMA A.R. and KRISHNA P. (1966)
'Polytypism and Polymorphism in Crystals',
John Wiley and Sons, New York.

WANG Y.F, CLAYTON C.R, HUBLER G.K, LUCKE W.H. and HIRVONEN J.K. (1979)
Thin Solid Films 63, 11.

WEBB R. and CARTER G. (1979)
Radn. Effects 42, 159.

WEILER W. (1973)
in 'The Science of Hardness Testing and its Research Applications'
Eds. J.H. Westbrook, H. Conrad,
Am. Soc. for Metals, Ohio, 1973.
p16.

WESTBROOK J.H. and CONRAD H. (Eds.) (1973)
'The Science of Hardness Testing and its Research Applications',
American Society for Metals, Ohio.

WESTWOOD A.R.C. and MACMILLAN N.H. (1973)
in 'The Science of Hardness Testing and its Research Applications'
Eds. J.H. Westbrook, H. Conrad,
Am. Soc. for Metals, Ohio, 1973.
p377.

WHAPHAM A.D. (1957)
Phil. Mag. 3, 103.

WHITE G. and DEARNALEY G. (1980)
Wear 64, 327.

WILSON G. (1980)
PhD. Thesis, University of Cambridge.

WOLF G.W. (1980)
Radn. Effects 48, 237.

YOFFE E.H. (1982)
Phil. Mag. 46A, 617.

ZELLAMA K, GERMAIN P, SQUELARD S, BOURGOIN J.C,
PIAGUET J. and ROBIC J.Y. (1978)
Solid State Comms. 26, 901.

ZIELINSKA-ROHOZINSKA E. and GERWARD L. (1980)
Phil. Mag. 41A, 321.

ZINNER E. (1980)
Scanning 3, 57.